DOI: 10.31577/ahs-2022-0023.02.0017

ACTA HYDROLOGICA SLOVACA

Volume 23, No. 2, 2022, 157–162

Modeling of soil water retention curves based on two programs

Justína VITKOVÁ*, Lucia TOKOVÁ, Natália BOTKOVÁ

We compared two methods of modeling soil water retention curves used by scientists in Slovakia. The first modeling was done using the GENRET program and the second using the RETC program. Samples of pure sandy soil and sandy soil with applied biochar in three different particle sizes were used for the simulation. Sandy soil has a very low retention capacity therefore the modeling of soil water retention curves is not easy. Our results showed that the GENRET program can model the curve even at high pressures, which the RETC program modeled only in one variant, but the RETC program had better agreement with measured data. The most significant differences between the programs were at the lowest and highest pressures.

KEY WORDS: soil water retention curve, modeling, RETC, GENRET

Introduction

The soil water retention curve (SWRC) is the relationship between water content and matric potential. It is one of the most significant hydraulic functions for modeling flow transport in porous media (Zha et al., 2015). SWRC is one of the most important and complex hydro-physical characteristics of the soil, because we can determine: a) energetic characteristics of soil water, b) qualitative and quantitative characteristics of soil pores, c) hydrolimits, d) changes in physical and hydro-physical characteristics due to the action of natural factors or human activity, e) design parameters for irrigation and soil drainage and f) input data for the calculation of other soil hydro-physical characteristics (Antal and Fídler, 1989). Therefore, SWRC is considered as one of the most fundamental soil hydraulic properties, and the accurate acquisition of SWRC and its parameterization have great significance in understanding soil moisture dynamic and soil hydrology.

There are two main approaches to obtaining SWRC. The first is experimental determination and the second is derivation from basic soil properties by using pedotransfer functions (PTF). Although, experimental approach is time consuming and costly, it is undoubtedly more precise and reliable for SWRC of specific soils (Pan et al., 2019). SWRC is affected by many soil environmental factors, and thus it is very difficult to accurately determinates relationship with these factors. The course of SWRC depends on the granular and mineralogical composition of the soil, on the content of humus, exchangeable cations, structure and bulk density. For that reason, it is established for each soil, or for each horizon separately (Fulajtár, 2006). The SWRC can be measured by a variety of techniques. Among the available techniques, the most commonly used are the Richards' pressure apparatus (Dane and Hopmans, 2002; Richards, 1948; Richards, 1965), also called pressure plates (and hereafter called pressure plates apparatus). We have used this technique for our experiment, as well.

The SWRCs are usually measured during the drainage process, starting with soil saturated with water (this is the preferred case), or during soil wetting, then starting with air-dry soil. Both SWRC main branches are typical of a particular soil; the shape and position of the SWRC reflect porous space dimensions, and porous space reflect soil texture (Novák and Hlaváčiková, 2019). Several mathematical formulations for describing the SWRC are available (Brooks and Corey, 1966; van Genuchten, 1980; Vogel and Cislerova, 1988). Early empirical models primarily describe the wet end of the SWRC. For example, the Brooks and Corey (1966) and van Genuchten (1980) models (abbreviated the BC and VG models, respectively) are the most popular for predicting SWRC under wet conditions. However, the two models do not predict the SWRC at oven dryness, because they assume the matric suction to be infinite when the soil moisture approaches the residual water content (Silvia and Grifoll, 2007). According to Bittelli and Flury (2009) directly observed soil suction is limited from 0 up to 1500 kPa (15 bars) and the measurements are time consuming and laborious at high suction values.

In our experiment we used a sandy soil, as not very

typical agricultural soil, but there are several countries and its locations where this type of soil has to be used for agricultural utilization. The biochar is one of tools to improve hydro-physical parameters and fertilization of sandy soils (Dokoohaki et al., 2017; Toková et al., 2022), that's why we present three variants of SWRCs with biochar and one variant without biochar. However, in this study we present only SWRC modeling differences and program selection.

Material and methods

Preparation of soil and soil-biochar mixtures

The sandy soil used in this experiment was taken from Plavecký Štvrtok area at Záhorská lowland. Particle size distribution was measured by the hydrometer method (Velebný, 1981). It consists of 91% sand, 7.5% silt and 1.5% clay, so it is classified as sand, based on the USDA classification. The soil was sieved to a fraction with particle diameter size ≤2 mm. Used biochar was produced from willow trees by pyrolysis temperature at 300°C. The size of biochar was 0–10 mm, so it was homogenized using a hammer mill and sieved to a fraction with a particle size 125 μm and 2 mm.
Samples of soil-biochar mixtures were prepared in laboratory conditions with a biochar application rate of 20 t ha^{-1} in Kopecky cylinders with a volume of 100 cm^3. Overall four variants were prepared: pure sandy soil (control), mixture of soil and biochar with particle size <125μm, mixture of soil and biochar with particle size 125μm–2mm and mixture of soil and biochar with particle size >2mm. For each variant were prepared three repetitions.

Overpressure equipment (pressure plate method)

To determine the SWRC of the soil, we used 9 measurement points at pressure potentials of 0; 0.002; 0.06; 0.1; 0.3; 0.56; 1; 3 and 4.8 bars. For the analytical construction of the SWRC, it was necessary to calculate the residual soil moisture – θ_r, because the relationship between soil moisture and soil water potential is determined only in the range of θ_r and θ_s (saturated water content) (Skalová et al., 2015). We determined the residual moisture of the soil using the measured points with the trend line and saturated soil moisture was measured. In this study, we present the average soil moisture values for each variant.

Soil water retention curve simulations

GENRET
The GENRET program is a part of the *GLOBAL* model, which was developed at the Institute of Hydrology SAS (Majerčák and Novák, 1995). Non-linear least-squares analysis of the SWRC is approximated by van Genuchten method (1980) and SWRC hysteresis is considered based on Kool-Parker theory (1987). Input data are saturated hydraulic conductivity, saturated water content and measured points of SWRCs. Residual water content could be computed or fitted; parameters *alpha* and *n* can be computed based on Mualem's or Burdine's theory or fitted. In our study were parameters *alpha* and *n* determinated based on the Mualem's theory. The unsaturated hydraulic conductivity is computed based on Mualem's theory (1976).

RETC
The RETC (*RETention Curve*) is a program for analyzing the hydraulic conductivity properties of unsaturated soils (van Genuchten et al., 1991). The parametric models of Brooks-Corey and van Genuchten are used to represent the SWRC. The theoretical pore-size distribution models of Mualem and Burdine predict the unsaturated hydraulic conductivity function. The simulation can be generated from observed soil water retention data assuming that one observed conductivity value (not necessarily at saturation) is available (van Ganuchten et al., 1991). The program also permits users to fit analytical functions simultaneously to observed water retention and hydraulic conductivity data. The RETC program assign fixed parameters *alpha* and *n* for sandy soil.
In our study we used van Genuchten model for SWRC simulation. It is widely used expression for describing the soil water retention function (1):

$$\theta(h) = \theta_r + \frac{\theta_s - \theta_r}{[1+|\alpha h|^n]^m} \quad h < 0$$
$$\theta(h) = \theta_s \quad h \geq 0 \qquad (1)$$

where
θ – is soil moisture,
h – is soil water potential,
r and s – denote residual and saturated water contents, respectively,
n and m – are dimensionless empirical shape factors,
1 – is a pore-size distribution index. For practical purposes it is also denoted as n in the program RETC,
α – is also empirical shape parameter.

Statistical analysis

Comparison of two programs for SWRC simulations was evaluated using the Microsoft Excel software. The statistical analysis was done by using standard box plot to show distribution of a set of data.

Results and discussion

Our results show that there are deviations in SWRC modeling when using two different programs (Fig. 1–4). The biggest differences were detected at the highest modeled pressures – a significant deviation between the curves was detected at pressures of pF 2.5 and above. It follows from the modeled SWRCs that at pF 3 soil moisture was 50% lower in the GENRET program compared to the RETC program, and at pF 3.5 it was up to 76% (Fig. 1). Higher differences in soil moisture were also detected for the variant with a particle size of biochar >2mm (Fig. 4), when at pF 3 it was 40% for the GENRET program and at pF 3.5 to 66% compared to the RETC

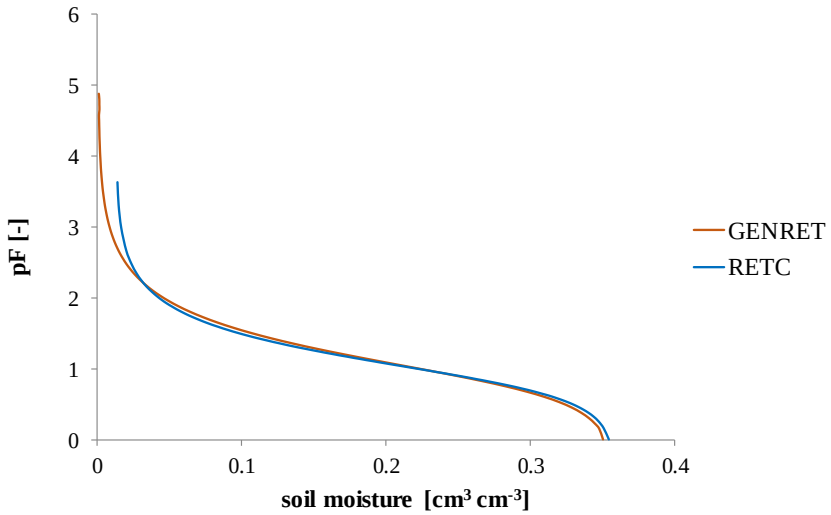

Fig. 1. Average SWRC for pure sandy soil modeled by GENRET and RETC programs.

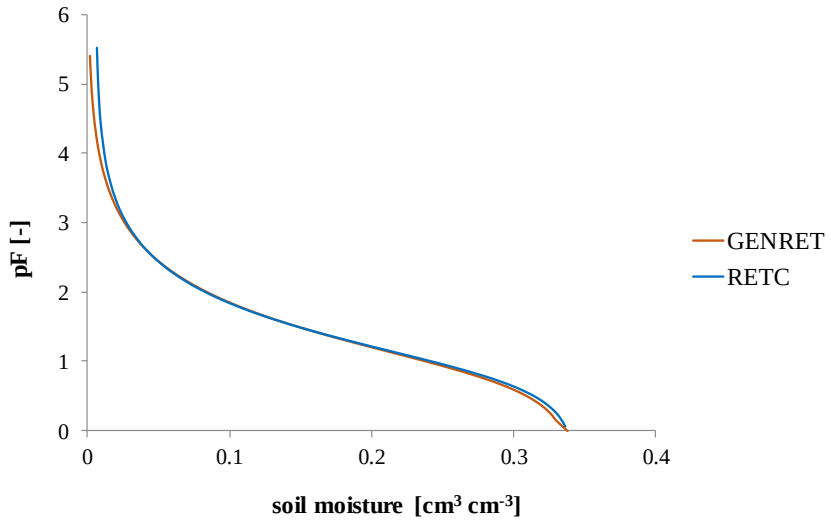

Fig. 2. Average SWRC for sandy soil and biochar with particle size <125µm modeled by GENRET and RETC programs.

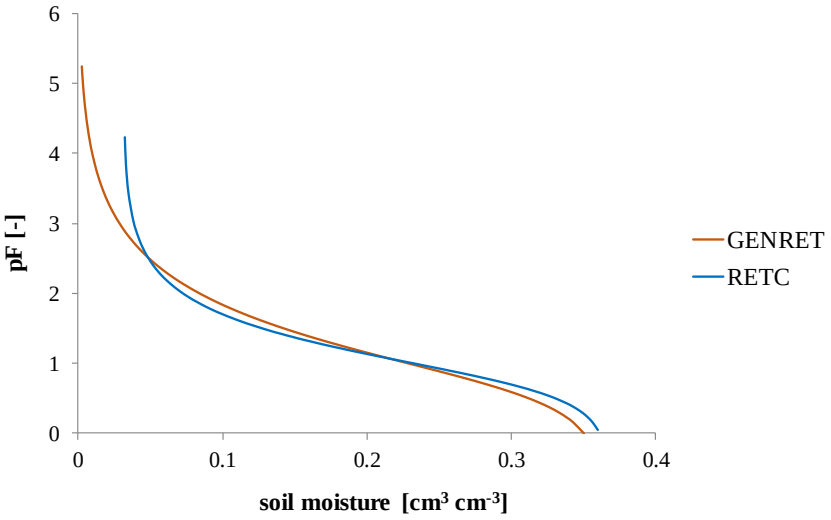

Fig. 3. Average SWRC for sandy soil and biochar with particle size 125µm–2mm modeled by GENRET and RETC programs.

program. At saturated soil values and low pressures, the difference was negligible – maximum to 6% (Fig. 3 and 4).

Almost identical SWRCs were simulated between GENRET and RETC programs for the variant of soil and biochar with particle size <125µm. The most significant difference was 13% at pF 3.5 (Fig. 2). From Fig. 1–4 it is clear that the GENRET program is able to model soil moisture even at higher pressures, despite the fact that the input data for sandy soil modeling deflect from the standard values. The statistical analysis (Fig. 5) shows that while the average soil moisture was modeled at 10% vol. with the GENRET program, it was around 18% vol. with the RETC program.

For better visualization are differences in measured and modeled SWRC points shown in Table 1. Better agreement was between measured data and modeled data by RETC program. In higher pressures were differences between programs and measured data higher, sometimes underestimated (more often GENRET program) and sometimes overestimated (more often RETC program). Soil moisture for pF 3.7 was not modeled by RETC program for variant soil + biochar >2mm.

The shape differences of the SWRCs were due to the different *alpha* and *n* parameters (Table 2). The fitted *alpha* parameter in RETC program was lower than the *alpha* values calculated by GENRET program; the parameter *n* was significantly higher in RETC compared to the calculated *n* value for all variants in GENRET.

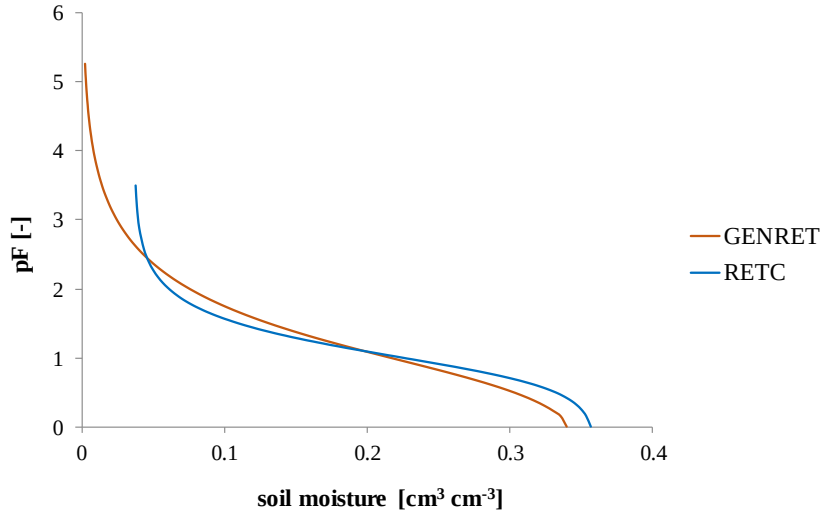

Fig. 4. Average SWRC for sandy soil and biochar with particle size >2mm modeled by GENRET and RETC programs.

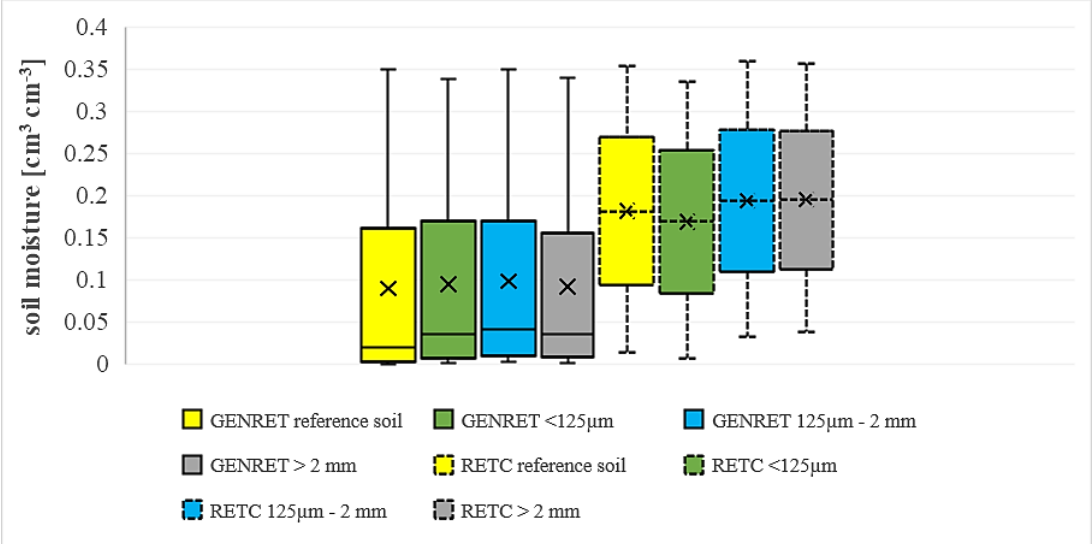

Fig. 5. Statistical analysis of SWRCs for GENRET and RETC programs means that the lower (Q1) and upper (Q3) quartile, representing observations outside the 9–91 percentile range. The diagram also shows the median (marked with line) and mean (marked with cross) observation. Data falling outside the Q1–Q3 range are plotted as outliers of the data.

Table 1. Differences in measured SWRC points and modeled by GENRET and RETC programs

		sandy soil			**soil + biochar <125µm**		
pF	bar	*measured*	*GENRET*	*RETC*	*measured*	*GENRET*	*RETC*
0.3	0.002	0.347	0.340	0.344	0.330	0.324	0.326
1.78	0.06	0.054	0.064	0.062	0.103	0.106	0.106
2	0.1	0.049	0.043	0.044	0.078	0.082	0.082
2.5	0.3	0.029	0.017	0.023	0.062	0.044	0.047
2.78	0.56	0.0127	0.012	0.020	0.029	0.034	0.033
3	1	0.0122	0.008	0.016	0.023	0.026	0.027
3.5	3	0.0120	0.003	0.0144	0.017	0.014	0.016
3.7	4.8	0.011	0.002	0.0136	0.014	0.011	0.013

		soil + biochar 125µm – 2mm			**soil + biochar >2mm**		
pF	bar	*measured*	*GENRET*	*RETC*	*measured*	*GENRET*	*RETC*
0.3	0.002	0.355	0.333	0.346	0.352	0.325	0.347
1.78	0.06	0.078	0.104	0.090	0.067	0.094	0.077
2	0.1	0.074	0.082	0.073	0.065	0.073	0.060
2.5	0.3	0.067	0.047	0.049	0.060	0.040	0.044
2.78	0.56	0.054	0.037	0.042	0.049	0.031	0.040
3	1	0.041	0.029	0.039	0.039	0.024	0.039
3.5	3	0.027	0.017	0.035	0.031	0.013	0.038
3.7	4.8	0.020	0.013	0.034	0.026	0.010	x

Table 2. Differences in average modeled *alpha* and *n* parameters (GENRET) and fitted parameters (RETC)

	GENRET		**RETC**	
	alfa	*n*	*alfa*	*n*
sandy soil	0.147	1.33	0.145	2.68
soil + biochar <125µm	0.151	1.89		
soil + biochar 125µm – 2mm	0.219	1.58		
soil + biochar >2mm	0.221	1.54		

Conclusion

Sandy soil has a very low retention capacity; therefore, it is not completely suitable for agricultural use. By using biochar, it is possible to improve its basic hydro-physical properties. SWRC is one of the most important parameters that can be used to assess soil retention capacity. Measuring SWRC points for sandy soil is problematic because the infiltrated water drains away very quickly (even at the lowest pressures). In our experiment, soil moisture was significantly reduced already at a pressure of 0.06 bar (6 kPa), and from a pressure of 0.56 bar (56 kPa) it changed indistinctly. Therefore, SWRC modeling is also more complicated, and not every model can handle non-standard input data. We compared the SWRC simulations by using the GENRET and RETC programs. They showed dispersion mainly at higher pressures and also when applying biochar with the largest particles. The RETC program failed to complete the modeling at the highest pressures and only for the soil and biochar <125µm variant modeled SWRC above pF 5 (10 000 kPa). It can be explained by the fact, that the smallest biochar particles (<125µm) can fill the pores between the sandy soil particles and thereby increase its retention capacity, which was also reflected in the values of the input data to the programs. Other way round, the GENRET program had a problem only with the variant with pure soil, when the modeling ended at a pF 4.8 (6 309 kPa). For the other variants, it reached a value of pF 5.5 (31 622 kPa). Measured SWRC points had better agreement with RETC program.

We can conclude that both programs have their limitations for simulations the SWRC of sandy soil. Our next research is continuing by using different method of θ_r determination for the GENRET program and calculating parameters *alpha* and *n* for RETC program.

Acknowledgement

This work was supported by Scientific Grant Agency No. VEGA 2/0155/21 and by EIG CONCERT-Japan No. EIG JC2019-074.

References

Antal, J., Fídler, J. (1989): Poľnohospodárske meliorácie, Príroda, Bratislava, 463 p.

Bittelli, M., Flury, M. (2009): Errors in water retention curves determined with pressure plates. Soil Science Society of America Journal, vol. 73, 1453–1460.

Brooks, R. H., Corey, A. T. (1966): Properties of porous media affecting fluid flow. Journal of the Irregation and Drainage Division, vol. 92, 61–88.

Dane, J. H., Hopmans, J. W. (2002): Pressure plate extractor. In: Dane, J. H., Topp., G. C. (Eds.) Methods of Soil Analysis. Part 4. Physical Methods. SSSA, Madison, WI, 688–690.

Dokoohaki, H., Miguez, F. E., Laird, D., Horton, R., Basso, A. S. (2017): Assessing the Biochar Effects on Selected Physical Properties of a Sandy Soil: An Analytical Approach, Communications in Soil Science and Plant Analysis, DOI: 10.1080/00103624.2017.1358742

Fulajtár, E. (2006): Fyzikálne vlastnosti pôdy, VÚPOP, Bratislava, 142 p.

Kool, J. B., Parker, J. C. (1987): Development and evaluation of closed-form expression for hysteretic soil hydraulic properties. Water Resour. Res., vol. 23, no. 1, 105–114.

Majerčák, J., Novák, V. (1995): GLOBAL – a numerical model for water movement in the soil root zone. Research Report, IH SAS, Bratislava, 75 p.

Mualem, Y. (1976): A new model for predicting the hydraulic conductivity of unsaturated porous media. Water Resour. Res., vol. 12, no. 3, 513–522.

Novák, V., Hlaváčiková, H. (2019): Applied Soil Hydrology. In Theory and Applications of Transport in Porous Media. Springer International Publishing: Cham, Switzerland. 342 p. ISBN 978-3-030-01805-4.

Pan, T. Hou, S., Liu, Y., Tan, Q. (2019): Comparison of three models fitting soil water retention curves in a degraded alpine meadow region. Scientific Reports, vol. 9, 18407.

Richards, L. A. (1948): Porous plate apparatus for measuring moisture retention and transmission by soils. Soil Sci., vol. 66, 105–110.

Richards, L. A. (1965): Physical condition of water in soil. In: Black, C. A. (Ed.), Methods of Soil Analysis, Part 1. Agron. Monogr. ASA, Madison, WI, 128–152.

Silvia, O., Grifoll, J. (2007): A soil–water retention function that includes the hyper–dry region through the bet adsorption isotherm. Water Resources Research, vol. 43, 1–13.

Skalová, J., Kotorová, D., Igaz, D., Gomboš, M., Nováková, K. (2015): Regionalizácia pedotransferových funkcií vlhkostných retenčných kriviek Slovenska. STU, Bratislava, 143 p.

Toková, L., Botková, N., Vitková, J., Šurda, P., Botyanszká, L., Rončák, P., Gaduš, J. (2022): Saturated hydraulic conductivity of sandy soil under application of two different biochar types. In Veda mladých 2022 – Science of Youth 2022: proceedings of reviewed contributions. – Nitra: Faculty of Horticulture and Landscape Engineering, 2022, 138–146. ISBN 978-80-552-2502-9. ISSN 2585-7398.

van Ganuchten, M. Th. (1980): A closed–form equation for predicting the hydraulic conductivity of unsaturated soil. Soil Science Society of America Journal, vol. 44, 892–898.

van Ganuchten, M. Th., Leij, T. F., Yates, S. R. (1991): The RETC Code for quantifying the hydraulic functions of unsaturated soils, Version 1.0. EPA Report 600/2–91/065, U.S. Salinity Laboratory, USDA, ARS, Riverside, California.

Velebný, V. (1981): Hydropedológia – učebná pomôcka na cvičenie. SVŠT. Bratislava. 173 p. ISBN 85–341–81.

Vogel, T., Cislerova, M. (1988): On the reliability of unsaturated hydraulic conductivity calculated from the moisture retention curve. Transport Porous Media, vol. 3, 1–15.

Zha, Y., Wu, X., Gong, F., Xu, M., Zhang, H., Chen, L., Huang, S., Cai, D. (2015): Long–term organic and inorganic fertilizations enhanced basic soil productivity in a fluvo-aquic soil. Journal of integrative Agriculture, vol. 14, 2477–2489.

Ing. Justína Vitková, PhD. (*corresponding author, e-mail: vitkova@uh.savba.sk)
Ing. Lucia Toková, PhD.
Ing. Natália Botková
Institute of Hydrology SAS
Dúbravská cesta 9
841 04 Bratislava
Slovak Republic

Ing. Natália Botková
Institute of Landscape Engineering
Faculty of Horticulture and Landscape Engineering, SUA
Hospodárska 7
949 76 Nitra
Slovak Republic

DOI: 10.31577/ahs-2022-0023.02.0018

ACTA HYDROLOGICA SLOVACA

Volume 23, No. 2, 2022, 163–171

Drainage systems design in urbanized areas under land use changes scenarios: case study of Narok Town (Kenya)

Etienne UMUKIZA, James M. RAUDE, Andrea PETROSELLI, Simon M. WANDERA, John M. GATHENYA, Ciro APOLLONIO*

Land use/land cover (LULC) changes due to urbanization have a strong influence on runoff process. In the case of Narok town, in Kenya, several flash floods have caused human losses and economic damages. Design hydrograph and its peak flow are the key elements to determine hydraulic geometrical properties in designing an adequate drainage system. In consideration of LULC changes and consequent hydrograph variability, in this study existing channel geometric properties were verified, using field measurements through a ground survey employing Real-Time Kinematic equipment at Kakia and Esamburmbur channels of Narok town. To improve the drainage system, the evaluated peak flows under assumed future LULC scenarios were used to design hydraulic properties for a sustainable urban drainage system. Three hydrological/hydraulic models (EBA4SUB, Manning's equation, and Civil 3D) were used under different LULC scenarios for computing channel geometry and correspondent water level. The change in channel geometry was found to obstruct free flow for different scenarios of peak discharge and flow volume. The presented results could be used to support the design of storm water drainage systems by local authorities, in order to mitigate flood hazards and consequently to reduce the hydraulic risk.

KEY WORDS: Peak flow estimation, Rainfall-runoff modeling, LULC changes, Kenya case study, EBA4SUB model, Drainage systems.

Introduction

Land use/land cover (LULC) maps are a key input in environmental evaluations for the sustainable planning and management of socio-ecological systems (Pelorosso et al., 2021). In particular, urbanization is considered the most important driver in LULC changes due to developments of facilities such as roads, houses, schools (Habete and Ferreira, 2016; Han et al., 2009; Ohana-Levi et al., 2018).

Rapid socio-economic development and urbanization are drivers of significant changes in land use and can cause, as a consequence, high potential runoff (Blöschl et al., 2007, Apollonio et al., 2016). Additionally, various human activities have profoundly influenced the hydrological cycle and water resources management due to the growth of society and the economy (Apollonio et al., 2018; Umukiza et al., 2021; Pellicani et al., 2018). Uncontrolled land use is among the main reasons of variations in hydrologic and hydraulic processes (Zope et al., 2016; Apollonio et al., 2016). Moreover, urbanization processes as part of LULC tend to increase runoff rates and peak discharges due to the increased imperviousness and reduced infiltration along the built-up area (Ohana et al., 2013). As a matter of the fact, the process of urbanization is accompanied by vegetation removal as consequence, leading to increased runoff.

Novelli et al. (2016) proposed an efficient Artificial Neural Networks (ANN) classification method based on LANDSAT satellite data to evaluate LULC changes in a river basin area considering a time trend of 28 years. Shaina Beegam and Prince Arulraj (2018) reported urbanization as a direct effect on the environment which in turn affects the variations in runoff, that ultimately turn to flood. Recanatesi and Petroselli (2020), selecting a strategic case study in the periurban environment of the metropolitan area of Rome, determined that the increase in the flood risk is more pronounced in the part of the selected area that has been more extensively interested by the soil loss. In recent decades, urbanization has become an environmental concern in many developing countries (Guo et al., 2011; Fenner et al., 2019). Globally, floods are among the most devastating natural hazards and their frequency is increasing. There are several causes of floods, such as natural factors, and anthropogenic activities such as blocking of drainage channels, uncontrolled land use, and deforestation in headwater regions (Młyński et al., 2018). Each year, floods cause major disruption throughout the world, leading to loss of both human and animal life

and damage to properties (Sharif et al., 2016). However, some land-use actions if correctly planned and realized can help to reduce flooding problems. For instance, urbanization in floodplain areas increases the risk of flooding due to the increase of peak discharge (Suriya and Mudgal, 2012).

The problems outlined above are also found in Kenya. In the case of Narok town, Kenya, the increase in floods events was recognized in recent years, resulting from the fact that Narok county areas is urbanizing at a rapid rate like many county areas in developing countries (Mwangi et al., 2019). Furthermore, population growth commonly leads to urbanization and expansion of agricultural land; hence this circumstance adversely affects hydrological processes (Coomes et al., 2001). Also, the lack of an adequate urban drainage network can increase the flooding risk (Alfarajat et al., 2014).

In fact, hydraulic structures for water control are sized to resist a design event, characterized by a hydrograph associated with a probability of occurrence (Erpicum et al., 2021; Piscopia et al., 2015). Usually, hydraulic structures are designed based on design hydrograph and its peak discharge to ensure efficiency and safety during service life. In many parts of the world, hydraulic structures are mostly considered safety-focused, risk-averse, and display hesitancy to use unproven innovation over legacy tools. Indeed, hydraulic structures engineering should involve and respond to the increasing demands for sustainability to reverse the challenges of today and the future (Erpicum et al., 2021). Although obtaining runoff estimation in ungauged catchments is very important when designing hydraulic structures, it is indeed a challenging problem to predict runoff for these basins because of the difficulty in obtaining adequate historical flow observations (Petroselli et al., 2020).

A recent study (Umukiza et al., 2021) evaluated future projections on the Narok town watershed in terms of LULC scenarios and related design flows for the best mitigation of floods and effective land planning. The study investigated the effects of projected LULC changes on peak flow and total runoff for the two catchments (Kakia and Esamburmbur) of Narok town, Kenya using the Event-Based Approach for Small and Ungauged Basins (EBA4SUB) rainfall-runoff model (Petroselli and Grimaldi, 2018) to determine the design hydrographs and peak discharge in the investigated catchments. As consequence of the aforementioned study, the present work aims to 1) carry out the hydraulic and geometric properties design of Kakia and Esamburmbur channels based on the peak flow determined under forecasted LULC change scenarios on watersheds, and 2) propose adequate conveyance capacity of the channels based on predicted effects of LULC changes as future likely scenarios to occur on rainfall-runoff regime within the watershed.

Material and methods

Description of the study area

The County Government of Narok lies between latitudes 0°50′ and 1°50′ South and latitude 35°28′ and 36°25′ East. It borders the Republic of Tanzania to the South, Kisii, Migori, Nyamira, and Bomet counties to the West, Nakuru County to the North, and Kajiado County to the East. It covers a total area of 17,933 km^2. The study area, shown in Fig. 1, is a small portion of Narok county territory, being characterized by a total area of 46.2 km^2 and it pertains to the hydrographic catchments of two seasonal streams, Kakia and Esamburmbur.

An average rainfall of 750 mm per year characterizes the precipitations of the area, with the majority of

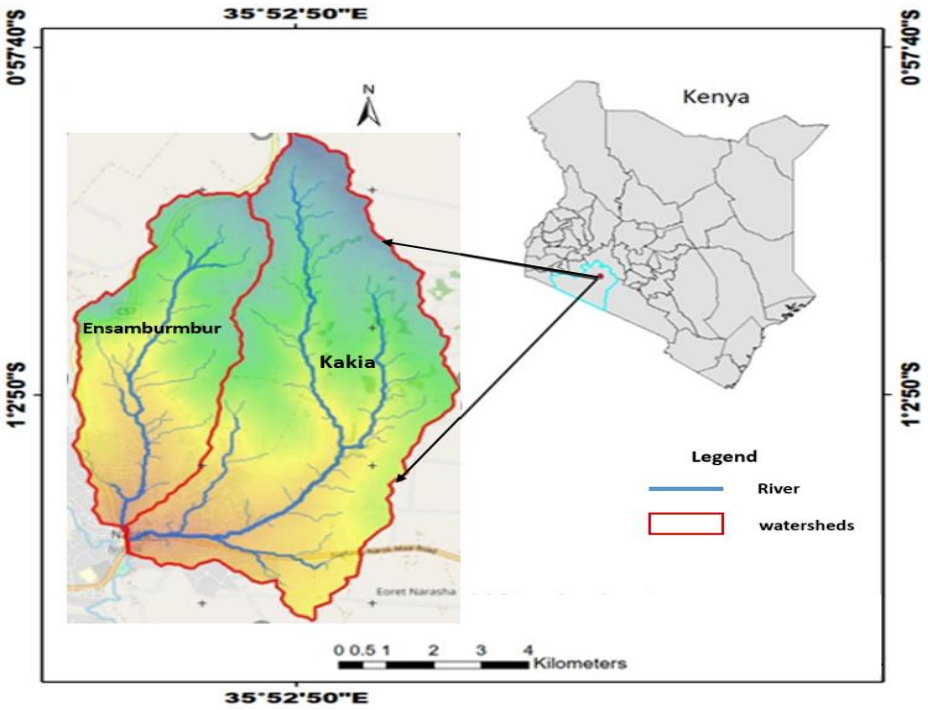

Fig. 1. Kakia and Esamburmbur sub-catchments.

the rainfall occurring in the March to May season. The temperature ranges from a minimum of 8°C to a maximum of 28°C.

The elevation of the investigated area lies between 1,844 m to 2,138 m above sea level and the water flow length is estimated to cover a maximum distance of 10,000 m to the outlet, for Kakia stream. The main economic activities are commercial farming (wheat, maize, and potatoes), livestock farming, and tourism in the famous Maasai Mara area.

LULC Changes in Narok Town Sub-catchment

The study by Marie Mireille et al. (2019) reported that LULC change that occurred in the investigated area in the period 1985–2019 showed a decrease in forest and pasturelands which were replaced by agriculture and built-up areas. Therefore, the major observed LULC changes were processed using supervised classification methods to assign different future scenarios starting from the Landsat image of November 2019, using Erdas Imagine 2015 (Umukiza et al., 2021).

To further understand the future likely impacts of various activities in the catchment, Umukiza et al. (2021) hypothesized four projected future scenarios (Table 1), based on major types of LULC identified in 2019 (scenario "0"). Therefore, due to LULC changes previously mentioned, Scenario one (1) considered that the built-up area is 20% of the total area, the agricultural area is 75%, and the pastureland is assumed to be in poor condition with a rate of 5% of the total area. In this scenario, intense increase in urbanization and agricultural activities were assumed, leading to a drastic decrease in forest areas and rangelands.

Scenario 2 consisted of 15% of the entire catchment for the built-up area, 40% for the agricultural area, 30% for pastureland, and 15% for the forest. In this scenario, a small increase in built-up area and reforestation was assumed, while agriculture is assumed to reduce and give an increase of rangeland.

Scenario 3 assumes 50%, 40%, and 10% for the built-up area, agricultural area, and rangelands, respectively, of the entire catchment. In this scenario, a considerable increase in a built-up area was assumed, maintaining the same extent of the agricultural area as Scenario 2, and reducing the forest with a small part of rangeland.

Scenario 4 assumed 20%, 5%, 30%, 40% and 5% for pastureland, forest, built-up area, agriculture and open space, respectively. In this scenario, a regular step of 10% of the proportion from pastureland, built-up area, an agricultural area, and a small rate for forest and open space, was assumed.

In the present work, we focus on design of channel geometry based on the peak discharges evaluated in Umukiza et al. (2021), under different scenarios of LULC. The effect of LULC changes have been expressed using the Natural Resources Conservation Services (NRCS) – Curve Number (CN). CN value was calculated with the combination of spatial LULC data, soil type, and assuming an Antecedent Moisture Condition (AMC) equal to II following what was done in Umukiza et al. (2021). The average CN value for the two investigated catchments from the projected LULC scenarios was determined according to Equation 1 (Gajbhiye et al., 2014):

$$CN = \frac{\sum CN_i A_i}{A} \quad (1)$$

where

CN_i, and A_i – are CN value [-] and area value [km^2], respectively, of the generic LULC parcel,

CN_i – is the weighted CN considering the specific areas as weights [-]

A – is the total area of the investigated catchment [km^2].

Evaluation of design peak discharge

Engineering designs of hydraulic structures require estimated design peak flow and flow volume for flood management. For small and ungauged catchments, like in our study area, usually enough observed flow data are not available, so calibration of the advanced hydrological and hydraulic model is difficult. Therefore, the Event-Based Approach for the Small and Ungauged Basins (EBA4SUB) rainfall-runoff model was used in Umukiza et al. (2021), since it is particularly suited to estimate design hydrograph, peak discharge, and flow volume in ungauged basins (Młyński et al., 2020). In detail, the inputs data needed by the model are the Digital Elevation Model (DEM) of the investigated catchments, the LULC data, and the rainfall data while the main parameters of the model are CN and time of concentration Tc (Petroselli and Grimaldi, 2018).

Based on this, the estimated values related to peak discharges for 50 and 100 years return periods for the different projected scenarios are summarized in Table 2.

Channel parameters

Channel dimensions at each cross-section were obtained using the RTK instrument. The main parameters like depth, width, and bottom slope for both streams for their complete length were determined. The inspections allowed to estimate Manning's roughness coefficients. The measurements of dimensions in terms of width, depth, and slope along the existing channels were carried out at an interval of 10 to 20 m (see Fig. 2).

The peak discharge estimated in Umukiza et al. (2021) under different LULC scenarios and assuming return periods equal to 50 and 100 years was used as a design discharge. Therefore, the following design considerations have been adopted in this study:

1. The flow is one-dimensional; depth and velocity vary only in the longitudinal direction of the channel. This implies that the velocity is constant and the water surface is horizontal across any section perpendicular to the longitudinal axis.
2. Flow is assumed to vary gradually along the channel so that hydrostatic pressure prevails and vertical accelerations can be neglected (Chow, 1959).

3. The longitudinal axis of the channel is approximated as a straight line.
4. The bottom slope of the channel is small and the channel bed is fixed; that is, the effects of scouring and deposition are negligible.
5. Resistance coefficients for steady uniform turbulent flow are applicable so that relationships such as Manning's equation can be used to describe resistance effects.

It is noteworthy that the assumption of the steady flow, used here, has some limits, related to neglecting the lateral inflow due to increase of catchment area of the basin, and to the existence of water structures in channel network locally effecting hydraulic characteristics and hence changing the supposed course of water depth along the channel. However, in our case, we did consider the whole catchment area for both Kakia and Esamburmbur. The uppermost contributing

Table 1. Details of Projected Scenarios Based on Major Types of LULC Transition Found for LULC in 2019. Source: Umukiza et al., 2021

	Different rates LULC [%] of the entire catchment				
LULC	**2019**	**Scenario 1**	**Scenario 2**	**Scenario 3**	**Scenario 4**
Forest	6.3	0	15	0	5
Pastureland	25.9	5	30	10	20
Agricultural	55.4	75	40	40	40
Open Space	0	0	0	0	5
Built-up area	12.5	20	15	50	30

Table 2. Peak discharge [$m^3 s^{-1}$] for different return periods (*Tr*, years) under various LULC Scenarios (Kakia and sub-catchment). Source: Umukiza et al., 2021

	Kakia		**Ensamburmbur**	
LULC Scenarios	**Tr50**	**Tr100**	**Tr50**	**Tr100**
2019	130.3	164.1	75.1	94.2
Scenario 1	154.2	191.1	88.9	110.1
Scenario 2	121.4	154.0	70.8	89.0
Scenario 3	172.2	210.4	100.6	121.8
Scenario 4	145.3	181.0	83.4	104.2

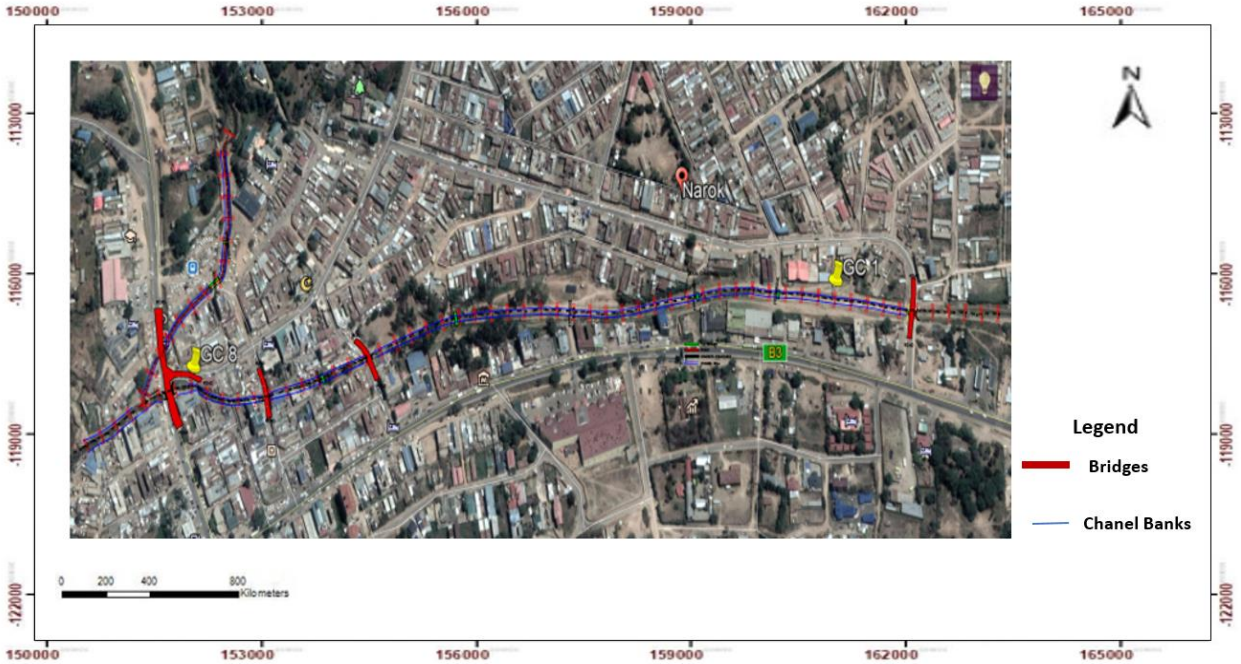

Fig. 2. Surveyed Channels and Identified Cross-Sections and Infrastructures.

inflow channel was considered in the downstream flow accumulation. Therefore, there will not be an additional drainage network with time due to the increase in the watershed basin.

In addition the assumption of steady uniform flow can be considered be valid, because the cross-section structures are at height of the channel banks and the flow is at the lower level of the height of the channel banks. For the channel design, the case of overflow due to overtopping of cross-sectioning structures has been avoided. Therefore, as there are no water structures that can disturb the flow, we can justify the steady uniform flow hypothesis.

Then, the estimated peak discharges were conveyed into the channel by using Manning's and continuity equations. For improving the existing lined channel (rectangular cross-section), the morphology of the channel is considered to be a rectangular cross-section for the first step, and trapezoidal in the second step for determining the suitable case to convey a given flow at the corresponding scenario of predicted runoff due to LULC. Under such hypothesis, Manning's Equation is expressed as follows.

$$Q = \frac{A * R^{\frac{2}{3}} \; S_f^{\frac{1}{2}}}{n} \qquad (2)$$

where:

n – is Manning's roughness value,
R – is Hydraulic radius [m],
Q – is peak flow [$m^3 s^{-1}$],
A – is the wetted area [m^2];
S_f – is the slope of hydraulic grade line [$m\ m^{-1}$].

The minimum velocity was checked to ensure that there is no scouring of the channel bed and no siltation as the water flows.

Results and discussion

Concerning Kakia channel, from the upstream to the downstream direction, the channel has varing height and width due to features constructed across the channel. For the Esamburmbur channel, it was observed that the channel narrowed downstream and that the banks decreased in height due to the bridge positioning. This state can obstruct the flow leading to overflowing. Therefore, the alterations in channel geometry affect the flow and may cause overflow in the narrower section of the channel. Table 3 presents the characteristics of analyzed the cross-sections.

The narrowed channel section of the active channel on the lowest 295 m of Esamburmbur channel may contribute to the overflow. The channel widths near the bridges were relatively narrow which can influence more overtopping discharge. The upstream and downstream of aligned channel with regard to the height and width were found to decrease due to features constructed across the channel. Moreover, Kiss and Blanka (2012) argued that streamflow derived from surface runoff is responsible for the determination of channel cross-section capacity. Thus, poor design of the channel especially narrowing of the channel towards the bridge is likely contributing to flooding. Therefore, the morphology of the channels and their conveyance capacity should be adjusted to prevent overflow conditions. It is evident that for better flood control, the construction of embankments should consider straightening the channel and maintaining a constant width.

From the survey data analysis, the real dimensions in terms of length, width, slope, and banks height of the channels were identified. The total lengths were found to be 1420 m and 360 m for Kakia and Esamburmbur respectively. While the elevation of the channel varies from 1827.59 m a.s.l and 1833.87 m a.s.l for the Esamburmbur channel and from 1826.42 m a.s.l to 1852.43 m a.s.l for Kakia. The slopes were found to be 0.018 [$m\ m^{-1}$] and 0.017 [$m\ m^{-1}$] for Kakia and Esamburmbur channels respectively. The calculation of geometric properties of the channel was performed with Civil 3D Hydraflow extension, based on the Manning

Table 3. Geometrical Parameters and Bridges on cross-sections of Kakia and Esamburmbur Channels

Distance from upstream to downstream [m]	Height of the banks [m]	Width [m]	Bridge type
Kakia Channel			
460	2.30	7.65	footbridge
650	3.45	7.27	footbridge
820	3.02	8.80	footbridge
1120	2.67	5.85	Bridge
1300	2.50	8.70	Bridge
Esamburmbur Channel			
120	2.55	7.10	footbridge
170	2.00	6.95	footbridge
295	2.50	4.00	Highway bridge

and continuity equations to obtain an accurate geometry of the channel, to convey designed peak discharge for all scenarios in different return periods. As the walls of the channel are formed with unfished concrete, the Manning's "*n*" coefficient for the concrete channel. It was hence selected here as equal to 0.017 (s $m^{-1/3}$). Consequently, Fig. 3 represents the water level and the variation of discharge for rectangular and trapezoidal shapes respectively.

The cross-section was taken at bridges surveyed along the channel. Channel crossings were found to require adequate and careful design. They must functionally allow for the passage of the maximum amount of water that can reasonably be expected to occur within the lifetime of the structure. For the case of Kakia and Ensamburmbur channels, many constructions across the channel were found downstream and the channel width changes from one point to the other in these locations. Also, the area is potentially an affected zone in the event of the flood occurring according to the inhabitants that were interviewed during the surveys. Regardless of the channel cross-sectional shapes (rectangular and trapezoidal), they should all conform to proper design standards with regard to alignment with the channel conveyance capacity. Therefore, the conveyance capacity was evaluated to cause no direct or indirect property damage and designed to accommodate increased runoff which could be occasioned by upstream land cover change and development. For rectangular cross-sections, the depth is the same considering a given section across an entire channel, while in a trapezoidal cross-section, the depth decreases with a bankside slope. The channel is gradually varied from cross-section to cross-section, hence the depth changes also. However, with the same bottom width, rectangular section was preferred compared to a trapezoidal section due to its necessity to increase the top width where space is critical, to efficiently allow the estimated peak flow. Hence, the designed peak discharge and corresponding channel properties, in consideration of their conveyance capacity for Kakia and Ensamburmbur channel, are presented in Table 4.

The results show a big difference between the current channel geometric properties of the two channels when compared to the required dimensions for both channels to convey the estimated peak flow in the different LULC scenarios and return periods. Thus the dimensions as per the current peak flow can be addressed either by adjusting the channel height or width to accommodate the extra flow water. For an appropriate design to convey the assumed peak discharge, the design should be based on a 50 years return period (SWMM, 2007). Also, it was noticed that for the same depth and peak flow, the shape of the rectangular sections is preferable since it presents the same dimensions at the bottom and top while for a trapezoidal section, the top width needs to be wider which could be difficult to realize. Therefore, knowing the peak flow that is more likely to happen, can give the idea of corresponding channel geometries that are adequate to carry the designed peak discharge.

The study by Jaeger et al. (2019) investigated different approaches to optimize flows in misaligned structures and concluded that aligned construction according to flow direction tailored reinforcement and redesigned stream embankment can contribute to containing overflow.

From the findings, we can suggest that the rate of urbanization assumed in Scenario 3 is not recommended

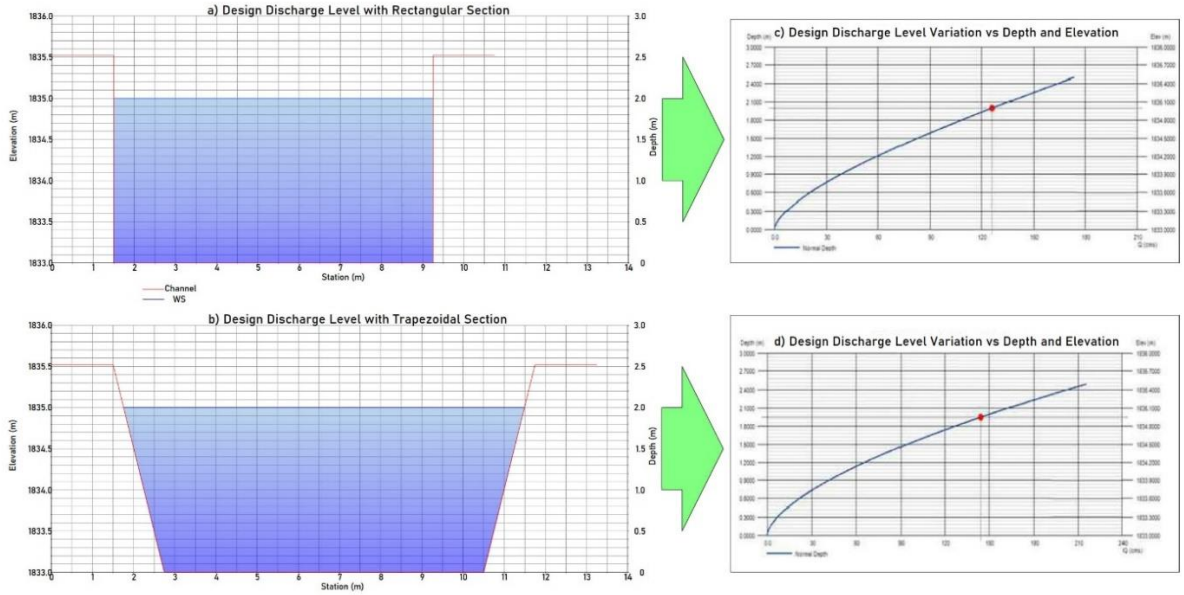

Fig. 3. a) Design Discharge Level with Rectangular Section; b) Design Level of Discharge with Trapezoidal Channel with 0.5 m; c) Maximum Depth vs Peak Discharge Variation for Trapezoidal; d) Maximum Design Depth vs Peak Discharge for Rectangular Section.

Table 4. Design discharges and hydraulic data for Kakia and Esamburmbur channel

Total Depth [m]	Flow depth [m]	Area [m^2]	Velocity [$m\ s^{-1}$]	Wetted Perimeter [m]	Width [m]		Discharge [$m^3\ s^{-1}$]	LULC Scenarios and Return Periods verified
					Bottom	Top		
Kakia channel								
2.5	2.0	17.1	8.4	12.1	7.8	9.75	**144.2**	Scenarios n.2 and 2019 with Tr50
2.5	2.0	20.0	8.5	14.0	10	10	**170.3**	Scenarios n.2 and 2019 with Tr100
2.6	2.1	21.6	8.8	14.3	10	10	**191.0**	All scenarios except n.3 with Tr100
2.8	2.3	17.1	8.4	12.1	7.5	7.5	**145.5**	Scenario n.4 with Tr50
3.0	2.4	20.3	8.8	13.2	8.5	8.5	**181.0**	Scenario n.4 with Tr100 Scenario n.3 with with Tr50
Esamburmbur channel								
2.5	2	8.0	6.5	8.0	4.0	4.0	**52.1**	Scenario n.4 with Tr10
2.8	2.3	9.4	6.8	8.7	4.0	4.0	**64.7**	Scenario 2019 with Tr25
2.7	2.2	9.9	7.0	8.9	4.5	4.5	**70.0**	Scenario n.2 with Tr50
2.8	2.2	11.3	7.3	9.5	5.0	5.0	**83.4**	Scenario n.4 with Tr50
2.8	2.3	14.0	7.8	10.6	6.0	6.0	**110.1**	Scenario n.1 with Tr50 and over design for others except scenario 3

as it can increase the flood risk. However, the application and implementation of some regulations related to LULC practices as in Scenario 2 show little increase in runoff response. From this, we conclude that an increase of green-areas as can influence positively runoff generation (Apollonio et al., 2021). These results are in line with previous studies. In fact, earlier studies highlighted that impervious area's growth due to uncontrolled LULC has a considerable effect on the increase of runoff volume (Dionizio and Costa, 2019). The land-cover trend is toward residential cover and urbanization, mostly occurring along the rural-urban fringe. This might be due to processes including immigration, natural growth and economic processes (Ohana et al., 2013).

Conclusion

In this work, the channel dynamics due to different scenarios of LULC for Kakia and Ensamburmbur sub-cathments have been investigated. Between the years 1985 and 2019 some changes in land-cover occurred in Narok town's watershed, and the same process is expected to continue occurring in future. This trend was a result of an alternation between agricultural and urbanized landscapes growth against forest, rangeland and open space; hence, the necessity to evaluate the channel's capacity in conveying the peak flow resulting from the future likely LULC transition.

The hydrological and hydraulic modelling results show that the current channel design requires improvement to accommodate the estimated peak flow. Additionally, the results from this study indicate that peak discharge is a key element to the design of channel geometry for improving the existing drainage system for the two investigated channels.

With regard to channel geometric properties under different scenarios, bridges contributed to channel narrowing down that may obstruct channel dynamics at different scenarios of peak discharge and flow volume. The channel geometric properties were designed as an improvement to convey the estimated peak flow for both the investigated channels by increasing their cross-sections.

In order to overcome some of the limitations highlighted by the present study, future research should concentrate on: 1) improving the surveys of the river network, using also UAV devices that proved to be effective in flood risk management (Annis et al., 2020); 2) using bidimensional hydraulic models to map eventual flood prone areas; 3) introducing and testing blue-green infrastructure in urban drainage to mitigate natural capital losses and contribute to other forms of capital crucial for human well-being (Cristiano et al., 2022).

Acknowledgement

This project was jointly funded by Pan African University Institute of Science, Technology & Innovation and Kenya National Research fund.

References

Alfarajat, et al. (2014): Mitigation Environmental Risk Of Floods In Jorthhwestern Parts Of Jordan. 300.

Annis, A.; Nardi, F.; Petroselli, A.; Apollonio, C.; Arcangeletti, E.; Tauro, F.; Belli, C.; Bianconi, R.; Grimaldi, S. UAV-DEMs for Small-Scale Flood Hazard Mapping. Water 2020, 12, 1717. https://doi.org/ 10.3390/ w12061717

Apollonio, C., Balacco, G., Novelli, A., Tarantino, E., Piccinni, A. F. (2016): Land use change impact on flooding areas: The case study of Cervaro Basin (Italy). Sustainability (Switzerland), 8(10). https://doi.org/ 10.3390/su8100996

Apollonio, C., Rose, M. D., Fidelibus, C., Orlanducci, L., Spasiano, D. (2018): Water management problems in a karst flood-prone endorheic basin. Environ. Earth Sci. 2018, 77, 676.

Apollonio, C., Petroselli, A., Tauro, F., Cecconi, M., Biscarini, C., Zarotti, C., Grimaldi, S. (2021): Hillslope Erosion Mitigation : An Experimental Proof of a Nature-Based Solution.

Blöschl, G., Ardoin-Bardin, S., Bonell, M., Dorninger, M., Goodrich, D., Gutknecht, D., Matamoros, D., Merz, B., Shand, P., Szolgay, J. (2007): At what scales do climate variability and land cover change impact on flooding and low flows? Hydrol. Process. 2007, 21, 1241–1247.

Chow, V. T. (1959) Open Channel Hydraulics. McGraw-Hill, New York.

Coomes, O. T., Lambin, E. F., Turner, B. L., Geist, H. J., Agbola, S. B., Angelsen, A., Folke, C., Bruce, J. W., Coomes, O. T., Dirzo, R., George, P. S., Homewood, K., Imbernon, J., Leemans, R., Li, X., Moran, E. F., Mortimore, M., Ramakrishnan, P. S., Richards, J. F., … Xu, J. (2001): The causes of land-use and land-cover change: Moving beyond the myths The causes of land-use and land-cover change: moving beyond the myths Helle Sk a. May 2014.

Cristiano, E., Annis, A., Apollonio, C., Pumo, D., Urru, S., Viola, F., Deidda, R., Pelorosso, R., Petroselli, A., Tauro, F., Grimaldi, S., Francipane, A., Alongi, F., Noto, L.V., Hoes, O., Klapwijk, F., Schmitt, B., Nardi, F.; Multilayer blue-green roofs as nature-based solutions for water and thermal insulation management. Hydrology Research 2022; nh2022201. doi: https://doi.org/10.2166/nh. 2022.201

Dionizio, E. A., Costa, M. H. (2019): Influence of land use and land cover on hydraulic and physical soil properties at the cerrado agricultural frontier. Agriculture (Switzerland), 9(1), 1–14. https://doi.org/10.3390/ agriculture9010024

Erpicum, S., Crookston, B. M., Bombardelli, F., Bung, D. B., Felder, S., Mulligan, S., Oertel, M., Palermo, M. (2021): Hydraulic structures engineering: An evolving science in a changing world. Wiley Interdisciplinary Reviews: Water, 8(2), 1–11. https://doi.org/10.1002/wat2.1505

Fenner, R., O'Donnell, E., Ahilan, S., Dawson, D., Kapetas, L., Krivtsov, V., Ncube, S., Vercruysse, K. (2019): Achieving Urban Flood Resilience in an Uncertain Future. Water 2019, 11, 1082. https://doi.org/10.3390/w11051082

Gajbhiye, S., Mishra, S. K., Pandey, A. (2014): Relationship between SCS-CN and Sediment Yield. Applied Water Science, 4(4), 363–370. https://doi.org/10.1007/s13201-013-0152-8

Guo, H., Li, X., Huang, Q., Zhang, D. (2011): Effect of lulc change on surface runoff inurbanization area Zhongchang SUN.

Habete, D., Ferreira, C. M. (2016): Impact of Forecasted Land Use Change on Design Peak Discharge at Watershed and Catchment Scales: Simple Equation to Predict Changes. Journal of Hydrologic Engineering, 21(7), 04016019. https://doi.org/10.1061/(asce)he.1943-5584.0001384

Han, J., Hayashi, Y., Cao, X., Imura, H. (2009): Evaluating Land-Use Change in Rapidly Urbanizing China: Case Study of Shanghai. Journal of Urban Planning and Development, 135(4), 166–171. https://doi.org/10.1061/ (asce)0733-9488(2009)135:4(166)

Jaeger, R., Jacobs, C., Tondera, K., Tindale, N. (2019): Improving flows in misaligned culverts. Water (Switzerland), 11(9), 1–15. https://doi.org/10.3390/ w11091932

Kiss, T., Blanka, V. (2012): River channel response to climate- and human-induced hydrological changes: Case study on the meandering Hernád River, Hungary. Geomorphology, 175–176, 115–125. https://doi.org/10.1016/j.geomorph. 2012.07.003

Marie Mireille, N., Mwangi, H. M., Mwangi, J. K., Mwangi Gathenya, J. (2019): Analysis of Land Use Change and Its Impact on the Hydrology of Kakia and Esamburmbur Sub-Watersheds of Narok County, Kenya. Hydrology, 6(4), 86. https://doi.org/10.3390/hydrology6040086

Młyński, D., Petroselli, A., Walega, A. (2018): Flood frequency analysis by an event-based rainfall-runoff model in selected catchments of southern Poland. Soil & Water Res., 13: 170–176.

Młyński, D., Wałęga, A., Ozga-Zielinski, B., Ciupak, M., Petroselli, A. (2020): New approach for determining the quantiles of maximum annual flows in ungauged catchments using the EBA4SUB model, Journal of Hydrology, Volume 589, 125198, ISSN 0022-1694, https://doi.org/10.1016/j.jhydrol.2020.125198.

Mwangi et al. (2019): Understanding urban environment problems in the newly urbanizing areas of kenya, a case of narok town. International Journal of Scientific and Technology Research, 8(6), 236–241.

Novelli, A.,Tarantino, E., Caradonna, G., Apollonio, C., Balacco, G., Piccinni, F. (2016): Improving the ANN Classification Accuracy of Landsat Data Through Spectral Indices and Linear Transformations (PCA and TCT) Aimed at LU/LC Monitoring of a River Basin. In Proceedings of the 16th International Conference on Computational Science and Its Applications, Beijing, China, 4–7 July 2016; Gervasi, O., Murgante, B., Misra, S., Rocha, A.M.A.C., Torre, C.M., Taniar, D., Apduhan, B.O., Stankova, E., Wang, S., Eds.; Springer: Beijing, China, 2016; pp. 420–432.

Ohana, N., Karnieli, A., Egozi, R., Peeters, A. (2013): Effects of land-cover change on rainfall-runoff relationships: a case study of the Yarkon-Ayalon watershed, Israel. First International Conference on Remote Sensing and Geoinformation of the Environment (RSCy2013), 8795, 87951G. https://doi.org/10.1117/12.2027190

Ohana-Levi, N., Givati, A., Alfasi, N., Peeters, A., Karnieli, A. (2018): Predicting the effects of urbanization on runoff after frequent rainfall events. Journal of Land Use Science, 13(1–2), 81–101. https://doi.org/10.1080/1747423X. 2017.1385653

Pellicani, R., Parisi, A., Iemmolo, G., Apollonio, C. (2018): Economic Risk Evaluation in Urban Flooding and Instability-Prone Areas: The Case Study of San Giovanni Rotondo (Southern Italy). Geosciences 2018, 8, 112. https://doi.org/10.3390/geosciences8040112

Pelorosso, R., Apollonio, C., Rocchini, D., Petroselli, A. (2021): Effects of Land Use-Land Cover Thematic Resolution on Environmental Evaluations. Remote Sens. 2021, 13, 1232. https://doi.org/10.3390/rs13071232

Petroselli, A., Grimaldi, S. (2018): Design hydrograph estimation in small and fully ungauged basins: a preliminary assessment of the EBA4SUB framework. Journal of Flood Risk Management, 11, S197–S210. https://doi.org/10.1111/jfr3.12193

Petroselli, A., Asgharinia, S., Sabzevari, T., Saghafian, B. (2020): Comparison of design peak flow estimation methods for ungauged basins in Iran. Hydrological Sciences Journal, 65 (1), 127–137. https://doi.org/10.1080/02626667.2019.1686506

Piscopia, R., Petroselli, A., Grimaldi, S. (2015): A software package for predicting design-flood hydrographs in small and ungauged basins. Journal of Agricultural Engineering, 46(2), 74–84. https://doi.org/10.4081/jae.2015.432

Recanatesi, F., Petroselli, A. (2020): Land Cover Change and Flood Risk in a Peri-Urban Environment of the Metropolitan Area of Rome (Italy). Water Resour Manage 34, 4399–4413 (2020). https://doi.org/10.1007/s11269-020-02567-8

Shaina Beegam, N., Prince Arulraj, G. (2018): A review article on impact of urbanization on hydrological parameters. International Journal of Civil Engineering and Technology, 9(199–208), 199–208.

Sharif, H. O., Al-Juaidi, F. H., Al-Othman, A., Al-Dousary, I., Fadda, E., Jamal-Uddeen, S., Elhassan, A. (2016): Flood hazards in an urbanizing watershed in Riyadh, Saudi Arabia. Geomatics, Natural Hazards and Risk, 7(2), 702–720. https://doi.org/10.1080/19475705.2014.945101

Storm Water Drainage System Design Manual. (2007). August.

Suriya, S., Mudgal, B. V. (2012): Impact of urbanization on flooding: The Thirusoolam sub watershed – A case study. Journal of Hydrology, 412–413, 210–219. https://doi.org/10.1016/j.jhydrol.2011.05.008

Umukiza, E., Raude, J. M., Wandera, S. M., Petroselli, A., Gathenya, J. M. (2021): Impacts of Land Use and Land Cover Changes on Peak Discharge and Flow Volume in Kakia and Esamburmbur Sub-Catchments of Narok Town, Kenya. Hydrology, 8(2), 82. https://doi.org/10.3390/hydrology8020082

Zope, P. E., Eldho, T. I., Jothiprakash, V. (2016): Impacts of land use-land cover change and urbanization on flooding: A case study of Oshiwara River Basin in Mumbai, India. Catena, 145, 142–154. https://doi.org/10.1016/j.catena.2016.06.009

Etienne Umukiza, MSc
Pan African University
Institute of Science, Technology and Innovation, Civil Engineering and Environmental,
Jomo Kenyatta University of Agriculture and Technology
P. O. Box 62000 – 00200 Nairobi
Kenya

James M. Raude Associate Professor, PhD
Soil, water, and Environmental Engineering Department,
Jomo Kenyatta University of Agriculture and Technology
P. O. Box 62000 – 00200 Nairobi
Kenya

John M. Gathenya Full Professor, PhD
Soil, water, and Environmental Engineering Department,
Jomo Kenyatta University of Agriculture and Technology
P. O. Box 62000 – 00200 Nairobi
Kenya

Andrea Petroselli Associate Professor, PhD
Department of Economics, Engineering, Society and Business
Tuscia University
01100 Viterbo
Italy

Simon M. Wandera, PhD
Department of Civil, Construction and Environmental Engineering
Jomo Kenyatta University of Agriculture and Technology
00200 Nairobi
Kenya

Ciro Apollonio Associate Professor, PhD (*corresponding author, e-mail: ciro.apollonio@unitus.it)
Department of Agriculture and Forest Sciences
Tuscia University
01100 Viterbo
Italy

DOI: 10.31577/ahs-2022-0023.02.0019

ACTA HYDROLOGICA SLOVACA

Volume 23, No. 2, 2022, 172–179

Model of urban groundwater level management in drainage systems

Aybek ARIFJANOV*, Luqmon N. SAMIEV, Zokhidjon ABDULKHAEV, Dilbar ABDURAIMOVA, Shodiyor YUSUPOV, Tatiana KALETOVÁ

Currently, it is proposed to design horizontal drains for the city of Fergana to reduce the negative impact of the rise in the level of groundwater on the environment, agricultural crops, buildings, and structures, as well as on underground communications. Groundwater depth measurements were carried out in observation wells in the city area and the results were analysed. The depth of groundwater level drop within the horizontal drainage effect is physically and mathematically modelled. For this, long-term data from observation wells were analysed and the hydraulic parameters of horizontal drainage were selected considering the hydrogeology of the area. Taking into account the terrain and characteristics of the soil layers, the possibility of diverting the collected water outside the city through the "Margilan Say" waterwork passing through the city centre has been developed. The differential equation of groundwater movement is solved by numerical calculation and the results are analysed graphically. According to the analysis of the results of numerical calculation, it is proved that it is possible to control the groundwater level with horizontal drainage. The adequacy of the results was assessed by comparing data collected in natural field conditions.

KEY WORDS: horizontal drainage, groundwater, depth of groundwater, coefficient of hydraulic conductivity, mathematical model.

Introduction

The rapid development of construction is exacerbating the engineering geological and environmental problems of groundwater. In many cases, for example, when excavating a foundation pit, soil deformation or cracking of the deep bottom, subsidence in underground construction by dewatering, piping or sand liquefaction, the problem of stability in the rock layer, concrete, iron and steel corrosion of manufactured fittings has always been one of the problems to be solved. Researchers and engineers are paying close attention to engineering geological and hydrogeological problems or construction disasters. There has been new information about groundwater engineering over the last decade (Tang et al., 2017).

Determining the impact of groundwater on the surrounding area is a major problem in groundwater hydrogeology (Mulligan and Ahlfeld, 2016). Urban groundwater collection and assessment are of great importance for irrigated agriculture and urban water supply, and this topic has been modelled by many researchers (e.g. Arnold et al., 1993; Sophocleous et al., 1999; Bredehoeft, 2011; Rossman and Zlotnik, 2013; Maxwell et al., 2014). The development and application of groundwater models is the basis for the application of modern and efficient methods of groundwater management. The study of groundwater flow systems has used mainly sandbox models, analogue models, and mathematical models (Istok, 1989; Arifjanov et al., 2021). Models often allow the physical and geological state of spatially variable aquifers to be determined, which is difficult to calculate and study. However, because this calculation is complex and time-consuming, such calculations are performed based on modern software. Over the years, many researchers have used a physical model of groundwater and a variety of mathematical methods to reduce computational time. Typically, the reduction in model time depends on the accuracy of the model (Gosses et al., 2018; Abdulkhaev et al., 2021). The mathematical model based on the groundwater process consists of an equation describing physical processes in the area, initial and boundary conditions of the flow.

Mathematical models can be solved analytically or numerically and are solved for steady and unsteady groundwater flow conditions (Anderson et al., 2015). Analytical models require a high degree of simplification of the problem that can be solved mathematically. Simple analytical solutions can be solved using a calculator, but more complex solutions are often obtained using a spreadsheet, computer program or special software (Barlow and Moench, 1998). Assumptions based on analytical solutions are justified for relatively simple

systems and therefore do not apply to many practical groundwater issues. Nevertheless, analytical solutions are still useful for some problems and provide important insights into the behaviour of groundwater systems. Analytical models can be useful tools for building more complex digital models, i.e., they are used to verify that the codes that solve the digital models are programmed correctly (Haitjema, 2006). The analytical element method provides analytical solutions to complex problems. The analytical element method is based on Green's functions and relies on computer code to locate certain types of analytical solutions called analytical elements (Strack, 1989; Haitjema, 1995). Currently, analytical element models are most commonly used in the two-dimensional and time-constant state of the groundwater flow problem (Haitjema 2006; Hunt 2006). Analytical element models are also useful for three-dimensional and time-variable modelling. Usually, numerical models based on the finite element or finite element method allow to calculate the movement of groundwater in three-dimensional porous media with complex initial and boundary conditions, stable and unstable flow (Anderson et al., 2015).

The rise of the underground water level in the centre of Fergana city, Beshbola, Yormazor and Joydam regions is causing many problems in residential areas. To solve this problem, deep ditches are being dug, and water is being collected, which causes various problems and inconveniences in the city. Therefore, it is relevant to design horizontal drainage for urban groundwater management and to develop a mathematical model of groundwater level change within the drainage effect.

Materials and methods

The rising groundwater level in the Fergana region (Fig. 1) in recent years has caused many problems. The groundwater level was measured, and the results were analysed from observation wells in the area. For areas above groundwater, the hydraulic parameters of the horizontal drainage were selected using the hydrogeology of the area. The selected hydraulic parameters and measurement results were taken as the initial data for the mathematical model, and the groundwater level in the urban area was calculated based on this model.

Central Fergana region is divided into 5 regions according to water permeability: (i) rapid seepage area (mountainous areas, where underground water is deep); (ii) the area located above the Big Fergana canal (including areas with poor drainage); (iii) the area with poor drainage (the area between the Katta Fargona kanali and the Janubiy Fargona kanali); (iv) central region (the region located below the Katta Fargona kanali); (v) non-flow area (flat area along the Syrdarya river bed).

Hydrogeological studies in the city of Ferghana show that the main factor of the rise of groundwater is mountain rivers (Shoxmardon soy, Isfayram soy), reservoirs (Karkidon reservoir), canals (Janubiy Fargona kanali) and water causes the water of the structures to soak into the ground and accumulate on the waterproof layer. According to engineering research, the area receives the most annual rainfall in the fall, winter, and spring months, as it receives more rain during this period and less during the summer months. The average annual

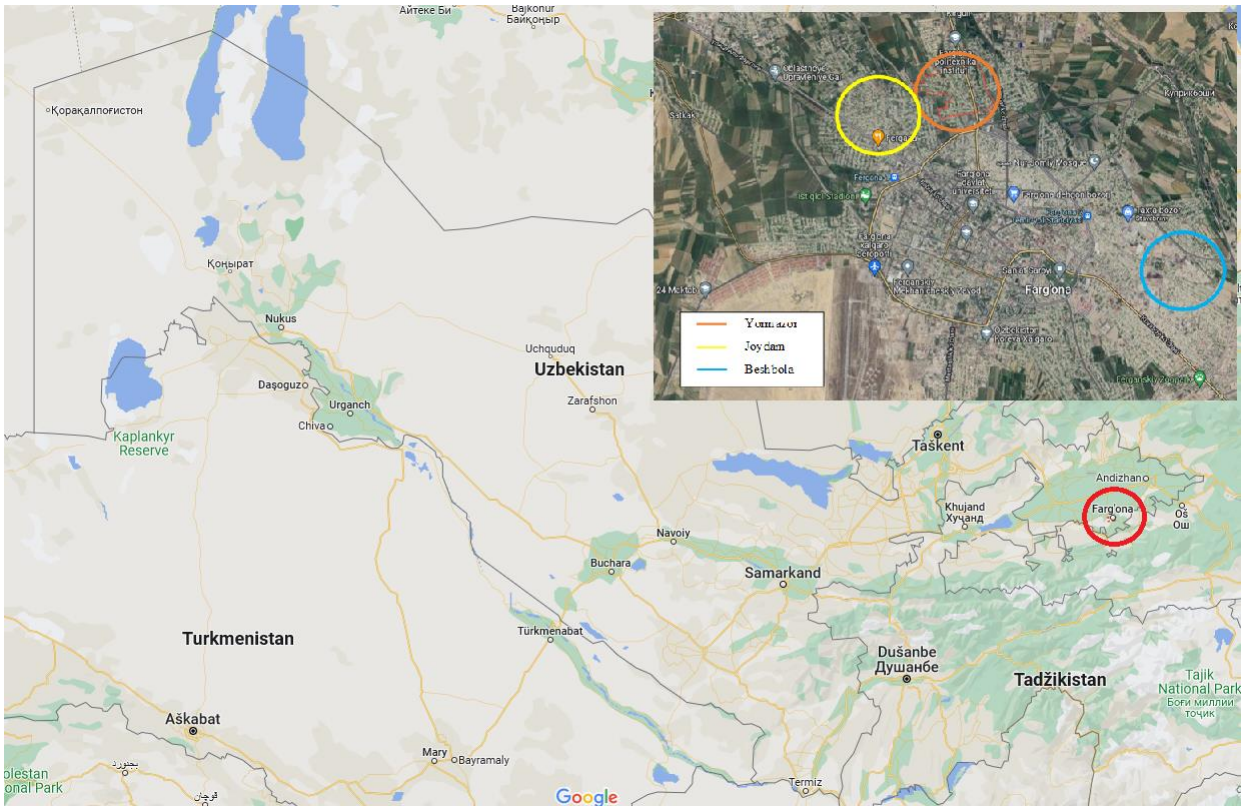

Fig. 1. The location of Fergana region within Uzbekistan and districts of Fergana city.

rainfall is 181.1 mm, and the daily rainfall is 0.496 mm. From July to September, the weather is dry, with less rainfall. The coefficient of hydraulic conductivity of the area is K=0.000436 m s^{-1}, and in most places, the depth of impermeable layer is 40 m.

Currently, rising groundwater levels in the area have a negative impact on buildings and structures, the environment, crop fields and underground communications. There are open horizontal canals and ditches in the city area, which are rapidly filling up and have a negative impact on the environment. Such structures occupy a large area when considered in general (Akmalov and Gerts, 2016). The best solution to these and similar problems is to collect groundwater through closed horizontal drains and supply it to irrigated areas outside the city. Studies of the hydrogeological condition of the area have proven that the topography is suitable for the discharge of the collected water out of the city through the "Margilan Say" waterworks passing through the city centre (Arifjanov et al., 2019; Arifjanov et al., 2021; Erkinjonovich et al., 2021).

The depth of groundwater table below the surface was measured from observation wells located in the studied area for 6 years (Fig. 2 and 3). According to the measured

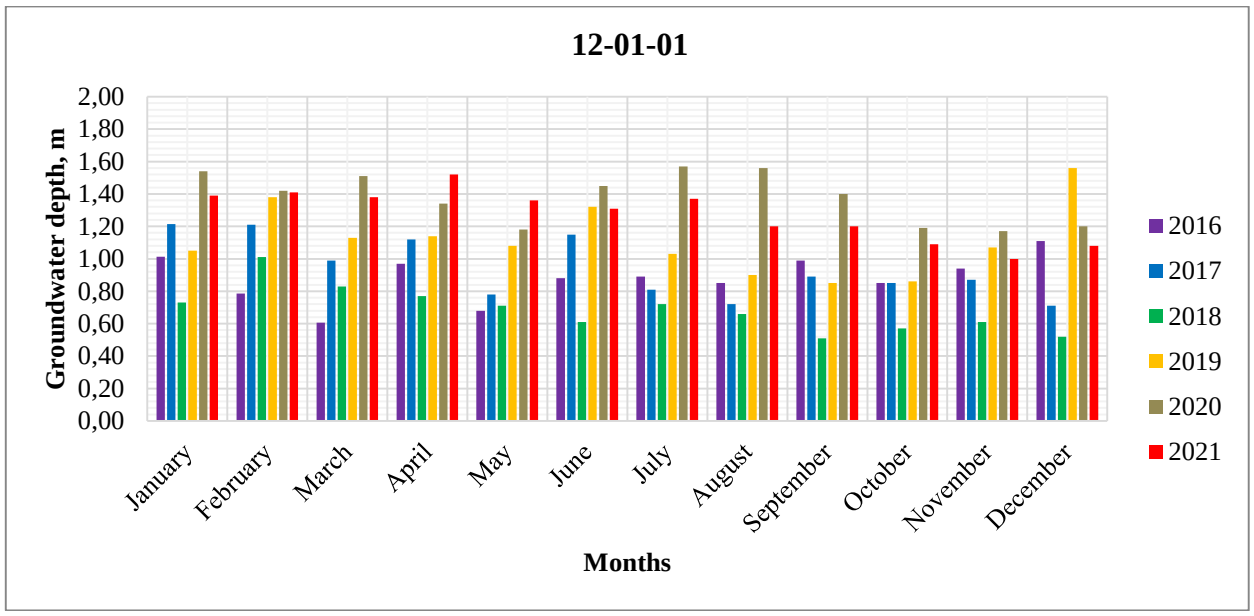

Fig. 2. The depth of groundwater table below the surface in the observation well No. 12-01-01 in the Yormazor area.

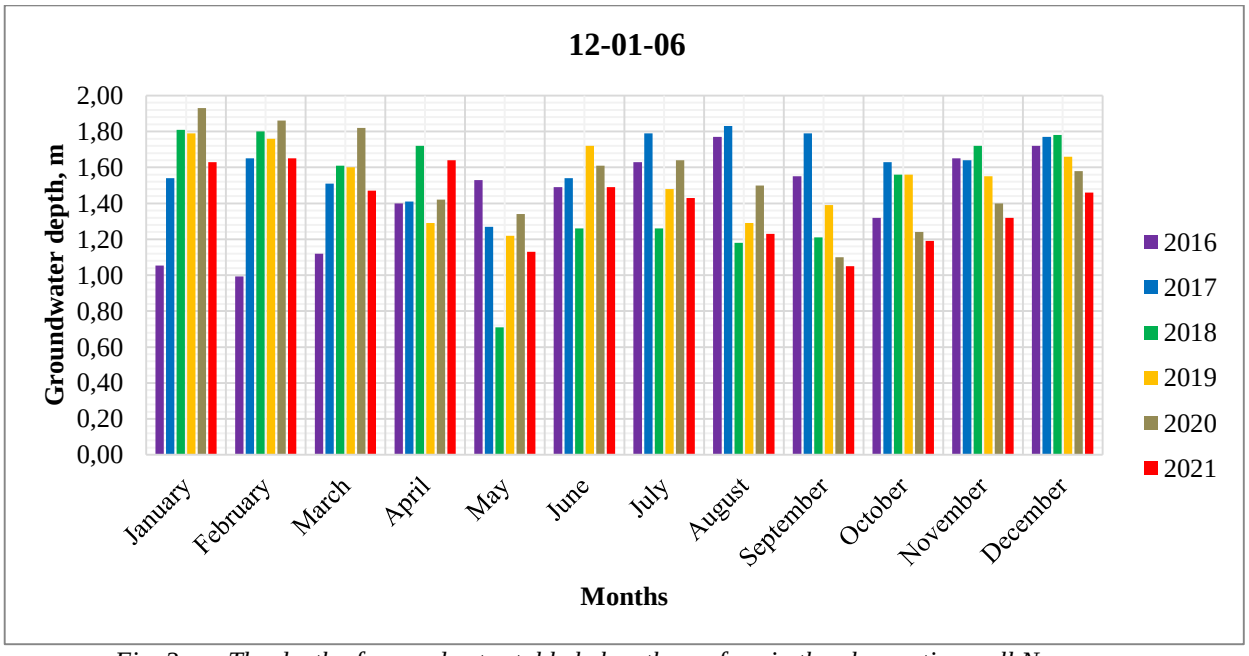

Fig. 3. The depth of groundwater table below the surface in the observation well No. 12-01-06 in the Yormazor area.

data, the depth of groundwater table below the surface in the observation well No. 12.01.01 varies from 0.4 to 1.5 m, and in observation well No. 12.01.06 varies from 0.7 to 1.9 m.

The specific filtration rate for imperfect horizontal drainage (Fig. 4) is:

$$q = \frac{K(H^2 - H_D^2)}{2 \cdot (L + \Delta f_{(H_D)})} \quad (1)$$

where

H – the height of the groundwater table above the impermeable layer [m],

H_D – the height from the impermeable layer to the drainage centre [m],

K – coefficient of hydraulic conductivity [m s^{-1}],

L – the length of the affected area of horizontal drainage [m],

Δf_{HD} – additional filtration resistance.

Since the soil of the study area consists of 2 different layers, the coefficient of hydraulic conductivity is found as follows:

$$K = \frac{K_1 h_1 + K_2 h_2}{h_1 + h_2} \quad (2)$$

The additional filtration resistance is found as follows (Averyanov, 2015):

$$\Delta f_{H_D} = 0.73 \cdot H_D \cdot \frac{2 \cdot H_D}{\pi H_D \cdot d} \quad (3)$$

where

d – drainage diameter [m].

The ordinate Z from the impermeable layer to the depression line at a distance x from the centre of the drain is found as follows:

$$Z = \sqrt{(H_D^2 + (H^2 - H_D^2) \cdot \frac{x}{L}} \quad (4)$$

The time taken for groundwater to recede in the area affected by drainage is as follows (Averyanov, 2015):

$$t = \sqrt{\frac{L^2}{3 \cdot \frac{K}{S_s} \cdot h_a}} \quad (5)$$

where

S_s – soil water removal coefficient [m^{-1}],

h_a – the average capacity of the area where groundwater levels are declining [m].

The following formula is used to determine the average capacity of an area where groundwater levels are declining:

$$h_a = \frac{S}{2} \quad (6)$$

where

S – the height from the centre of the drain to the groundwater table [m].

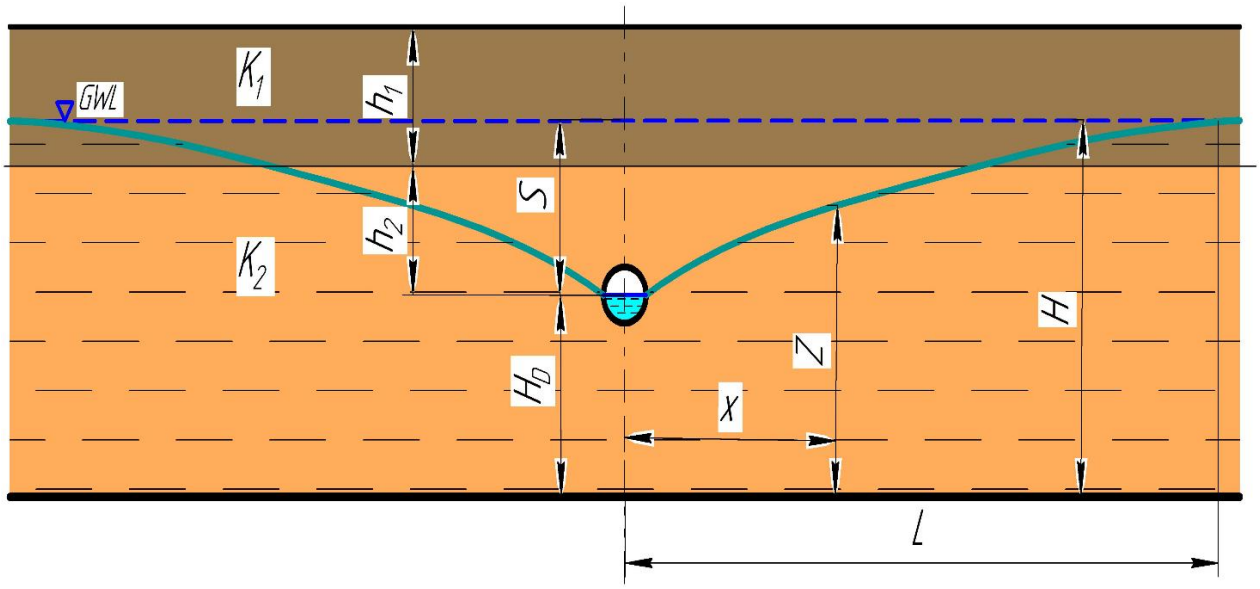

Fig. 4. Scheme of hydrodynamically imperfect horizontal drainage; GWL – groundwater level, x – length from the centre of the drainage, h_1 – thickness of the first layer, h_2 – distance between the top of the second layer and drainage centre, S – distance between GWL and drainage centre, HD – distance from impermeable layer to drainage, H – thickness of the aquifer, K_1 and K_2 – coefficient of hydraulic conductivity of the first and second layer, respectively, L – the length of the affected area of horizontal drainage, Z – the difference between impermeable layer and depression line at a distance x.

Using the above formulas, the water consumption received by the horizontal drainage of length L was calculated.

Mathematical model

The relationship and mass conservation law expressed in Darcy's law represent the process of groundwater flow. The Laplace equation is used to express the flow of groundwater by the method of finite separations. The two-dimensional Laplace equation appears as follows:

$$\frac{\partial^2 h}{\partial x^2} + \frac{\partial^2 h}{\partial y^2} + \frac{Q}{T \cdot \Delta\omega} = 0 \qquad (7)$$

where

T – transmissivity coefficient, which depends on the coefficient of hydraulic conductivity and the thickness of the layer, $T = K_h \cdot b$, [m^2 s^{-1}].

K_h – the coefficient of hydraulic conductivity in the horizontal direction, [m s^{-1}],

b – the thickness of the layer, [m],

$\Delta\omega$ –elementary surface, [m^2],

Q – water consumption, [m^3 s^{-1}].

The general water balance equation was expressed by S. F. Averyanov as follows:

$$Q = Q_{com} + Q_{e.g} + Q_{at} - Q_{dr} - (Q_{eva} + Q_{pla}) - Q_{exit} \qquad (8)$$

where

Q_{com} – the amount of water coming into the area, [m^3 s^{-1}],

$Q_{e.g}$ – amount of surface water, [m^3 s^{-1}],

Q_{at} – waters formed from atmospheric precipitation, [m^3 s^{-1}],

Q_{dr} – the amount of water collected from the area through drains, [m^3 s^{-1}],

Q_{eva} – the amount of evaporation from the soil surface, [m^3 s^{-1}],

Q_{pla} – the absorption of water from the ground by plants, [m^3 s^{-1}],

Q_{exit} – the amount of groundwater that has flowed out of the area, [m^3 s^{-1}].

After determining the boundaries of the study area, the selected area is divided into segments. Each node in the segment has 4 adjacent points, and the secondary product on the *x*- and *y*-axes can be written as (Fig. 5 and 6) (Istok, 1989):

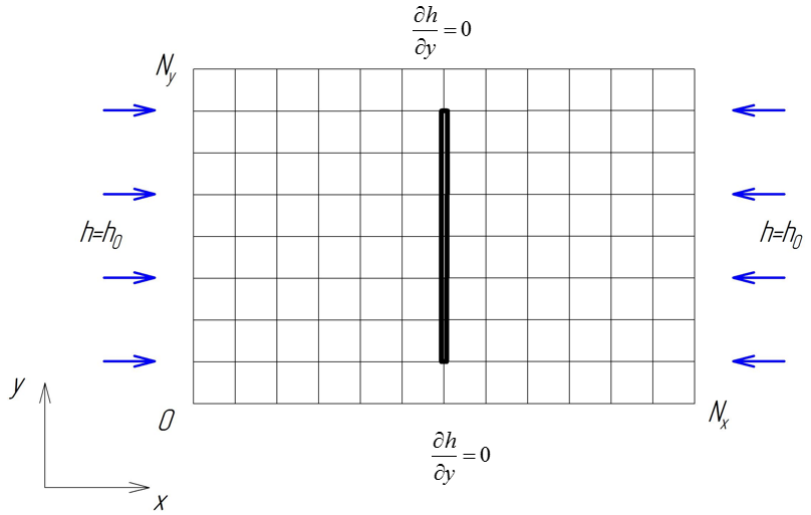

Fig. 5. Dividing the area of interest into a net.

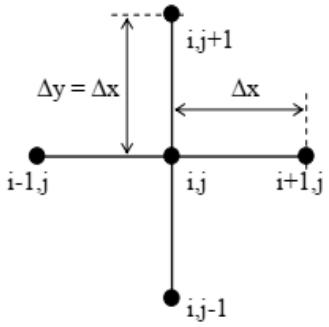

Fig. 6. Internal nodes of the finite element mesh.

$$\frac{\partial^2 h}{\partial x^2} = \frac{h_{i-1,j} - 2h_{i,j} + h_{i+1,j}}{(\Delta x)^2} \quad (9)$$

$$\frac{\partial^2 h}{\partial y^2} = \frac{h_{i,j-1} - 2h_{i,j} + h_{i,j+1}}{(\Delta y)^2} \quad (10)$$

By substituting Equations (9) and (10) to Equation (7), we obtain a limited difference equation:

$$\frac{h_{i-1,j} - 2h_{i,j} + h_{i+1,j}}{(\Delta x)^2} + \frac{h_{i,j-1} - 2h_{i,j} + h_{i,j+1}}{(\Delta y)^2} \pm \frac{Q_{i,j}}{T(\Delta x)^2} = 0 \quad (11)$$

$$h_{i-1,j} + h_{i,j-1} - 4h_{i,j} + h_{i+1,j} + h_{i,j+1} \pm \frac{Q_{i,j}}{T(\Delta x)^2} = 0 \quad (12)$$

We find $h_{i,j}$ from Equation (12) as follows:

$$h_{i,j} = \frac{h_{i-1,j} + h_{i,j-1} + h_{i+1,j} + h_{i,j+1}}{4} \pm \frac{Q_{i,j}}{4T(\Delta x)^2} \quad (13)$$

If the calculation is repeated many times, the number of iterations is expressed in terms of m:

$$h_{i,j}^{m+1} = \frac{h_{i-1,j}^{m} + h_{i,j-1}^{m} + h_{i+1,j}^{m} + h_{i,j+1}^{m}}{4} \pm \frac{Q_{i,j}}{4T(\Delta x)^2} \quad (14)$$

The above equation is valid for the internal nodes of the bounded region. If we assume that $h_{i,j-1} = h_{i,j+1}$ for the boundary on the x -axis, we make the following changes to Equations (13) and (14) for the boundary nodes on the x -axis:

$$h_{i,j} = \frac{h_{i-1,j} + h_{i+1,j} + 2h_{i,j+1}}{4} \pm \frac{Q_{i,j}}{4T(\Delta x)^2} \quad (15)$$

or

$$h_{i,j}^{m+1} = \frac{h_{i-1,j}^{m} + h_{i+1,j}^{m} + 2h_{i,j+1}^{m}}{4} \pm \frac{Q_{i,j}}{4T(\Delta x)^2} \quad (16)$$

For all boundary nodes, changes are made as in Equations 15 and 16. The following initial and boundary conditions are used to solve the problem numerically:

$$h(0;y) = h_0, \qquad h(x;0) = \frac{\partial h}{\partial y} = 0, \qquad h(x;N_y) = \frac{\partial h}{\partial y} = 0,$$

$$h(N_x;y) = h_0, \qquad {}_{(x,0)}\left|\frac{\partial h}{\partial y} = h_{i,0} = h_{i,1}\right., \qquad {}_{(x,N_y)}\left|\frac{\partial h}{\partial y} = h_{i,Ny} = h_{i,Ny-1}\right.,$$

where

h_0 – initial depth of groundwater, [m],

N_x, N_y – the number of nodes on the x and y axis, respectively.

In the calculation, the groundwater level in all parts of the region was assumed to be 2 m, and the infiltration coefficient was 0.496 m d^{-1}. Based on the above conditions, the differential equation (16) is solved numerically.

Results and discussion

Groundwater levels have risen in the Beshbola, Joydam and Yormazor districts of Fergana (Fig. 1). The use of horizontal drains to reduce groundwater is one of the most effective methods. Based on the above initial and boundary conditions, a mathematical model of the groundwater table under the influence of drainage was developed. The results of the numerical calculation are presented in the form of a graph in Fig. 7. The colours in the graph show the change in the groundwater level within the drainage area.

In fact, it can be seen that the groundwater level has risen significantly during the months of heavy rainfall. The depth of groundwater table below the surface fluctuated from 0.4 to 1.5 m in observation well

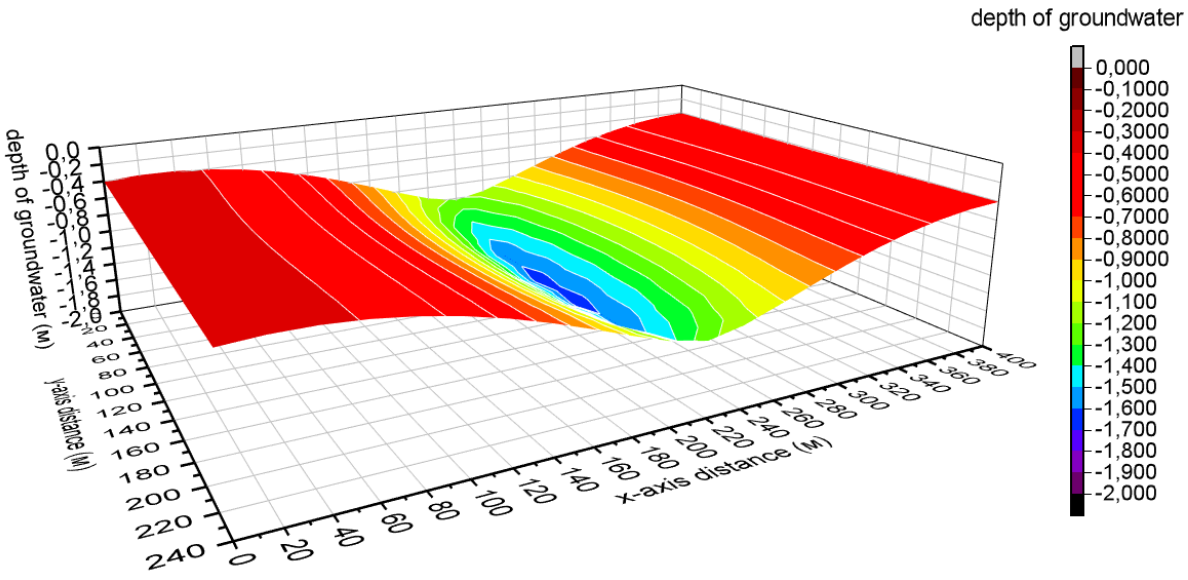

Fig. 7. Changes in the depth of groundwater in the area of drainage influence.

No. 12.01.01, and from 0.7 to 1.9 m in observation well No. 12.01.06 (Fig. 2 and 3).
In the initial case, the level of underground water is 0.4 m, and this value was obtained based on the results of measurements in observation wells. The area of the modelled area is 400x300 m, and the change of groundwater at every 10 cm depth is highlighted in different colours.
Based on the Fig. 7, it is possible to construct a depression curve and predict the depth of the groundwater level at a distance x from the drain.

Conclusion

In recent years, the rise in the level of underground water in residential areas and urban areas has caused many problems. In the central parts of the city of Fergana, in the regions of Yormazor, Beshbola and Joydam, the level of groundwater table below the surface is 1–1.5 meters. To solve this problem, deep pits are dug and water is collected. The ditches built in different parts of the city are causing various problems and inconveniences. It is planned to manage urban groundwater table through horizontal drainage, improve the environmental condition of the city, and reduce the negative impact of underground water on buildings and engineering communications in the city. Collected water is supplied to agricultural fields outside the city through the Margilan stream.
The use of horizontal drains is one of the most effective ways to reduce groundwater. The hydrogeology of the area, field research experiments, initial and boundary conditions, mainly the change of the groundwater level within the framework of the drainage effect, are physically and mathematically modelled. Numerical results of physical and mathematical calculations are presented in graphic form for the convenience of scientists. Each change in groundwater level is highlighted in the graph with colours and lines. According to the results of the analysis, it has been proven that it is possible to control the level of groundwater through horizontal drains in the places where the groundwater has risen.

Acknowledgements

The authors acknowledge "TIIAME" NRU, Slovak University of Agriculture in Nitra, Scientific Grant Agency project VEGA 1/0747/20 and the project "Sustainable smart farming systems taking into account the future challenges 313011W112", co-financed by the European Regional Development Fund within the operational program Integrated infrastructure for their material and financial support.

References

Abdulkhaev, Z. E., Madraximov, M. M., Axmadjon O'g'li, M. S. (2021): Reducing the Level of Groundwater. In The City of Fergana. International Journal of Advanced Research in Science, Communication and Technology 2(2): 67–72.

Akmalov, Sh. B., Gerts, J. V. (2016): Using Remote Sensing Very High Resolution Data in Observation of Open Drainage System Conditions in Syrdarya Province. Irrigatsiya va Melioratsiya (2): 26–29.

Anderson, M. P., Woessner, W. W., Hunt, R. J. (2015): Applied Groundwater Modeling: Simulation of Flow and Advective Transport. Academic press.

Arifjanov, A., Samiev, L., Yusupov, S., Khusanova, D., Abdulkhaev, Z., Tadjiboyev, S. (2021): Groundwater Level Analyse in Urgench City with Using Modflow Modeling and Forecasting System. In E3S Web of Conferences, EDP Sciences, 3010.

Arifjanov, A., Otaxonov, M., Abdulkhaev, Z. (2021): Model of Groundwater Level Control Using Horizontal Drainage. Irrigation and Melioration 2021(4): 21–26.

Arifjanov, A., Otaxonov, M., Samiev, L., Akmalov, S. (2019): Hydraulic Calculation of Horizontal Open Drainages. In E3S Web of Conferences, EDP Sciences, 5039.

Arnold, J. G., Allen, P. M., Bernhardt, G. (1993): A Comprehensive Surface-Groundwater Flow Model. Journal of hydrology 142(1–4): 47–69.

Averyanov, S. F. (2015): Management of the water regime of reclaimed agricultural lands / Monograph / – Moscow: Russian State Agrarian University – Moscow Agricultural Academy named after K. A. Timiryazev. 542 p.

Barlow, P. M., Moench, A. M. (1998): 98 Analytical Solutions and Computer Programs for Hydraulic Interaction of Stream-Aquifer Systems. US Department of the Interior, US Geological Survey.

Bredehoeft, J. (2011): Hydrologic Trade-offs in Conjunctive Use Management. Groundwater 49(4): 468–75.

Erkinjonovich, A. Z., Mamadaliyevich, M. M., O'G'Li, S. M. A., Egamberdiyevich, T. N. (2021): Farg'ona Shahar Yer Osti Sizot Suvlarining Ko'tarilish Muammosi Va Yechimlari. Oriental renaissance: Innovative, educational, natural and social sciences, 1(3), 138–144.

Gosses, M., Nowak, W., Wöhling, T. (2018): Explicit Treatment for Dirichlet, Neumann and Cauchy Boundary Conditions in POD-Based Reduction of Groundwater Models. Advances in water resources 115: 160–71.

Haitjema, H. (2006): The Role of Hand Calculations in Ground Water Flow Modeling. Groundwater 44(6): 786–91.

Haitjema, H. M. (1995): Analytic Element Modeling of Groundwater Flow. Bloomington: Academic Press.

Hunt, R. J. (2006): Ground Water Modeling Applications Using the Analytic Element Method. Groundwater 44(1): 5–15.

Istok, J. (1989): Groundwater Modeling by the Finite Element Method. Washington, DC (USA) American Geophysical Union.

Maxwell, R. M., Putti, M., Meyerhoff, S., Delfs, J-O., Ferguson, I. M., Ivanov, V., Kim, J., Kolbitz, O., Kollet, S. J., Kumar, M., Lopez, S., Niu, J., Paniconi, C., Park. Y-J., Phanikumar, M. S., Shen, C., Sudicky, E. A., Sulis, M. (2014): Surface-subsurface Model Intercomparison: A First Set of Benchmark Results to Diagnose Integrated Hydrology and Feedbacks. Water resources research 50(2): 1531–1549. https://doi.org/10.1002/2013 WR013725

Mulligan, K. B., Ahlfeld, D. P. (2016): Model Reduction for Combined Surface Water/Groundwater Management Formulations. Environmental Modelling & Software 81: 102–10.

Rossman, N. R., Zlotnik, V. A. (2013): Regional Groundwater Flow Modeling in Heavily Irrigated Basins of Selected States in the Western United States. Hydrogeology Journal 21(6): 1173–1192.

Sophocleous, M. A., Koelliker, J. K., Govindaraju, R. S., Birdie, T., Ramireddygari, S. R., Perkins, S. P. (1999): Integrated Numerical Modeling for Basin-Wide Water Management: The Case of the Rattlesnake Creek Basin in South-Central Kansas. Journal of Hydrology 214(1–4): 179–196. https://doi.org/10.1016/S0022-1694(98)00289-3

Strack, O. D. L. (1989): Groundwater Mechanics. Prentice Hall.

Tang, Y., Zhou, J., Yang, P., Yan, J., Zhou, N. (2017): Groundwater Engineering. 2nd ed. Shanghai: Springer. 423 p.

Prof. Aybek Arifjanov (*corresponding author, e-mail: obi-life@mail.ru)
Dr. Luqmon N. Samiev
Shodiyor Yusupov
Dilbar Abduraimova
Ing. Tatiana Kaletová, PhD.
Department of Hydraulics and Hydroinformatics
Tashkent Institute of Irrigation and Agricultural Mechanization Engineers
39 Kari Niyazov
Tashkent 100000
Uzbekistan

Ing. Tatiana Kaletová, PhD.
Faculty of Horticulture and Landscape Engineering
Slovak University of Agriculture in Nitra
Tulipánová 7
94976 Nitra
Slovak Republic

Abdulkhaev Zokhidjon, PhD student
Department of Construction of Engineering Communications
Fergana Polytechnic Institute
86 Fergana
Fergana 150107
Uzbekistan

DOI: 10.31577/ahs-2022-0023.02.0020

ACTA HYDROLOGICA SLOVACA

Volume 23, No. 2, 2022, 180–189

Hydraulic conductivity of saturated bed silts in Chotárny channel, ŽO area, Slovakia

Renáta DULOVIČOVÁ*, Radoslav SCHŰGERL, Yvetta VELÍSKOVÁ

This paper deals with the comparison of two different ways used for determination of saturated hydraulic conductivity values of bed silts located along the Chotárny channel, obtained from field measurements in 2018. The Chotárny channel is one of three selected monitored channels at the ŽO area – the flat lowland with channel network. The permeability of bed silts impacts water flow between surface water in the channel and surrounding groundwater in the scope of their interaction at this area. It is expressed by its value of saturated hydraulic conductivity. The bed silts along Chotárny channel were extracted and obtained by two ways, as disturbed samples and as undisturbed samples. The selection of sampling place was made by thickness of bed silt in the measured profiles. The samples were extracted in three different vertical parts of bed silt – from top, middle and bottom part of bed silt layer. In case of the disturbed samples the empirical formulas based on the grain size analysis were used for determination of saturated hydraulic conductivity value. In case of undisturbed samples was used the falling head method for determination of saturated hydraulic conductivity value. The values of saturated hydraulic conductivity obtained from disturbed samples of bed silts K_d were calculated by using of several empirical formulas: 1. Bayer – Schweiger; 2. Špaček I.; 3. Špaček II.; 4. Hazen I.; 5. Bayer; 6. USBR and 7. Orechova. The results in Table 1 show that the valid values K_d for Chotárny channel in 2018 were from 1.00×10^{-10} to 1.19×10^{-04} m s^{-1}. The recommended formula for calculation of K_d of bed silts by empirical formulas in Chotárny channel, based on criterium of the largest number of valid obtained results, is Hazen I. formula. The values of saturated hydraulic conductivity obtained from undisturbed samples of bed silts K_u were determined according the relation for calculation of average value of saturated hydraulic conductivity (by falling head method in laboratory). These values are illustrated in Table 2. The values K_u for Chotárny channel in 2018 reached values from 7.68×10^{-08} – 4.53×10^{-05} m s^{-1}. All the results from both methods of determination of saturated hydraulic conductivity were compared.

KEY WORDS: bed silts, permeability of bed silts, saturated hydraulic conductivity, disturbed and undisturbed samples, grain size analysis, falling head method

Introduction

Žitný Ostrov (ŽO), Rye Island – Fig. 1a on the left – was created by sediments transport from upper part of the Danube River. This area formed as a flat plain with only small differences in altitude. Its average slope is about 0.25 ‰ and it was one of the reasons for building channel network here. The channel network at ŽO area was built already in the late 19th century with primary aim to drain the wet places of this area. Thereafter its utilization began also to surface irrigation during dry periods and also to groundwater resources regulation in some ŽO localities. The silting up of channel bottom by bed sediments has impact to bottom permeability of channels in time and by this way to interact with surrounding groundwater. This permeability is expressed by the value of saturated hydraulic conductivity of bed silts. Engineering practice often requires the investigation of ground water movement, volumes in storage and computation of the amount of infiltrated water into or from the aquifer. Hydraulic engineers, hydrologists and hydrogeologists have been studying this topic with a variety of conclusions. In the current literature research papers usually focus on a wide variety of saturated hydraulic conductivity related topics. Habtamu et al. (2019) evaluate saturated hydraulic conductivity with different land uses of disturbed and undisturbed soil, Duong et al. (2019) clarify the effects of soil hydraulic conductivity and rainfall intensity on riverbank stability, Říha et al. (2018) present the verification of validity of various published porosity functions and empirical formulae with the use of the experimental data, Wang et al. (2018) present an alternative model to predict soil hydraulic conductivities, Hwang et al. (2017) compare saturated hydraulic conductivities of sandy soils to characterize properties of water retention, Gadi et al. (2017) studied spatial and temporal variation of hydraulic conductivity and vegetation growth in green infrastructures, Hussain and Nabi (2016) used seven empirical formulas to calculate hydraulic conductivity, based on grain size distribution of unconsolidated aquifer materials, Kutílek (1978) or Kasenow (2010)

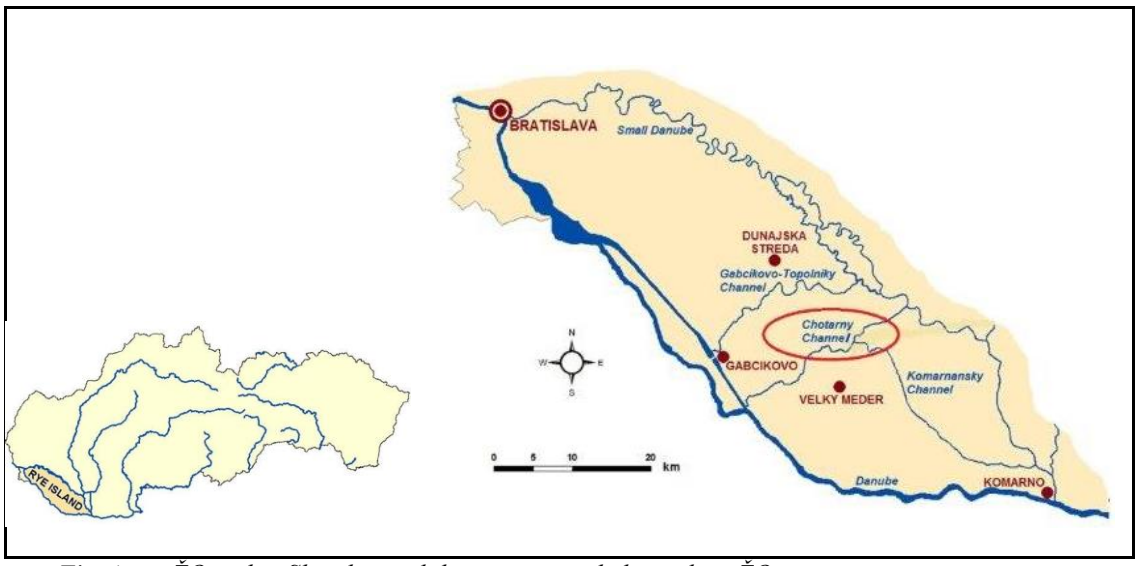

Fig. 1a. ŽO within Slovakia and three monitored channels at ŽO area.

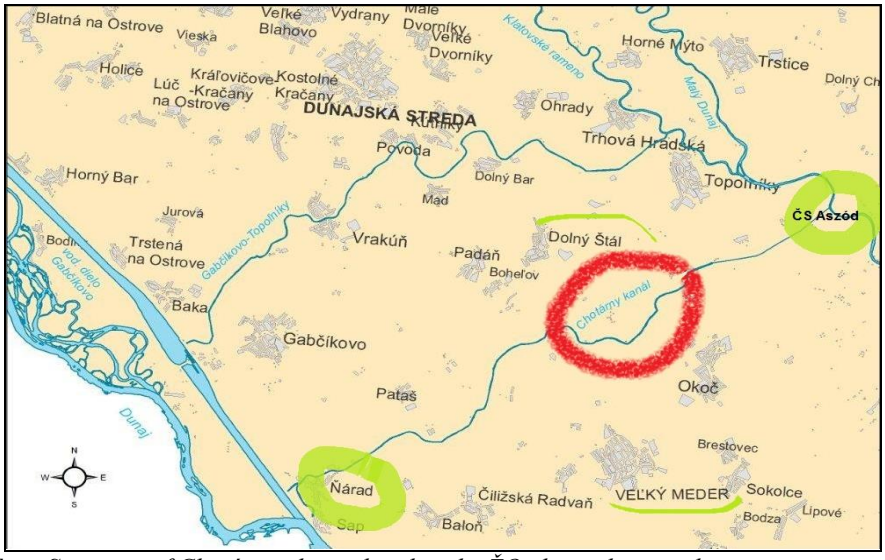

Fig. 1b. Situation of Chotárny channel within the ŽO channel network.

calculated the value of saturated hydraulic conductivity by empirical formulas coming out from grain size analysis, Šurda et al. (2013); Dulovičová et al. (2018) used simplified equipment for measuring of saturated hydraulic conductivity from undisturbed samples by falling head method, etc.

This paper relates to results of field measurements along Chotárny channel – one of three main monitored channels at the ŽO area (Fig. 1a, Fig. 1b). Saturated hydraulic conductivity values of bed silts were determined on the base of two ways of bed silt samples extraction (disturbed and undisturbed samples). The channel network aggradation at ŽO has been monitored and studied by many our regional specialists – Kosorin (1997), Mucha et al. (2006), Štekauerová et al. (2009), Baroková and Šoltész (2014), Kováčová (2017), etc. This paper shows some results of field measurements along the Chotárny channel in 2018 – Fig. 1b.

Material and methods

Chotárny channel is one from three channels of the ŽO channel network monitored by Institute of Hydrology SAS since 1993. Geometrical parameters of this channel observed during the last measurements were: the channel length was approximately 27 km, the channel width was in range 11–17.5 m, the channel depth run into maximal values up to 3.15 m (according to cross-section location). The registered values of hydraulic conductivity in aquifers nearby this channel K_{fs} are 0.40–3.4 x 10^{-3} m s^{-1} (Mišigová, 1988). Chotárny channel receives water from drain channel of Gabčíkovo waterworks. The tributaries of Chotárny channel are channel Gabčíkovo – Ňárad, Čilížsky stream, channel Jurová – Veľký Meder, channel Kračany – Boheľov, Belský channel and Býčí channel. The water from Chotárny channel is used for irrigation by another channels which

are connected to this channel network by sluices (Dušek and Velísková, 2014). The collection facility for the Chotárny channel is situated in left-hand embankment of the drain (outflow) channel (in km 1.25) and is permanently closed. Water supply to Chotárny channel is provided by underground seepage pipe. In km 10.15 of Chotárny channel occures the water measuring station Jánošíkovo na Ostrove. The Chotárny channel connects to Little Danube through pumping station eastward of village Topoľníky.

The measurements of bed silt thicknesses along the Chotárny channel in 2018 were performed from the displaceable inflatable boat by simple drill hole. The distance of cross-sections along the channel varied between 1.0–1.5 km. In all channel cross-sections there was measured the water depth and bed silt thicknesses with step 1.0–2.0 m along the channel width. The samples of channel bed silt were extracted in these selected cross-sections where the largest channel bed silt thickness was noticed – in 8 cross-sections of Chotárny channel. Sediment sampling was conducted using the 04.23 Sediment Core Sampler, a rod operated type Beeker. This instrument collected the samples of silts in 1 m long acrylic tube as shown in Fig. 2a.

The Fig. 2b illustrates the sediment sampling from field measurement in one of cross-sections of Chotárny channel.

There was possible to take undisturbed samples of bed silt with this device and from each whole sample there was extracted a part from top, middle and bottom layer of silt. After experimental determination of saturated hydraulic conductivity for each layer of sample from one cross-section, the sample was broken and changed to disturbed sample. Next, for each disturbed sample it was done the granularity analysis and determined the value of saturated hydraulic conductivity.

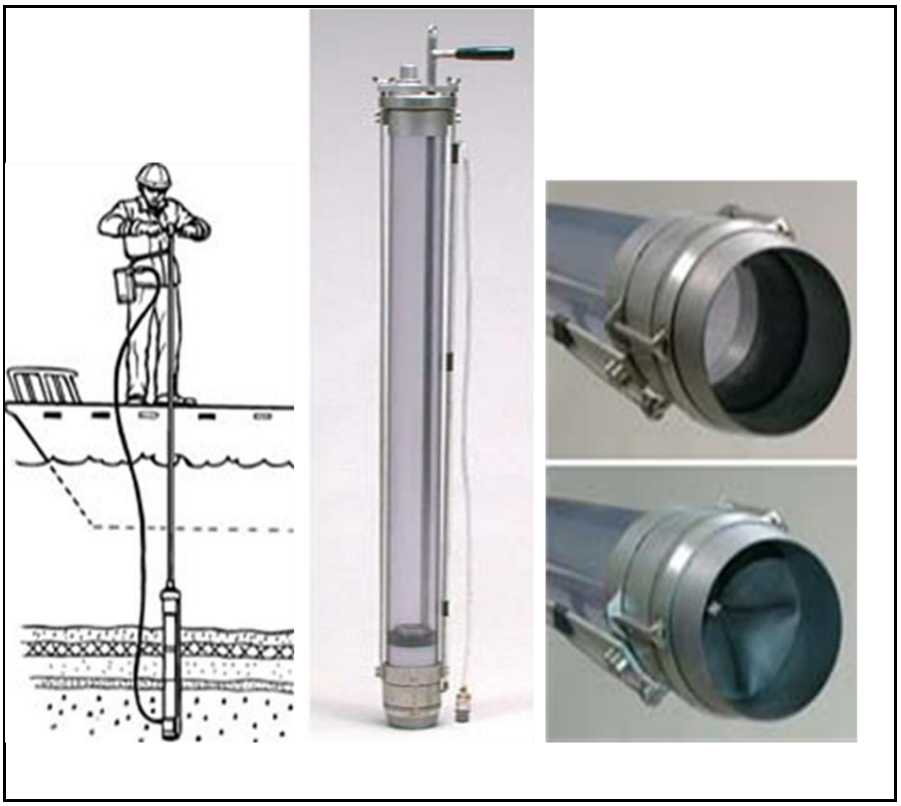

Fig. 2a. Measuring device for sediment samples extraction– the Beeker sampler.

Fig. 2b. Sediment sampling from boat at Chotárny channel in 2018.

The disturbed samples – determination of saturated hydraulic conductivity

Determination of saturated hydraulic conductivity from disturbed samples of bed silts can be calculated by empirical formulas coming out from grain size analysis (Kutílek, 1978; Kasenow, 2010). Several empirical formulas for determination of hydraulic conductivity from granularity exist, but it is possible to apply only a few of them because their limited validity. Therefore we used at first the relationships by Beyer-Schweiger and Špaček (Špaček, 1987) and later we added yet using of another four empirical formulas according to authors Hazen I., Bayer, USBR and Orechova (User's manual of software GeoFil). In all these mentioned relationships the value of saturated hydraulic conductivity K_d is function of d_{10}, d_{17}, d_{20} or d_{60} (particle diameters in 10%, 17%, 20% and 60% of soil mass). These parameters were determined from granularity curves of all extracted disturbed samples at Chotárny channel.
Beyer-Schweiger formula, used for determination of saturated hydraulic conductivity from disturbed samples K_{dBS} [m s^{-1}], is:

$$K_{dBS} = 7.5x10^{6}\, C\,(d_{10})^{2} \qquad (1)$$

where C=1.5961x10^{-3} $(d_{60}/d_{10})^{-0.20371}$, d_{10} – particle diameter in 10% of soil mass [m], d_{60} – particle diameter in 60% of soil mass [m] and conditions of validity are:

$$0.06 \le d_{10} \le 0.6 \quad \text{and} \quad 1 \le \frac{d_{60}}{d_{10}} \le 20$$

Špaček formulas I., II. [m d^{-1}] for saturated hydraulic conductivity from disturbed samples K_d are:

$$K_{d\,ŠI.} = 20.577(d_{10})^{1.013}\left(\frac{0.5}{d_{60}-d_{10}}\right)^{0.059} \qquad (2)$$

$$K_{d\,ŠII.} = 108.4386(d_{10})^{0.8866}(d_{60})^{0.7726} \qquad (3)$$

where conditions of validity for application of eq. (2) are:
$d_{10} < 0.01$mm
or
$0.01 \le d_{10} < 0.13 \;\wedge\; d_{60} < 0.0576 + 0.5765 d_{10}$
and conditions of validity for application of eq. (3) are:
$d_{10} \ge 0.13$mm
or
$0.01 \le d_{10} < 0.13 \;\wedge\; d_{60} > 0.0576 + 0.5765 d_{10}$
Hazen I. formula, used for determination of saturated hydraulic conductivity $K_{d\,HI.}$ [m s^{-1}], is:

$$K_{dHI.} = \frac{116(d_{10})^{2}}{100} \qquad (4)$$

where d_{10} is particle diameter in 10% of soil mass [cm], the condition of validity is: $d_{15} < 0.6$ [cm].

Bayer formula $K_{d\,B}$ [m s^{-1}] is:

$$K_{dB} = U^{b}\mathrm{a}(d_{10})^{2} \qquad (5)$$
$$U = \frac{d_{60}}{d_{10}}$$

where d_{10} is particle diameter in 10% of soil mass [cm]; d_{60} is particle diameter in 60% of soil mass (cm); a, b are constant factors – for consolidated soils a=0.01; b=-0.23; U is coefficient of uniformity; the conditions of validity are: 0.06 (cm) < d_{10} < 0.6 (cm) $\wedge$ U < 20.

USBR formula $K_{d\,USBR}$ [m s^{-1}] is:

$$K_{dUSBR} = \frac{0.36(d_{20})^{2.3}}{100} \qquad (6)$$

where d_{20} is particle diameter in 20% of soil mass [mm]; the condition of validity is: 0.01 [mm] < d_{20} < 2.0 [mm].

Orechova formula $K_{d\,Or}$ [m s^{-1}] is:

$$K_{dOr} = \frac{640(d_{17})^{2}}{86400} \qquad (7)$$

where d_{17} is particle diameter in 17% of soil mass [mm]; the condition of validity is: $g_{0,063}$ [mm] < 35%, it means that is valid for soils with fraction less than 0.063 mm content < 35 %.

The valid values of saturated hydraulic conductivity from disturbed samples of silts along the Chotárny channel K_d according to these 7 formulas were calculated and summarized in Table 1. The samples of silts were extracted in those selected cross-sections along the Chotárny channel where the larger thicknesses of silt were measured within that cross-section – in 8 locations (as the 1st column of Table 1 and Table 2 cites) – in km 1.2, 6.0, 8.6, 16.3, 18.0, 20.0, 24.6 and 25.5.

The undisturbed samples – determination of saturated hydraulic conductivity

In case of undisturbed samples of bed silts the values of saturated hydraulic conductivity were obtained by using of falling head method – direct measurement in laboratory. There was used the simplified equipment for measuring of saturated hydraulic conductivity from undisturbed samples – Fig. 3a (Šurda et al., 2013).
The formula for calculation of average value of saturated hydraulic conductivity K_u according to scheme on Fig. 3a is:

$$K_u = \frac{l}{\Delta h}\, ln\, \frac{h2}{h1} \qquad (8)$$

where K_u is the saturated hydraulic conductivity of undisturbed samples [cm.s^{-1}], l is a sample height [cm], h_1, h_2 – variable static head [cm] – see Fig. 3a.

The values of saturated hydraulic conductivity from undisturbed samples, extracted from 8 selected cross-

sections at Chotárny channel (as was described above also in case of disturbed samples), were determined by the relationship (8) according to scheme on Fig. 3a. The results of values of saturated hydraulic conductivity from undisturbed samples K_u along the Chotárny channel are summarized in Table 2.

Table 1. Chotárny channel –values of K_d from disturbed samples of the bed silt layers in year 2018

Chotárny channel – 2018								
Channel stationing [km]	***Bed silt layer***	***K_d [m s^{-1}]***						
		Bayer-Schweiger	***Špaček I.***	***Špaček II.***	***Hazen I.***	***Bayer***	***USBR***	***Orechova***
1.2	top	3.81x10^{-08}	6.03x10^{-07}	(-)	6.14x10^{-08}	2.98x10^{-10}	(-)	(-)
	middle	(-)	(-)	1.02x10^{-06}	9.09x10^{-08}	(-)	(-)	(-)
	bottom	(-)	5.06x10^{-07}	(-)	4.64x10^{-08}	(-)	(-)	(-)
6.0	top	4.13x10^{-06}	(-)	2.62x10^{-05}	7.25x10^{-06}	3.20x10^{-08}	3.36x10^{-08}	2.24x10^{-07}
	middle	1.80x10^{-08}	4.23x10^{-07}	(-)	2.97x10^{-08}	1.40x10^{-10}	(-)	(-)
	bottom	6.30x10^{-05}	(-)	1.19x10^{-04}	9.40x10^{-05}	4.97x10^{-07}	5.84x10^{-07}	8.64x10^{-07}
8.6	top	(-)	7.64x10^{-07}	1.69x10^{-06}	1.19x10^{-07}	(-)	1.34x10^{-09}	(-)
	middle	(-)	(-)	2.04x10^{-05}	3.35x10^{-06}	(-)	1.84x10^{-08}	9.07x10^{-08}
	bottom	1.68x10^{-07}	1.24x10^{-06}	1.70x10^{-06}	2.90x10^{-07}	1.30x10^{-09}	1.15x10^{-09}	(-)
16.3	top	1.99x10^{-08}	4.45x10^{-07}	(-)	3.35x10^{-08}	1.54x10^{-10}	(-)	(-)
	middle	(-)	5.05x10^{-07}	(-)	4.64x10^{-08}	(-)	(-)	(-)
	bottom	3.32x10^{-08}	5.69x10^{-07}	(-)	5.61x10^{-08}	2.58x10^{-10}	(-)	(-)
18.0	top	2.15x10^{-08}	4.61x10^{-07}	(-)	3.55x10^{-08}	1.68x10^{-10}	(-)	(-)
	middle	(-)	4.11x10^{-07}	(-)	2.97x10^{-08}	(-)	(-)	(-)
	bottom	1.59x10^{-08}	3.99x10^{-07}	(-)	2.61x10^{-08}	1.24x10^{-10}	(-)	(-)
20.0	top	1.97x10^{-08}	4.44x10^{-07}	(-)	3.35x10^{-08}	1.53x10^{-10}	(-)	(-)
	middle	1.29x10^{-08}	3.66x10^{-07}	(-)	2.27x10^{-08}	1.00x10^{-10}	(-)	(-)
	bottom	1.37x10^{-08}	3.72x10^{-07}	(-)	2.27x10^{-08}	1.06x10^{-10}	(-)	(-)
24.6	top	(-)	5.50x10^{-07}	6.29x10^{-07}	5.61x10^{-08}	(-)	6.89x10^{-10}	(-)
	middle	(-)	1.66x10^{-06}	4.28x10^{-06}	5.68x10^{-07}	(-)	1.75x10^{-09}	1.90x10^{-08}
	bottom	(-)	5.16x10^{-07}	2.61x10^{-06}	6.14x10^{-08}	(-)	8.29x10^{-10}	(-)
25.5	top	1.06x10^{-07}	9.95x10^{-07}	1.27x10^{-06}	1.86x10^{-07}	8.15x10^{-10}	9.83x10^{-10}	(-)
	middle	(-)	6.60x10^{-07}	1.03x10^{-06}	8.46x10^{-08}	(-)	1.15x10^{-09}	(-)
	bottom	(-)	(-)	1.29x10^{-05}	1.23x10^{-06}	(-)	2.23x10^{-09}	2.27x10^{-08}

Symbol (-) means the conditions of validity for application of empirical formula are not maintained, e.g. the input values are located outside the range for this formula's application.

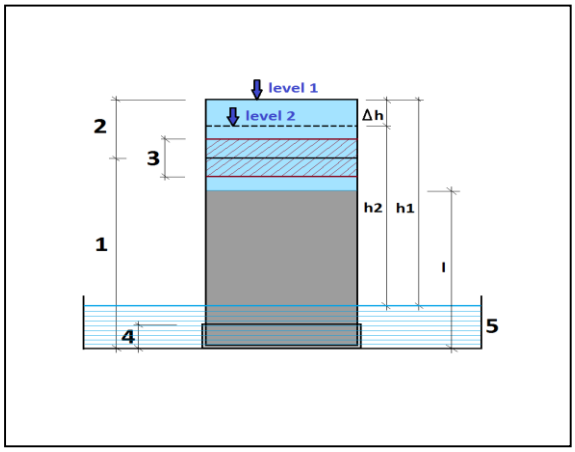

Fig. 3a. Simplified equipment for measuring saturated hydraulic conductivity of undisturbed sample: 1 – sampling tube height, 2 – Kopecky's roller, 3 rubber ring, 4 – filter paper and wire strainer, 5 – Petri dish.

Fig. 3b. The demonstration of application of falling head method to 24 undisturbed samples from Chotárny channel.

Table 2. Chotárny channel – values of K_u from undisturbed samples of the bed silt layers in year 2018

Chotárny channel – 2018		
Channel stationing [km]	***Bed silt layer***	***K_u [m s^{-1}]***
1.2	top	1.83×10^{-07}
	middle	1.19×10^{-07}
	bottom	8.12×10^{-07}
6.0	top	1.91×10^{-06}
	middle	1.53×10^{-07}
	bottom	4.53×10^{-05}
8.6	top	3.72×10^{-07}
	middle	1.62×10^{-06}
	bottom	3.20×10^{-07}
16.3	top	2.50×10^{-06}
	middle	3.01×10^{-07}
	bottom	3.18×10^{-07}
18.0	top	9.69×10^{-07}
	middle	1.07×10^{-06}
	bottom	7.68×10^{-08}
20.0	top	7.62×10^{-07}
	middle	1.01×10^{-07}
	bottom	8.08×10^{-08}
24.6	top	5.82×10^{-06}
	middle	2.57×10^{-06}
	bottom	$1,51 \times 10^{-06}$
25.5	top	$1,00 \times 10^{-06}$
	middle	2.76×10^{-07}
	bottom	7.25×10^{-06}

The results at every single cross-section are quite various – km 1.2 is pretty consistent 10^{-07}, km 6.0 shows huge differences from 10^{-05} to 10^{-07}, km 8.6 is somewhat consistent from 10^{-07} to 10^{-06}, km 16.3 is also somewhat consistent from 10^{-06} to 10^{-07}, km18.0 shows huge differences from 10^{-06} to 10^{-08}, km 20.0 and km 25.5 are also somewhat consistent and km 24.6 is also pretty consistent 10^{-06}. We can conclude that in single layers of silt at single cross-sections the differences between top, middle and bottom layer there were not any in two cross-sections (km 1.2 and 24.6), in four cross-sections the differences between top, middle and bottom layer were on order of tenfold (km 8.6, 16.3, 20.0 and 25.5) and in two cross-sections these differences were on the order of a hundredfold (km 6.0 and 18.0). We could try to clarify the cause of these differences in another paper in the future.

In case of comparison of the values of K_u in its single layers - between top, middle and bottom layer within one cross-section – there was no significant impact

of the level and the results were scattered throughout the cross section, except in two cases – the cross-section in km 6.0 and in km 18.0.

Results and discussion

As was mentioned before there were used two ways for determination of saturated hydraulic conductivity values of bed silts at the Chotárny channel. The results obtained from both were compared in this study. The values of saturated hydraulic conductivity were in both cases determined for the top, middle and bottom layer of extracted bed silt samples.

The value of saturated hydraulic conductivity, as the indicator of bed silt permeability, was calculated at first for disturbed samples of bed silts – by seven empirical formulas. Each of them determines this variable quantity as a function of d_{10}, d_{17}, d_{20} and d_{60} (particle diameter in 10, 17, 20 and 60% of soil mass). Conditions of validity for application of these seven formulas also depend on value of d_{10}, d_{17}, d_{20} and d_{60}. The values of saturated hydraulic conductivity of disturbed samples K_d, computed from 7 empirical formulas, are summed in Table 1. The valid values of saturated hydraulic conductivity of bed silt from single layers reached from $1.00\text{x}10^{-10}$ to $1.19\text{x}10^{-04}$ m s^{-1}, depending on the formula. The range of these results is in the order of thousand. This enormous difference could be caused by influence of the bed silt grain size which is determined from the grain size curve. Perhaps also other phenomenon, such as thickness of layer, temperature, etc. could be responsible for this difference.

In comparison with saturated hydraulic conductivity values of surrounding aquifer near the Chotárny channel the values of bed silts are severalfold lower.

For comparison of results mentioned in Table 1 we used the count of valid results, computed from each empirical formula according seven authors, as a criterion for recommending relevant formula for computation of bed silt values of saturated hydraulic conductivity K_d. The recommended formula for calculation of K_d based on this criterium for Chotárny channel is Hazen I. formula – from 24 extracted disturbed samples we obtained 24 valid values of saturated hydraulic conductivity. Fig. 4 represents the statistical presentation of number of K_d.

The other method of determination of the values of saturated hydraulic conductivity for undisturbed samples was falling head method. The results obtained by this way are summed in Table 2. The valid values of channel bed silt saturated hydraulic conductivity from undisturbed samples K_u reached from $7.68\text{x}10^{-08}$ to $4.53\text{x}10^{-05}$ m s^{-1}.

We made the comparison of the values of saturated hydraulic conductivity obtained from disturbed and undisturbed samples of bed silts at Chotárny channel in 2018.

In case of disturbed samples the values of saturated hydraulic conductivity K_d run into 10^{-10} to 10^{-05}, whereby the values 10^{-08} predominated (Table 1). In case of undisturbed samples the values of saturated hydraulic conductivity K_u run into 10^{-08} to 10^{-05}, predominant values were 10^{-07} (Table 2).

At comparison of single layers of bed silts, extracted as disturbed samples, we found out that between top, middle and bottom layers were almost none differences or in a few cases only ten to hundred fold.

In case of comparison of undisturbed silt samples in its single layers the differences between top, middle and bottom layer were tenfold up-to hundredfold.

At last it was made comparison of values of saturated hydraulic conductivity from disturbed samples according Hazen I. (selected by criterion of the largest number of obtained results) and from undisturbed samples. From this comparison arised the interesting outcome which showed that in case of disturbed samples the values of saturated hydraulic conductivity according Hazen I. 10^{-08} predominate and these values are tenfold-to hundredfold less than the values from undisturbed samples. Fig. 5a represents the illustration of saturated hydraulic conductivity values from disturbed samples, for comparison at Fig. 5b are saturated hydraulic conductivity values from undisturbed samples at Chotárny channel in 2018.

The scales of both graphs are different due to the big differences in the values of saturated hydraulic conductivity. Further study in the future will be conducted to investigate the reasons why the values differ vastly.

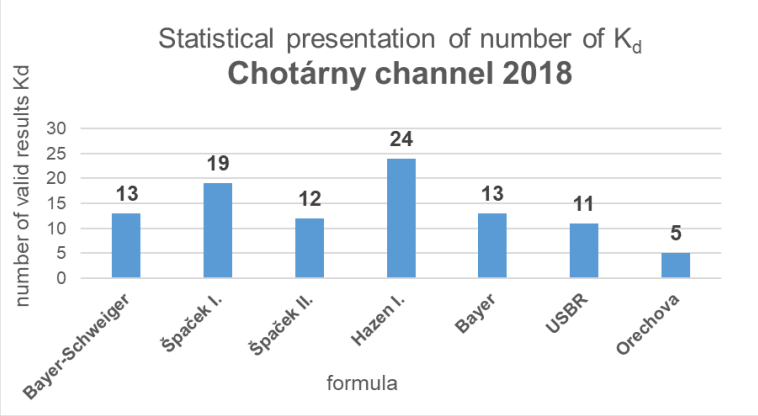

Fig. 4. The illustration of statistical evaluation of data range.

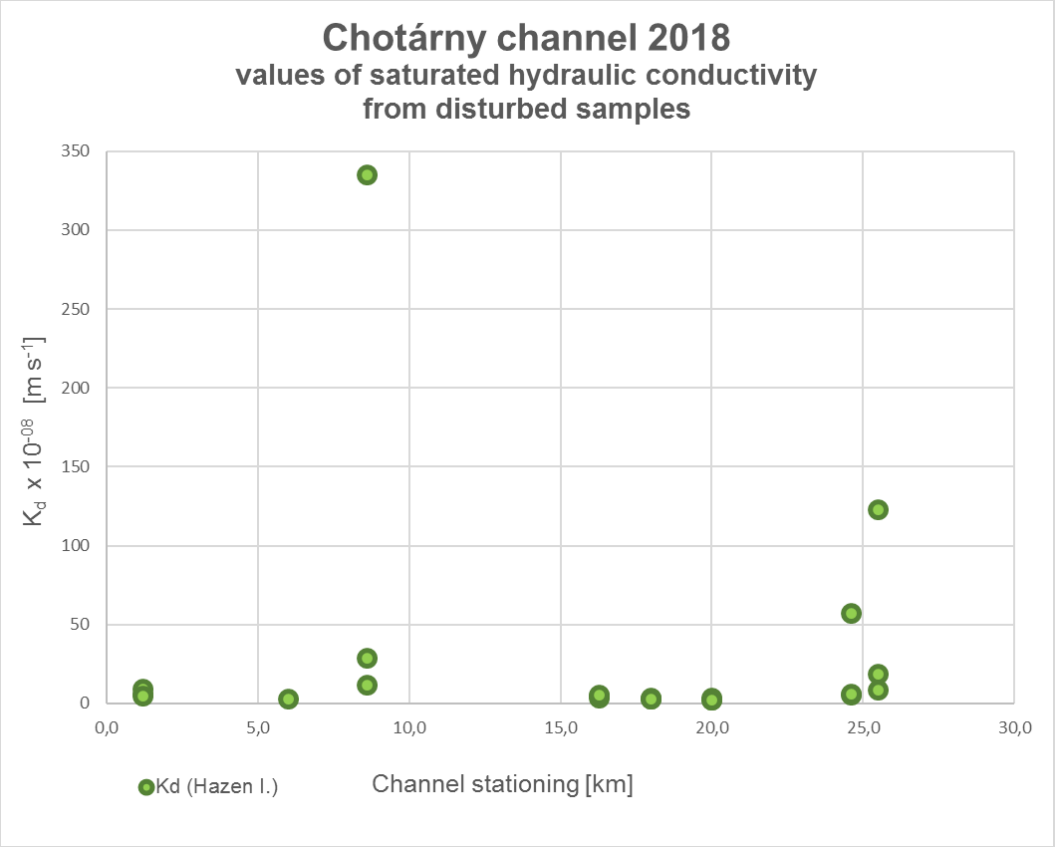

Fig. 5a. The illustration of saturated hydraulic conductivity values from disturbed samples at Chotárny channel in 2018.

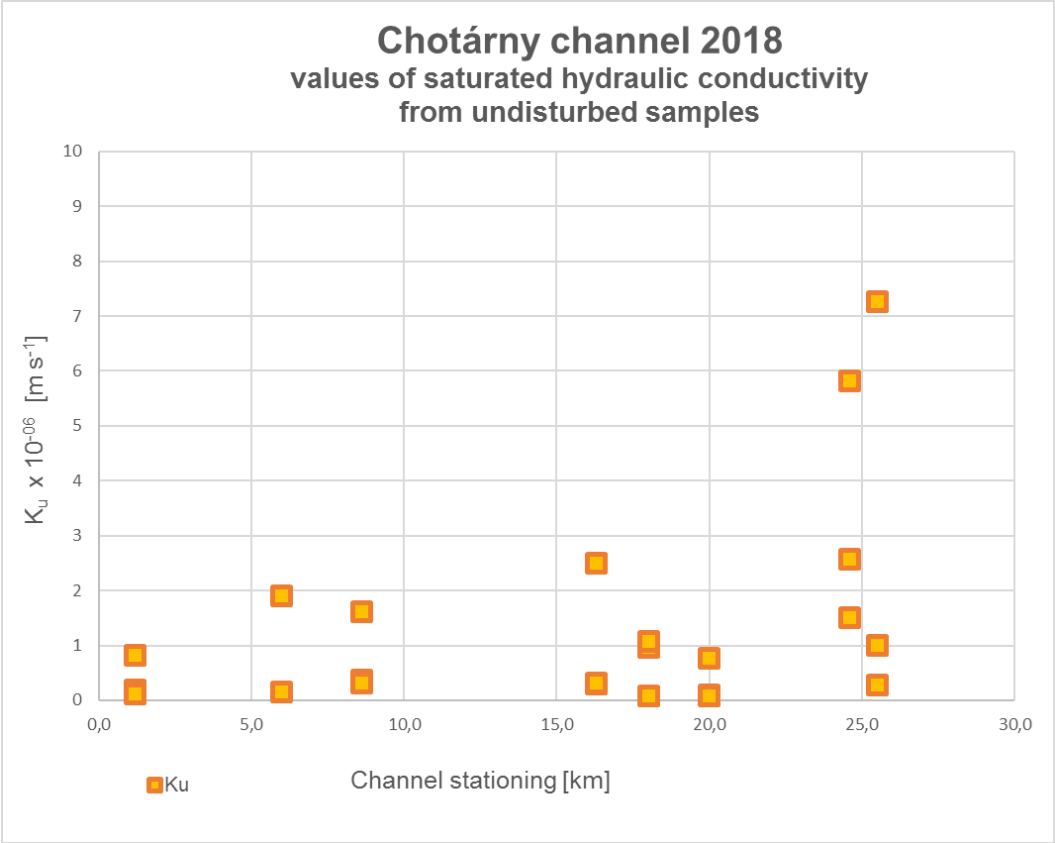

Fig. 5b. The illustration of saturated hydraulic conductivity values from undisturbed samples at Chotárny channel in 2018.

Conclusion

This study directs at the determination of bed silt permeability along the Chotárny channel on base of field measurements performed during 2018 and comparison of two ways for determination of its saturated hydraulic conductivity. The thickness of bed silts and its permeability fundamentally influence and determine the rate of mutual interaction between surface water in the Chotárny channel and groundwater in its surroundings. For this reason, it is important to research and monitor continuously the state of channel bed aggradation and to know the permeability of bed silts, expressed by its value of saturated hydraulic conductivity.

The values of saturated hydraulic conductivity of bed silts along the Chotárny channel were determined by two ways. The first way was by using of calculation according to seven empirical formulas applicable for disturbed samples of bed silts based on granularity analysis of disturbed samples. The resultant values are presented in Table 1. The valid values of saturated hydraulic conductivity for single parts of bed sediment layers reached from $1.00x10^{-10}$ to $1.19x10^{-04}$ m s^{-1}.

The second way was using of falling head method by direct measurement in laboratory applicable for undisturbed samples of bed silts. The resultant values are presented in Table 2. These values of saturated hydraulic conductivity for single parts of bed silt layers reached from $7.68x10^{-08}$ to $4.53x10^{-05}$ m s^{-1}.

The comparison of the values of saturated hydraulic conductivity obtained from disturbed and undisturbed samples of bed silts at Chotárny channel in 2018 was made. The comparison of these results concluded that the values differ to a great extent.

In case of comparison of undisturbed silt samples in its single layers the differences between top, middle and bottom layer were tenfold up-to hundredfold.

From the comparison of values of saturated hydraulic conductivity from disturbed samples according Hazen I. and undisturbed samples was that in case of disturbed samples the values of saturated hydraulic conductivity according Hazen I.

All obtained information about bed silt thicknesses supplemented by values of saturated hydraulic conductivity of bed silt can be eligible for numerical simulation models and simultaneously they represent valuable information for any future way of groundwater level regulation in surroundings of the Chotárny channel and other channels at the ŽO area.

Acknowledgement

This work is support by the contract VEGA-02/0025/19.

References

Baroková, D., Šoltész, A. (2014): Analysis of surface and groundwater interaction in the Danube river branch system., SGEM Conference Proceedings, 14th SGEM Geo-Conference on Water Resources. Forest, Marine And Ocean Ecosystems, Vol. I., www.sgem.org, ISBN 978-619-7105-13-1/ ISSN 1314-2704, 51–58

Dulovičová, R., Velísková, Y., Schűgerl, R. (2018): Hydraulic conductivity of bed silts in Komárňansky channel – Žitný ostrov. Acta Hydrologica Slovaca, Vol. 19, No. 1, 117–125 (in Slovak)

Duong, T. T, Minh, D. D, Yasuhara, K. (2019): Assessing the Effects of Rainfall Intensity and Hydraulic Conductivity on Riverbank Stability. MDPI Water Journal 2019, 11(4), 741: Available on https://doi.org/10.3390/w11040741

Dušek, P., Velísková, Y. (2014): Hydrological and hydrogeological conditions at Žitný ostrov channel network area. Acta Hydrologica Slovaca, Vol. 15, No. 2, 361–369 (in Slovak)

Gadi, V. K., Tang, Y.R., Das, A., Monga, Ch., Garg, A. Berretta, Ch. and Sahoo L. (2017). Spatial and temporal variation of hydraulic conductivity and vegetation growth in green infrastructures using infiltrometer and visual technique. Catena, Vol. 155: 20–29. https://doi.org/10.1016/j.catena.2017.02.024

Habtamu, F.M., Tamene, M., and B. Geremew Sinshaw, B.G. (2019). Evaluating Saturated Hydraulic Conductivity under Different Land Use types, Gumara Watershed, Tana Sub-basin. Journal of Academia and Industrial Research (JAIR), Vol. 7, Issue 9: 124, ISSN: 2278-5213

Hussain F. Nabi G. (2016): Empirical Formulae Evaluation for Hydraulic Conductivity Determination Based on Grain Size Analysis. Original Research Paper. Pyrex Journal of Research in Environmental Studies, Vol 3 (3): 026-032, Available on http://www.pyrexjournals.org/pjres

Hwang, H. T., Jeen, S. W., Suleiman, A. A. Lee, K. K. (2017): Comparison of Saturated Hydraulic Conductivity Estimated by Three Different Methods. Water – Open Access Journal, MDPI, 9, 942: 1–15. Available on https://creativecommons.org/licenses/by/4.0. doi:10.3390/w9120942

Kasenow, M. (2010): Determination of hydraulic conductivity from grain size analysis, Water Resources Publications, LLC, Textbook

Kosorin, K. (1997): Spatial groundwater dynamics of the Rye Island aquifer. J. Hydrol. Hydromech., Vol. 45, 348 – 364.

Kováčová, V. (2017): Trends of nitrate ions content in Žitný Ostrov channel network. Acta Hydrologica Slovaca, Vol. 18, No. 1, 57–67 (in Slovak)

Kutílek, M. (1978): Vodohospodářská pedologie, Alfa Bratislava, SNTL 04-721-78, 296 p., (in Czech)

Mišigová, I. (1988): Methods of regional assessment of hydraulic properties of the rocks on the Žitný Ostrov. Report IHH SAS, (in Slovak)

Mucha, I., Banský Ľ., Hlavatý Z., Rodák D. (2006): Impact of riverbed clogging colmatation on ground water, Riverbank Filtration Hydrology: Impacts on System Capacity and Water Quality. NATO Science Series: IV. Earth and Environmental Sciences – Vol. 60, Springer, 43–72. (printed in the Netherlands)

Říha, J., Petrula, L., Hala, M., Alhasan, Z. (2018): Assessment of empirical formulae for determining the hydraulic conductivity of glass beads. J. Hydrol. Hydromech., 66, 3, 337–347 DOI: 10.2478/johh-2018-0021 337

Špaček, J. (1987): Determination of filtration coefficient from total grain-size curves. J. Meliorace, Vol. 23, No.1, 1–13 (in Czech)

Šurda, P., Štekauerová, V., Nagy, V. (2013): Variability of the saturated hydraulic conductivity of the individual soil types in the area of the Hron catchment. Nővénytermelés, Vol. 62, supplement, 323–326

Štekauerová, V., Nagy, V., Šútor, J., Milics, G., Neményi, M. (2009): Influence of groundwater level on soil water regime of Žitný ostrov. In V. Növénytermesztési Tudományos Nap - Növénytermesztés: Gazdálkodás - Klímaváltozás – Társadalom, Akadémiai Kiadó, Budapest, 197–200

User's manual of software GeoFil

Wang, Y., Jin, M., Deng, Z. (2018): Alternative Model for Predicting Soil Hydraulic Conductivity Over the Complete Moisture Range. American Geophysical Union, Available on https://doi.org/10.1029/2018 WR023037

Ing. Renáta Dulovičová (*corresponding author, e-mail: dulovicova@uh.savba.sk)
Mgr. Radoslav Schügerl, PhD.
Ing. Yvetta Velísková, PhD.
Institute of Hydrology SAS
Dúbravská cesta 9
841 04 Bratislava
Slovak Republic

DOI: 10.31577/ahs-2022-0023.02.0021

ACTA HYDROLOGICA SLOVACA

Volume 23, No. 2, 2022, 190–196

Neurohydrological prediction of water temperature and runoff time series

Zoltan Arpad LIPTAY *

In this paper we give an overview of experiments with artificial neural networks on the Hungarian reach of the Danube River carried out by the Hungarian Hydrological Forecasting Service. Two areas were selected: rainfall-runoff modelling and water temperature simulation. The statistical machine learning method is a universal interpolation and classification tool, but showed poor performance when applied for correlation in complex hydrological situations. Despite very strong learning skills of neural networks even a conceptual model gave more consistent and superior results through validation, and the statistic method is more sensitive to overlearning than deterministic methods. Despite deterministic models being superior artificial neural networks still provide satisfactory results that confirms their application.

KEY WORDS: hydrology, artificial neural networks, modelling, forecast

Introduction

The machine learning type artificial intelligence approaches have a long history reaching back to the work of McCulloch and Pitts (1943). Later on Rosenblatt (1957) presented the concept of a perceptron but it got great interest only after its rediscovery by Rumelhart et al. (1986). The nonlinearity of Rumelhart's multilayer perceptron (MLP) was a significant advantage compared to the linear behaviour of the Rosenblatt perceptron, and by the back error propagation method it was possible to find the weights of the internal synapses. An artificial neural network (ANN) is non-parametric statistical method, it is considered as a black box model and by opening this box one does not find the representation of the physical processes, and thus method extraction is not yet possible. It is an artificial architecture consisting of neurons and synapses resembling the biological cognition and its information processing characteristics. The information is distributed throughout the network, and the information processing is a parallel process, so even a significant change in some of the weights of the synapses has only a minor effect on the performance of the entire network. The information processing and learning capabilities of the ANN are utilized in the main application areas. General application areas are for example interpolation, categorization, classification, while higher level applications are for example image processing, image classification, language processing and language generation, machine translation, spell checking, named entity recognition, part-of-speech tagging, semantic parsing and question answering, paraphrase detection. However certain application areas require more complex approaches than regular artificial networks, such as the convolutional neural networks for high resolution image processing.

The first published hydrological application of the artificial neural network (ANN) was by Daniel (1991) but it was followed by a great number of studies and it is still an intensively studied area. Comprehensive reviews on neural hydrology (or neurohydrology) were made by Govindaraju (2000a and 2000b), Tanty and Desmukh (2015) and Lange and Sippel (2020), while numerous case studies are also available (Rabi et al., 2015; Temizyurek and Dadaşer-Çelik, 2018; Zhu et al., 2018; Zhu et al., 2019; Van Leeuwen et al., 2020; Jakab et al., 2021).

The aim of this paper is to compare the performance of an artificial neural network with regular hydrological calculations of deterministic and conceptual types. Rainfall-runoff modelling of a small lower mountainous catchment was one of the areas where a conceptual approach was compared to the ANN. The second experiment was the water temperature simulation of a river where both a deterministic and a conceptual method were compared to the ANN.

Materials and methods

Artificial neural networks

The feed forward multi-layer perceptron (MLP) stands of at least three layers of neurons: input, hidden and output layers. Classifications and regressions are two possible

applications of ANNs. Speaking of either application some inputs are given at the input layer and outputs are received at the output layer. These outputs are compared to target values and based on the errors the ANN is able to learn (Rumelhart et al., 1986). This training method requires a great number of training data carefully selected to describe the general range of the resembled process because the extrapolation capabilities of an ANN are poor (Govindaraju, 2000b). We used the widely applied error back-propagation with added momentum for the training process. The algorithms used for this study were programmed in C# in Microsoft Visual Studio, but nowadays more and more ANN related tools and solutions are available online that need no programming skills to apply.

A schematic representation of a neuron is presented on Fig. 1.

From left to right the *j*-th neuron (N_j) has *n* number of inputs (I_n) with w_{jn} weights of the synapses and it has a *b* bias value. These are summed as:

$$S_j = \sum_{i=1}^{n} I_i w_{ji} + b \quad (1)$$

where
I – input neuron,
w – weights of the synapses,
b – bias value ,
S – sum of input synapses and bias value.

All neurons have a transfer or activation function (A_j) which is usually of sigmoid type. If we take the aforementioned logistic function, the O_j output of the neuron will be written as:

$$O_j = A_j = \frac{1}{1+e^{-S_j}} \quad (2)$$

where
O – output of the neuron,
A – activation function,
S – sum of input synapses and bias value.

The feed forward MLP stands of at least three layers of neurons: input, hidden and output layers. The neurons of the input layer have only one input per neuron and boththe input and output layers have linear transfer function, thus:

$$O_j = S_j \quad (3)$$

where
O – output of the neuron,
S – sum of input synapses and bias value.

The schematic diagram of a feed forward multilayer perceptron is shown on Fig. 2.

Classifications and regressions are two possible applications of ANNs. Speaking of either application some inputs are given at the input layer and outputs are received at the output layer. These outputs are compared to target (*T*) values and based on the errors (*E*) the ANN is able to learn (Rumelhart et al. 1986).

$$E = \frac{1}{2}\sum_{k=1}^{M}(T_k - O_k)^2 \quad (4)$$

where
E – error value,
T – target value,
O – output of the neuron.

This training method requires a great number of training data carefully selected to describe the general range of the resembled process because the extrapolation capabilities of an ANN are poor (Govindaraju, 2000b). We used the widely applied error back-propagation with added momentum for the training process. For any weight (Formula 5) and bias (Formula 6) in the network the formula is written as:

$$w_{kj}(t+1) = w_{kj}(t) - \alpha \frac{\partial E}{\partial w_{kj}} + \beta \Delta w_{kj}(t-1) \quad (5)$$

$$b_j(t+1) = b_j(t) - \alpha \frac{\partial E}{\partial b_j} + \beta \Delta b_j(t-1) \quad (6)$$

where
α – learning rate,
β – momentum,
t – training step,
E – error value,
b – bias value.

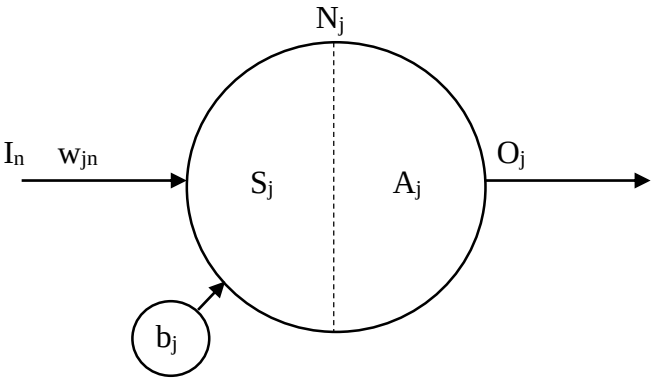

Fig. 1. Schematic diagram of a neuron.

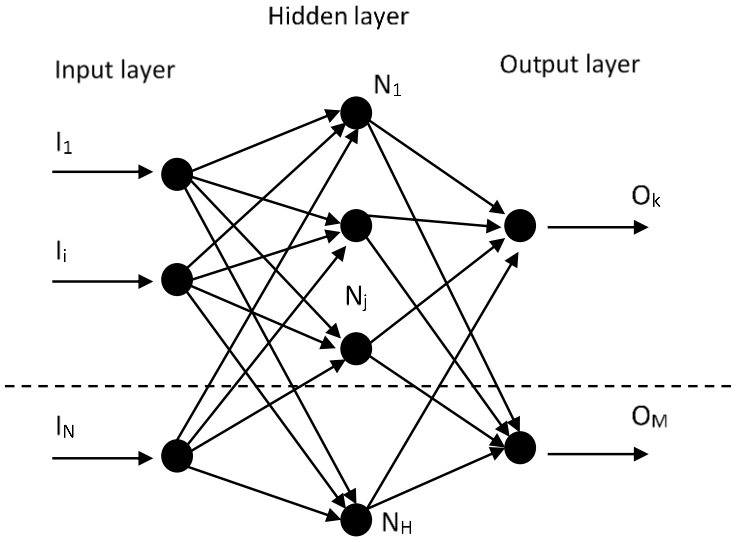

Fig. 2. Schematic diagram of a feed forward multilayer perceptron.

We used the tangent hyperbolic function as an activation function, thus the partial derivative of the error after the application of the chain rule in the output layer is:

$$\frac{\partial E}{\partial w_{kj}} = \frac{\partial E}{\partial O_k}\frac{\partial O_k}{\partial S_k}\frac{\partial S_k}{\partial w_{kj}} = -(T_k - O_k)O_j \quad (7)$$

In the hidden layer it is:

$$\frac{\partial E}{\partial w_{ji}} = \sum_{k=1}^{M}\left(\frac{\partial E}{\partial w_{kj}}w_{kj}\right)\tanh'(S_j)O_i \quad (8)$$

where
E – error value,
T – target value,
O – output of the neuron,
S – sum of input synapses and bias value,
w – weights of the synapses.

The formulas for the biases (b) are similar except they do not have any inputs so the multiplication with the output (O) of the previous layer is missing.

Rainfall-runoff modelling

The study area for rainfall-runoff modelling was the lower mountainous catchment of Galga River in Hungary upstream of Galgamácsa gauging station. This station is 29.8 kilometres upstream from the confluence with its recipient, the Zagyva River, the area of its catchment is 288 km^2. It is a small catchment with complex hydrological behaviour where conceptual hydrological modelling has not provided satisfactory results yet. The applied rainfall-runoff model was of conceptual type developed and operated by the Hungarian Hydrological Forecasting Service. The input of the model is a rainfall time series already processed by a spatially distributed snow calculation to add molten and extract frozen snow water. The potential and the actual evapotranspiration values are then estimated by the Thornthwaite equation (Thornthwaite 1948) and the Mintz-Walker formula (Mintz and Walker 1993). The output time series of the distributed module are surface water income or active precipitation series. The active precipitation values of the distributed model are then summed on every subcatchments of the model domain such as the Galga subcatchment used in this study.
The rainfall-runoff model uses a modified version of the Horton equation (Horton, 1933) to calculate infiltration. The modification in the Horton equation is the substitution of the exponential term with the relation of the saturated water content and the actual water content of the specific soil, and it also takes frozen soil into account. The active precipitation is separated by the above formulas to evapotranspiration, and three runoff components: surface runoff, rootzone runoff and groundwater.
The separated runoff components are then tranformed to the outflow section of the subcatchment by discrete linear cascade models (DLCM). DLCM is a flood routing method originally published by Kalinin and Milyukov (1957), and later by Nash (1960), details are also available in Chow et al. (1988). The analitic solution of the DLCM is done with a state-space approach and with a non-integer number of cascades based on the work of Szilagyi (2006).
Calibrations were carried out on the data from 2015 to 2019, validation on 2013–2014 and 2020.

Water temperature simulation

The selected site for water temperature simulations was on the Danube River at Paks gauging station. This station is of high importance due to the cooling water outlet of the nuclear power plant located nearby. Two methods were compared to the artificial neural network, a physically based energy balance estimation and

a simplified conceptual model ignoring all the terms but the sensible heat with an added transfer coefficient.

The estimation of the energy balance

First of the methods is the estimation of the terms of the energy balance of water published by Starosolszky (1969) and many other e.g. Mohseni and Stefan (1999). The model uses the observed water temperature as an initial condition and estimates the daily changes based on the energy balance driven mainly by the predicted air temperature of the ECMWF meteorological model. The governing equation of the energy balance is:

$$E_0 - E_u = (1 - A) \cdot E_{sw} + E_{lw} - E_s + E_c + E_e + E_p \qquad (9)$$

where
E_o – total energy emitted or absorbed,
E_u – energy flux through the river bed,
E_{sw} – net solar (shortwave) radiation,
A – albedo,
E_{lw} – atmospheric (longwave) radiation,
E_s – emitted longwave radiation of water surface,
E_c – sensible heat transfer on the water-air boundary layer (convective heat flux),
E_e – energy loss or gain from evaporation or vapor condensation (latent heat transfer or evaporative heat flux),
E_p – energy from precipitation.

Equations for direct solar radiation are available (Dozier, 1979), its value can be estimated with sufficient accuracy based on the formulas of spherical trigonometry. However the estimation of the diffuse component of shortwave radiation is not as exact, there are formulas also available (Liu and Jordan, 1960; Gates, 1980; Linacre, 1992; Oliphant et al., 2006). The longwave atmospheric radiation is based on the Stefan-Boltzmann Law (Stefan, 1879; Boltzmann, 1884).

The weighted mean temperatures

The theory, published by the Swedish meteorologist Olof Bertil Rodhe in 1952 and later in 1955, was an answer to the uncertain approach of temperature sum based methods (Östman, 1950; Nusser, 1950; Palosuo, 1951) of that era. This approach was specifically developed for marine application, to predict the appearance and later the extension of shore ice along the Baltic coastline. The U.S. Army Cold Regions Research and Engineering Laboratory experimented with river application and presented promising results (Bilello, 1963), and also recommended Rodhe's method for further testing on river ice prediction. Liptay (2018a) also applied the method for the Hungarian Danube reach with promising results.
Although the theory of energy balance had been known for a long time, meteorological measurements were unable to provide the necessary input data for the calculation of the energy balance till the end of the 1960s (Csoma, 1968). Rhode assumed that all terms of the full energy balance are neglected but the direct energy transfer between water and air.

$$\frac{d\tau}{dt} = k(T - \tau) \qquad (10)$$

where
T – air temperature [°C],
τ – water temperature [°C],
t – time [s],
k – time inverse coefficient [1 s^{-1}] or a constant with inverse dimension of time.

After the solution and discretization of the basic differential equation (10), the final form is equation 11.

$$\tau_n = \tau_{n-1} + \left(1 - e^{-k\Delta t}\right)(T_n - \tau_{n-1}) \qquad (11)$$

where
T_n – average air temperature at a time step tn-1-tn [°C],
τ_n – temperature of the water surface at tn [°C],
τ_{n-1} – the temperature of the water surface at tn-1 [°C]
Δt – time step [s].

In the theory of weighted mean temperatures k is considered to be a constant, and its value is selected to drive Eq. 11. to zero when ice is expected. It is also possible to find a value for k where the series of calculated and observed water temperatures have the highest correlation (Liptay, 2018b). Mohseni and Stefan (1999) presented that the air temperature and water temperature has an S-shaped relation. This relation of the weekly average values from 01. 07. 2008 to 31. 08. 2017 is presented for Paks on Fig. 3. A polynomial trend line is also shown with the coefficient of determination of 0.92. We consider this relation as a sigmoid function ($\sigma(x)$) such as the standard logistic function, the normal cumulative distribution function, or the tangent hyperbolic function just to name a few. The first derivative of $\sigma(x)$ gives the measure of the rate at which water temperature changes with respect to the change of air temperature as a continuous function. Considering a more general form of the logistic function:

$$\sigma(x) = \frac{a}{1 + e^{(-\frac{x}{b} + c)}} \qquad (12)$$

where
$\sigma(x)$ – logistic function,
a – scale,
b – steepness,
c – shift for the transformation of the standard function.

Finally the formula for k is written as:

$$k = k_m\left(1 - \sigma'(x)\right) \qquad (13)$$

where
k – time inverse coefficient [1 s^{-1}] or a constant with inverse dimension of time,
k_m – maximum value for k at the lowest and highest water temperatures,
$\sigma(x)$ – logistic function.

A significant increment in model performance was achieved by substituting the local air temperature with a simple formula representing the convection of wate temperature from an upstream station. Another major advance was the introduction of the appearance on the surface of rivers, because the process of energy exchange is influenced. In order to describe this effect in a simple yet appropriate way we introduced an additional factor for *k* when the calculated water temperatures are under 0°C.

The data set for calibration was from summer 2015 to 2017, while the validation was done on data from summer 2017–2018, and summer 2018–2019 periods.

Results

Rainfall-runoff modelling

The ANN based method provided superior results on the learning data, but showed poor performance during any validation attempts. The conceptual rainfall-runoff calculation showed consistent performance during both of the calibration and the validation runs. The observed and simulated discharges were compared at Galgamácsa station based on the RMSE and water balance (accumulated discharges) values. Results are in Table 1.

Water Temperature Simulation

We used two different neural network architectures for water temperature simulation. The first approach was a single output multilayer perceptron (MLP) predicting only one day at a time. The inputs include the latest observed water temperature and the daily air temperature predictions regarding the lead time. For example for 1 day lead time it had two input neurons, while for 10 days it had 11 neurons on the input layer. This approach resulted in 10 separate neural networks for all the 10 days. The second approach was an architecture for the entire 10 days of lead time, so the number of input neurons was 11 (1 observed water temperature and 10 daily air temperature predictions) and the number of output neurons was 10.

Zhu et al. (2019) analysed the possibilities of artificial neural networks in water temperature simulation and documented increased efficiency when introducing streamflow and the day of year (DOY) as inputs. They also highlighted that streamflow has a decreasing impact on the accuracy on rivers with lower bed slope. We also analysed the possibilities of these two additional inputs but did not obtain any positive results.

The greater details of the methods and calculations are available in Liptay and Gauzer (2021).

The estimation of the energy balance showed consistent performance in every situation always giving satisfactory results. The conceptual model performed slightly poorer and showed less consistency on the validation time series. The ANN reached the tightest fit during calibration even better than the physical model, but did not perform well in the validation scenarios.

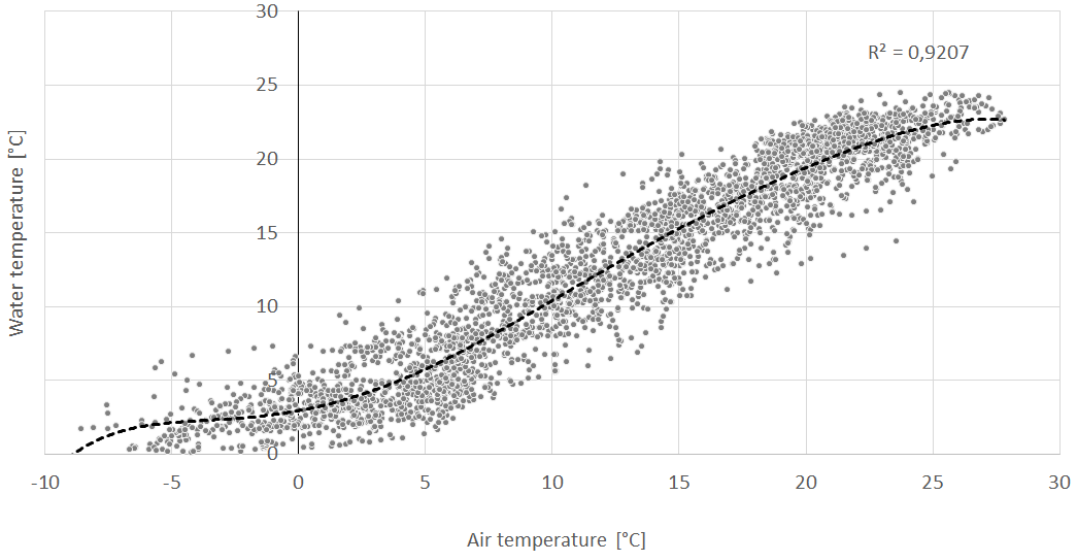

Fig. 3. The relation of air temperature and water temperature at Paks.

Table 1. Results of rainfall-runoff modelling (RMSE, water balance)

	Learning (2015–2019)	Validation (2013–2014)	Validation (2020)
observed	–	–	–
	0.0630 km^3	0.0167 km^3	0.0041 km^3
MLP	0.40 $m^3 s^{-1}$	0.0095 km^3	0.21 $m^3 s^{-1}$
	0.0630 km^3	0.49 $m^3 s^{-1}$	0.0045 km^3
GAPI	0.57 $m^3 s^{-1}$	0.28 $m^3 s^{-1}$	0.25 $m^3 s^{-1}$
	0.0566 km^3	0.0208 km^3	0.0024 km^3

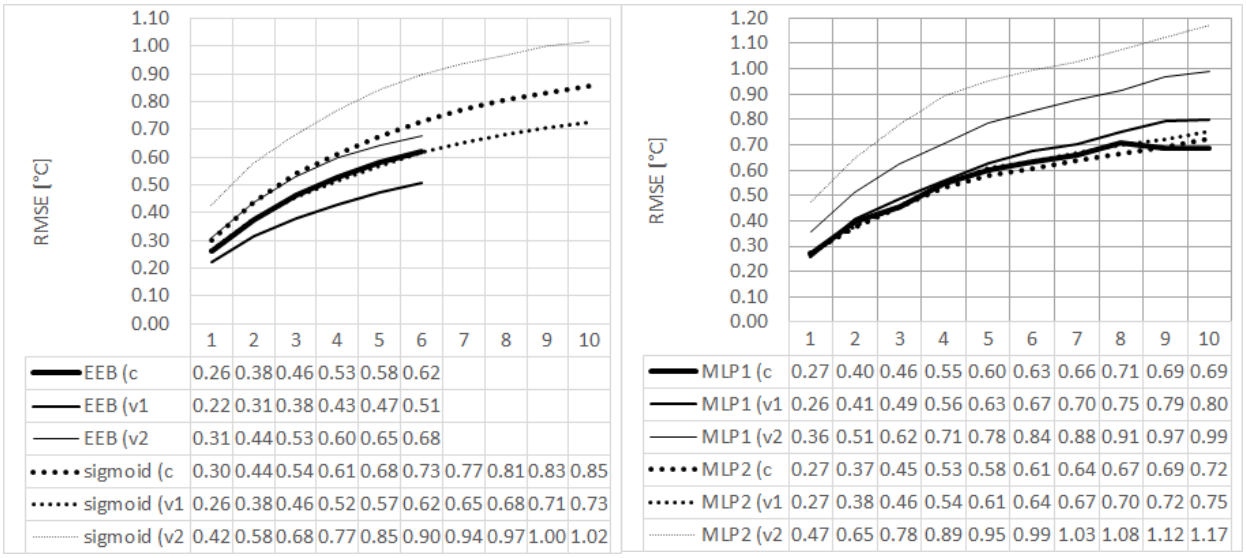

Fig. 4. Results of water temperature simulation (RMSE).

Conclusion

The time series forecasting capabilities of feed-forward multilayer neural networks were compared to deterministic models in this paper. The main difference between the non-parametric statistic and deterministic methods is the consistency of the performance. While the ANN is able to achieve superior calibration results, it is easily overtought. ANN water temperature and rainfall-runoff models were good tools to analyse a set of data, but any step outside of the already introduced set of information leads to extrapolation which is a weakness of ANNs. This makes ANNs a very good tool for the quick evaluation of time series and for the analysis of correlation between data. Statistical models do not need any information about the catchment or the physical environment of the data and this advantage is very important in case of insufficiently monitored areas. Time series forecasting with deep learning methods is a continuously growing and developing field such as almost any application of artificial intelligence methods. For example convolutional neural networks (CNNs) are widely applied also in time series forecasting besides image processing and are also discussed by Lange and Sippel (2020).

References

Bilello, M. E. (1963): Method of predicting river and lake ice formation. U.S. Army Cold Regions Research and Engineering Laboratory, Hanover.

Boltzmann, L. (1884): Ableitung des Stefan'schen Gesetzes, betreffend die Abhängigkeit der Wärmestrahlungvon der Temperatur aus der electromagnetischen Lichttheorie. Ann. der Phys. und Chemie. 22, 291(1884)

Chow, V. T., Maidment, D. R., Mays, L. W. (1988): Applied Hydrology. New York, McGraw-Hill Inc.

Csoma, J. (1968): A Tisza jégjelenségeinek előrejelzése. Vízügyi Közlemények. 50/3, 326-365.

Daniel, T. M. (1991): Neural networks – application in hydrology and water resources engineering. Proc. Int. Hydrol. and Water Resour., Institution of Engineers, Perth, Australia.

Dozier, J. (1979): A solar radiaton model for a snow surface in mountainous terrain. In "Modeling Snow Cover Runoff" (S. C. Colbeck and M. Ray, eds.), 144–153. U.S. Army Cold Reg. Re. Eng. Lab., Hanover, New Hampshire

Gates, D. M. (1980): Biophysical ecology.New York: Springer-Verlag. 611 pp.

Govindaraju, R. (2000a): Artificial Neural Networks in hydrology. I: Preliminary concepts. J. Hydrol. Eng. 5/2. 115–123.DOI:10.1061/(ASCE)1084-0699(2000)5:2(115)

Govindaraju, R. (2000b): Artificial Neural Networks in hydrology. II: Hydrologic applications. J. Hydrol. Eng. 5/2. 124–137. DOI: 10.1061/(ASCE)1084-0699(2000) 5:2(124)

Horton, R. E. (1933): The role of infiltration in the hydrologic cycle. Trans. Am. Geophys. Union. 14th Ann. Mtg (1): 446–460. doi:10.1029/TR014i001p00446.

Jakab, B., Van Leeuwen, B., Tobak, Z. (2021): Detection of Plastic Greenhouses Using High Resolution Rgb Remote Sensing Data and Convolutional Neural Network. Journal of Environmental Geography. 14. 38–46. 10.2478/jengeo-2021-0004.

Kalinin, G. P., Milyukov, P. I. (1957): Raschete neustanovivshego- sya dvizheniya vody v otkrytykh ruslakh On the computation of un- steady flow in open channels. Met. i Gydrologia Zhurnal, 10, 10–18 Leningrad.

Lange, H., Sippel, S. (2020): Machine Learning Applications in Hydrology. In book: Forest-Water Interactions (233–257). 10.1007/978-3-030-26086-6_10.

Linacre, E. T. (1992): Data-sparse estimation of lake evaporation, using a simplified penman equation. Agricultural and Forest Meteorology 64, 237–256.

Liptay, Z. Á. (2018a): Jégmegjelenés előrejelzése a súlyozott középhőmérsékletek elve alapján a Duna hazai szakaszára. Hidrológiai Közlöny 98, 1, 25–32

Liptay, Z. Á. (2018b): Numerikus hidrológiai modellezés és folyami jégviszonyok előrejelzése. Pécsi Tudományegyetem, Pécs.

Liptay, Z. Á., Gauzer, B. (2021): Operational river ice and water temperature forecasting on the Hungarian Danube reach. FLOODrisk 2020 – 4th European Conference on Flood Risk Management, Science and practice for

an uncertain future. 10.3311/FloodRisk2020.17.11

Liu, B. Y. H., Jordan, R. C. (1960): The interrelationship and characteristic distribution of direct, diffuse and total solar radiation. Solar Energy 1960;4(3): 1

McCulloch, W. S., Pitts, W. (1943): A logic calculus of the ideas immanent in nervous activity. Bull. of Math. Biophys., 5, 115–133.

Mintz, Y., Walker, G. K. (1993): Global fields of soil moisture and land surface evapotranspiration derived from observed precipitation and surface air temperature. J. Appl. Meteorol., 32. 1305–1335.

Mohseni, O., Stefan, H. G. (1999): Stream temperature/air temperature relationship: a physical interpretation. Journal of Hydrology. 218, 128–141.

Nash, J. E. (1960): A unit hydrograph study, with particular reference to british catchments. Hydraulics Research Station, Department of Scientific and Industrial Research, p.n. 6433

Nusser, F. (1950): Gebiete gleicher Eisvorbereitungszeit an den deuschen Küsten. Deutsche Hydrographische Zeitschrift. 3, 3/4.

Oliphant, A., Susan, C., Grimmon, B., Schmid, H. P., Wayson, C. A. (2006): Local-scale heterogeneity of photosynthetically active radiation (PAR), absorbed PAR and net radiation as a function of topography, sky conditions and leaf area index. Remote Sensing of Environment. 103/324–337

Östman, C. J. (1950): Om sambandet mellan köldsummor, isläggning och istjocklek. Meddelanden iråan Sveriges meteorologiska och hydrologiska institut. Serie A. No 1.

Palosuo, E. (1951): Ice in the Baltic and the Meteorological Factors. Journal du Conceil International pour l'Exploration de la Mer. 17,2

Rabi, A., Hadzima-Nyarko, M., Sperac, M. (2015): Modelling river temperarure from air temperature: case of the River Drava (Croatia). Hydrological Sciences Journal. 60/9:1490–1507.
https://doi.org/10.1080/02626667.2014.914215

Rodhe, B. (1952): On the relation between air temperature and ice formation in the Baltic. Geografiska Annaler. 34, 175–202, Stockholm

Rodhe, B. (1955): A study of the correlation between the ice extent, the course of air temperature and the sea surface tenperature in the Åland Archipelago. Geografiska Annaler, 37, 141–163, Stockholm

Rosanblatt, F. (1957): The perceptron. A perceiving and recognizing automaton. Cornell Aeronautical Laboratory, Buffalo, New York.

Rumelhart, D. E., Hinton, G. E., Williams, R. J. (1986): Learning internal representations by error propagation. Parallel distributed processing, MIT Press, Cambridge. 1, 318–362.

Starosolszky, Ö. (1969): A jég a vízépítésben. Vízgazdálkodási Tudományos Kutató Intézet. Budapest.

Stefan, J. (1879): Über die beziehung zwischen der wärmestrahlung und der temperatur. Wiener Ber. II 79, 391 (1879)

Szilagyi, J. (2006): Discrete State-Space Approximation of the Continuous Kalinin-Milyukov-Nash Cascade of Noninteger Storage Elements. Journal of Hydrology. 328. 132–140. 10.1016/j.jhydrol.2005.12.015.

Tanty, R., Desmukh, T. (2015): Application of Artificial Neural Network in Hydrology – A Review. International Journal of Engineering Research and. 4/6. DOI: 10.17577/IJERTV4IS060247.

Temizyurek, M., Dadaşer-Çelik, F. (2018): Modelling the effects of meteorological parameters on water temperature using artificial neural networks. Water Sci Technol. 77(5–6):1724–1733. doi: 10.2166/wst.2018.058.

Thornthwaite, C. W. (1948): An approach toward a rational classification of climate. Geographical Review 38, 55–94

Van Leeuwen, B., Tobak, Z., Kovács, F. (2020): Machine Learning Techniques for Land Use/Land Cover Classification of Medium Resolution Optical Satellite Imagery Focusing on Temporary Inundated Areas. Journal of Environmental Geography. 13. 43–52. 10.2478/jengeo-2020-0005.

Zhu, S., Nyarko, E. K., Hadzima-Nyarko, M. (2018): Modelling daily water temperature from air temperature for the Missouri River. PeerJ 6:e4894; http://doi.org/10.7717/peerj.4894

Zhu, S., Nyarko, E. K., Hadzima-Nyarko, M., Heddam, S., Wu, S. (2019): Assessing the performance of a suite of machine learning models for daily river water temperature prediction. PeerJ. 7:e7065. http://doi.org/10.7717/peerj.7065

Zoltan Arpad Liptay, PhD (*corresponding author, e-mail: liptay.zoltan@ovf.hu)
Hungarian Hydrological Forecasting Service
General Directorate of Water Management
Márvány u. 1/d.
1012 Budapest
Hungary

DOI: 10.31577/ahs-2022-0023.02.0022

ACTA HYDROLOGICA SLOVACA

Volume 23, No. 2, 2022, 197–206

Trend changes and frequency analysis of the annual maximum volumes for various runoff duration on the Morava River at Moravský Svätý Ján

Veronika BAČOVÁ MITKOVÁ*

In the present paper we analyzed, the occurrence of annual maximum runoff volumes with t-day durations for a 99-year series (1920–2020) of mean daily discharge of the Morava River at Moravský Svätý Ján gauge (Slovakia). The runoff volume is, apart from the peak runoff, another very important hydrological characteristic of a river for flood hazard assessment. The maximum runoff volumes with *t*-day duration were determined. Subsequently, trends of the annual maximum runoff volumes with *t*-day durations were identified. We analyzed how the annual maximum runoff volumes of the Morava River have changed over the period 1922–2020 and how they have changed over dry and wet periods. The results indicate that the trends of the annual maximum runoff volumes with *t*-day durations decrease, especially in wet periods. On the Morava River usually the maximum annual discharges occur simultaneously with the annual maximum runoff volume of waves with a given duration *t*. However, the corresponding values in terms of significance are not equivalent. Based on the exceeding probability curves of the annual maximum runoff volumes, it is possible to determine to the selected volume V_{tmax} for different t-days the probability of its exceeding and return period. The Log-Pearson distribution type III was used to determine the T-year values of the maximum runoff volumes with t-day duration.

KEY WORDS: The Danube River, wave volume, Log-Pearson III probability distribution, *T*-year volume

Introduction

In the scientific and public spaces, there are ongoing discussions about the impact of climate change on the hydrological river regime and the frequency of extreme hydrological events (floods and drought). The confirmation or refutation of this information is only possible through statistical processing of long-term data series of the hydrological and meteorological cycle. Assessment of the impact of the notified climate change on the river regime and runoff of rivers from the basins has been a frequently discussed subject in many scientific studies (Bronstert et al., 2007; Szépszó et al., 2014; Pekárová et. al., 2016; Gaume et. al., 2016; Blöschl et al., 2017 and 2019; Didovetz, et al., 2019; Szolgay, et al., 2020). Some issues in water management and engineering hydrology require that peak discharge and the shape of a flood wave or a flood runoff volume are known. Not only high water level or peak discharge can cause damage to a protective dam, but also, the long-term high volumes – wetting, or overspill, e.g. two flood waves joining at the confluence. Such a situation was seen in the spring of 1941 on the River Morava when the flood lasted more than 2.5 months and the volume was almost twice as large as the volume of the flood wave in 1997 with an almost identical culmination. In applied hydrology, it is often difficult to assign exact values of a flood wave volume to a particular probability of exceedance and hence to its corresponding T-year discharges. Such relationships are very irregular in nature, so a flood wave hydrograph of a given exceedance probability must be a priory known. The work of the collective Hladný et al., (1970) dealt with the processing of volumes of flood waves from stations throughout the territory of Czechoslovakia. To define the volumes of individual waves, the authors introduced the parameter *t*. The parameter defines the duration of the flood wave in days. In this way, they determined maximum runoff volumes lasting 2-, 5-, 10- and 30-days. The statistical data series were compiled from the maximum annual volumes of the given duration. For the extrapolation of the T-year volumes, they used theoretical lognormal probability distribution.

Zatkalík (1970) dealt with similar processing of the calculation of the maximum volumes of the Danube. The author calculated maximum runoff volumes based on the maximum runoff duration *t*.

The introduction of the *t* parameter allows:

1) a clear assessment of the probability of exceedance of the volume of a selected flood wave,
2) to create a serious basis for solving the well-known design flood problem, which would be appropriate in assigning a volume that would be maximum for the given *T*-year culmination discharge.

Since a 99-year series of the mean daily discharge of the Morava River at Moravský Svätý Ján (Moravský Sv. Ján) gauging station is available from SHMI archives and yearbooks. Therefore, we could calculate the 99-year series of the highest (annually) 5-, 10-, 15-, and 30-consecutive days' wave volumes. Then their trends and probability distribution were analysed. The whole time data series was subsequently divided into dry and wet periods and changes in their trends were analysed.
The aim of this study is:

- assess the maximum annual runoff volumes V_{tmax} lasting 5-, 10-, 15-, and 30-days of the waves which belong to annual maximum discharges of the Morava River at Moravský Sv. Ján (1922–2020);
- analyze changes in the maximum annual runoff volumes V_{tmax} of the Morava River at Moravský Sv. Ján during the period (1922–2020);
- analyze the changes in the maximum annual runoff volumes V_{tmax} in wet and dry periods during the period 1922–2020;
- determine the theoretical exceedance probability curves;
- estimate the *T*-year annual maximum runoff volumes with *t*-day durations belonging to annual maximum discharges.

Methods and material

Determination of the maximum runoff volumes with t-day duration

In the present paper for determining the maximum annual runoff volumes (V_{tmax}) we used the procedure published in Zatkalík (1970). The hydrological events belonging to annual maximum discharges were selected for the set of volumes. To determine the volume of the wave belonging to annual maximum discharge, it is necessary to identify the beginning and end of the wave. It is quite difficult to identify the beginning and end of the discharge wave, in some cases. For such events, their beginning and their end approximately at the level of the long-term average daily discharge were determined. The series of mean daily discharges were used as input data to calculate volumes of the selected waves for given *t*-days durations. Next, the moving averages of the volume around the peak discharge for given *t*-days durations were calculated and the maximum volumes were selected. For example, in the case of t=10 days duration, ten daily move averages were calculated around the culmination. Consequently, only one maximum value was included into the statistical data set for analysis of maximum runoff volumes with t=10 days runoff duration. The detailed descriptions of the method are published in Mitková, et al. (2002) or Bačová Mitková and Halmová (2021). Fig. 1. illustrates an example of the determination of maximum volumes with a given runoff duration of t=10-days.

Trend detection in selected hydrological data series

The Mann-Kendall nonparametric test (M-K test) we used for the detection of trends in hydrological time series. The purpose of the Mann-Kendall (MK) test (Mann, 1945; Kendall, 1975; Gilbert, 1987) is statistically assessed if there is a monotonic upward or downward trend of the variable of interest over time. A monotonic upward (downward) trend means that the variable consistently increases (decreases) through time, but the trend may or may not be linear. The presence of a statistically significant trend is evaluated using the Z value. A positive (negative) value of Z indicates an upward (downward) trend. The statistic Z has a normal distribution. To test for either an upward or a downward monotone trend (a two-tailed test) at α level of significance, hypothesis *H0* (no trend) is rejected if the absolute value of $|Z|$ is greater than Z_1-$\alpha/2$, where Z_1-$\alpha/2$ is obtained from the standard normal cumulative distribution tables. The significance level of 0.001 means that there is a 0.1% probability that the value of x_i is from a random distribution and are likely to make a mistake if we reject hypothesis *H0*. The sig significance level of 0.1 means that there is a 10% probability that we make a mistake if we reject hypothesis *H0*. If the absolute value of Z is less than the level of significance, there is no trend. For the four tested significance levels the following symbols are used in the template:

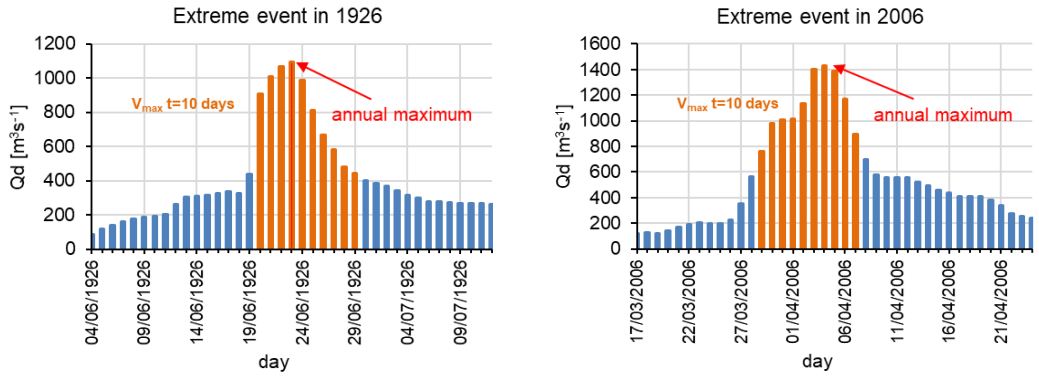

Fig. 1. Illustration of the determination of the maximum volume with a given runoff duration t=10 days on the Morava River at Moravský Sv. Ján (floods occurred in July 1926 and March–April 2006).

*** if trend at α = 0.001 level of significance – *H0* seems to be impossible
** if trend at α = 0.01 level of significance
* if trend at α = 0.05 level of significance – 5% mistake if we reject the *H0*
+ if trend at α = 0.1 level of significance
Blank: the significance level is greater than 0.1, cannot be excluded that the *H0* is true.

The most significant trend is assigned three stars (***), with a gradual decrease in importance, the number of stars also decreases.
For n (number of tested values) ≥ 10, the statistic S is approximately normally distributed with the mean and variance as follow

$$E(S) = 0 \tag{1}$$

$$VAR(S) = \frac{1}{18}\left[n(n-1)(n-2) - \sum_{p=1}^{q} t_p(t_p-1)(2t_p+5) \right] \tag{2}$$

where:
q – is the number of tied groups,
t_p – the number of data values in the p group.

Estimation of the T-year annual maximum runoff volumes

The maximum annual runoff volume V_{tmax} series were fitted with Log-Pearson type III distribution. The Log-Pearson distribution type III. is used to estimate the extrema in many natural processes and it is one of the most commonly used probability distributions in hydrology (Bobee, 1975; Pilon and Adamowski, 1993; Griffis and Stedinger, 2007; Pawar and Hire, 2018). For example, in the United States, since 1967, experts often choose this distribution as "The distribution of choice for floods" (Koutsoyiannis, 2005). The Log-Pearson Type III distribution is a three-parameter gamma distribution with a logarithmic transformation of the variable. The cumulative distribution function and probability distribution function according to Hosking and Wallis (1997) are defined as:

If $\gamma \neq 0$ let α=4/ γ2 and ξ=μ-2σ/ γ

If γ >0 then:

$$F(x) = G(\alpha, \tfrac{x-\xi}{\beta})/\Gamma(\alpha) \tag{3}$$

$$f(x) = \frac{(x-\xi)^{\alpha-1} e^{-(x-\xi)/\beta}}{\beta^{\alpha}\Gamma(\alpha)}, \tag{4}$$

where:
ξ – location parameter,
α – shape parameter,
β – scale parameter,
Γ – Gamma function.

If γ <0 then

$$F(x) = 1 - \frac{G\left(\alpha, \frac{x-\xi}{\beta}\right)}{\Gamma(\alpha)}, \tag{5}$$

$$f(x) = \frac{(\xi-x)^{\alpha-1} e^{-(\xi-x)/\beta}}{\beta^{\alpha}\Gamma(\alpha)}. \tag{6}$$

To estimate the distribution parameters, the method described in Bulletin17B (IACWD, 1982) was used. Bulletin 17B provided revised procedures for weighting station skew values with results from a generalized skew study, detecting and treating outliers, making two station comparisons, and computing confidence limits of the frequency curve.
The Kolmogorov-Smirnov test was performed to test the assumption that the discharge magnitudes follow the theoretical distributions. The p-value (p≥0.05) was used as a criterion for the rejection of the proposed distribution hypothesis. The second criterion was the comparison between the theoretical distribution and the empirical distribution of the data series. Probability estimates are calculated for chosen plotting positions. A basic plotting position formula for symmetrical distributions is given by (7):

$$Pi = \frac{m-\alpha}{N+1-2\alpha}. \tag{7}$$

where:
p_i – is the exceedance probability of the variable (V_{tmax}),
α – is a plotting position parameter ($0 \leq \alpha \geq 0.5$),
m – is the order number of the variable (descending rank),
N – is number of variables.

The relationship between the probability of exceedance of a given value in any year and its average return period T is (Szolgay et al., 1994):

$$p = 1 - e\text{-}1/T. \tag{8}$$

If $T \geq 10$ we can use simplified form of equation (8):

$$P = \frac{m}{T}. \tag{9}$$

where:
m –variable order number- descending order to the statistical series,
n – number of variables.

The Morava River and Input data

The Morava River originates on the Králický Sněžník mountain in the north-eastern corner of Pardubice Region an elevation 1 380 m n. m. (Czechia). It is the main river of Czech region Moravia, which derives its name from it The Morava River is a left tributary of the Danube River. The basin covers an area of 26 658 km^2 and a length is 352 km. Morava River has a vaguely southward trajectory. The lower part of the river's course forms the border between the Czech Republic and Slovakia and

then between Austria and Slovakia (Fig. 2).
The mean daily discharges (Fig. 3) and maximum annual discharges (Fig. 4a) of the Morava River at Moravský Sv. Ján from the period 1922–2020 were used as input data for analysis. The mean long-term daily discharges reached the value of 104.41 $m^3 s^{-1}$ (1922–2020) at Moravsky Ján gauge station.
The course of annual maximum discharges, long-term

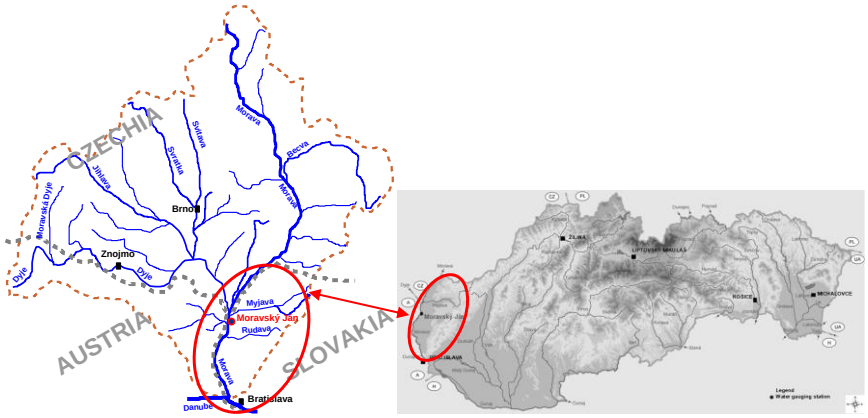

Fig. 2. Scheme of the Morava river basin and the location of the Slovak part of the Morava River basin.

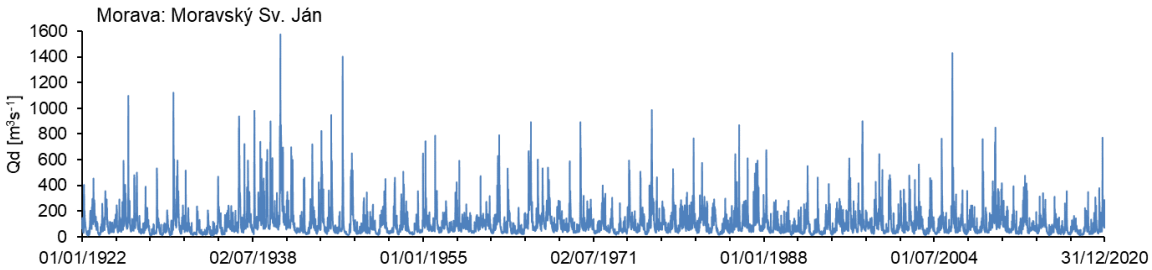

Fig. 3. The mean daily discharges of the Morava River at Moravský Sv. Ján (1922–2020).

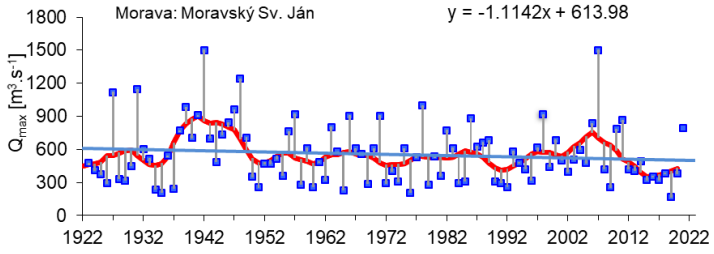

a)

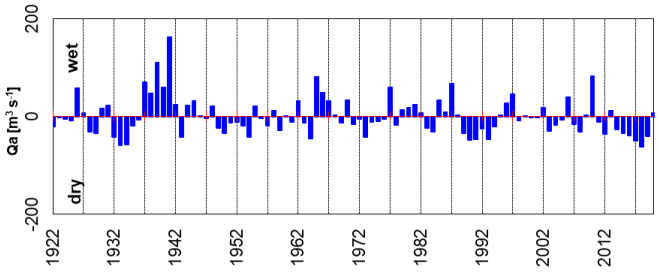

b)

Fig. 4. a) the maximum annual discharges of the Morava River at Moravský Sv. Ján (1922–2020), their linear trend and 5-year moving trend b) the deviation annual discharges from long-term annual discharge during the period of 1922–2020.

linear trend and 5-year moving trend are illustrated in Fig. 4a. The annual peak discharges of the Morava River at Moravský Sv. Ján show a slightly decreasing long-term linear trend during the selected period of 1922–2020. There also occurred some extreme floods above 1000 m^3s^{-1} (in 1926, 1930, 1941 or 2006 (Figure 4a). The largest one was in 2006 with a maximum discharge value of 1502 m^3s^{-1}. Fig. 4b shows several consecutive dry and wet years at intervals lasting approximately five or six years. The minimum annual discharge occurred in 2018 (43.82 m^3s^{-1}). From year 2011 to the year 2020 were recorded especially dry years (except 2013 and 2020). Fig. 5 illustrates the distribution of the annual maximum discharges occurrence in individual months during the period of 1922–2020 and in dry and wet years. The maximum number of the events with annual maximum discharges occurs in the month of March. It can be caused by spring rainfall in the middle and southern part of the basin and snowmelt, especially in the northern part of the basin (Fig. 5).

In the second part of the work, the sets of data were divided into two sub-sets based on dry and wet multiannual periods. The dry and wet periods we determined based on double 5-year moving averages of the Morava River discharges at Moravský Sv. Ján for the analyzed period 1922–2020 (Fig. 6). The wetness of individual years is different and more or less independent of each other. It is to be understood that the various physical causes also distort the action of the decisive factors to such an extent that we can speak of randomness. According to this, but also from experience, we can say that years of a similar nature usually group together, (Dub, 1957). The limit value for determining the dry and wet periods was the value of the long-term average annual discharge Q_a=104.41 m^3s^{-1}. Because we took the period as a result of the moving average, dry and wet years can also occur in it. The number of 42 years was included in the dry period and the number of 57 years in the wet period (Fig. 6). Fig. 6 also shows that from 2011 to 2019 the dry period is recorded.

Results and discussion

Based on the mentioned method, the waves that belong to the maximum annual discharge were selected. The mean daily discharges and the maximum annual discharges of the Morava River at Moravský Sv. Ján from the period 1922–2020 were used as input data for analysis. Subsequently, maximum annual runoff volume series for various duration of the discharge were calculated (Fig. 7). The maximum annual runoff volume was calculated for runoff
durations 5-, 10-, 15- and 30-days. Considering all the analysed t-days runoff durations the annual maximum runoff volume of the flood in 1941 was the highest one. Considering the runoff durations of about 10-days and 15-days the lowest annual maximum runoff volumes reached the event belong to annual maximum discharge in 2018, within the period of 1922–2020. On the Morava River usually the maximum

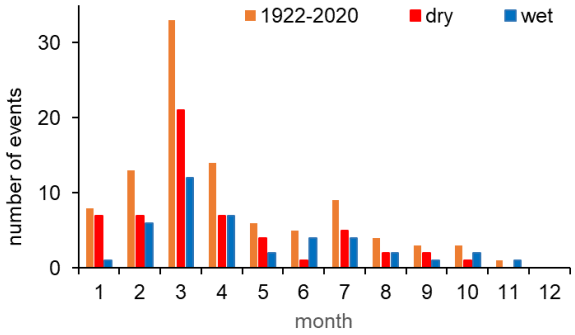

Fig. 5. Monthly distribution of the annual maximum discharges of the Morava River at Moravský Sv. Ján during the period of 1922–2020, for the dry and the wet years.

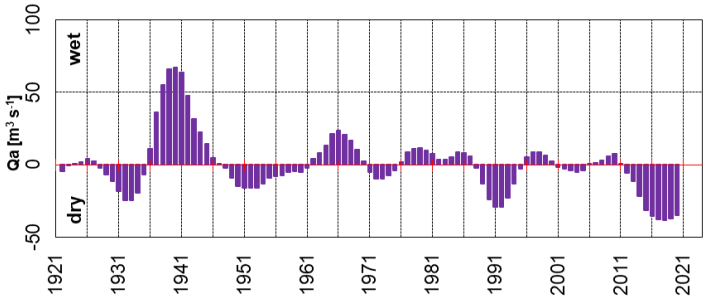

Fig. 6. Course of the dry and wet periods based on double 5-year moving averages of Morava discharges at Moravský Sv. Ján for the period 1922–2020.

annual discharge occurs simultaneously with the annual maximum runoff volume of waves with a given time duration *t*. The correlation of the annual maximum discharge and maximum annual runoff volume for selected runoff durations range between 0.90 (V_{30max}) and 0.97 (V_{5max}).

For example, correlations between Q_{max} and V_{tmax} range in similar values like the Danube River (Bratislava). On the other, hand the correlation between Q_{max} and V_{tmax} ranges from 0.76 to 0.59 for the Hron River (Banská Bystrica) and from 0.89 to 0.56 for the Váh River (Liptovský Mikuláš) (Pekárová et al. 2018).

The analyses of the long-term trends of V_{tmax} on some selected rivers in Slovakia (Topľa: Hanušovce, Váh: Liptovský Mikuláš Hron: Banská Bystrica and Hron: Brehy and Dunaj: Bratislava) showed that the annual maximum discharges and the annual maximum runoff volumes V_{tmax} with various duration of the runoff have decreasing trends for Topľa: Hanušovce and Hron: Banská Bystrica. (Bačová and Pekárová, 2020; Bačová Mitková, 2022). The trend analysis of the annual maximum runoff volumes V_{tmax} for Danube: Bratislava showed that the runoff volume regime during floods has not changed substantially during the last 134-years (Halmova et al., 2008) resp. 144 years (Bačová Mitková and Halmová, 2021).

Trend analysis of annual maximum runoff volumes V_{tmax} on the Morava River at Moravský Sv. Ján (1922–2020)

The M-K trend test shows significant long-term trends in annual maximum runoff volumes for the runoff duration of above 5 days. We can reject the hypothesis *H0* at significance levels α=0.1 (V_{5max}) and α=0.05 (V_{10max}, V_{15max} and V_{30max}), for the data period 1922–2020 (Table 1). The long-term trends of the M-K test for annual maximum runoff volumes with analysed durations *t*=10 days and *t*=30 days of the Morava River at Moravský Sv. Ján (1922–2020) are illustrated in Fig. 8. The trend analysis of the dry and the wet periods shows significant decreasing long-term trends in annual maximum runoff volumes in the wet period. We can reject the hypothesis *H0* at significance levels α=0.01 (V_{5max}, V_{10max}, V_{15max} and V_{30max}), for the data period of 1922–2020 (Table 2). The trend analysis of the dry period did not show any significant trends. Similar results were achieved for trend analysis of the dry and the wet years.

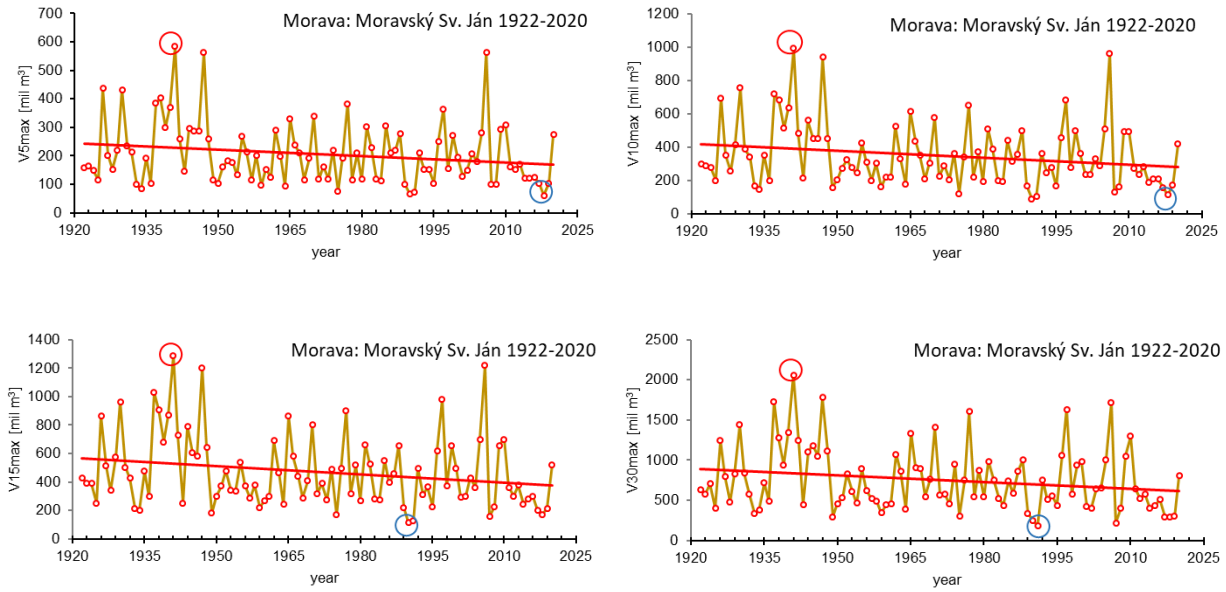

Fig. 7. Maximum annual volume series V_{tmax} of the Morava for various flood duration t (e.g. V_{20max} means maximal annual runoff volume in 20 days).

Table 1. Conclusions of Mann-Kendall trend test for annual maximum runoff volumes V_{tmax} with time duration *t* for waves belong to annual maximum discharges of the Morava River at Moravský Sv. Ján (1922–2020)

				Mann-Kendall trend		Sen's slope estimate	
V_{tmax} [mil m^3]	First year	Last Year	*n*	Test Z	Signific.	A	B
V_{5max}	1922	2020	99	-1.89	+	-0.59	213.5
V_{10max}	1922	2020	99	-2.20	*	-1.16	360.2
V_{15max}	1922	2020	99	-2.26	*	-1.66	496.7
V_{30max}	1922	2020	99	-2.13	*	-2.34	746.5

*(A, B are parameters of the linear trend line y = A*x+B, A is slope of the trend line)*

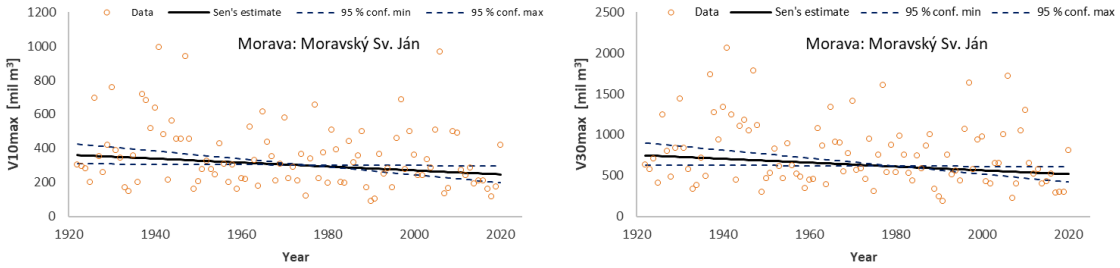

Fig. 8. Graphical results of Mann-Kendall trend test for annual maximum runoff volumes V_{tmax} with time durations t=10 days and t=30 days for waves belong to annual maximum discharges of the Morava River at Moravský Sv. Ján (1922–2020)

Table 2. Conclusions of Mann-Kendall trend test for annual maximum runoff volumes V_{tmax} with time duration *t* for waves belong to annual maximum discharges in wet periods of the Morava River at Moravský Sv. Ján (1922–2020)

				Mann-Kendall trend	Sen's slope estimate
V_{tmax} [mil m^3]	n	Test Z	Signific.	A	B
V_{5max}	57	-2.64	**	-2.72	293.8
V_{10max}	57	-3.13	**	-5.03	520.3
V_{15max}	57	-3.15	**	-6.99	695.4
V_{30max}	57	-3.20	**	-10.99	1120.5

*(A, B are parameters of the linear trend line y = A*x+B, A is slope of the trend line)*

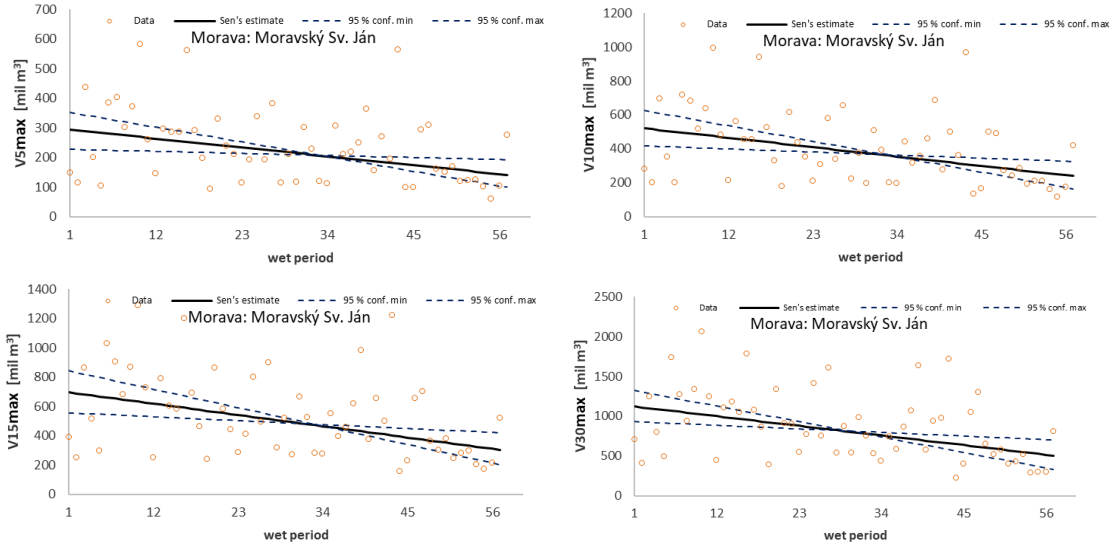

Fig. 9. The Mann-Kendall trend test for annual maximum runoff volumes V_{tmax} with runoff durations t=5-, 10-, 15-, and 30-days for waves belonging to annual maximum discharges of the Morava River at Moravský Sv. Ján (wet period).

Estimation of the T-year annual maximum runoff volumes V_{tmax} on the Morava River at Moravský Sv. Ján (1922–2020)

The estimation of the *T*-year annual maximum runoff volumes V_{tmax} with various duration of the runoff values by Log-Pearson III type probability distribution are presented in this part of the contribution. The frequency curve spreadsheet version 3.06 of IACWD, (1982) and bulletin of Flynn and al. (2006) were used to estimate the parameters of distribution function.

The calculated volumes were plotted on a log-probability scale. Fig. 9 illustrates theoretical exceedance curves of annual maximum runoff volumes with selected runoff durations on the Morava River at Moravský Sv. Ján during the period of 1922–2020.

The results suggest that for Q_{max} with T=100 years the annual maximum runoff volumes for analysed runoff duration with return period $T=100$ years are estimated at value 278 mil m^3 (V_{10max}), 238 mil. m^3 (V_{5max}), and 1098 mil. m^3 (V_{10max}) and at value 1708 mil m^3 (V_{15max}) (Table 3).

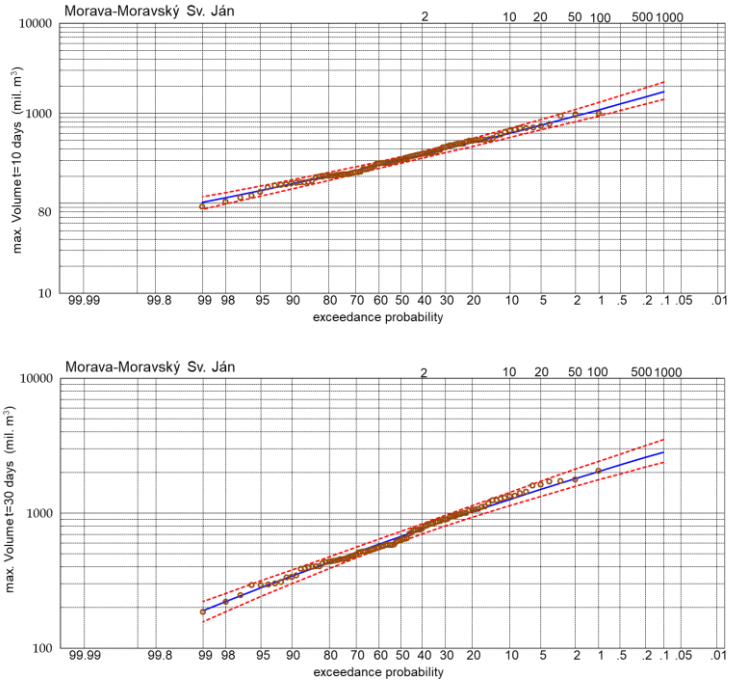

Fig. 10. Examples of the theoretical LPIII exceedance probability curves of the Morava maximum annual runoff volumes V_{10max}, and V_{13max} for Morava: Moravský Sv. Ján (1922–2020).

Table 3. ***T-year maximum discharges Q_{max} and T-year annual maximum runoff volumes V_{tmax} of the Morava River at Moravský Sv. Ján (1922–2020) (Log-Pearson III) ($P=p*100\%$; $p=1-e^{-1/T}$)***

River: Gauging station	Q_T [m^3 s^{-1}]	P [-]	t=5 days	t=10 days	t=15 days	t=30 days
Morava: Moravský Sv. Ján	Q_{50}	0.02	V_{50tmax} [mil. m^3]			
	1403.0		542.75	935.21	1254.45	1808.44
	Q_{100}	0.01	$V_{100tmax}$ [mil. m^3]			
	1631.0		638.21	1098.19	1472.03	2042.57
	Q_{500}	0.002	$V_{500tmax}$ [mil. m^3]			
	2232.0		895.28	1533.35	2049.81	2596.88
	Q_{1000}	0.001	$V_{1000tmax}$ [mil. m^3]			
	2524.0		1023.51	1748.61	2334.08	2841.53

Conclusion

In the present paper we analyzed, the occurrence of annual maximum runoff volumes with *t*-day durations for a 99-year series of mean daily discharges of the Morava River at Moravský Sv. Ján (Slovakia). The statistical methods were used to clarify how the maximum runoff volumes of the Morava River at Moravský Sv. Ján changed over the period 1922–2020 and over dry and wet periods. The M-K tests showed no significant trend in annual maximum discharges. The trend analysis of the annual maximum runoff volumes shows significant long-term trends in annual maximum runoff volumes for the runoff duration above 5 days. We can reject the hypothesis *H0* at significance levels α=0.1 (V_{5max}) and α=0.05 (V_{10max} and V_{15max}), for the data period 1922–2020. Based on the M-K test we can conclude that the runoff volume regime during floods has changed during the last 99 years, which is of importance to water management. This conclusion pertains not only to the short-term flood runoff episodes (V_{2max}), but also to the long-term ones (V_{30max}). Trend analysis of the dry and wet periods (also years) showed significant decreasing long-term trends in annual maximum runoff volumes in the wet period at significance levels α=0.01. It means, that there is a 5% resp. 1% portability that we make a mistake if we reject hypothesis *H0*. The result showed that the maximum annual discharges usually occur with the annual maximum runoff volume of waves with a given time duration *t*. However, the corresponding values in terms of significance are not equivalent. Based on the exceeding probability curves of the annual maximum runoff volumes, it is possible to determine the selected volume *V* for different *t* the probability of its exceeding and return period.

The second part of the paper dealt with estimating

the *T*-year annual maximum runoff volumes V_{tmax} on the Morava River at Moravský Sv. Ján for the period 1922–2020. For the estimation of *T*-year annual maximum runoff volumes V_{tmax} we used the Log-Pearson Type III distribution function. The results showed the high sensitivity of the LP3 distribution to extremes of the dataset. The Log-Pearson III distribution fits well with the observed data and it is an appropriate mathematical tool for estimating the design values with long return periods.

The results are useful in water planning and flood protection and can help mapping flood risk areas and develop river management plans in the Morava River basin. In frequency analyses, it is important to note, that the process is never-ending and, if anything, will change according to catchment; thus, it is necessary to recalculate distribution curves and define new design discharges for recent periods for particular stations.

Acknowledges

This work was supported by the project VEGA No. 2/0004/19 "Analysis of changes in surface water balance and harmonization of design discharge calculations for estimation of flood and drought risks in the Carpathian region".

References

Bačová Mitková, V., Pekárová, P. (2020): Analysis of Maximum Runoff Volumes with Different Time Durations of Flood Waves: A Case Study on Topľa River in Slovakia. In IOP Conference Series: Earth and Environmental Science: 5th World Multidisciplinary Earth Sciences Symposium, WMESS 2019; Prague; Czech Republic; 9 September 2019 through 13 September 2019. – Prague, vol. 362, iss. 1, art. no. 012013. doi.org/10.1088/1755-1315/362/1/012013

Bačová Mitková, V., Halmová, D. (2021): Analyzing changes and frequency distribution in maximum runoff volumes with different duration of the Danube River at Bratislava. In Acta Hydrologica Slovaca, 2021, vol. 22, no. 1, 50–60. doi.org/10.31577/ahs-2021-0022.01.0006

Bačová Mitková, V. (2022): Estimation, trend detection and temporal changes in maximum annual discharge volume series of the Hron River in Slovakia. In Acta Hydrologica Slovaca, 2022, vol. 23, no. 1, 42–51. doi.org/10.31577/ahs-2022-0023.01.0005

Blöschl, G. et al. (2017): Changing climate shifts timing of European floods. Science 357, 588–590. DOI: 10.1126/science.ann2506

Blöschl, G., Hall, J., Viglione, A. et al. (2019): Changing climate both increases and decreases European river floods. Nature 573, 108–111. https://doi.org/10.1038/s41586-019-1495-6

Bobee, B. (1975): The Log Pearson Type 3 Distribution and Its Application in Hydrology. Water Resources Research, Vol. 11, No. 5, 681–689.

Bronstert, A., Kolokotronis, V., Schwandt, D., (2007): H. Straub Comparison and evaluation of regional climate scenarios for hydrological impact analysis: general scheme and application example Int. J. Climatol., 27, 1579–1594, 10.1002/joc.1621

Didovets, I., Krysanova, V., Bürger, G., Snizhko, S., Balabukh, V., Bronstert, A. (2019): Climate change impact on regional floods in the Carpathian region. Journal of Hydrology: Regional Studies, 22, 100590. doi.org/10.1016/j.ejrh.2019.01.002

Dub, O. (1957): Hydrológia, Hydrografia, Hydrometria. Sloveské vydavateľstvo technickej literatúry. Bratislava, 266 p.

Flynn, K. M., Kirby, W. H., Hummel, P. R. (2006): User's Manual for Program Peakfq, Annual Flood-Frequency Analysis Us-ing Bulletin 17b Guidelines; U.S. Geological Survey: Reston, VA, USA, 2328–7055

Gaume, E., Borga, M., Llassat, M. C., Maouche, S., Lang, M., Diakakis, M. (2016): Mediterranean extreme floods and flashfloods. The Mediterranean Region under Climate Change. AScientific Update, IRD Editions, 133–144, Coll. Synthèses, 978-2-7099-2219-7. hal-01465740v2

Gilbert, R. O. (1987): Statistical Methods for Environmental Pollution Monitoring. John Wiley & Sons, Inc., New York.

Griffis, V. W., Stedinger, J. R. (2007): The Log-Pearson type III distribution and its application in flood frequency analysis. I: Distribution characteristics. J. of Hydrologic Engineering, 12, 5, 482–491.

Halmova, D., Pekarova, P., Pekar, J., Onderka, M. (2008): Analyzing temporal changes in maximum runoff volume series of the Danube River. IOP Conf. Series: Earth and Environmental Science 4, IOP Publishing. 1–8. doi:10.1088/1755-1307/4/1/012007.

Hosking, J. R. M., Wallis, J. R. (1997): Regional Frequency Analysis. Cambridge University Press. Cambridge.

Hladný, J., Doležal, F., Makeľ, M., Sacherová, D. (1970): Peak runoff volumes of a given duration (in Czech) Hydrological conditions of the CSSR Volume III.

IACWD (1982): Guidelines for determining flood discharge frequency, Bulletin 17-B. Technical report, Interagency Committee on Water Data, Hydrology Subcommittee. 194 p.

Kendall, M. G. (1975): Rank Correlation Methods, 4th edition, Charles Griffin, London.

Koutsoyiannis, D. (2005): Uncertainty, entropy, scaling and hydrological statistics. Hydrological Sciences Journal, 50, 3, 381–404.

Mann, H. B. (1945): Non-parametric tests against trend, Econometrica 13: 163–171.

Mitková, V., Pekárová, P., Babiaková, G. (2002): Maximálne objemy odtoku Dunaja daného trvania v suchých a vodných obdobiach (Maximum runoff volumes of the Danube of a given duration in dry and water periods). In Acta Hydrologica Slovaca, Vol. 3, No. 2, 185–191. ISSN 1335–6291. (In Slovak)

Pawar, U.; Hire, P. (2018): Flood Frequency Analysis of the Mahi Basin by Using Log Pearson Type III Probability Distribution. Hydrospatial Analysis 2(2), 102–112. Dx.doi. org/10.21523/gcj3.

Pekárová, P., Bačová Mitková, V. Pekár J., Miklánek P., Halmová D., Liova S. (2018): Historical food on the territory of Slovakia and their importance in hydrology. (In Slovak: Historické povodne na území Slovenska a ich význam v hydrológii. Bratislava: Veda, SAS, 135 p. ISBN 978 -80-224-1684-9.

Pekárová, P., Pramuk, B., Halmová, D., Miklánek, P., Prohaska, S., Pekár, J. (2016): Identification of long-term high-flow regime changes in selected stations along the Danube River. In Journal of Hydrology and Hydromechanics, 2016, vol. 64, no. 4, 393–403.

Pilon, P. J., Adamowski, K. (1993): Asymptotic variance of flood quantile in log Pearson type III distribution with historical information, J. of Hydrol., 143, 3–4, 481–503.

Szépszó, G., Lingemann, I., Klein, B., Kovácz, M. (2014):

Impact of climate change on hydrological conditions of Rhine and Upper Danube rivers based on the results of regional climate and hydrological models. Nat Hazards 72, 241–262. https://doi.org/10.1007/s11069-013-0987-1.

Szolgay, J., Blöschl, G., Gribovszki, Z., Parajka, J. (2020): Hydrology of the Carpathian Basin: interactions of climatic drivers and hydrological processes on local and regional scales – HydroCarpath Research. J. Hydrol. Hydromech., 68, 2, 128–133. DOI: 10.2478/johh-2020-0017

Szolgay, J., Dzubák, M., Hlavčová, K. (1994): Hydrology. Runoff process and surface water hydrology. STU v Bratislave, 277p. (In Slovak: Hydrológia. Odtokový proces a hydrológia povrchových vôd.)

Zatkalík, G. (1970): Calculation of the basic parameters of the discharge waves. PhD. thesis. 71 p. (In Slovak)

Ing. Veronika Bačová Mitková, PhD. (*corresponding author, e-mail: mitkova@uh.savba.sk)
Institute of Hydrology SAS
Dúbravská cesta 9
841 04 Bratislava
Slovak Republic

DOI: 10.31577/ahs-2022-0023.02.0023

ACTA HYDROLOGICA SLOVACA

Volume 23, No. 2, 2022, 207–216

Impact of climate change and human factors on the water regime of the Danube Delta

Viktor VYSHNEVSKYI*, Serhii SHEVCHUK

Climate changes in the Danube Delta, as well as changes in water temperature, water runoff and sediment yield, have been identified on the basis of available observational data. It has been shown that the intra-annual distribution of water runoff has become more uniform in recent decades. It decreased in April-May and increased in February-March. At the same time, there has been a significant decrease in sediment transport. Changes due to anthropogenic impact were detected in water runoff in the largest river branches, in particular, the reduction of the share of the Kiliyskyi branch. Over the past 60 years, the water temperature in the Danube Delta has increased significantly, by more than 2°C. In general, the water temperature is higher than the air temperature, especially in autumn. Some features of the delta formation have been identified.

KEY WORDS: the Danube River; delta, water discharge, sediment yield, air and water temperature

Introduction

The Danube is the second largest river in Europe in terms of catchment area, length and water runoff. At the same time, the Danube River is the most international river in the world, with a catchment area of 19 countries. 10 of these countries have direct access to the Danube River. An important feature of the Danube River is the presence of the large delta, which is the second largest in Europe after the Volga Delta (Olson and Krug, 2020).

It is concidered (Panin and Jipa, 2002; Olson and Krug, 2020; The Lower Danube River..., 2022) that the catchment area of the Danube River is 817,000 km^2 and the length is 2860 km. There are also slightly different data (Habersack et al., 2013; Stagl and Hattermann, 2015; Romanova et al., 2019), but the difference is small.

The water regime of the Danube River and, in particular its delta, largely depends on climate, which is unstable. Many papers (Webb and Nobilis, 2007; Pekarova et al., 2008; Marin et al., 2014; Vyshnevskyi and Donich, 2021) contain information on air temperature increase within the Danube River catchment area. At the same time, the results of studies on precipitation show that there are no significant changes (Marin et al., 2014; Vyshnevskyi and Donich, 2021).

There are many scientific works devoted to the Danube Delta itself (Panin and Jipa, 2002; Hydrology..., 2004; Gastescu, 2009; Gatejel, 2018; Tanasescu and Constantinescu, 2020; Covaliov et al., 2022).

One of the most important issues is the delta size. According to the data (Hydrology..., 2004), its area is estimated at 4200 km^2, including the Ukrainian part – 830 km^2, the Romanian one – 3370 km^2. Some other data about the delta area (4152 km^2) and its Romanian part (3446 km^2) are given in the paper (Olson and Krug, 2020). If we consider the Razim-Sinoe lagoon as part of the Danube Delta, its total area reaches 5165 km^2 (Olson and Krug, 2020). In general, the boundaries of the delta and, accordingly, its area are somewhat debatable.

The important issue of the lower course of the Danube River is water runoff and its distribution by the delta branches. This issue is considered in the works (Mikhailova et al., 2002; Hydrology..., 2004; Gastescu, 2009; Romanova et al., 2019). However, the distribution of runoff is unstable – it changes due to natural and anthropogenic factors.

An important feature of the river is the sediment yield, which significantly affects the delta size. According to the studies (Mikhailova et al., 2002; Panin and Jipa, 2002; Levashova, 2004, Gastescu, 2009; Habersack et al., 2013) the sediment yield has the tendency to significant decrease. The creation of reservoirs upstream the Djerdap-I HPP and Djerdap-II HPP is considered to be an important factor of this tendency (Mikhailova et al., 2002; Panin and Jipa, 2002; Gastescu, 2009).

The issues related to the Danube Delta, are the water temperature, water quality etc. These issues are studied in the works (Hydrology..., 2004; Gastescu, 2009; Covaliov et al., 2022; The Lower Danube River …, 2022).

It is important that part of the delta is a protected area. The Danube Delta Biosphere Reserve was created in the Romanian part of the delta, and the Danube

Biosphere Reserve in the Ukrainian part. At the same time, there are various economic activities in the delta: crop production, fisheries, reed harvesting, tourism. Some areas which were previously transformed, have regained their natural status (Gastescu, 2009; Tanasescu and Constantinescu, 2020; Covaliov et al., 2022).

In general, not all issues related to the Danube Delta are properly studied, some results are outdated. This is partly due to the fact that recent years have been very warm and low water. This affected both water temperature and the ecological state of the delta. In this regard, the main purpose of this study is to identify the impact of climate change and human activity on the water regime of the Danube Delta.

Material and methods

The Danube Delta is generally located in the south of Europe, on the border of two countries: Romania and Ukraine. As it was mentioned, most of the Danube Delta belongs to Romania, less – to Ukraine. Near the delta there are several large lakes, that connected with the Danube River (Fig. 1).

The Danube Delta begins some upstream the city of Izmail, where the river for the first time is divided into two branches: the left – Kiliyskyi, the right – Tulchynskyi. This place is called the Izmail Chatal. 17 km downstream from this place the Tulchynskyi branch is again divided into two: the left – Sulinskyi, the right – Georgievskyi. The width of these branches is less than the width of the river upstream of its branching. Thus, the width of the Kiliyskyi branch is about 400–450 m. As we approach the sea, the main branches are divided several more times, which determines the existence of a large number of watercourses and islands. In particular, the Kiliyskyi branch in the delta is divided into the Ochakivske (in the northeasten direction), the Bystre (in the eastern), the Starostambulskyi (in the southeastern) branches. In addition, there are many lakes within the delta (Fig. 2)

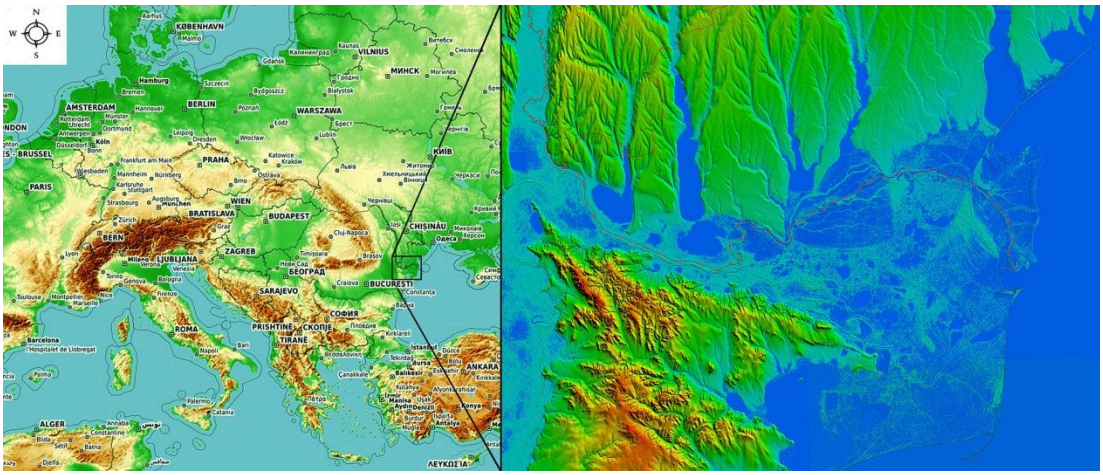

Fig. 1. The location of the Danube Delta and its volumetric image.

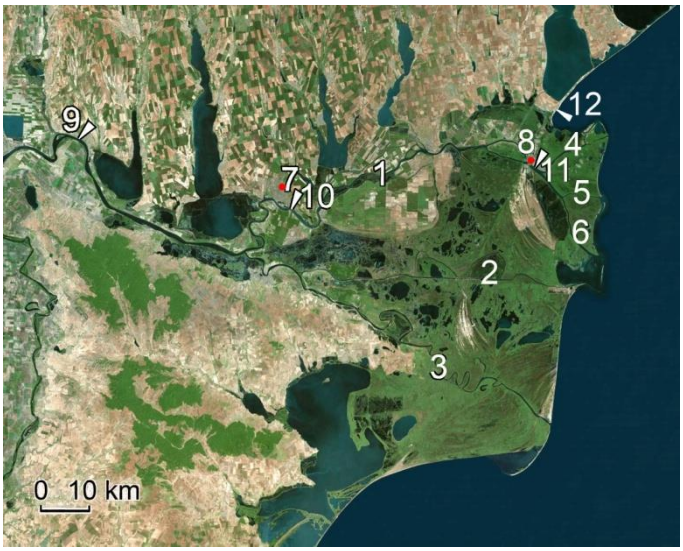

Fig. 2. The main water bodies in the Danube Delta and the available network of observations. The river branches: 1– Kiliyskyi, 2– Sulinskyi, 3 – Georgievskyi, 4 – Ochakivskyi, 5 – Bystre, 6 – Starostambulskyi. Meteorological stations: 7 – Izmail, 8 – Vylkove. Hydrological stations: 9 – Reni, 10 – Izmail, 11 – Vylkove, 12– Prymorske.

The length of the delta from its top to the sea edge in a straight line is 80 km. Approximately the same is the length from the north to the south.
The paper used the data from observations at meteorological and hydrological stations of Ukraine, which are summarized in the Danube Hydro-meteorological Observatory (Izmail).
In addition to regular monitoring data remote sensing data were also used in the paper. Most attention was paid to the data of Landsat 8 and Sentinel 2 satellites, which are available at https://earthexplorer.usgs.gov and https://scihub.copernicus.eu. The volumetric image of the Danube Delta was created on the basis of SRTM and GlobalMapper program.

Results and discussion

The air temperature and its changes

The climatic conditions of the Ukrainian part of the Danube Delta were studied on the basis of data meteorological stations Izmail and Vylkove. Meteorological station Izmail is located on the northern outskirts of Izmail city, 4.7 km from the Danube River, meteorological station Vylkove – almost on the river bank (see Fig. 2).
The mean annual air temperature at Izmail meteorological station during 1991–2020 was 11.7°C, and at Vylkove station – 12.2°C. The mean air temperature in January is minus 0.5°C and plus 0.4°C, respectively, the mean air temperature in July – respectively 23.6°C and 24.1°C.
Over the past 60 years, namely 1961–2020, mean air temperature in the studied area has increased significantly. Its changes during this period are 0.36–0.38°C per decade. The highest air temperature for the entire observation period was in recent years, namely in 2019 and 2020 (Fig. 3).
The air temperature in 2021 was smaller than in two previous years (Izmail station –11.9°C, Vylkove station – 12.4°C), but higher than mean value in 1991–2020.

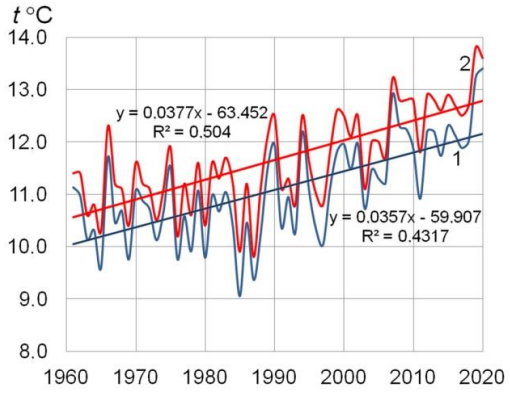

Fig. 3. Changes in mean annual air temperature at Izmail (1) and Vylkove (2) meteorological stations during 1961–2020.

Precipitation

Another important factor influencing the Danube Delta state is the amount of precipitation. Mean annual precipitation during 1991–2020 at Izmail meteorological station was 449, at Vylkove station – 463 mm. In the previous 30 years (1961–1990) the precipitation was some larger – 490 and 481 mm, respectively.
As the precipitation is characterized by considerable spatial and temporal variability, averaging was carried out at two mentioned meteorological stations to assess the changes. It turned out that the smallest precipitation was in 2019 (Fig. 4).
The intra-annual distribution of precipitation is rather even. However, the largest precipitation is observed in June: at Izmail station – 59 mm, at Vylkove station – 44 mm.

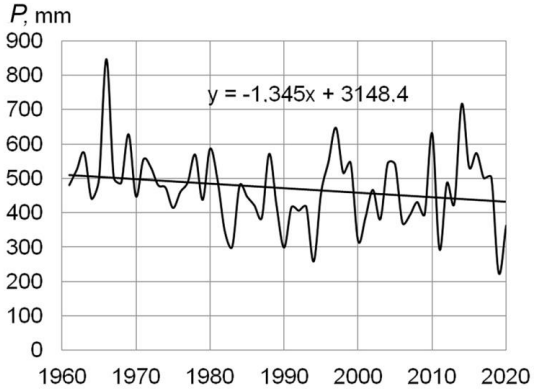

Fig. 4. Changes in averaged annual precipitation at Izmail and Vylkove meteorological stations during 1961–2020.

Evaporation from the water surface

Evaporation from the water surface in the Danube Delta was estimated on the basis of data from meteorological station Vylkove, where the observations are carried out using GGI-3000 evaporator, the water surface of which is 3000 cm^2.
According to the available observations the daily evaporation layer in summer days can reach 6.0–7.0 mm and the monthly evaporation can exceed 200 mm. It was identified that evaporation from the water surface is highly dependent on air temperature. It is important, that this dependence is nonlinear. The same results were obtained for many meteorologicas stations and for the different conditions (Vyshnevskyi, 2022) (Fig. 5).
Based on the obtained dependence shown in Fig. 5 it is possible to determine the changes in evaporation from the water surface over a long period (Fig. 6).
These data show that in recent decades, evaporation from the water surface has increased significantly – from about 900 mm to 1080 mm. The obtained result is similar to those given for the adjacent territory of Romania (Neculau and Stan, 2016), where the fact of evaporation over 1000 mm was determined as well.

The largest increase in evaporation is observed in July and August. While in 1961–1990 the mean daily values were close to 5.0 mm, now they are close to 6.0 mm (Fig. 7).

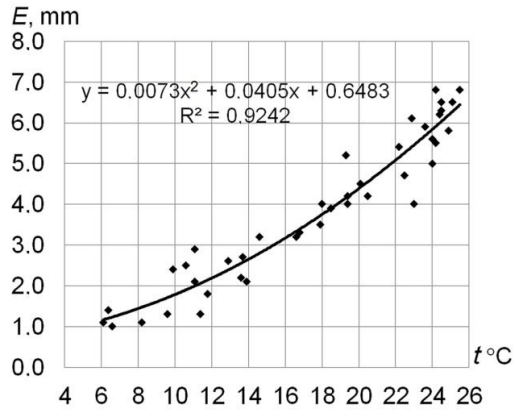

Fig. 5. The dependence of water surface evaporation on air temperature at Vylkove meteorological station.

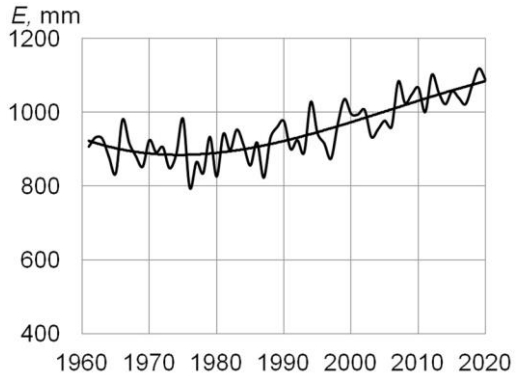

Fig. 6. The long-term changes of calculated annual evaporation from the water surface at Vylkove meteorological station.

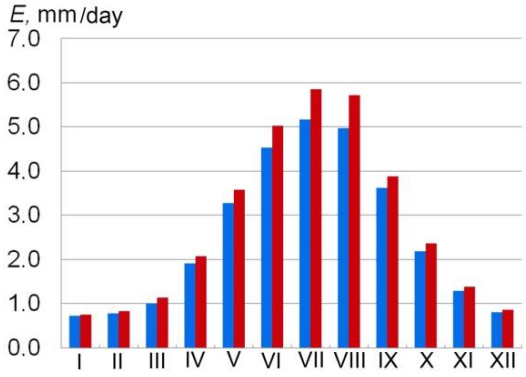

Fig. 7. The long-term changes in mean daily evaporation from the water surface at Vylkove meteorological station by months: left columns – 1961–1990, right columns – 1991–2020.

The results of studies presented in the paper (Vyshnevskyi, 2022), show that the evaporation from the evaporation basins (and, accordingly, from natural reservoirs) is slightly smaller than from the evaporator GGI-3000 due to less water heating. It makes approximately 0.9 from the data of evaporator GGI-3000. With this in mind, we obtained the next mean annual evaporation from the water surface for the different periods: 1991–2000 – 853 mm, 2001–2010 – 905 mm, 2011–2020 – 952 mm.

These data suggest that part of the river flow in the Danube Delta is lost as a result of evaporation, as it is twice larger than precipitation. In summer period mean evaporation layer exceeds precipitation by about four times.

It should be borne in mind that most of the delta is not a water space. The main territory is shallow water covered with air-water vegetation, which is dominated by reed (Covaliov et al., 2022). According to the studies (Stan et al., 2016) carried out in Romania, evaporation from such reservoirs is about twice as much as evaporation from the water surface. It means that evaporation from such water bodies can reach 1900 mm and additional evaporation 1450 mm. According to these data, it is possible to estimate the loss of water in the Danube Delta due to evaporation. Taking into account the delta area of 4200 km^2, the additional evaporation from natural landscapes can be estimated as 4–5 km^3. This is quite a noticeable value even for such a large river as the Danube.

Economic activity in the delta

The economic activity in the Danube Delta is long-term and varied. Some of its kinds have almost no effect on the water regime of the river, others affect – and quite noticeable. One of the first measures that significantly affected the Danube Delta was the construction in the early XX century the directing flow dam (training dike) at the place of Izmail Chatal. This dam was constructed from the stone and it is periodically repaired. Currently it reaches almost the middle of the Danube River width, which significantly affects the redistribution of the river flow in favor of the Tulchynskyi branch (Fig. 8).

To a large extent, the construction of this directing flow dam was associated with measures to improve navigation – especially in the Sulinskyi branch, which is the middle one of the three largest delta branches. This branch was straightened and deepened in some places. In addition, in order to reduce the sedimentation in the river mouth two parallel dams were built in the direction of the sea (Gatejel, 2018). Due to this, the Sulinskyi branch became the most important navigable route in the delta.

Measures to improve navigation in the Ukrainian part of the delta at the mouth of the Bystre branch were similar. The bar at the mouth of this branch was deepened. In addition, to the north of the mouth of this branch was built a dam in order to minimize the sedimentation by the coastal flow of sediments which moves from the north.

Fig. 8. The directing flow dam (shown by the arrow) at the division of the Danube River into Kiliyskyi and Tulchynskyi branches.

Another important measure that affected the delta was the construction of dikes on the river banks in order to use the adjacent territory in the economic sphere – primarily for agriculture. Such measures were carried out in both the Ukrainian and Romanian parts of the delta. In particular, on the left bank of the Danube River in the late 1950s and early 1960s was built a dike about 200 km long, which protected the adjacent lands from the flooding. At the same time, 21 sluice-gates were built on the watercourses connecting the Danube River with the lakes. As a result, these lakes were partly transformed into reservoirs.

In 1979–1980, another project was implemented, namely the construction of the Danube-Sasyk canal. The purpose of this project was to transform Lake Sasyk in fresh water body and to use it for irrigation. In the early 1980s, this canal supplied 0.5–1 km^3 of water. However, the water in the lake still remained brackish and therefore the water intake from it was stopped. Currently, only a small volume of water is taken from the canal itself for irrigation and fish farming.

A small volume of water is taken from the Danube River as well. In particular, the Danube water is used for the cities of Kilija and Vylkove.

Water runoff

Long-term observations of the Danube River runoff at Reni station, which started 100 years ago, make it possible to study the most important features of the river water regime. The mean long-term runoff of the Danube River at the top of the delta during 1921–2020 is 6510 $m^3 s^{-1}$, or 205 km^3 per year. Almost the same value is given in other works (Levashova et al., 2004; Gastescu, 2009; Stagl and Hattermann, 2015). The largest mean annual water discharge (9950 $m^3 s^{-1}$) over the past 100 years was observed in 1941, the lowest one (3920 $m^3 s^{-1}$) – in 1921 (Fig. 9).

As can be seen in Fig. 9, over the past 100 years there have been no significant changes in the water runoff of the Danube River. At the same time, the river is characterized by redistribution of runoff by separate branches. On the one hand, they are due to natural factors, on the other – human impact. In the latter case, the greatest impact was caused by the above-mentioned directing flow dam at the site of the first division of the Danube River into two branches. As a result, the share of the Kiliyskyi branch river flow has significantly decreased. While in the early XX century this share reached 70%, in recent decades it has significantly decreased. Thus, in 1991–2000, the share of the Kiliyskyi branch was 58.1% of the total runoff of the Danube River, in 2001–2010 – 53.4%, in 2011–2020 – 49.8%.

The share of the Kiliyskyi branch runoff slightly increases in case of large river flow and decreases at low water. Thus, in 2010, when the river flow was large, the share of this branch was 53.5% of the total. Next year, when the river flow was small, this share was only 49.7%. Significant redistribution of water runoff occurred and continues to occur between the branches located downstream of Vylkove. To some extent, this is due to human activities, including dredging to improve shipping conditions. In particular, the deepening of the Bystre branch and removing the shallow at its mouth caused the increase of its share. In 2000, this branch accounted for 17.9% of total runoff, in 2020 – 19.2%. In turn, this led to a reduction of the river flow in the adjacent branches.

As it was already mentioned, evaporation, as well as water intake for economic needs, have a certain influence on water runoff at the mouth of the river. Thus, the mean discharge of the Kiliyskyi branch in recent years at Izmail station is larger than at Vylkovo station by 70–80 $m^3 s^{-1}$ or 2.2–2.5 km^3 per year. The main part of this volume is losed for evaporation.

During the year, the largest water runoff of the lower Danube River is observed in April, slightly less – in May. The lowest discharges are observed in September. It is important that over the past decades the intra-annual distribution of river flow has become more even,

in particular, the maximum runoff in April–May has become lower. The discharges also decreased in the summer. Meanwhile, the flow increased in February and March (Fig. 11).

As a result of climate change, there was some approach of flood peak to the beginning of year. Currently, this peak at Reni station is observed closer to May 1. A similar result regarding the reduction of flood discharges and the approach of the flood peak to the beginning of the year was obtained in the works (Stagl and Hattermann, 2015; Blöschl, et al., 2017; Vyshnevskyi and Donich, 2021). For the future there is a forecast of runoff increase in winter and decrese for summer (Stagl and Hattermann, 2015).

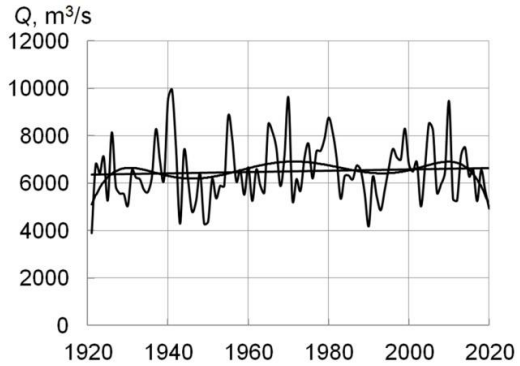

Fig. 9. Fluctuations of mean annual water runoff of the Danube River at Reni station during 1921–2020.

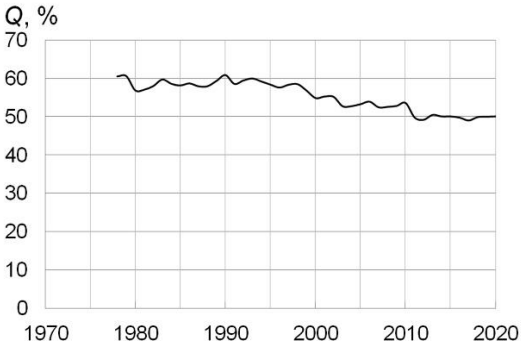

Fig. 10. Change in the share of Kiliyskyi branch runoff at Izmail station to the total at the top of the Danube Delta at Reni station.

Water turbidity and transport of sediment

The Danube River is one of the rivers with a fairly high water turbidity, and in terms of sediment yield, it ranks the first in Europe. Ultimately, this determines the existence of large delta, the size of which is growing. The average long-term transport of sediment at Reni station during 1978–2020 was 30 million tons, at Izmail station – 15 million tons. However, during this period transport of sediment decreased significantly and now it is two to three times smaller than the mean value for period from 1978 (Fig. 12).

The mean water turbidity during 1978–2020 at Reni station was 145 g m^{-3}, at Izmail station – 131 g m^{-3}. In recent years, under conditions of relatively small water runoff of the Danube River, the water turbidity has essentially decreased. In particular, in 2020 at Reni station it was 57 g m^{-3}, at Izmail station – 56 g m^{-3}, at Vylkove station – 50 g m^{-3}.

Reduction of water turbidity and sediment yield in the Danube River has been recorded in other works as well. In particular, in the paper (Mikhailova et al., 2002), it was noted that in natural conditions (1840–1920), the transport of sediment was 62.7 million t/year. The volume for the period 1921–2000, given in the paper (Gastescu, 2009), is slightly smaller – 58.75 million tons. However, the difference between these data is small. According to the paper (Gastescu, 2009), the modern transport of sediment is 25–35 million t/year.

As can be seen, during 1978–2020, compared to natural conditions, transport of sediment decreased by half and continues to decrease markedly. One of the factors of this is considered (Panin and Jipa, 2002; Levashova et al., 2004) the creation of reservoirs upstream the Djerdap-I HPP and Djerdap-II HPP. However, these reservoirs were built 40–50 years ago (Djerdap-I – in 1972, Djerdap-II – in 1984), but the sediment yield decrease continues. According to (Habersack et al., 2013) one of

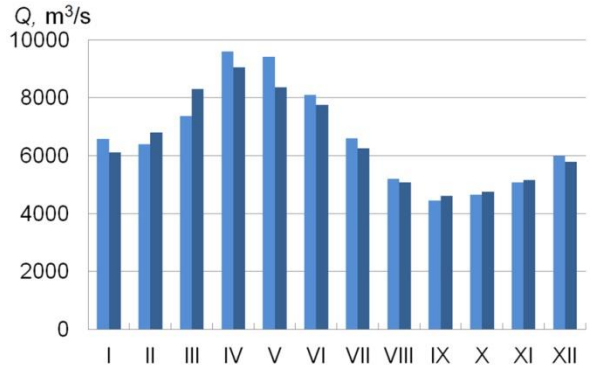

Fig. 11. Intra-annual distribution of the Danube River runoff at Reni station during 1981–2020. Left columns – 1981–2000, right columns – 2001–2020.

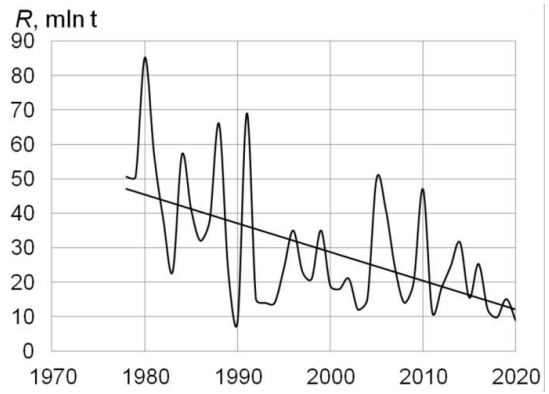

Fig. 12. The long-term changes of sediment yield at the top of the Danube Delta at Reni station.

the reasons of sediment yield decrease is the dredging to improve the navigation conditions. In our opinion, there are other factors related to climate change. Due to the increase of air temperature, in paricular in winter, soil freezing decreases and, accordingly, the share of surface runoff decreases as well. The second consequence of climate change is the reduction of maximum spring flood and flow velocity during this period. This trend of sediment yield decrease is observed in many regions of Europe, including the rivers that have not been regulated. A certain role in reducing of sediment trasport can be caused by environmental activities – increasing forest cover in the mountains and anti-erosion measures.

Water temperature

The location of the Danube Delta in the southern Europe determines a fairly high water temperature. It is important that in the Romanian section of more than 200 km the river flows from the south to the north. Being in this section the water temperature has time to rise. Another factor to consider is the location of places of water temperature observation. All hydrological stations within Ukraine are located on the left bank of the river, which is oriented to the south. This contributes to the fact that the water temperature here can be a few tenths of a degree higher than in the middle of the river.

These factors determine that the water temperature in the Danube Delta is high. In particular, at Izmail hydrological station, mean monthly water temperature in July and August during 1991–2020 was 25.4 and 25.7°C. It is important that the water temperature in the Danube Delta is essentially higher than the air temperature. In particular, the mean monthly water temperature at Izmail station during 1991–2020 in July is 1.8°C higher than air temperature. Excess of water temperature over air temperature is even greater in autumn and December. The largest difference is observed in October, when the mean air temperature is 11.9°C and the mean water temperature is 16.1°C. Even in March–April, when the rapid increase of air temperature is observed, water temperature is higher than air temperature (Fig. 13).

This rather significant excess of water temperature over air temperature is explained by the fact that the main absorption of solar energy occurs in the upper layer of water, where, in fact, the temperature is measured. Another probable factor in the excess of water temperature over air temperature is the above mentioned fact of water flow in the adjacent section from the south to the north. In addition, fresh water temperature has minimum 0°C, which air temperature does not have. Similar results showing an excess of water temperature over air temperature were obtained in many other works (Webb and Nobilis, 2007; Pekarova et al., 2008; Ptak et al., 2018; Vyshnevskyi, Shevchuk, 2021; Ptak et al., 2022), but the excess in the Danube Delta is larger than in many other rivers.

Importantly, water temperatures, like air temperatures, have risen essentially in recent decades. The increase is observed throughout the year (Fig. 14).

Fig. 14 shows that water temperature rose especially markedly in July and August, which corresponds to an increase of air temperature. At the same time, the increase in water temperature in April is small.

It is important, that observed increase of annual water temperature is a little bit larger, than the increase in air temperature. Over the past 60 years the increase in mean annual water temperature near Izmail is 0.38°C per decade and the increase of air temperature is 0.36°C per decade (Fig. 15).

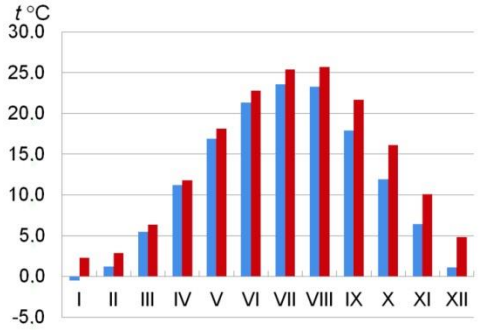

Fig. 13. Intra-annual distribution of air temperature (left columns) and water temperature (right columns) in Izmail during 1991–2020.

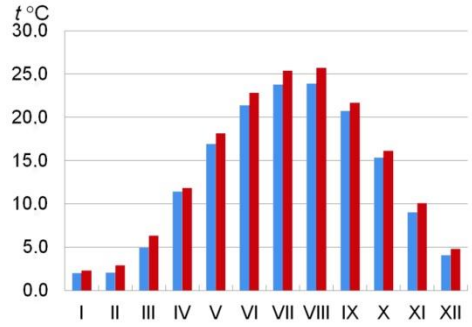

Fig. 14. Intra-annual distribution of water temperature at Danube–Izmail. Left columns – 1961–1990, right columns – 1991–2020.

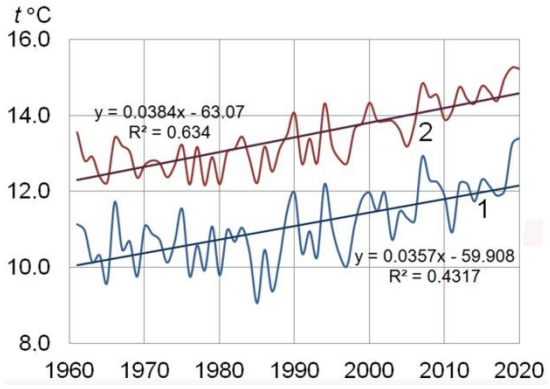

Fig. 15. The long-term changes in mean annual air (1) and water (2) temperature at Izmail meteorological and Izmail hydrological stations.

The conclusion about the increase in water temperature is contained in many other works (Webb and Nobilis, 2007; Basarin et al., 2016; Marszelewski and Pius, 2016; Czernecki and Ptak, 2018; Vyshnevskyi and Shevchuk, 2021; Ptak et al., 2022; Wrzesiński and Graf, 2022), but the excess of water temperature increas over air temperature increase is somewhat unusal. It can be assumed that the found feature on the Danube Delta is caused by the decrease of the river flow. But during long-time period the annual water runoff of the Danube River is practically stable. Another factor can be wastewater discharge, but the local cities are small without powerful enterprises. In fact, the main cause of the discovered feature is noticeable decrease of the Kiliyskyi branch river flow during observed period. Whereas in the early 1960's its share was about 60% of the total, by nowadays it is about 50%. It means that artifical decrease of the Kiliyskyi branch water runoff contributed to the increase in water temperature.

The available data show that water temperature depends on the water runoff of the Danube River. As river flow decreases, its heating in the warm period increases, in particular, due to the simultaneous reduction of mixing and depth. The opposite is observed at large discharges, when the water temperature may even be lower than the air temperature. Regression analysis also shows the inverse effect of the river flow on its temperature during main part of year except January–February. The most essential impact of water runoff on water temperature is observed in June. Taking into account two arguments (air temperature and water runoff) it is possible to obtain a close relationship between actual and calculated water temperature. A similar result was obtained in papers (Pekarova et al., 2008; Wrzesiński and Graf, 2022).

Delta size change

The change in delta size is primarily due to its advance towards the sea, because most of the sediment is deposited there. For a long period of time, the study can be carried out using Landsat satellite images. The first satellite images of the delta by Landsat 5 satellite were obtained in 1984. In particular, the image dated September 7, 1984 is of high quality. The image of Landsat 9 satellite dated August 07, 2022 is also of high quality. According to these data, it is possible to determine the changes which have occured over the past 38 years (Fig. 16).

A comparison of these images shows some differences between them. First of all, the appearance of an elongated island between the Starostambulskyi and the Sulinskyi branches is noteworthy. Its northern part belongs to Ukraine, the southern part – to Romania. Currently, in this island is the only land border between these states. Another place where the delta has moved towards the sea is located at the exit from the Ochakivskyi branch, which is oriented to the northeast. In this place several elongated islands were created.

In general, the changes in the size of the delta during the last decades are small. This is primarily due to the decrease of the Danube River sediment yield, as it was mentioned above. There is also another factor namely sea level rise. At Prymorske station, located near

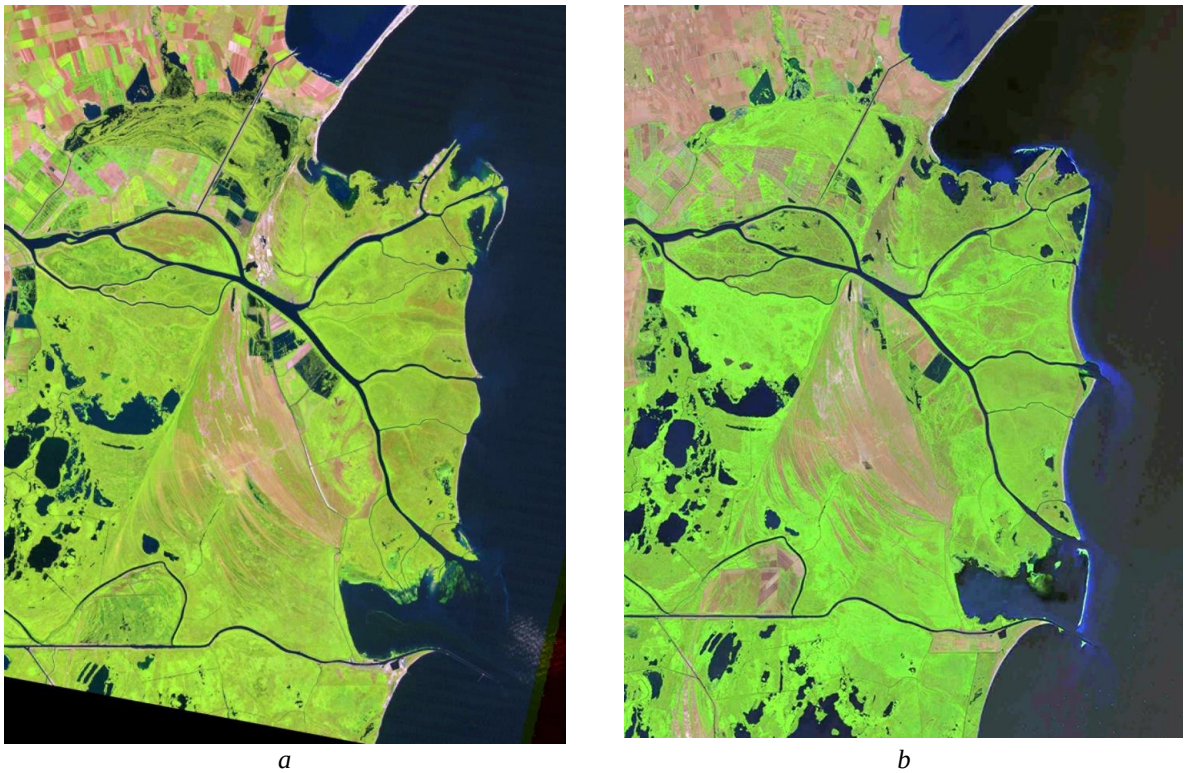

a *b*

Fig. 16. Satellite images of the Danube Delta obtained by Landsat 5 on 07.09.1984 (a) and Landsat 9 on 07.08.2022 (b).

the mouth of the river, the mean sea level in 1981–1985 was minus 0.17 m, in 2017–2021 – minus 0.05 m. This means that the water level rose by about 12 cm, which also affected the delta.

Conclusions

The water regime of the Danube Delta is influenced by natural and human factors. Over the past 60 years, air temperature in the area of the Danube Delta has risen. This caused the essential increase in water temperature which is slightly larger than the increase of air temperature. The highest increase of water temperature is observed in summer period. The water temperature in the Danube Delta is higher than the air temperature. In spring this excess is about 1°C, in autumn – it reaches 4°C.

Despite climate change, the mean water runoff at the top of the Danube Delta remains stable at about 205 km^3. Meanwhile, intra-annual river flow distribution has become more even than it was some decades ago. In particular, the maximum runoff in April–May have become less. At the same time, it increased in February and March. The changes of flow regime has affected the sediment yield, which tends to essential decrease. In turn, the reduction of sediment yield has led to the fact that the movement of the delta towards the sea has slowed. Another factor, which impacted the delta, is the sea level rise.

One of the most important factors of human influence on the delta was the construction in the early twentieth directing flow dam at the site of the first division of the Danube River into two branches. As a result, the share of the Kiliyskyi branch has decreased from 60% to 50% in the last 40 years alone. It has some impact on the water temperature in this river branch.

References

Basarin, B., Lukić, T., Pavić, D., Wilby, R. L. (2016): Trends and multi-annual variability of water temperatures in the river Danube, Serbia. Hydrological Processes, 30, 18, 3315.

Blöschl, G., Hall, J., Parajka, J. et al. (2017): Changing climate shifts timing of European floods. Science 357, 588–590.

Czernecki, B., Ptak, M. (2018): The impact of global warming on lake surface water temperature in Poland – the application of empirical-statistical downscaling, 1971–2100. Journal of Limnology. 77 (2). 340–348.

Covaliov, S., Doroftei, M., Mierla, M., Trifanov, C. (2022): Natural vegetal resources of the Danube Delta territory – present status and trends. Scientific Annals of the Danube Delta Institute. 27. 25–33.

Gastescu, P. (2009): The Danube Delta Biosphere Reserve. Geography, biodiversity, protection, management. Rom. Journal Geogr. 53, (2), 139–152.

Gatejel, L. (2018): Building a better passage to the sea: engineering and river management at the mouth of the Danube, 1829–61. Technol. Cult. 59, 925–953.

Habersack, H., Jäger, E., Hauer, C. (2013): The status of the Danube River sediment regime and morphology as a basis for future basin management. International Journal of River Basin Management, 11: 2, 153–166.

Hydrology of the Danube Delta. Under editorship of Mikhajlov V.N. (2004): Moscow: GEOS, 448 p. (in Russian).

Levashova, E. A., Mikhailov, V. N., Mikhailova, M. V., Morozov, V.N. (2004): Natural and anthropogenic changes in water and sediment runoff at the mouth of the Danube River. Water resources. Volume 31. N. 3. 261–272 (in Russian).

Marin, L., Birsan, M.-V., Bojaru, R., Dumitrescu, A. et al. (2014): An overview of annual climatic changes in Romania: trends in air temperature, precipitation, sunshine hours, cloud cover, relative humidity and wind speed during the 1961–2013 period. Carpathian Journal of Earth and Environmental Sciences, November, 9, 4, 253–258.

Marszelewski, W., Pius, B. (2016): Long-term changes in temperature of river waters in the transitional zone of the temperate climate: A case study of Polish rivers. Hydrol. Sci. J. 61, 1430–1442.

Mikhailova, M. V., Mikhailov, V. N., Levashova, E. A., Morozov, V. N. (2002): Natural and anthropogenic changes in water and sediment runoff of the Danube at the delta head (1840–2000). Proc. XXIth Conference of the Danubian countries on hydrological forecasting and hydrological bases of water management, Bucharest, 1–7.

Neculau, G., Stan, F.-I. (2016): Evaporation and evapo-transpiration in Romania. Forum geografic. Studii și cercetări de geografie și protecția mediului. Volume XV, Supplementary Issue (December 2016). 39–48.

Olson, K. R., Krug, E. (2020): The Danube, an Empire Boundary River: Settlements, Invasions, Navigation, and Trade Pathway Journal of Water Resource and Protection. 12, 10, 884–897.

Panin, N., Jipa, D. (2002): Danube River Sediment Input and its Interaction with the North-western Black Sea Estuarine, Coastal and Shelf Science. 54, 551–562.

Pekarova, P., Halmova, D., Miklanek, P., Onderka, M., Pekar, J., Skoda, P. (2008): Is the water temperature of the Danube River at Bratislava, Slovakia, rising? Journal of Hydrometeorology, 9, 5, 1115–1122.

Ptak, M., Sojka, M., Choiński, A., Nowak, B. (2018): Effect of environmental conditions and morphometric parameters on surface water temperature in Polish lakes. Water, 2018, 10, 580.

Ptak, M., Sojka, M., Graf, R., Choiński, A., Zhu, S., Nowak, B. (2022): Warming Vistula River – the effects of climate and local conditions on water temperature in one of the largest rivers in Europe. J. Hydrol. Hydromech., 70, 1, 1–11.

Romanova, Y., Shakirzanova, Zh., Ovcharuk, V. et al. (2019): Temporal variation of water discharges in the lower course of the Danube River across the area from Reni to Izmail under the influence of natural and anthropogenic factors. Energetika. 65 (2–3). 144–160.

Stagl, J. C., Hattermann, F. F. (2015): Impacts of climate change on the hydrological regime of the Danube River and its tributaries using an ensemble of climate scenarios. Water. 7, 6139–6172.

Stan, F.-I., Neculaub, G., Zaharia, L. et al. (2016): Study on the evaporation and evapotranspiration measured on the Căldărușani Lake (Romania). Procedia Environmental Sciences, 32, 281–289.

Tanasescu, M., Constantinescu, S. (2020): The human ecology of the Danube Delta: A historical and cartographic perspective. Journal of Environmental Management. 262.

The Lower Danube River: Hydro-Environmental Issues and Sustainability (2022): Editors Abdelazim Negm, Liliana Zaharia, Gabriela Ioana-Toroimac. 582 p.

Vyshnevskyi, V. I. (2022): The impact of climate change on evaporation from the water surface in Ukraine. Journal of Geology, Geography and Geoecology. Vol. 31. N 1. 163–170.

Vyshnevskyi, V. I., Donich, O. A. (2021): Climate change in the Ukrainian Carpathians and its possible impact on river runoff. Acta Hydrologica Slovaca. Vol. 22, № 1, 3–14.

Vyshnevskyi, V., Shevchuk, S. (2021): Thermal regime of the Dnipro Reservoirs. J. Hydrol. Hydromech., 69, 3, 300–310.

Webb, B. W., Nobilis, F. (2007): Long-term changes in river temperature and the influence of climatic and hydrological factors. Hydrolog. Sci. J., 52, 74–85.

Wrzesiński, D., Graf, R. (2022): Temporal and spatial patterns of the river flow and water temperature relations in Poland. J. Hydrol. Hydromech., 70, 2022, 1, 12–29.

Prof. Viktor Vyshnevskyi (*corresponding author, e-mail: vishnev.v@gmail.com)
National Aviation University
Liubomyra Huzara Ave, 1
Kyiv, 03058
Ukraine

Serhii Shevchuk, seniour researcher
Central Geophysical Observatory
Nauky Ave., 39/2
Kyiv, 03028
Ukraine

DOI: 10.31577/ahs-2022-0023.02.0024

ACTA HYDROLOGICA SLOVACA

Volume 23, No. 2, 2022, 217–225

Changes in the hydrological balance in the Litava river basin during the 90-years period 1931–2020

Pavla PEKÁROVÁ*, Zbyněk BAJTEK, Pavol MIKLÁNEK, Ján PEKÁR, Katarína JENEIOVÁ, Jakub RIDZOŇ

During last twenty years, a number of extremely dry years have occurred in a number of European river basins. In Slovakia, the lowland streams of southern Slovakia have been particularly affected by drought. One of these streams is the Ipeľ River. In this basin we have three continuous observations of daily flows since 1931: from Krupinica at Plášťovce, Litava at Plášťovce, and from Ipeľ at Holiša station. The first part of the paper is devoted to the statistical analysis of the Litava flow series. In the second part, the hydrological balance in the Litava basin for the three subperiods (1931–1960, 1961–1990, and 1991–2020) in annual time step has been elaborated. The first thirty years 1931–1960 were the wateriest (runoff was 205 mm). In the last thirty years, the runoff coefficient was only 0.2 (runoff 131 mm) in Litava basin. In the final part of the study, the BILAN balance model (in a monthly step) was used to compute the contribution of several runoff components in the Litava basin during period 1930/31–2019/20. The long-term average baseflow accounts for 40.7% of the total modelled runoff, interflow accounts for 46.8% and direct runoff accounts for 12.5% of the total modelled runoff.

KEY WORDS: Litava River, hydrological balance, simulation, model BILAN

Introduction

In the last two decades, a decline in flows has been recorded in several streams in Slovakia. The hydrological balance in Slovakia did not change significantly until 2000. However, after 2000, we observe more significant changes in the hydrological balance (Fenkeková and Blaškovičová, 2018; Ďurigová et al., 2019; Halmová et al., 2022). Due to higher air temperature and higher precipitation, potential evapotranspiration and balance evaporation from the territory of the Slovak Republic are increasing. In eastern Slovakia, this trend is not as pronounced (Pavelková et al., 2016). In the period 1991–2015, annual precipitation in Slovakia increased overall by about 5% compared to the period 1961–1990, which amounts to almost 40 mm in absolute values. Despite higher rainfall totals, streamflows are decreasing. The decline in flows is most pronounced in the lowland streams of southern Slovakia.

In long-term water management planning, it is necessary (or at least advisable) to take into account the expected impact of climate change on the hydrological regime. For example, when permitting new abstractions (or increasing the capacity of existing abstractions), it is necessary to have information on water quantity. In view of this, it is recommended to include among the standard tasks of hydrology the study of the impact of climate change on the hydrological balance of river basins.

The hydrological balance of river basins in Slovakia has been addressed by a number of authors (e.g. Holko et al., 2001; Kostka and Holko, 2001; Majerčáková et al., 2004; Horvát et al., 2009; Pekárová et al., 2010; Porubská at al., 2012, 2013; Garaj et al., 2019; Keszeliová et al., 2021; Výleta et al., 2022).

The most comprehensive hydrological balance for the period 1961–1990 for 109 sub-basins in the entire Danube river basin was compiled by Petrovič et al. (2006, 2010). Sleziak et al. (2021) evaluate the possible climate change impacts on the runoff regime in eight selected basins located in the whole territory of Slovakia. The projected runoff in the basins they simulated using the HBV model.

For these reasons, we focused on assessing the long-term water balance in the relatively anthropogenically unaffected Litava river basin for the 90-year period 1931–2020.

The present study is divided into three parts.

1. The first part deals with a detailed statistical analysis of the Litava flows at the Plášt'ovce station;
2. in the second part we deal with the hydrological balance of the Litava in annual step;
3. the third part focuses on the modelling of the monthly water balance by the BILAN model.

Material and methods

River basin description

The Litava is an important left-side tributary of the Krupinica. It has a total length of 45 km. It rises in the Krupina plain, the spring lies at an altitude of about 650 m above sea level on the southern slope below the saddle between Kopaný závoz (775 m above sea level) on the western side and Jaseňový vrch (724 m above sea level) on the eastern side (Fig. 1). The area belongs to the upland-lowland region with a rain-snow type of runoff regime with accumulation in December-January, high water levels in February-April. There is a significant increase in water levels in late autumn and early winter. The Litava catchment area to Plášťovce gauging station is 214.27 km^2. The streams in the river basin form a mostly parallel river system. Due to the not very rugged terrain, the average altitude reaches 450 m above sea level.

The average monthly values of precipitation from the stations Krupina (latitude 48°22'51'', longitude 19°06'42''; 470 m a.s.l.), Bzovík (latitude 48°19'09'', longitude 19°05'38''; 355 m a.s. l.) and Senohrad (latitude 48°22', longitude 19°12'; 586 m a.s.l.), air temperature, and average monthly discharges from the gauging station Litava: Plášťovce for the 90-years period 1931–2020 were used to evaluate the hydrological balance.

Data

For the watershed balance, we need a measured series of discharge from the watershed and areal precipitation and mean temperature on the watershed. There is a problem in Slovakia with obtaining continuous series of daily precipitation and air temperature data for the period 1931–1960. From the point of view of protection of our country before floods there was build-up a network of precipitation stations at the end of the 19. century. The average monthly precipitation series from 203 stations (period 1901–1970) were published in the Collection of papers of the SHMI. Therefore, when processing the water balance, we only worked with stations published in Šamaj and Valovič (1978). The following data were used in the analysis of the flows:

– Average daily discharge of the Litava at the station Plášťovce, 1931–2020;
– Average monthly air temperatures at Bzovik, and Banská Štiavnica stations (Petrovič and Šoltís, 1984);
– Monthly precipitation totals from stations Bzovík, Krupina, and Senohrad (Šamaj and Valovič, 1978).

Methods

Considerable attention has been paid to catchment hydrological balance methods. The hydrological balance quantifies the circulation of water in a closed catchment system with one concentrated outlet in the final profile on a watercourse. Assume that the only input to the watershed is atmospheric precipitation in the watershed and that there are no withdrawals or inflows from neighbouring areas. Then we can use a balance equation of the form:

$$P = R + ET + \Delta S \quad (1)$$

where:
P – mean annual precipitation depth [mm];
R – mean annual runoff depth [mm];
ET – balance evaporation [mm];
ΔS – change of water retention in the basin during the time Δt.

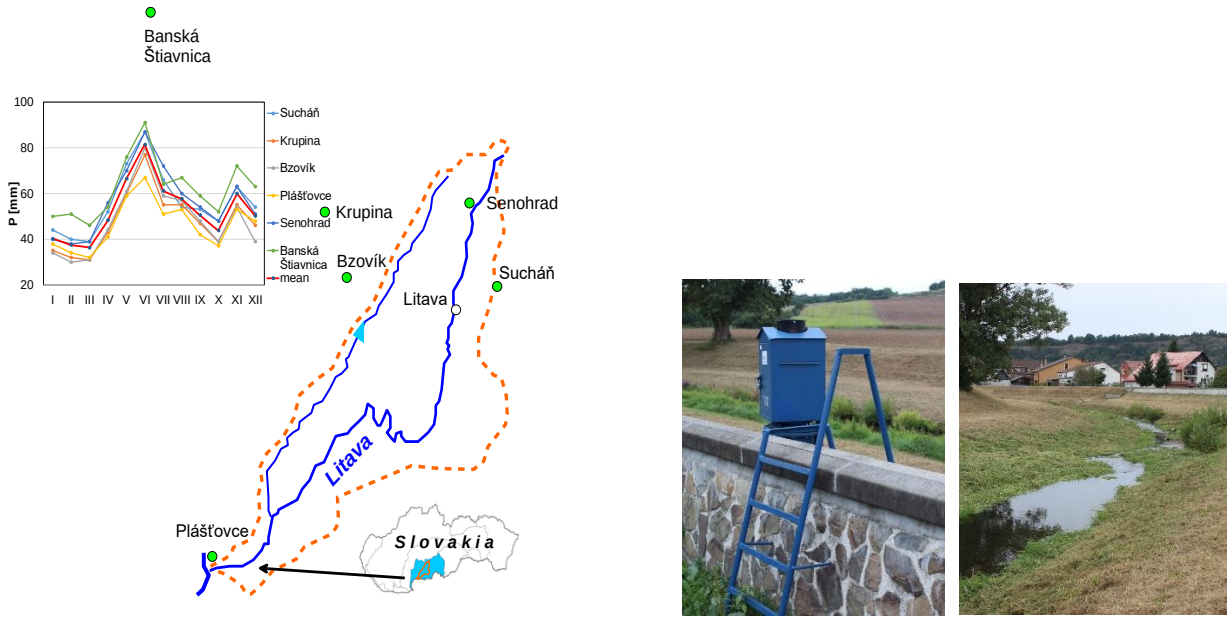

Fig. 1. Location and scheme of the Litava basin, precipitation stations (green points) and course of the monthly precipitation (1961–1990), Slovakia (left); water gauge of the SHMI at Plášťovce on Litava River. (Photo: J. Mészáros, 2021).

The difference in water storage in the saturated and unsaturated zones of the soil and in snow at the beginning (1 November) and at the end (31 October) of the balance period can be neglected for a sufficiently long period (e.g. 30 years) (Majerčáková et al. 2004). In that case, we can identify the annual actual evapotranspiration (AET) with the difference between precipitation and runoff, which is the annual balance evaporation (ET).

Over the last decades, hydrological rainfall-runoff models in a basin scale have become an important tool in the water management. The user has been able to choose the right model depending on the topic of study. The biggest problem remains the problem of getting high-quality, sufficiently long series of input data. After proper model selection and calibration, its subsequent use has irreplaceable contribution either in the water management or ex post evaluation of specific situations in river basins.

Among the conceptual models with lumped parameters there belong e.g. monthly water models BILAN, WBMOD, WatBal, or rainfall runoff models in daily time step HBV, SAC SMA Sacramento soil moisture model, HEC-HSM model or GLOBAL model (Garaj et al, 2019).

In this study, we used the hydrological model BILAN with a monthly time step to assess the individual components of the water balance of the Litava basin up to station Plášťovce. Model BILAN belongs to a group of conceptual models with lumped parameters (Tallaksen and van Lanen, 2004; Kašpárek and Novický, 1997, 2004a, b; Horáček et al., 2009; Vizina et al., 2015). The model schematizes (simplifies) catchment areas into three water reservoirs. The structure of the model consists of a system of relations describing the basic principles of water balance of the unsaturated and saturated zones, including the impact of vegetation cover and groundwater. Measured time series of monthly precipitation, air temperature and potential evapotranspiration, or relative humidity are the inputs into the model BILAN.

The aim of the model is to simulate monthly time series of hydrological variables and apply it to the entire river basin. Total runoff in the month consists of three components: base flow, interflow (hypodermic) and direct flow. Direct flow is considered as fast runoff component of total runoff, which does not affect the evaporation, and soil water balance. Hypodermic flow is considered as the water excess in the aeration zone. In winter, during snowmelt, this runoff component also includes direct runoff. The base flow is the slow component of the total runoff, the delay in the basin may be longer than one month. The model in the vertical direction distinguishes three levels, namely the surface, soil zone and groundwater zone. The size of the flows between the reservoirs is determined by the model algorithms, which are controlled by eight free parameters.

Time series of measured monthly discharges (runoff) in the closing profile Litava are used for model calibration. The model parameters include: soil water storage, direct flow, snow melt factor, factor to calculate the amount of water in liquid form in the winter, the parameter managing percolation distribution, hypodermic flow and groundwater recharge in terms of the melting snow in the winter and summer, parameter managing drainage from groundwater aquifer.

Eight free model parameters have to be identified to simulate the streamflow generation by the model:

- ***Spa*** – capacity of soil moisture [mm],
- ***Alf*** – parameter for rainfall-surface runoff equation (direct runoff),
- ***Dgm*** – snow melting factor,
- ***Dgw*** – factor for calculating the quantity of liquid water available on the land surface under winter conditions,
- ***Mec*** – parameter controlling distribution of percolation into through flow (interflow) and groundwater; recharge under conditions of snow melting
- ***Wic*** – parameter controlling distribution of percolation into through flow (interflow) and groundwater; recharge under winter conditions,
- ***Soc*** – parameter controlling distribution of percolation into through flow (interflow) and groundwater; recharge under summer conditions,
- ***Grd*** – parameter controlling outflow from groundwater storage (base flow).

Model parameters are identified (calibrated) by using an optimization algorithm. The optimization aims at attaining the best fit between observed and simulated runoff series.

The calibration of the parameters is executed in two steps. In the first step, *the standard error* of estimate (standard deviation between the observed and simulated runoff series) or *mean absolute error* (mean calculated from absolute deviations between the observed and simulated runoff series, where 'absolute' means that negative deviations are converted to positive values) is used as the optimization criteria to calibrate ***Spa, Dgm, Dgw,*** and ***Alf*** parameters that affect significantly the mean runoff.

The remaining four parameters (***Mec, Wic, Soc, Grd***) affecting the runoff distribution into its individual components are then calibrated by using the mean of absolute values of relative deviations (relative means that each deviation is divided by observed value).

The values of model parameters obtained from the optimization algorithm can be influenced by the maximum number of iterations performed by the algorithm. In case that we achieved the optimal model parameters, we can proceed to the simulation. Initial conditions in the basin can significantly influence the results of the simulation of water balance, especially in the first year. These conditions can be specified by the initial groundwater reserves setting. These conditions can be specified by setting the initial groundwater storage. The default initial groundwater storage is 50 mm. It can be changed based on the current state in the basin in the first month, or is derived from interim simulations.

Results and discussion

Statistical analysis of changes in the runoff regime of the Litava to station Plášťovce

The assessment of the hydrological regime of the Litava River was based on measurements of average daily discharge at the Plášťovce station for the period 1931–2020. Fig. 2a shows the course of the average daily discharge of the Litava. The average annual discharge of the Litava at Plášťovce for the period was 1.09 $m^3 s^{-1}$, the annual runoff depth was 160.5 mm. The highest average daily discharge was recorded on 22 June 1999 (69.48 $m^3 s^{-1}$). The wettest decade was 1931–1940, the driest 1981–1990 (Fig. 2b). Comparing the 30-year periods, the first period 1931–1960 was the wettest, the period 1961–1990 the most equable, and the last period 1991–2020 was marked by several floods and droughts.

The wettest month is April and the driest months are August-September (Fig. 2c). The highest flood flow of the Litava in Plášťovce was also recorded on 22 June 1999 Q_{max}=125.1 $m^3 s^{-1}$. The minimum flow Q_{min}=0.01 $m^3 s^{-1}$ was recorded on 1 September 1961 and on 13. July 1988. A water reservoir Kozí Vrbovok is built on a tributary of the Litava. As can be seen in Fig. 2d, the extreme peak discharges of the Litava in Plášťovce have increased significantly in the last 30 years. As a consequence, a flood dike has been built in Plášťovce (see Fig. 1).

Hydrological balance in the Litava basin during three 30-years periods

The annual rainfall (per calendar year) for the Litava to Plášťovce catchment was determined from measurements at the Krupina, Bzovík and Senohrad stations in the period 1931–2020 (Fig. 3). Monthly precipitation totals were used to calculate the annual precipitation in the Litava basin, which were converted to the average elevation of the basin according to precipitation gradient (Petrovič et al., 2006). Basin air temperature was determined from stations Banská Štiavnica and Bzovík. The long-term average for the period 1931–2020 was 8.61°C. Fig. 3 shows the average annual values of the individual components of the hydrological balance, the air temperature in the basin, and the runoff coefficient ($k=R/P$) of the Litava River.

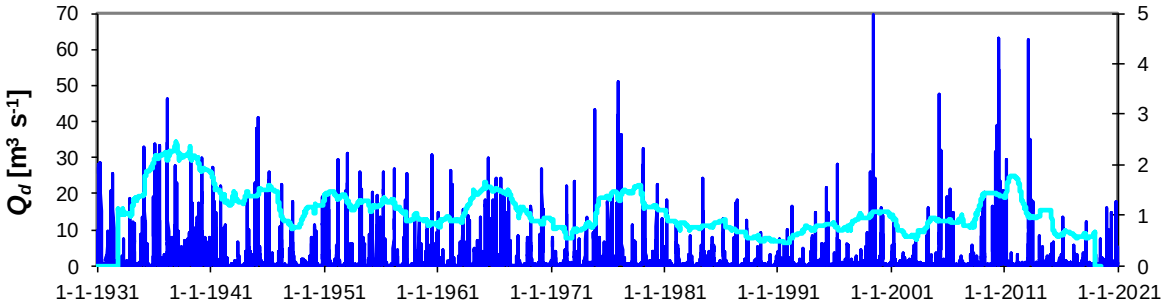

a)

Fig. 2. a) Mean daily discharge of Litava at Plášťovce station (dark blue line, left scale) and double 4-year moving averages of the daily discharge (light blue line, right scale).

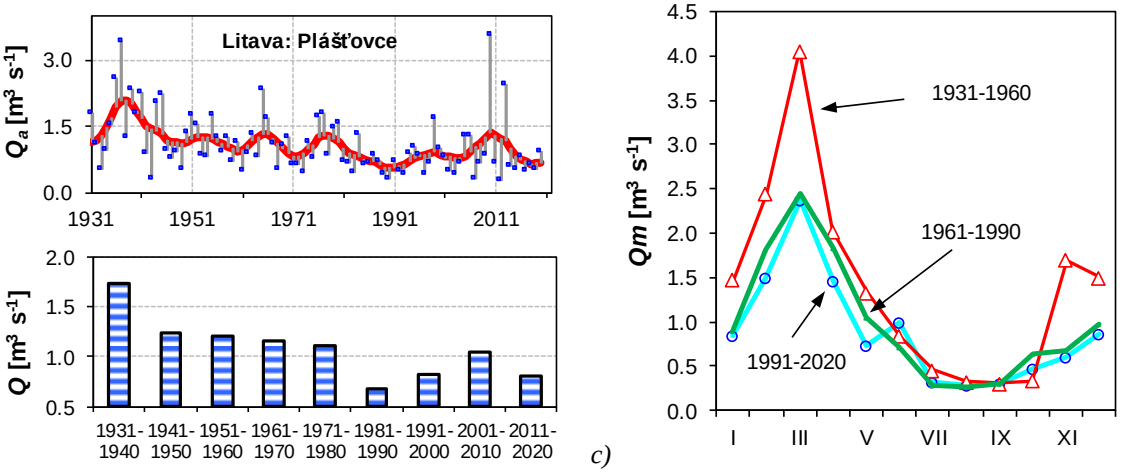

b) c)

Fig. 2. b) Variability of the mean annual discharge (above) and 10-year mean values of the Litava discharge, period 1931–2020. c) Changes of the mean monthly discharge in three periods 1931–1960, 1961–1990, and 1991–2020.

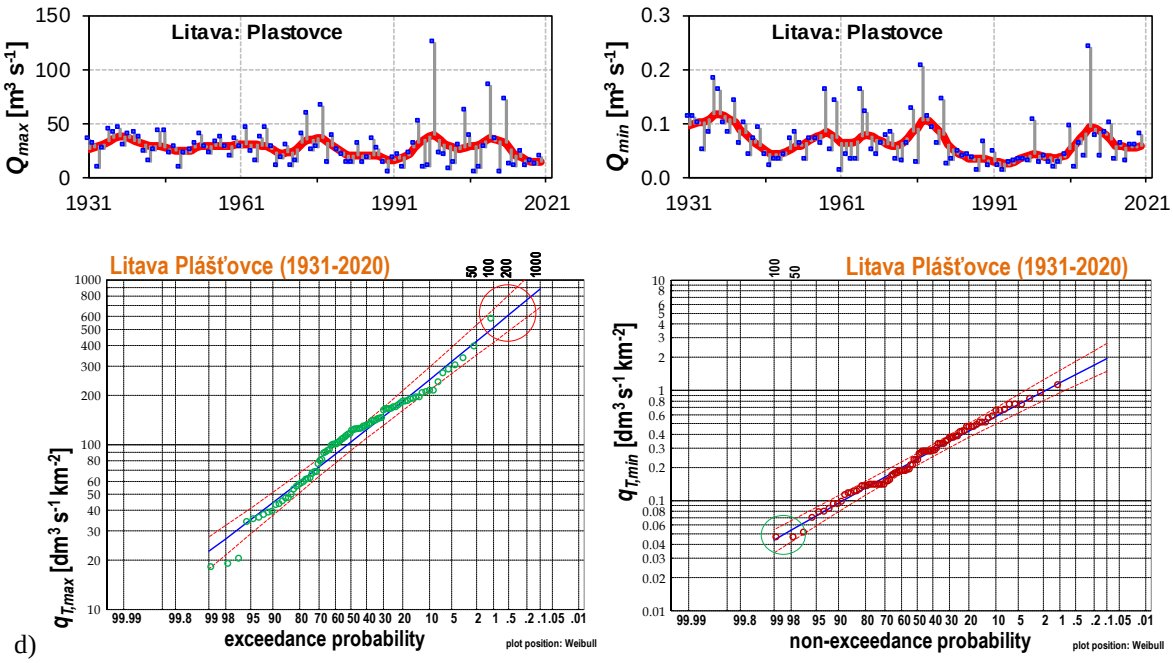

d)

Fig. 2. d) Course of annual maximum Q_{max} (left) and minimum Q_{min} (right) discharge series of Litava, values of the maximum $q_{T,max}$ and minimum $q_{T,min}$ discharge per unit area (specific runoff) calculated according to log-Pearson type III distribution, Litava River at Plášťovce, 1931–2020.

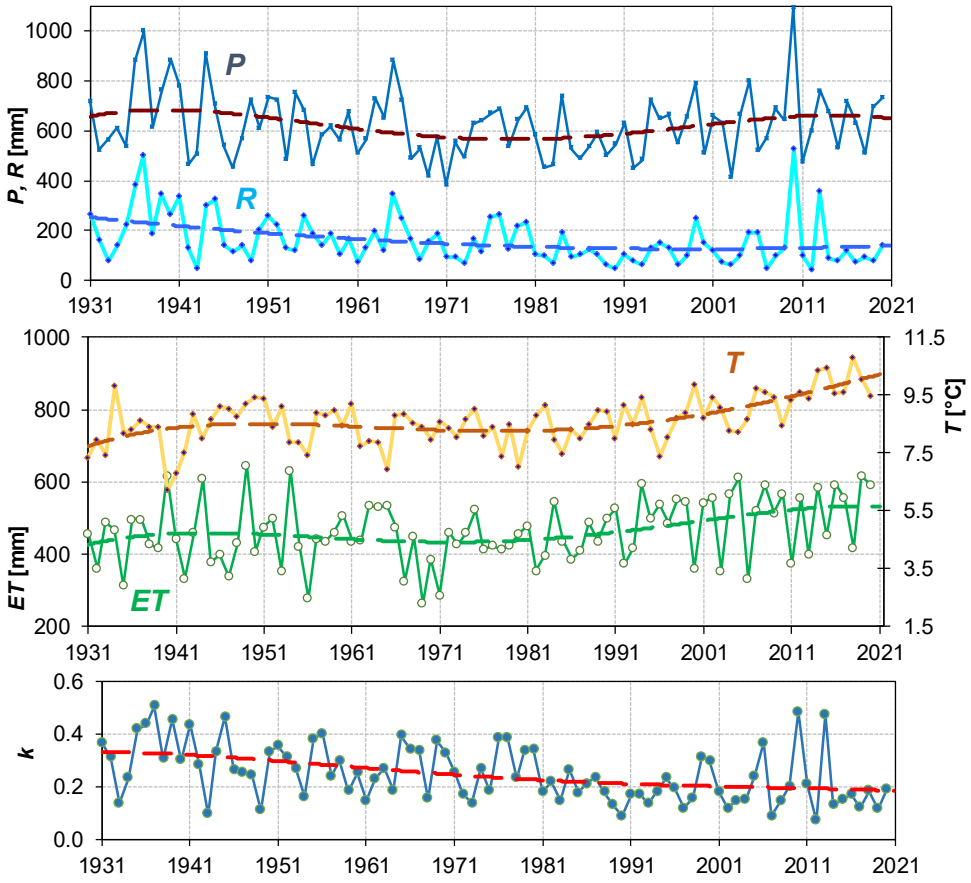

Fig. 3. Annual precipitation depth P and annual runoff R of the basin; annual balance evaporation ET, and the mean annual basin air temperature T; runoff coefficient k in the Litava basin up to Plášťovce, (period 1931–2020).

The values of the basic components of the water balance of the Litava basin for the three 30-year periods are presented in Table 1. The first thirty years 1931–1960 were the wettest, the runoff reached 205 mm, the runoff coefficient was 0.3. The years 1936–1940 were extremely wet, the average rainfall in this period reached 927 mm. The second thirty years had the lowest rainfall totals, 582 mm, but because it was the coldest, the balance evaporation was only 438 mm. The runoff coefficient dropped significantly – to 0.24. The 1990–2022 thirty-year period was the warmest, resulting in high evapotranspiration – 507 mm per year. Despite the higher rainfall, runoff fell to only 131 mm and the runoff coefficient fell to 0.2.

From the measured annual values over a 90-year period, a regression analysis was used to derive an empirical relationship for estimating the future development of runoff from the Litava basin (between runoff, precipitation and air temperature (Halmová et al., 2022):

$$Rmod = 23.38 + 0.522\ P - 22.01\ T \quad (2)$$

where:
Rmod – mean annual runoff from the Litava basin;
P – annual areal precipitation in the Litava basin;
T – mean annual air temperature in the basin.

A multiple correlation coefficient of 0.77 was obtained in the calculation. From relation (2), it can be seen that a 100 mm decrease in precipitation in the Litava basin causes a 52 mm decrease in runoff. A 1°C increase in annual mean temperature results in a 22 mm decrease in runoff.

More detailed runoff balance results for individual months and for several runoff components (base runoff, direct runoff) can only be obtained by mathematical modelling - using the balance model in a monthly (daily) step (Hanel et al., 2012; Sleziak et al., 2021).

Runoff balance by BILAN model in monthly step

Modelling of water balance components during the whole period 1930/31–2019/2020

We calibrated the BILAN model on data from the Litava to Plášťovce basin for the period 1930/31–2019/2020 (hydrological year). Table 2 shows the resulting model parameters for the whole period 1930/31–2019/2020. We can visually assess the success of the model calibration in Fig. 4a. The correlation coefficient between measured and modelled values is relatively low at 0.72 (R^2=0.51). This results from the fact that we calibrated the model over a long period of 90 years. Conditions – e.g. vegetation - have changed in the catchment. If we had chosen shorter periods, the results would have been better, but we would have had different sets of parameters. This way we have one set of parameters for the whole period, and we can compare different periods with each other – which is our goal.

Fig. 4b and 4c show the individual components of the hydrological balance from the Litava basin for the whole period – outputs from the BILAN model. The long-term average baseflow (*BF*) accounts for 40.7% of the total modelled runoff (*Rmod*), interflow (*I*) accounts for 46.8% and direct runoff (*DR*) accounts for 12.5% of the total modelled runoff (*Rmod*).

The long-term average monthly water storage in snow (*SS*) and soil (*SW*) was highest in February (35.9 mm / resp. 79.2 mm). In groundwater (*GS*), the highest retention was in the month of March – 30.9 mm. Cumulatively, the highest water retention in the basin was in the month of February (138.3 mm), the lowest in the month of August (20 mm).

Changes of the hydrological balance during the three 30-years periods

Changes in selected components of the hydrological balance of the Litava in monthly steps for three 30-year periods: I. 1930/31–1959/60; II. 1960/61–1989/91 and III. 1990/91–2019/20 are graphically presented in Figures 5 and 6. The first and second graph of Figure 5, top left, plot the measured (*Robs*) and modelled (*Rmod*) long-term average runoff depth for the three periods. The following graphs plot the monthly courses of the evapotranspiration (*ET*), base flow (*BF*), interflow (*I*), and direct runoff (*DR*) over the three periods.

A comparison of the three 30-year periods shows:

The first period 1930/31–1959/60 and the third 30-year period are overestimated by the model. In contrast, the second period is underestimated by the modelled runoff – the model gives lower runoff values on average. Table 3 shows the annual values of base flow (*BF*), hypodermic runoff (*I*) and direct runoff (*DR*) for the three periods studied in millimetres (and as a percentage of total runoff). The results of the BILAN model show that the percentage of base runoff decreases and soil – hypodermic runoff increases.

Table 1. The Litava river basin annual water balance for 3 periods 1931–1960; 1961–1990; 1991–2020. *P*– precipitation depth, *R* – runoff depth, *ET* – annual balance evaporation, *T* – average annual air temperature in basin, *k* – runoff coefficient

Year	*P* [mm]	*R* [mm]	*ET* [mm]	*T* [°C]	*k*
1931–1960	655	205	451	8.38	0.30
1961–1990	582	145	438	8.29	0.24
1991–2020	638	131	507	9.16	0.20

Table 2. Model BILAN parameters for the Litava river basin, period: 1930/31–2019/2020

Period	*Spa*	*Dgw*	*Alf*	*Dgm*	*Soc*	*Wic*	*Mec*	*Grd*
1930/31–2019/20	80.00	6.674	0.001	14.441	0.383	0.465	0.742	0.327

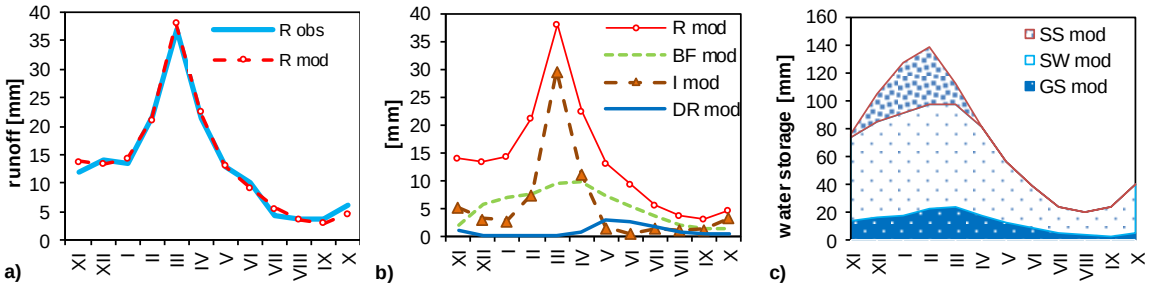

Fig. 4. a) Comparison of the long-term mean monthly runoff R (measured) and Rmod (modelled); (b) Long-term modelled mean monthly runoff Rmod, base flow BF, interflow I, and direct runoff DR; c) snow water storage SS, soil water storage SW, and groundwater storage GS; period 1930/31–2019/2020.

Table 3. The Litava river basin long term annual water balance for 3 periods. *Robs*– observed runoff depth, *Rmod* – modelled runoff depth, *BF* – base flow, *I* – interflow; *DR* – direct runoff

Period	*Robs* [mm]	***Rmod*** [mm]	*BF* [mm]	*BF* [%]	*I* [mm]	*I* [%]	*DR* [mm]	*DR* [%]
1930/31–2019/20	161	**171**	70.07	*40.7*	80.44	*46.8*	21.45	*12.5*
1930/31–1959/60	206	**226**	95.58	*42.2*	103.04	*45.58*	27.92	*12.3*
1960/61–1989/90	145	**129**	51.61	*39.9*	61.20	*47.3*	16.67	*12.9*
1990/91–2019/20	130	**159**	63.01	*39.4*	77.07	*48.2*	19.75	*12.4*

Discussion and conclusions

1. Statistical analysis of the daily flows of the Litava River shows:
   – The first thirty years 1931–1960 were the wateriest in the Litava basin. In the last thirty years, although the runoff coefficient was only 0.2 (runoff of 131 mm), the average daily flows of the Litava in Plášťovce reached the highest values. This is evidence of either more extreme rainfall events or poorer drainage conditions in the catchment (or a combination of both). To estimate future runoff trends from the basin, we used a simple regression relationship between runoff, precipitation, and air temperature, derived from the 90-year period 1931–2020, *Rmod = 23.38 + 0.522 P - 22.01 T*. This relationship shows that a 100 mm decrease in precipitation in the Litava basin causes a 52 mm decrease in runoff. A 1°C increase in mean annual temperature results in a 23.4 mm decrease in runoff. The results of the balance of the Litava: Plášť'ovce catchment are very similar to the results from the neighbouring Krupinica: Plášť'ovce catchment (Halmová et al., 2022).
2. The modelled results of the components of the hydrological balance for the whole period 1930/31–2019/20 by the BILAN model show:
   – Long-term average baseflow accounts for 40.7% of the total runoff, hypodermic runoff accounts for 46.8% and direct runoff accounts for 12.5% of the total runoff of the Litava in Plášťovce.
   – Cumulatively, the highest water retention in the basin was in the month of February (138.3 mm), the lowest in the month of August only (20 mm).
3. The results of the BILAN model for each 30-year period show that:
   – In absolute terms, soil water, snow and ground-water supplies in the Litava basin have declined.
   – In relative numbers, the percentage of base runoff decreases and soil - hypodermic runoff increases.

In this paper, we focused on the assessment of the long-term balance over a 90-year period with the BILAN model. Such a long period in Slovakia was first treated by a unified balance sheet model in Halmová et al. (2022). It should be noted that it is difficult to collect the necessary homogeneous input data for 90 years from the same location and with comparable instruments.

In addition, the assessed catchment must not be significantly anthropogenically influenced. There are only a few such catchments left in Slovakia. It is therefore necessary to focus on the assessment of changes in the hydrological balance in these catchments.

Acknowledgement

This work was supported by the project APVV No. 20-0374 "Regional detection, attribution and projection of impacts of climate variability and climate change on runoff regimes in Slovakia", and the project VEGA No. 2/0004/19 "Analysis of changes in surface water balance and harmonization of design discharge calculations for estimation of flood and drought risks in the Carpathian region".

References

Ďurigová, M., Ballová, D., Hlavčová, K. (2019): Analyses of monthly discharges in Slovakia using hydrological exploratory methods and statistical methods. Slovak J. Civ. Eng. 27, 36–43. https://doi.org/10.2478/sjce-2019-0014

Fendeková, M., Blaškovičová, L. (Eds.) (2018): Prognosis of hydrological drought development in Slovakia. (Authors Bochníček, O., Blaškovičová, L. – Damborská, I, Fendek, M. Fendeková, M., Horvát, O., Pekárová, P., Slivová, V., Vrablíková, D.). Bratislava: UK in Bratislava, 181 p. ISBN 978-80-223-4673-3, http://europeandroughtcentre.com/2020/04/03/open-access-book-on-prognosis-of-hydrological-drought-development-in-slovakia/

Garaj, M., Pekárová, P., Pekár, J., Miklánek, P. (2019): The Changes of Water Balance in the Eastern Slovakia. IOP Conf. Ser.: Earth Environ. Sci. 362 012014. ISSN 1755-1307. https://iopscience.iop.org/article/10.1088/1755-1315/362/1/012014

Halmová, D., Pekárová, P., Podolinská, J., Jeneiová, K. (2022): The assessment of changes in the long-term water balance in the Krupinica River basin for the period 1931–2020. Acta Hydrologica Slovaca, 23, 1, 21–31, https://doi.org/10.31577/ahs-2022-0023.01.0003

Hanel, M., Vizina, A., Máca, P., Pavlásek, J. (2012): A multi-model assessment of climate change impact on hydrological regime in the Czech Republic. J. Hydrol. Hydromech., 60, 3, 152–161. https://doi.org/10.2478/v10098-012-0013-4

Holko, L., Parajka, J., Majerčáková, O., Faško, P. (2001): Hydrological balance of selected catchments in the Tatra Mountains region in hydrological years 1989–1998. J. Hydrol. Hydromech., 49, 3–4, 200–222.

Horvát, O., Hlavčová, K., Kohnová, S., Danko, M. (2009): Application of the FRIER distributed model for estimating the impact of land use changes on the water balance in selected basins in Slovakia. J. Hydrol. Hydromech., 57, 4, 213–225. https://doi.org/10.2478/v10098-009-0020-2

Horáček, S., Rakovec, O., Kašpárek, L., Vizina, A. (2009): Development of the model of hydrological balance – BILAN. Vodohospodárské technicko-ekonomické informace, 51, 2–5. (In Czech.)

Kašpárek, L., Novický, O. (1997): Application of a physically-based model to identify factors causing hydrological droughts in western and central European basins. In: FRIEND'97 – Regional Hydrology: Concepts and Models for Sustainable Water Resource Management (ed. by A. Gustard, S. Blazkova, M. Brilly, S. Demuth, J. Dixon, H. van Lanen, C. Llasat, S. Mkhandi & E. Servat), IAHS Publ. no. 246, 197–204. https://www.researchgate.net/publication/242413031_Application_of_a_physically-based_model_to_identify_factors_causing_hydrological_drought_in_western_and_central_European_basins

Kašpárek, L., Novický, O. (2004a): Background information BILAN, CD ROM, 9 pp.

Kašpárek, L., Novický, O. (2004b): Users guide BILAN, CD ROM, 12 pp.

Keszeliová, A., Hlavčová, K., Danáčová, M., Danáčová, Z., Szolgay, J. (2021): Detection of changes in the hydrological balance in seven river basins along the Western Carpathians in Slovakia. Slovak Journal of Civil Engineering, 29, 4, 49–60. https://doi.org/10.2478/sjce-2021-0027

Kostka, Z., Holko, L. (2001): Runoff modelling in a mountain catchment with conspicuous relief using TOPMODEL. (In Slovak). J. Hydrol. Hydromech., 49, 3–4, 149–171.

Majerčáková, O., Škoda, P., Šťastný, P., Faško, P. (2004): The development of water balance components for the periods 1931–1980 and 1961–2000. J. Hydrol. Hydromech. 52, 4, 355–364. (In Slovak).

Pavelková, D., Kandra, B., Hlavatá, H., (2016): Evaluation of long-term precipitation and temperature development in the central part of the East Slovakian Lowland, Acta Hydrologica Slovaca, 17, 1, 13–21. (In Slovak.)

Pekárová, P., Martincová, M., Miklánek, P. (2010): Water balance of the Belá River basin in 1940/41–2004/05 period (Part I.: Basin water storage change in two 30-years periods). Acta Hydrologica Slovaca, 11, 1, 3–11.

Petrovič, Š., Šoltís, J. (1984): Temperature conditions in Slovakia, Part 1. Zborník prác SHMÚ 23/1, Alfa, Bratislava. 220 pp. (In Slovak.)

Petrovič, P. et al., (2006): Basin-wide water balance in the Danube river basin. The Danube and its basin – Hydrological monograph Part VIII-3, ISBN 80-89062-49-0, IHP UNESCO & VÚVH, Bratislava, 161 pp.+4 maps.

Petrovič, P., Mravcová, K., Holko, L., Kostka, Z., Miklánek, P. (2010): Basin-Wide Water Balance in the Danube River Basin. In: Brilly, M. (eds) Hydrological Processes of the Danube River Basin. Springer, Dordrecht. https://doi.org/10.1007/978-90-481-3423-6_7

Porubská, D., Fendeková, M., Machlica, A. (2012): Assessment of the hydrological balance elements valuein the Ľupčianka basin.– Podzemná voda ISSN 1335-1052, XVIII, 2/2012, 173–182. (In Slovak.)

Porubská, D., Holko, L., Fendeková, M. (2013): Impact of input data on the simulation results of the rainfall-runoff model.– Podzemná voda ISSN 1335-1052, 19, 2/2013, 78–90. (In Slovak.)

Sleziak, P., Výleta, R., Hlavčová, K., Danáčová, M., Aleksić, M., Szolgay, J., Kohnová, S., (2021): A Hydrological Modeling Approach for Assessing the Impacts of Climate Change on Runoff Regimes in Slovakia. Water, 13, 23, 3358. ISSN 2073-4441. https://doi.org/10.3390/w13233358

Šamaj, F., Valovič, Š. (1978): Long-term precipitation depths during the period 1901–1970 in Slovakia. Zborník prác SHMÚ 14/1, Alfa, Bratislava, 413 pp. (In Slovak.)

Tallaksen, L. M., van Lanen, H. A. J. (eds) (2004): Hydrological Drought – Processes and Estimation Methods for Streamflow and Groundwater. vol. 48, Elsevier, Amsterdam

Vizina, A., Horáček, S., Hanel, M. (2015): New capabilities of the model BILAN. Vodohospodářské technicko-ekonomické informace. roč. 57, č. 4–5, str. 7–10. ISSN 0322-8916. (In Czech.)

Výleta, R., Sleziak, P., Hlavčová, K., Danáčová, M., Aleksić,

M., Szolgay, J., Kohnová, S. (2022): An HBV-model based approach for studying the effects of projected climate change on water resources in Slovakia. In EGU General Assembly 2022. – Vienna: eGU22-2409. ISSN 1607-7962. Available on: https://meetingorganizer.copernicus.org/EGU22/EGU22-2409

RNDr. Pavla Pekárová, DrSc. (*corresponding author, e-mail: pekarova@uh.savba.sk)
Ing. Zbyněk Bajtek, PhD.
RNDr. Pavol Miklánek, CSc.
Institute of Hydrology SAS
Dúbravská cesta 9
841 04 Bratislava
Slovak Republic

Assoc. Prof. RNDr. Ján Pekár, CSc.
Faculty of Mathematics, Physics, and Informatics
Department of Applied Mathematics and Statistics
Comenius University in Bratislava
Mlynská dolina
842 48 Bratislava
Slovak Republic

Ing. Katarína Jeneiová, PhD.
Mgr. Jakub Ridzoň
Slovak Hydrometeorological Institute
Jeséniova 17
833 15 Bratislava
Slovak Republic

DOI: 10.31577/ahs-2022-0023.02.0025

ACTA HYDROLOGICA SLOVACA

Volume 23, No. 2, 2022, 226–233

Comparison of spatial interpolation methods of hydrological data on example of the Pripyat river basin (within Ukraine)

Kostiantyn SOKOLCHUK*, Marek SOKÁČ

The article considers four methods of spatial interpolation: method of inverse weighted distances (IDW), triangulation (TIN), Spline interpolation and Kriging. The Pripyat basin was chosen as the study area, and the regularities of the spatial distribution of hydrological characteristics across the territory were assessed. For this territory, maps of spatial distribution of the specific discharge by four chosen methods were created; the accuracy of the obtained results was assessed. Based on the results of the work it was determined that the IDW method with a distance coefficient P=2 gives better results for the generalization of hydrological data over the studied area. The next most reliable methods are Kriging, which shows small errors, and Spline, with smooth transitions. The least suitable among the studied methods is TIN method. To study boundaries and territories that are outside the boundaries defined by GIS based on input data, in this case – Pripyat basin, IDW method is recommended to use, while every other can be used to study the central part of the catchment, with different reliability for the boundary territories.

KEY WORDS: spatial interpolation, geographic information systems, map creation, IDW method, Kriging method, spline, TIN, Pripyat.

Introduction

In order to obtain a continuous map of the distribution for runoff characteristics over the areas, which are insufficiently covered with measuring stations, it is necessary to apply various methods of spatial interpolation. There are various methods of interpolation, but the choice of the optimal one depends on the data sample, the density of the network of observations, the physical and geographical conditions of the territory and the features of the spatial distribution of each specific characteristic (Ghasemi et al, 2015). Nowadays, the most convenient methods of interpolation involve the use of GIS technologies.

In hydrology and engineering hydrology, hydrological data modelling and analysis are necessary, at different scales and for various purposes (Sui and Maggio, 1999). GIS technologies are necessary and useful tools in surface water management, which allow presenting the relationship between spatial and hydrological data of river basins (Kusre et al, 2010). A description of this topic and the benefits of using GIS technologies can be found in the works of Ukrainian (Korniienko et al, 2021; Pochaievets et al, 2021) and international researchers (Hammouri and El-Naqa, 2007; Sami et al, 2013). However, despite a number of works devoted to the interpolation of hydrological data within the Pripyat basin, full-fledged comparisons of different interpolation methods were not carried out in practice. Analyses of this type are carried out all over the world (Dzhalalvand et al, 2019), but their results cannot be accurately extrapolated to areas with other natural conditions. All this determines the relevance of this topic.

This type of researches is also important as the Pripyat River basin has an insufficiently dense network of observation stations and an uneven distribution of hydrological posts throughout the basin. This requires spatial interpolation in the study of river basins and river basins management (Sokolchuk, 2019).

The goal of this paper is to compare the effectiveness of the IDW, Spline, Kriging and TIN methods in the spatial interpolation of specific hydrological data on the territory of the Pripyat River basin within Ukraine, determine the optimal settings for each method.

Material and methods

The studied area is the Pripyat River basin, within Ukraine. Pripyat is a river in Ukraine, located in Volyn, as well as partly in Rivne and Kyiv regions, and in Belarus. It is the largest river among the right Dnipro river tributaries, and flows into the Kyiv reservoir. The total area of the river basin is 121 000 km^2. The Belarusian part of the basin is approximately 43% of the catchment area, the Ukrainian – around 57% (Palamarchuk and Zakorchevna, 2001). The flat nature of

the river and slight slopes of the water surface create difficulties in determining hydrological parameters of the river and basin, which is why the values of the basin area and river length can vary according different literature sources (Obodovskii et al, 2012).

The Pripyat basin occupies almost the entire north-western part of Ukraine (Fig. 1). Permanent posts of the hydrological measuring network are located on the right bank of Pripyat River. In view of the foregoing, obtained results can be applied only for this part of the basin, which, however, is most of the Pripyat basin within Ukraine. The Pripyat basin has a well-developed hydrographical network, approximately 10.5 thousand of rivers and streams. Among the right-bank tributaries flowing through the territory of Ukraine the most significant are Turia, Stokhid, Styr, Horyn, Stvyha, Ubort, Slovechna, Solon, Uzh. The Pripyat basin is located within two physical and geographical zones, this river basin is one of the most swampy and forested area in Ukraine.

The climate in the territory of the studied basin is moderately continental with warm and humid summers and fairly mild winters. Spring is long and unstable, with frequent alternating cold and warm periods, summer is warm and rainy. The annual amount of precipitation in the territory of the basin varies from 550 to 600 mm (EUWI+, 2019).

The water regime is characterized by a long spring flood, a short-term summer low, which is disturbed by rain floods and almost annual autumn water level rises. Spring accounts for 65% of the annual runoff (Susidko and Lukianets, 2004).

Most of the Pripyat basin is located within the Poliska Lowland, the south-western part of the basin is on the Volyn Upland. The relief is mainly flat and undulating lowlands and plains. Widespread denudation forms of relief, which are formed on crystalline rocks (EUWI+, 2019). The relief is homogeneous, the landscape and meteorological conditions change smoothly. Therefore, physical and geographical conditions within the territory of the Pripyat basin allow making spatial interpolation. Considering similar physical and geographical conditions of neighbouring watersheds, also data from the Teteriv River basin and the South Bug River was used.

Methodology and input data

As a basic hydrological characteristic for this study, the average annual specific discharge was chosen. It was calculated based on data from stationary flow measurement stations. This characteristic is used to create cartographic materials, compare watersheds, etc. Using GIS were calculated the centre points of the catchments area for particular catchments, defined by the hydrological stations. The general picture of division is presented in figure 2. The study is based on data from 33 permanent hydrological observing posts, 28 within the Prypiat basin and 5 outside this river basin.

The long-term averaged value of specific discharge for the right side of Prypiat basin according to observations ranges from its smallest value 2.10 l s^{-1} km^{-2} in the upper reaches of the Prypiat (Lyubyaz), the eastern part of the basin, to its highest value of 5.94 l s^{-1} km^{-2} for the river Radostavka above Triytsya, in the north-western part of the basin. The area of the basin does not have a predominant effect on the specific discharge; mainly this characteristic depends on the physical and geographical conditions of the territory. Similar patterns of spatial changes can be observed on all obtained maps, which allow comparison of the interpolation methods accuracy. Taking into account a certain unevenness of the development of the hydrological observation network, further evaluation and averaging of data, all available data from hydrological stations were used. Most series of observations begin in the period from the late 1940s to the early 1960s, the average duration of water runoff observations is more than 60 years. In the presence of individual gaps, they were filled with the help of correlation dependencies. Series of observations are sufficiently representative, and runoff parameters in general are reliable and unbiased. This pattern is disturbed for two data series: at the posts Pripyat – Richitsa and Norin-Slovenia. Physical and geographical features of their basins and anthropogenic activities influenced the average annual runoff in these stations. Considering that interpolation comes from watershed centres, and the probable causes of abrupt changes in the average annual runoff are specific to the territory of these watersheds, these data were also used to study spatial generalizations patterns (Sokolchuk, 2019).

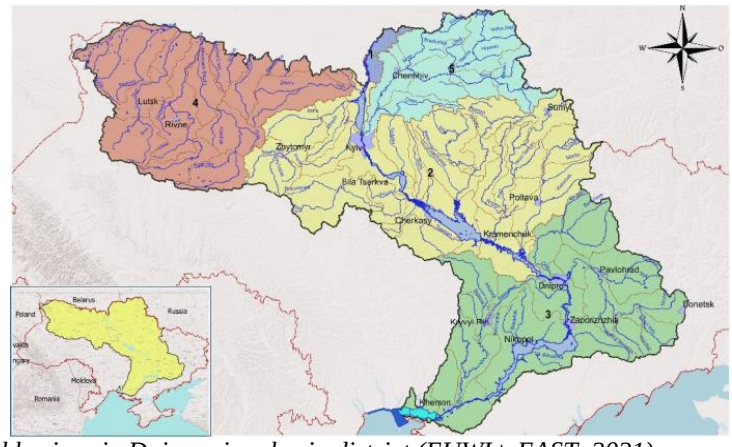

Fig. 1. Subbasines in Dnipro river basin district (EUWI+ EAST, 2021).

During the research, four spatial interpolation methods were compared, for some of them different settings were used. First method- the triangulation (TIN), is based on linear interpolation and it is close to the manual linear interpolation. The starting points are connected in such a way that the resulting surface is covered by triangles, and none of the sides of the triangle intersects the sides of the other triangles (Fig. 3). The surface values at the points of the grid network, which are inside the triangle, are calculated based on the fact that they belong to the plane passing through the vertices of the specific triangle. The obtained surface necessarily passes through all the starting points at which the surface values are determined by observation. Insufficient number of starting points leads to the appearance of large rectilinear segments on the map; the result obtained in this case would be a method error.

The second method used is method of inverse weighted distances IDW. It is based on the calculation of weights by which the values of the surface at the starting points are "weighed" when constructing the interpolation function. The weighting factor assigned to a single starting point for calculating the surface value at the grid node is proportional to the degree of inverse distance from the starting point to the calculated grid node.

In order to calculate the surface value at the grid node, the sum of all the weights of the starting points is equal to one, and the weight of each starting point is the fraction of this total unit weight. Structure of isolines can form concentric areas of the same value around known data points, generally around one with large or small values of the surface area. It is known as "bull's eye effect", which is the disadvantage of the IDW method. To reduce the influence of these points when implementing the method, it is necessary to set the value of the parameter that smoothest the interpolation function. The larger the smoothing parameter, the less influence each starting point has on the calculated value in the Grid node (Ishchuk et al, 2003). For this research two values were used, P=2 and P=5, they are indicative and within which the results are approximately reliable for the available data.

Spline is the third interpolation method, tool that estimates values using a mathematical function that minimizes overall surface curvature, resulting in a smooth surface that passes exactly through the input

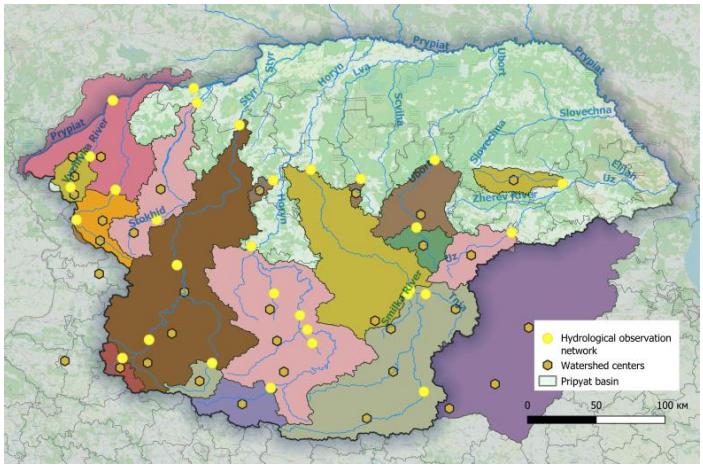

Fig. 2. Division of the Pripyat basin into separate watersheds.

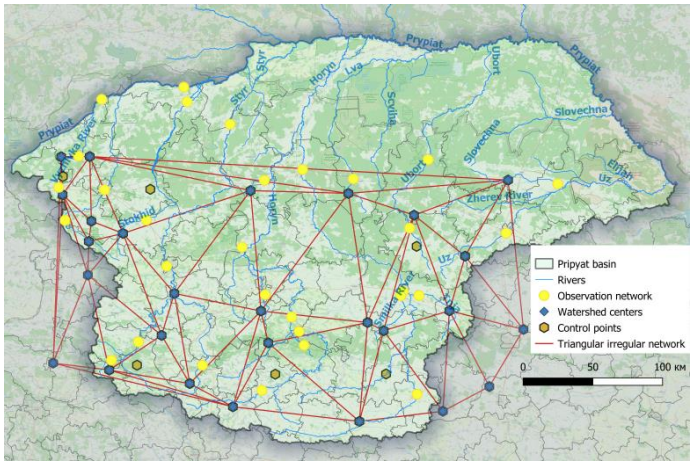

Fig. 3. Triangular irregular network for watershed centres for Pripyat basin within Ukraine.

points. Conceptually, the sample points extrude to the height of their magnitude. The spline works on the principle of a surface that passes through the input points while minimizing its total curvature. It fits a mathematical function to a specified number of nearest input points while passing through the sample points. This method is highly useful for generating smoothly varying surfaces such as elevation, water table heights or pollution concentrations. We can assume that the hydrological characteristics of the watersheds have similar distribution features.

The IDW and Spline interpolation tools are referred to as deterministic interpolation methods as they are directly based on the surrounding measured values or on specified mathematical formulas that determine the smoothness of the resulting surface. Another type of interpolation methods consists of geostatistical methods, such as Kriging, which are based on statistical models that include autocorrelation, the statistical relationships among the measured points. Due to this, geostatistical techniques not only have the capability of producing a prediction surface but also provide some measure of the certainty or accuracy of the predictions (ESRI, 2016; Watson and Philip, 1985).

Kriging is the fourth method, which was chosen for comparison. It assumes that the distance or direction between sample points reflects a spatial correlation that can be used to explain variation in the surface. The Kriging tool fits a mathematical function to a specified number of points, or all points within a specified radius, to determine the output value for each location (ESRI, 2016).

The evaluation of the used methods was performed by determining the differences between the actual values of the specific discharge and the values taken from the created maps. The evaluation was performed in two ways. The first one was the evaluation of the differences of the observation points, used for the interpolation procedures (22 observation "non-control points" out of total 28 points). This type of the evaluation aims to determine how accurate the interpolation procedures are with respect to the existing (specified) observation points. In the second type of evaluation, 6 points out of 28 within the study area were selected and excluded from the interpolation procedure ("control points"). The evaluation was done based on the comparison between the measured (real) and interpolated values in these control points. This was done to test the feasibility of using the interpolated maps obtained during the research to study hydrologically unexplored watersheds. Points were selected on the principle of even distribution across the territory. The hydrological stations of the catchments adjacent to the Pripyat basin were not taken into account in this assessment.

To calculate the mean absolute error (MAE) of the obtained results, all individual regression residues are squared, summed, and the sum is divided by the total number of checked points (Azpurua and Ramos, 2010):

$$\mathrm{MAE} = \frac{\sum_{i=1}^{n}|(y_i - y_p)|}{n} \quad (1)$$

where

y_i – actual value, obtained from observations,

y_p – predicted value, obtained by interpolation,

n – number of points.

The square root of this value is denoted as RMSE (Root Mean Square Error):

$$\mathrm{RMSE} = \sqrt{\frac{\sum_{i=1}^{n}(y_i - y_p)^2}{n}} \quad (2)$$

The deviation is also presented as a percentage, by dividing the average absolute error by the average real specific discharge.

A comparison of this type cannot be based solely on a mathematical assessment of the results. We estimated as well as the shape of the isolines, the presence of numerical errors on the interpolated surface which called artifacts - unwanted effects which result from using a high- precision GIS to process low-accuracy spatial data, from positional errors, not attribute errors etc. (Goodchild and Kemp, 1990). Also were taken into consideration the overall compliance of the distribution of the annual average specific discharge within the studied area.

Results

As a result of the research maps of the distribution of the specific discharge were created using different methods of spatial interpolation. The nature and features of spatial changes of the selected hydrological characteristic within the basin was analysed. Surfaces of mathematically calculated values are presented in the form of gradient with extracted isolines on Fig. 4a, 4b and 5a–e.

The results of the comparison of actual and interpolated values are shown in Table 1 and 2. In absolute values the lowest error has the method of Kriging exponential, the second most accurate method is the IDW method. The highest errors are shown by values, taken from surfaces, interpolated by the TIN linear and Kriging exponential. Despite the difference in accuracy between the methods is 100%, on average obtained values deviate from the actual values of the specific discharge by less than 6%, i.e. all methods give a result close to the actual values.

The assessment of the accuracy of the obtained maps during the inspection for the previously extracted control points (Table 2), as expected, showed greater errors, but the general trends remain. Kriging shows the most accurate results, followed by IDW, TIN and Spline in sequence. Last one showing more than 15% error for the assessment of basins within the study area.

Of all the four methods used, only one, IDW, also allows data extrapolation beyond conditional boundaries formed by geographically boundary points (Fig. 4a and 4b). This allows estimating values for most of the Pripyat basin within Ukraine. However, due to the absence of observation posts, the assessment of their accuracy in the most remote parts is difficult. The figures (Fig. 4a

and 4b) also show the formation of "bull's eyes" effect, information is not interpolated on the entire territory, especially when increasing the distance factor. However, given the interpolation from the centres of catchments, mostly slow changes in physical and geographical conditions of runoff formation in the study area, which is indirectly confirmed by small errors, the application of the method is rather justified.

Interpolations by the other three methods give results only within the limits, set automatically by the QGIS, defined by input data. It is more mathematically correct, but does not allow to fully assess the watersheds, not sufficiently covered with hydrological observation network. Each of the methods has its advantages, disadvantages and features, caused by both the mechanisms of their work and the peculiarities of the mechanism in the GIS environment used.

When interpolating by the Kriging method, shown in Fig. 5a and 5b, the data are interpolated over the area, the transitions are smoother. However, a more detailed analysis of maps and isolines extracted from them showed that at some points of the isolines make sharp changes in direction of isolines and artefacts are widely formed. Therefore, the use of this method for a detailed study of the area might require additional operations.

Figures 5.c and 5.d show that when interpolated using the TIN method, the isolines are not sufficiently smooth. Some large rectangular areas with the same values of the specific discharge can be seen, i.e. the method might give inaccurate results. The results at the boundary of the obtained interpolation site in the north are strongly distorted when using TIN cubic (Fig. 5d) due to the peculiarities of the interpolation mechanism in QGIS. It is not possible to take reliable values for the boundary points for their verification, which was also considered in the calculations for Table 1 and 2.

Table 1. Evaluation of interpolation methods in non-control points

Parameter	Indicator	Methods of interpolation						
		Spline	Kriging spherical	Kriging exponential	TIN cubic	TIN linear	IDW. P=5	IDW. P=2
Errors of average annual runoff modules	MSE	0.14	0.17	0.08	0.15	0.18	0.11	0.10
	RMSE	0.38	0.41	0.29	0.38	0.43	0.33	0.31
Average deviation	%	4.03	4.78	2.25	3.85	5.07	3.02	2.73

Table 2. Evaluation of interpolation methods by control points

Parameter	Indicator	Methods of interpolation						
		Spline	Kriging spherical	Kriging exponential	TIN cubic	TIN linear	IDW. P=5	IDW. P=2
Errors of average annual runoff modules	MSE	0.55	0.35	0.31	0.43	0.36	0.42	0.18
	RMSE	0.74	0.59	0.56	0.65	0.60	0.65	0.43
Average deviation	%	15.13	9.70	8.42	11.63	10.20	11.66	5.43

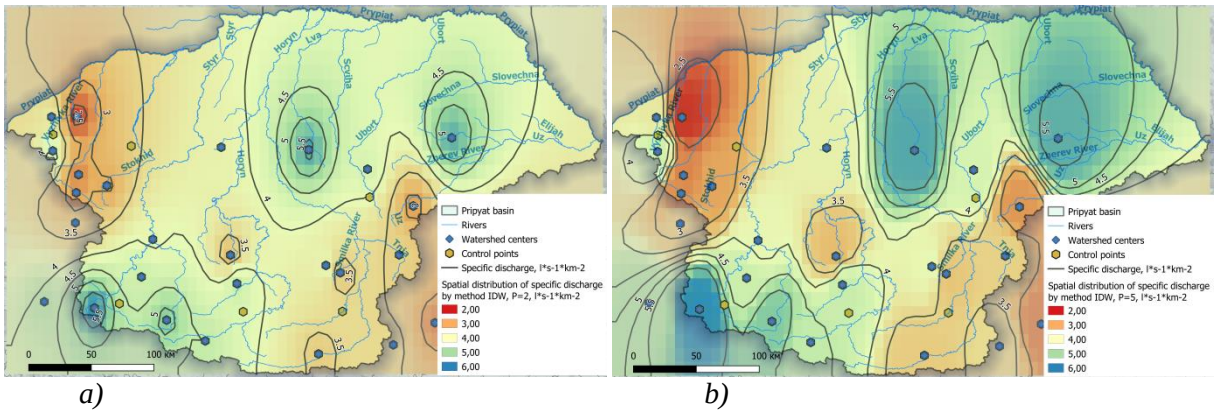

a) *b)*

Fig. 4. Spatial distribution of specific discharge for Pripyat basin within Ukraine, created by the method of IDW a) with P=2; b) with P=5.

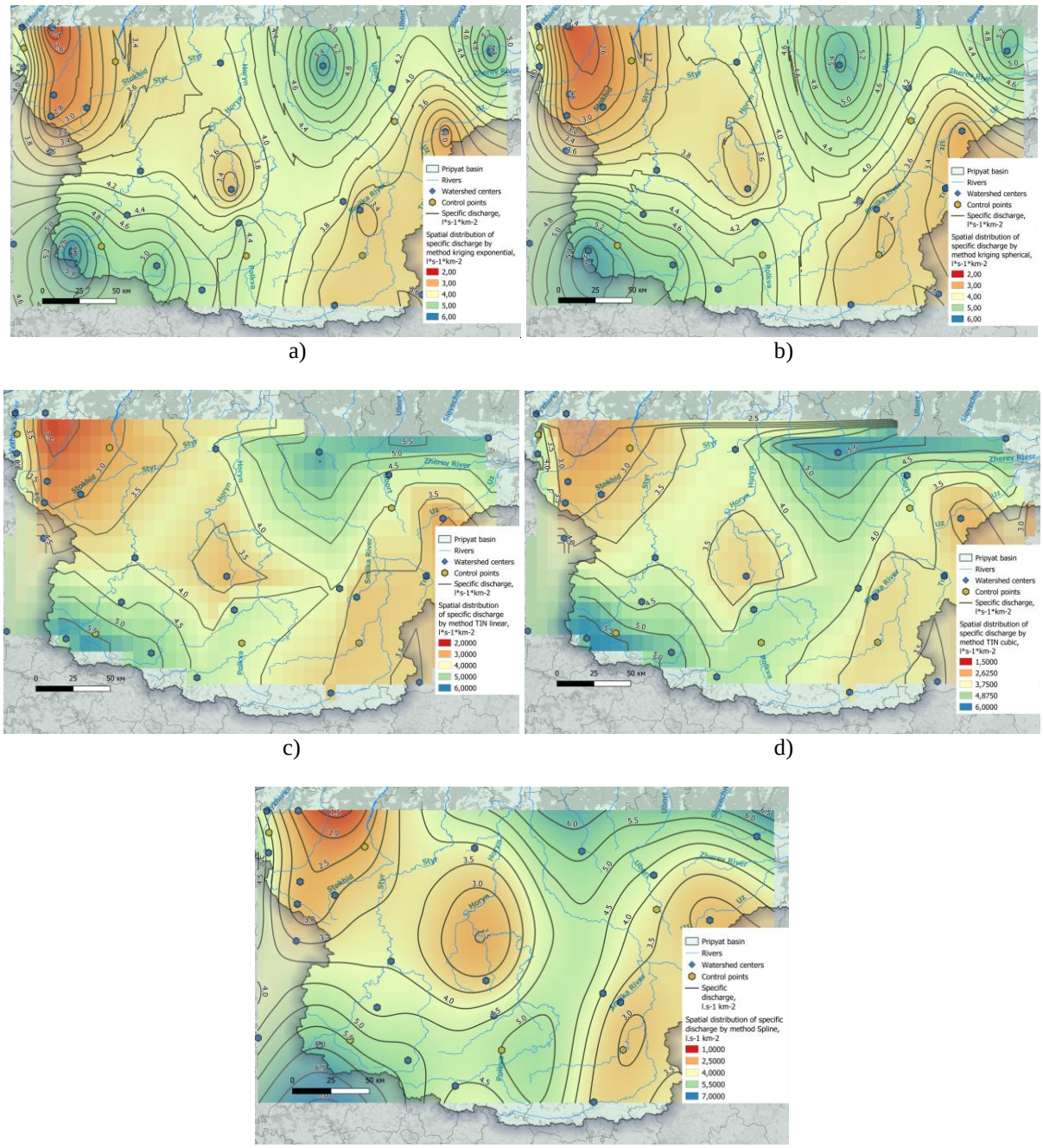

Fig. 5. Spatial distribution of specific discharge for Pripyat basin within Ukraine, created by method: a) Kriging exponential; b) Kriging spherical; c) TIN linear; d) TIN cubic; e) Spline.

The transitions and isolines obtained by the Spline method are the smoothest, sharp outlines are not present. The interpolation results are also distorted in the north of the basin due to the mechanism of the algorithm, but to a lesser extent than when using TIN cubic.

Conclusions

According to the results of the work, considering both errors and visual assessment, came to the conclusion that the IDW method is better for data interpolation over the study area. The isolines are smooth and it is possible to obtain an approximate estimate for the entire catchment, which may be particularly important for regions, where there are not enough observation stations. Despite the error of the obtained values is not the smallest for it with distance coefficient P=5, using higher coefficient is necessary to identify zones with significant deviations from the average, as well as to reconcile the boundaries of the zones of influence of the points with the boundaries of watersheds.

Kriging method allows obtaining specific discharge with

relatively small errors; however, the results require significant refinement or improvement of the source programs that provide interpolation.

TIN method in none of the variants can be used to accurately study the boundaries of the catchment and areas outside the defined area. Given the inability to rapidly increase the number of reference points and the above aspects, TIN in these conditions can be used only to refine data in the central part of the right bank of the Pripyat river basin. Compared to linear TIN, TIN cubic showed lower accuracy.

The Spline method, despite relatively significant errors and some implementation problems, was proven to be a promising option for further research. Significant advantages are smooth isolines, absence of artefacts. The prevalence of the method for hydrological interpolation was not presented in the Ukrainian scientific literature, which may be due to the small number of such estimates and the lack of this method in the standard set of tools of one of the most common GIS (QGIS).

The obtained results can be used to analyse patterns of spatial distribution of hydrological characteristics in the Pripyat basin and preliminary research of catchments, which are not sufficiently covered by observation stations. These conclusions can be cautiously applied to catchments of other rivers with similar conditions, i.e. for plain catchments with smooth changes in the conditions of flow formation, with an average catchment area ranging from 1,000 to 10,000 km^2. Considering the complete absence of rivers with a catchment area of less than 100 km^2 in the database, the obtained conclusions require separate confirmation of their suitability for the analysis of small rivers. This article also could be used as an illustrative example of the differences between various interpolation methods. It is planned to conduct additional assessment of the accuracy of these methods on watersheds with different hydrologic conditions.

Acknowledgment

The authors would like to express his thanks for the support to the Taras Shevchenko National University of Kyiv, Faculty of Geography, Department of Hydrology and Hydroecology, namely to docent Olga Lukianets, and to Olena Pochaievets, for their help during this research.

References

Azpurua, M. A, Ramos K. D. (2010): Comparison of spatial interpolation methods for estimation of average electromagnetic field magnitude. Progress in Electromagnetics Research, Vol. 14, 2010. 135–145.

Dzhalalvand A., Gaidukova E.V., Burlov V. G. et al. (2019): Applying methods of spatial interpolation to hydrological data on example of reception basin of Karun river (Iran). International Research Journal.– 2019. – №2 (80). – URL: https: //research-journal.org/archive/2-80-2019-february/ primenenie-metodov-prostranstvennoj- interpolyacii-k-gidrologicheskim-dannym-na-primere-vodosbora-r-karun-iran (accessed: 09. 09. 2022). – doi: 10.23670/IRJ.2019. 80.2.006

ESRI (2016): How Kriging works. ArcGIS for Desktop [Electronic resource] // Environmental Systems Research Institute, 2016. – URL: https://desktop.arcgis.com/en/ arcmap/10.7/tools/3d-analyst-toolbox/how-kriging-works.htm (accessed 02. 06. 2022)

EUWI+EAST (2022): River basin management plan in Ukraine. [Electronic resource] International Office of Water, 2021. – URL: https://www.euwipluseast.eu/en/ partners-countries-activities-ukraine/ukraine/river-basin-management-plan (accessed 09. 09. 2022)

EUWI+ (2019): Nabyvanets, Y., Osadcha, N., Hrebin, V., Vasylenko, Y., Koshkina, O.: Development of draft river basin management plan for Dnipro river basin in Ukraine: phase 1, step 1 – Description of the characteristics of the river basin. EUWI+ Project.

Ghasemi, M., Mahdavi, A., Jafarzadeh A. A. (2015): Compare Kriging and IDW interpolation methods for soil mapping. The 2nd National Conference on Environment Hazard of Zagros, Tehran, 5 March 2015.

Goodchild, M. F., Kemp, K. K. (1990): NCGIA Core Curriculum in GIS. National Center for Geographic Information and Analysis, University of California, Santa Barbara CA

Hammouri, N., El-Naqa, A. (2007): Hydrological modeling of ungauged wadis in arid environments using GIS: a case study of Wadi Madoneh in Jordan. Revista mexicana de ciencias geológicas, 24, 2007. – Pages 185–196.

Ishchuk, O. O., Korzhnev, M. M., Koshlyakov, O. E. (2003): Просторовий аналіз і моделювання в ГІС: Навчальний посібник (Spatial analysis and modeling in GIS: Training manual.) - K.: Publishing and Printing Center "Kyiv University". [in Ukrainian]. 2003. – 200 p.

Korniienko, V., Obodovskyi, O., Snizhko, S. (2021): The spatial analysis of the hydropower modules distribution for the Pripyat basin within Ukraine using open GIS technologies. 20th International Conference Geoinformatics: Theoretical and Applied Aspects, 2021(1), 1–6. https://doi.org/10.3997/2214-4609. 20215521142

Kusre, B. C., Baruah C., Bordoloi P. K., Patra S. C. (2010): Assessment of hydropower potential using GIS and hydrological modeling technique in Kopili River basin in Assam (India). Applied Energy, Volume 87, Issue 1, January, 2010. – Pages 298–309, doi.org/10.1016/j. apenergy.2009.07.019.

Obodovskii, A. G., Stankevich, A. P., Afanasiev, S. A. (2012): Управление трансграничным бассейном Днепра: суббасейн р.Припяти: монография (Management of transboundary Dnieper river basin: sub-basin of the r. Pripyat: monograph). Kyiv: Kafedra. [in Russian]. 448 p.

Palamarchuk, M. M., Zakorchevna, N. B. (2001): Водний фонд України: довідковий посібник. (Water Fund of Ukraine: reference manual), ed. Khoreva, V. M. , Aliyeva, K.A.; K- Nika-Center. [in Ukrainian], 2001. 392 p.

Pochaievets, O., Obodovskyi, O., Lukianets, O., Grebin, V. (2021): Algorithm research and evaluation of minimum water flow of mountain rivers using GIS. 20th International Conference Geoinformatics: Theoretical and Applied Aspects. https://doi.org/10.3997/2214-4609. 20215521123

Sami, K., Mohsen, B. A., Afef, K., Fouad, Z. (2013): Hydrological Modeling Using GIS for Mapping Flood Zones and Degree Flood Risk in Zeuss-Koutine Basin (South of Tunisia). Journal of Environmental Protection, 4(12), 1409–1422. https://doi.org/10.4236/JEP.2013. 412161

Sokolchuk, K. I. (2019) Evaluation of the representativeness

of the series of observations and sampling parameters of the distribution of the mean annual runoff of the rivers in the right bank of the Pripyat basin. Hidrolohiia, hidrokhimiia i hidroekolohiia. 2019. № 2 (53) 31–37. [in Ukrainian].

Susidko M. M., Lukianets O. I. (2004): Районування території України за ступенем гідрологічної небезпеки (Zoning of the territory of Ukraine by the degree of hydrological danger). Scientific project of UkrNDGMI. [in Ukrainian], – 2004. Issue 253. 196–200.

Sui, D. Z., Maggio, R. C. (1999): Integrating GIS with hydrological modelling: practices, problems, and prospects, Computers, Environment and Urban Systems; Volume 23, Issue 1. 1999. – Pages 33–51, doi.org/ 10.1016/S0198-9715(98)00052-0

Watson, D. F., Philip G. M. (1985): "A Refinement of Inverse Distance Weighted Interpolation." Geoprocessing 2: 315–327. 1985.

Kostiantyn Sokolchuk, M.Sc. (*corresponding author: sokolcuk@uh.savba.sk)
Assoc. Prof. Ing. Marek Sokáč, PhD.
Institute of Hydrology SAS
Dúbravská cesta 9
841 04 Bratislava
Slovak Republic

Kostiantyn Sokolchuk, M.Sc.
Institute of Landscape Engineering, Faculty of Horticulture and Landscape Engineering
Slovak University of Agriculture in Nitra
Tulipánová 7
949 76 Nitra
Slovak Republic

DOI: 10.31577/ahs-2022-0023.02.0026

ACTA HYDROLOGICA SLOVACA

Volume 23, No. 2, 2022, 234–240

Verification of the automated flood forecasting system on the Stryi River

Borys KHRYSTIUK, Liudmyla GORBACHOVA*, Vitalii SHPYG

The physical and geographical location of the Stryi River Basin causes the formation of catastrophic floods, which are regularly forming in this region and cause significant material damage and, sometimes, the death of people. The last catastrophic flood took place on the Stryi River in June 2020. Thus, the creation of a modern system for forecasting the streamflow of the Stryi River is a very important task. This paper describes such an automated flood forecasting system (FFS Stryi) that is developed at the Ukrainian Hydrometeorological Institute of the State Emergency Service of Ukraine and the National Academy of Sciences of Ukraine. The basis of the system is the hydrological module NAM of the Rainfall-Runoff software complex MIKE 11 (Denmark), which uses the forecasted weather parameters from the numerical mesoscale atmospheric model WRF ARW v. 3.6.1 (USA). The objective of this study is to verify this system and identify the factors that affect the accuracy of flood forecasting of the Stryi River. The system of streamflow forecasting of the Stryi River uses the continuous series of calculated (historical) levels and discharges, air temperature, precipitation, evaporation, as well as the forecast of meteorological indicators for 5 days. The system is set to work with a three-hour time step in the automatic regime. Verification of FFS Stryi according to the historical meteorological data showed that the system reproduces the streamflow of the Stryi River with satisfactory quality. The accuracy of discharge forecasting depends on the accuracy of weather parameters forecasting and, above all, the quantity of precipitation and the time of their falling out. Errors of hydrological forecasting are caused by an imperfect hydrometeorological network of observations (number of points and frequency of measurement), a digital model of the relief of the Stryi River basin and errors of weather parameters forecasts.

KEY WORDS: short-term forecasting, weather forecast, NAM RR MIKE 11, WRF ARW v. 3.6.1, Stryi River

Introduction

The formation of extreme floods is a common problem around the world, and in particular in Ukraine (Susidko and Luk'yanets, 2004; Sofia and Nikolopoulos, 2020; Khrystiuk et al., 2020; Merz et al., 2021; Yang et al., 2021). The most flood-prone region of Ukraine is the Carpathians, where frequent rain floods, sometimes catastrophic, cause significant material damage associated with the destruction of settlements, agricultural lands, communications, etc. (Susidko et al., 2011). Of course, early warning about future floods is the paramount importance for this area, both in view of the timely implementation of flood control measures, and to improve the efficiency of the operation of hydropower and other water facilities (Romashchenko and Savchuk, 2002; Gorbachova, 2012).

In the world, modern hydrological services are using computer simulation systems for river runoff forecasting, which are based on a hydrological model that works automatically using weather forecast (WMO, 2009; Roelevink et al., 2010; Gorbachova, 2012; Shakirzanova et al., 2019). Today in Ukraine such a modern direction is insufficiently developed. In Ukraine, a lot of scientific developments in hydrological forecasting use methodological achievements that were formed in the 60-70s of the twentieth century (Susidko, 2000; Luk'yanets, 2004; Priymachenko, 2010; Susidko et al., 2011; Dutko and Sosedko, 2011; Moskalenko, 2012; Khrystyuk, 2014; Shakirzanova et al., 2019). This applies to the development of methods for short-term forecasting of floods in the Dniester River Basin, which were started at the Ukrainian Hydrometeorological Institute of the State Emergency Service of Ukraine and the National Academy of Sciences of Ukraine (UHMI) in the 70s of last century. The methods were based on the regression dependences or on the mathematical models of rain and snow-rain runoff formation that were proposed by the specialists of the Hydrometeorological Center of the former USSR (GHF, 1989; Priymachenko, 2010).

It should be noted that the former models of rain and snow-rain runoff formation on the Carpathian rivers have not lost their physical nature so far, but their practical use is limited by the lack of observation points for hydrometeorological indicators in the areas of the intensive runoff formation and the low observation

frequency of these indicators, as well as the imperfect technology of observation, transmission and processing of hydrometeorological data. In addition, the forecasts of river runoff according to these models offer slight lead time, as they do not fully take into account the forecasts of weather parameters. Another disadvantage is that different models are used to forecast floods of different genesis. It is clear that modern hydrological forecasts should be based on a detailed (in space and time) forecast of weather parameters that can be obtained by the numerical meteorological models (WMO, 2009; Roelevink et al., 2010). For the above reasons, in the UHMI there has been created, as an alternative to the existing models of short-term forecasting of rivers runoff on the Dniester Mountain tributaries, an automated short-term flood forecasting system on the example of the Stryi River Basin (FFS Stryi), which uses the MIKE module 11 (Denmark) and the numerical mesoscale atmospheric model WRF ARW v. 3.6.1 (USA). Thus, the objective of this paper is to verify this system and identify factors that affect the accuracy of streamflow forecasting of the Stryi River.

Materials and methods

The Stryi River Basin is located on the eastern slopes of the Carpathian Mountains (Fig. 1). The Stryi River belongs to the right-bank tributaries of the Dniester River, which are mountain rivers with significant slopes of channels and terrain and with little permeable soil cover (Kaganer, 1969). In their basins, the mean annual rainfall is 750–1000 mm and they are the main area of formation of the Dniester River (Priymachenko, 2010; Khrystiuk, 2017).

Melting snow in the mountains in spring and winter, during thaws, as well as prolonged rains and rain showers by summer and autumn, combined with a well-developed hydrographic network, cause the floods of varying duration and discharges on the Stryi River. Particularly dangerous are the floods of the warm season, which are formed after heavy rains in the mountains (Priymachenko, 2010).

During the whole period of observations on the Stryi River at Verkhne Synovydne village, the largest catastrophic flood was the flood in June 1969. The maximum discharge consisted of 2610 $m^3 s^{-1}$ and was observed on June 9. This flood was the most dangerous not only in the Stryi River Basin, but also in the entire Carpathian region. Its frequency is estimated as once in 100 years. In the recent past, high rain floods were observed in 2008, 2010 and 2020. The floods of 2008 were caused by heavy rains with thunderstorms that covered the basins of the Tysa, Dniester and Prut rivers. The consequence of this catastrophic flood was not only the destruction of the region infrastructure, but also, unfortunately, the death of people. At the hydrological gauge of the Stryi River - Verkhne Synovydne village the maximum discharge consisted of 1720 $m^3 s^{-1}$ and was observed on July 25. In 2010, a catastrophic flood occurred in June and the first half of July in the basins of the Dniester and Eastern Carpathian Mountain. At the hydrological gauge of the Stryi River – Verkhne Synovydne village the maximum discharge consisted of 932 $m^3 s^{-1}$ and was recorded on July 8. (Adamenko, 2014; Lyalko et al., 2017). So, the rain flood of 2010 was chosen to verify the automated system of short-term flood forecasting on the Stryi River (FFS Stryi). This is due to the fact that the flood of 2010 was quite high, but not catastrophic, as the flood of 2020, during which there was a significant destruction of the regional infrastructure. Usually, after such catastrophic events, the maximum discharge in rivers is determined by an approximate method, namely by high water marks. Thus, the historical observation materials for the 2010

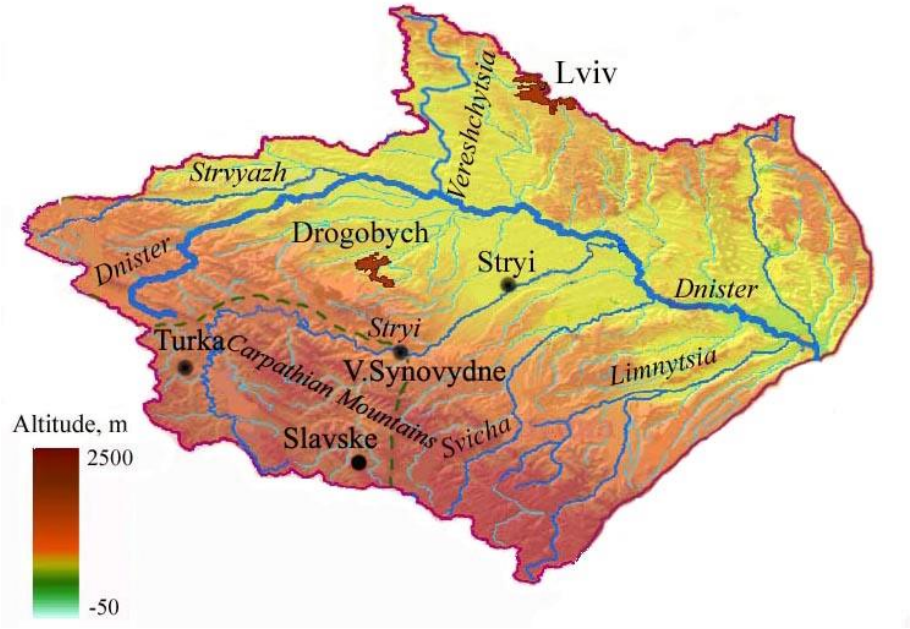

Fig. 1. Location of the Stryi River and the meteorological stations in its basin.

flood are of higher quality, which will improve the verification of the hydrological model.

The MIKE 11 software complex (developed by the Danish Hydraulic Institute) is widely recognized worldwide and is used for research and operational forecasting (Gorbachova, 2012; WMO, 2009; Roelevink et al., 2010; MIKE11, 2012; Shamsudin and Hashim, 2002). The MIKE 11 has a modular structure, which consists of the following basic modules: hydrological, hydrodynamic, advection-dispersion and bound sediments transport, water quality, transport of unbound sediments. Each of these modules has additional more detailed modules. The Rainfall-Runoff (RR) hydrological module contains additional modules, among which are the hydrological module (NAM), the unit hydrograph module (UHM), and the soil moisture accumulation model (SMAP). The NAM module is the most widely used, as it allows the best simulation of the streamflow from the catchment area, which is formed by melting snow and rainfall (Kumar et al., 2022; Bahremand and De Smedt, 2008; Shamsudin and Hashim, 2002). Therefore, the NAM module is suitable for simulating streamflow in the Stryi River Basin, which is characterized by snow-rain and rain floods. The Rainfall-Runoff NAM module is the balance model with lumped parameters. It takes into account the inflow of water to the catchment surface after rains and snowmelt, evaporation from the catchment surface and the formation of surface, subsurface and groundwater flow.

The input data of the Rainfall-Runoff NAM module are the continuous series of air temperature, rainfall and evaporation and discharge with a certain step in time and for a long period (up to 3 years). All these data can be obtained from the archives of the Central Geophysical observatory named after Boris Sreznevsky (CGO), except for evaporation from the catchment surface, as direct measurements of this characteristic are not carried out. Usually, the evaporation values from the Ukrainian catchment are calculated according to methodological approaches by Konstantinov, Polyakov, Buduko et al. (Iofin, 2016). Such calculations require the information on the radiation balance, air and soil humidity, etc. Observations of these indicators are not carried out in all river basins, which significantly complicates, and sometimes makes it impossible to calculate the evaporation from the surface of some watersheds. The paper of Iofin (2016) notes that the factors that affect the evaporation from the soil have much in common with the factors that determine the evaporation from the water surface. Thus, the evaporation depth (*E, mm*) from the catchment of the Stryi River was determined by an empirical formula, the structure of which has the form:

$$E=0,21*(0,255+0,1*V)*d^{0,78} \quad (1)$$

where:
d – is the air moisture deficit [hPa];
V – is the wind speed [$m\ s^{-1}$].

After automatic calibration of the parameters of the NAM module of the Rainfall-Runoff model for a specific catchment, the streamflow forecast was carried out with use of the forecasted weather parameters, which are calculated by the numerical mesoscale atmospheric model WRF ARW 3.6.1 (Wang et al., 2015). The WRF ARW 3.6.1 model is intended for both research of atmospheric processes and for operational forecasting. In the UHMI, calculations according to different versions of the WRF model have been carried out regularly since 2008 of 4 times a day (Doroshenko et al., 2020; Gorbachova et al., 2021).

The quality of streamflow modeling according to the NAM module of the Rainfall-Runoff model was evaluated by the ratio of the standard deviation of the actual discharges from the mean value ($\overline{\sigma}$) to the mean square error of the simulated discharges ($\overline{S}$), i.e. $\overline{S}/\overline{\sigma}$. Such values are determined by formulas (GOH, 2012):

$$\overline{\sigma} = \sqrt{\sum_1^n (y_i - \overline{y})^2 / (n-1)} \quad (2)$$

$$\overline{S} = \sqrt{\sum_1^n (y_i - y_i')^2 / n} \quad (3)$$

where:
y_i – is the actual discharge;
$\overline{y}$ – is the mean discharge;
y_i' – is the simulated discharge;
n – is the members number of the series.

The calibration quality determines by indicators according to Table 1.

Periodicity of operational information receipt from the observation network of the Department of Hydrometeorology of the State Emergency Service of Ukraine and weather forecasts according to the model WRF ARW 3.6.1 is 3 hours. Thus, the NAM module of the Rainfall-Runoff model was set to work with a three-hour step in time.

Results and discussion

The Stryi River Basin is characterized by the formation of dangerous floods of different genesis. Thus, the priority aim is the simulation namely maximum discharges. So, the calibration of the NAM module was carried out with the definition of parameters set that well provide exactly this type of simulation.

Parameters calibration of the NAM module of the Rainfall-Runoff model of the MIKE 11 software complex for the catchment of the Stryi River – Verkhne Synovydne village was carried out according to the hydrometeorological data for the period 01.07.2007–30.06.2010. The historical discharges of the Stryi River at the Verkhne Synovydne village water gauge were used for modeling, as well as data on air temperature, precipitation, air humidity deficit and wind speed at Turka, Slavske and Stryi meteorological stations. The mean values of meteorological indicators for the catchment of the Stryi River at the Verkhne Sinyovydne village water gauge were calculated taking

into account the weight coefficients of each meteorological station. These coefficients were determined by the combined approach based on the Thiessen polygons taking into account the topography of the catchment area, as well as partial optimal selection in the calculations (Befani and Kalinin, 1983; WMO, 2009) (Table 2). To calibrate the NAM module of the Rainfall-Runoff model by interpolation a historical continuous series of observations of the discharges and precipitation with a step in time of 3 hours for the period 01.07.2007–30.06.2010 were created. Continuous series of evaporation depth (*E, mm*) for three-hour time intervals are determined by formula 1.

Calibration results of the NAM module of the Rainfall-Runoff model for the catchment area of the Stryi River - Verkhne Synovydne village for the period 01.07.2007-30.06.2010 are quite satisfactory because the coefficient of determination is 0.84 according to Table 1. The highest historical and simulated discharges are generally well coordinated (Fig. 2). The difference between the mean year historical and mean year simulated discharges range from -10.5 % (01.07.2009–30.06.2010) to +2.3 % (01.07.2008–01.07.2009) and in mean consist -3.5 % for the period calibration. The calibration quality by ratio $\overline{S}/\overline{\sigma}$ was 0.40, which corresponds to the "good" category according to Table 1. This calibration quality indicator allows full use of the NAM module of the Rainfall-Runoff model for historical and forecasting modeling for the catchment area of the Stryi River – Verkhne Synovydne village.

The flood, which was observed on July 7–10, 2010 on the Stryi River near the village of Verkhne Synovydne, was caused by heavy rainfall that fell in its catchment area during July 6–8, 2010. During this period the precipitation depth at meteorological stations in the Stryi River Basin reached: Turka – 51.6 mm, Slavske – 94.0 mm and Stryi – 70.5 mm. The flood started at 2 pm on July 7, 2010 and reached its peak at 8 am on July 8, 2010. The peak discharge of this flood was 932 $m^3 s^{-1}$.

Table 1. Indicators quality of the calibration at the members number of the series $n \geq 25$ (GOH, 2012)

Category	Indicators quality	
	$\overline{S}/\overline{\sigma}$	coefficient of determination *(R)*
good	≤ 0.50	≥ 0.87
satisfactory	0.51 – 0.80	0.86 – 0.60

Table 2. List of meteorological stations, the data of which were used for the catchment of the Stryi River to the Verkhne Synovydne village

№	Meteorological station name	Height above sea level [m]	Weight coefficient	Meteorological station code
1	Turka	594	0.33	33511
2	Slavske	592	0.33	33516
3	Stryi	294	0.33	33513

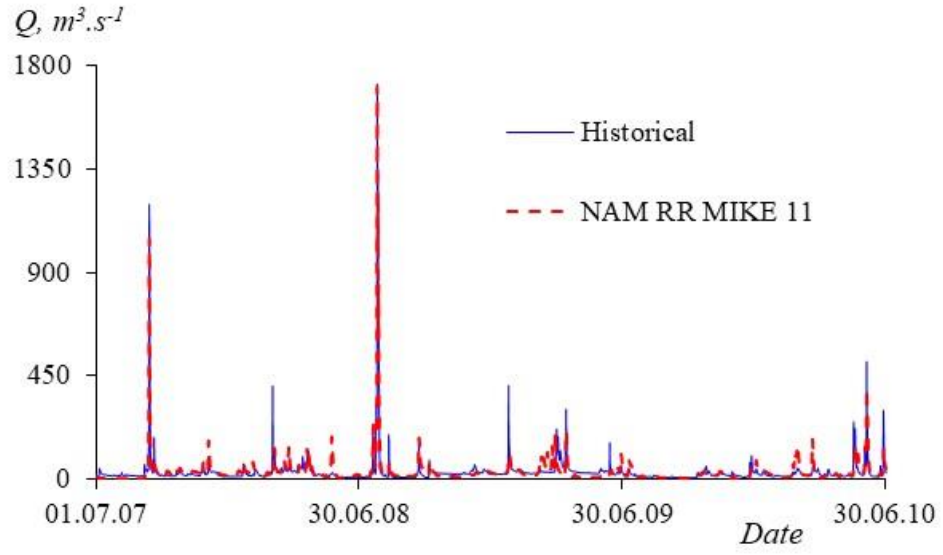

Fig. 2. Calibration results of NAM module of the Rainfall-Runoff model for the Stryi River at the Verkhne Synovydne village water gauge, 01.07.2007–30.06.2010.

Both the increase and decrease of levels and discharges during the flood were quite quick (Fig. 3). Analysis of simulation results, which are shown in Fig. 3 shows that the NAM module of the Rainfall-Runoff model quite satisfactorily reproduced discharges according to historical data of weather parameters. The simulated flood peak time differs from the historical (actual) time by 3 hours, and the simulated maximum discharge (724 $m^3 s^{-1}$) differs from the historical discharge by 22%. The discrepancy between the simulated time of the flood peak and the historical is explained by the fact that the amount of precipitation at meteorological stations in the Stryi River Basin is measured twice a day, while the NAM module of the Rainfall-Runoff model requires the meteorological data every three hours. The values of the precipitation amount that fell on the surface of the river catchment with a frequency of three hours were determined by linear interpolation, which introduced errors in the simulated values of discharges and the time of their occurrence, and in the model parameters during their calibration. The quality of streamflow modeling and calibration of the NAM module of the Rainfall-Runoff model parameters is also affected by the insufficient number of meteorological stations in the Stryi River Basin. So, only three meteorological stations are characterizing the river basin with the difficult mountainous terrain and catchment area is 2400 km^2.

Discharges that are modeled using the forecasted indicators of weather parameters according to the model WRF ARW 3.6.1 from July 6, 2010, were significantly lower than the historical discharges (Fig. 3). This result is due to a significant underestimation of the forecasted amount of precipitation that formed the rain flood. In addition, the WRF ARW 3.6.1 model is inflating the forecasted values of air temperature, humidity deficit and wind speed compared to historical values (Fig. 4). This contributes to the fact that when modeling in the NAM module of the Rainfall-Runoff model, the evaporation depth from the catchment surface is increasing and, consequently, the forecasted discharges are decreasing (Fig. 3). Also, one of the reasons for the forecast errors of numerical atmospheric models for specific meteorological stations, is the imperfection of the digital terrain model.

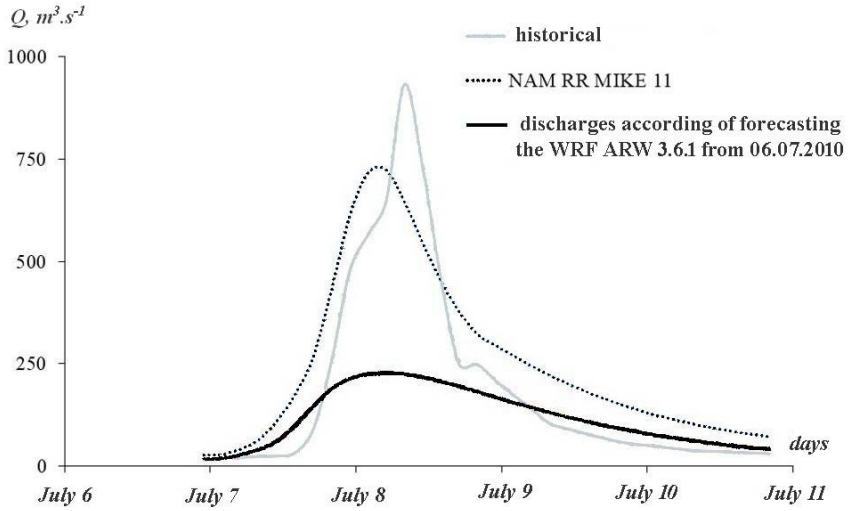

Fig. 3. Historical and modeled by the NAM module of the Rainfall-Runoff model according to the historical data and weather parameters forecast (WRF ARW 3.6.1) discharges on the Stryi River – Verkhne Synovydne village for July 7–10, 2010.

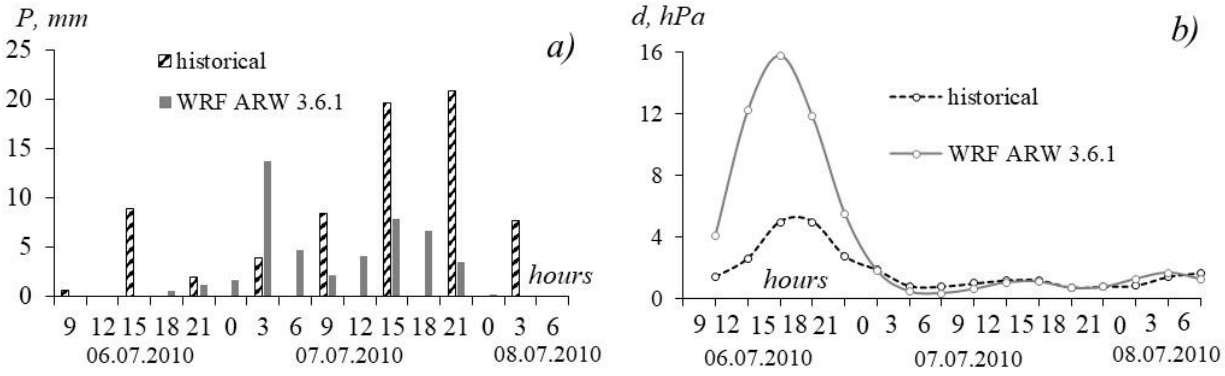

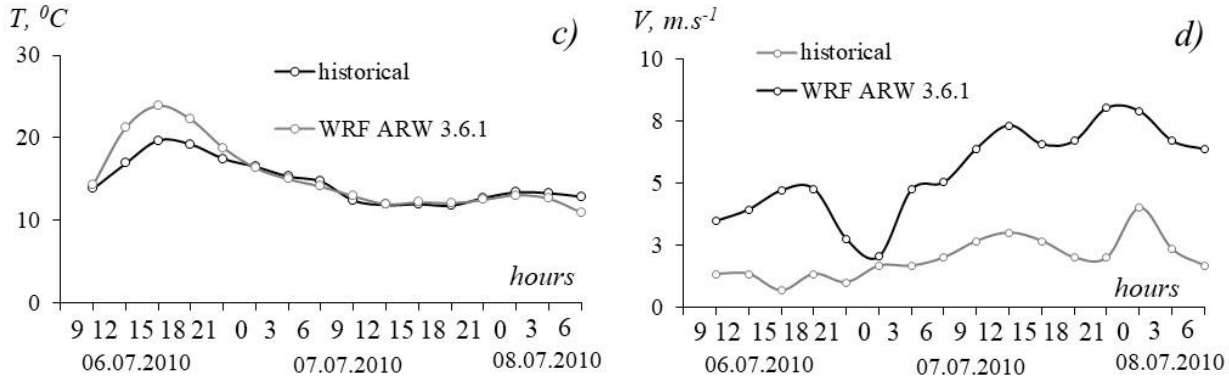

Fig. 4. Historical and forecasting values according to the WRF ARW 3.6.1 model of precipitation (a), air moisture deficit (b), air temperature (c) and wind speed (d) that are averaged over the basin of the Stryi River – Verkhne Synovydne village

Conclusions

The results of the verification of the automated system (FFS Stryi) show a satisfactory reproduction of the discharges of the Stryi River according to historical meteorological data. At the same time, on the Stryi River the accuracy of forecasting discharges of rain floods depends on the accuracy of forecasted weather parameters and, above all, the amount of precipitation and the time of their falling. Also, significant errors in hydrological forecasting are due to insufficient frequency of precipitation measurements (twice a day) at meteorological stations and too few of these stations in the river basin, which does not allow to accurately determine the average meteorological indicators for catchment, which are used to forecast discharges and to calibrate the parameters of the NAM module of the Rainfall-Runoff model. Thus, on the Stryi River the results improving of forecasting the discharges of rain floods is possible by increasing the observation points for meteorological indicators in its basin and the frequency of precipitation measurements and, of course, improving weather forecasts according to WRF ARW 3.6.1. However, it should be noted that the obtained results of verification FFS Stryi show that even with the above problems, this system makes it possible to forecast dangerous floods which will no doubt improve the operative and timely informing of relevant management bodies to prevent their consequences.

Acknowledgement.

This research was conducted within project № 1/Ф-2017 "Development of a software and modeling complex for short-term forecasting of extreme floods on the rivers of the Upper Dniester basin" of the National Academy of Sciences of Ukraine (state registration № 0117U002571).

References

Adamenko, O. (2014): On the causes and consequences of floods in the Dniester Valley. Visnyk of the Lviv University. Series Geography, Vol. 48, 141–49. http://dx.doi.org/10.30970/vgg.2014.48.1302 (in Ukrainian with English abstract)

Bahremand, A., De Smedt, F. (2008): Distributed Hydrological Modeling and Sensitivity Analysis in Torysa Watershed, Slovakia. Water Resour Manage, 2008, Vol. 22, 393–408.

Befani, N. F., Kalinin, G. P. (1983): Practices and methodological developments in hydrological forecasts. Leningrad: Hydrometeoizdat, 390 p. (in Russian)

Doroshenko, A., Shpyg, V., Budak, I., Huda, K. (2020): Numerical atmospheric models and their application in different areas of economics. In: Kvasniy L. and Tatomyr I. (eds). Ukraine in the context of global and national modern servisation processes and digital economy: monograph. Praha: Oktan Print, 155–171. https://doi.org/10.46489/UITCOG0909

Dutko, V. O., Sosedko, M. M. (2011): From the experience of identifying the parameters of the mathematical model of rain runoff depending on the orography of the area. Hydrology, Hydrochemistry and Hydroecology, Vol. 3, no. 24, 73–80. (in Ukrainian)

Guide to Hydrological Forecasts (GHF) (1989): Short-term forecast of the discharge in rivers. Leningrad.: Hydrometeoizdat, Vol. 2, 246 p. (in Russian)

Guidelines for operational hydrology (GOH) (2012): Forecasts of the land water regime. Hydrological support and service. K.: PP "Verlan", 120 p. (in Ukrainian)

Gorbachova, L. O. (2012): Adaptation of the hydrological "Rainfall-Runoff" Mike 11 model to Mountain Rivers. Proceedings of Ukrainian Hydrometeorological Institute, Vol. 263, 71–77. (in Ukrainian)

Gorbachova, L. O., Khrystiuk, B. F., Shpyg, V. M., Huda, K. V. (2021): Short-term forecasting of floods on the rivers of the Upper Dniester basin: methodology, forecasting system and first results. Abstracts of the reports of the Second All-Ukrainian Hydrometeorological Congress, 7–9 October 2021. Odessa: Odessa State Environmental University, 49–50. (in Ukrainian)

Iofin, Z. K. (2016): Development of methodology for assessing the water balance of river basins. Thesis for the degree of Doctor of Technical Sciences. Moscow: A. N. Kostyakov Institute for Environmental Engineering, 244 p. Available at: http://old.timacad.ru/catalog/disser/dd/Iofin/disser.pdf (in Russian)

Khrystyuk, B. (2014): The short-term forecast of the water levels in the Kiliya channel of the Danube River. Energetika, Vol. 60, no. 1, 69–75. https://doi.org/10.6001/energetika.v60i1.2874

Khrystiuk, B. F. (2017): Short-term forecasting of water inflow to the Dniester reservoir taking into account the numerical forecast of weather parameters. Abstracts of the First All-Ukrainian Hydrometeorological Congress with international participation, March 22–23, 2017. Odesa: Odesa State Ecological University, 179–180. (in Ukrainian)

Khrystiuk, B., Gorbachova, L., Pekárová, P., Miklánek, P. (2020): Application of the commensurability method for long-term forecasting of the highest summer floods on the Danube River at Bratislava. Meteorology Hydrology and Water Management. Research and Operational Applications, Vol. 8, no. 1, 70–76. https://doi.org/10.26491/mhwm/114482

Kumar, R., Huda, M., Maryam, M., Lone, M. (2022): Research Rainfall runoff modeling using MIKE 11 NAM of Jhelum river of Kashmir Valley, India. MAUSAM, Vol. 73, no. 2, 365–372. https://doi.org/10.54302/mausam.v73i2.804

Luk'yanets, O. I. (2004): The forecasting floods system in Transcarpathia on the basis of the investigates and mathematical model of the processes of forming the runoff. Abstract of thesis for the degree of cand. geogr. sciences. Kyiv: KNU, 20 p. (in Ukrainian with English summary)

Lyalko, V. I., Apostolov, A. A., Elistratova, L. A. (2017): Influence of natural and anthropogenic factors on the formation of dangerous situations: landslides, floods (on the example of the upper course of the Dniester River). Ukrainian Journal of Remote Sensing, Vol. 15, 31–39. Available at: file:///E:/Завантаження/112-Article%20Text-446-1-10-20180211.pdf (in Ukrainian)

Merz, B., Blöschl, G., Vorogushyn, S., Dottori, F., Aerts, J. C. J. H., Bates, P., Bertola, M., Kemter, M., Kreibich, H., Lall, U., Macdonald, E. (2021): Causes, impacts and patterns of disastrous river floods. Nature Reviews Earth & Environment, Vol. 2, 592–609. https://www.nature.com/articles/s43017-021-00195-3

Moskalenko, S. O. (2012): Estimation of reliability of determination of water formation parameters of mathematical model of rain floods for small catchments of the Right Bank of Pripyat. Hydrology, Hydrochemistry and Hydroecology, Vol. 2, no. 27, 23–29. Available at: http://www.library.univ.kiev.ua/ukr/host/viking/db/ftp/univ/ggg/ggg_2012_27 (in Ukrainian with English abstract)

A Modelling System for River and Channels (MIKE11) (2012): User guide. DHI, 2, 204 p.

Roelevink, A., Udo, J., Koshinchanov, G., Balabanova, S. (2010): Flood forecasting system for the Maritsa and Tundzha Rivers. Proceeding International Conference on water, climate and environment: BALWOIS-2010, 25–29 May 2010, Ohrid, Republic of Macedonia. Available at: https://balwois.com/wp-content/uploads/old_proc/ffp-1570.pdf

Romashchenko, M. I., Savchuk, D. P. (2002): Water elements. Carpathian floods: statistics, causes, regulation. K.: Agrarian science, 304 p. (in Ukrainian)

Priymachenko, N. V. (2010): Grounding of the flood characteristics system calculation on mountain rivers of the Dniester basin based on the mathematical modeling of the forming processes rain runoff. Abstract of thesis for the degree of cand. geogr. sciences. Kyiv: KNU, 19 p. (in Ukrainian with English summary)

Shakirzanova, J. R., Dokus, A. O., Serbova, Z. F., Shvets, N. M. (2019): Complex method of long-term forecasting of the hydrological characteristics of the spring flood of rivers. Problems of Hydrology, Hydrochemistry, Hydroecology: monograph / Osadchyi V.I. et al. (eds). Kyiv: Nika-Center, 58-74. ISBN 978- 966-7067-39-7 (in Ukrainian with English summary)

Shamsudin, S., Hashim, N. (2002): Rainfall runoff simulation using Make11 NAM. Jurnal Kejuruteraan awam (Journal of Civil Engineering), Vol. 15, no. 2, 1-13. Available at: https://fdocuments.in/reader/full/2002-rainfall-runoff-simulation-using-mike11-nam

Sofia, G., Nikolopoulos, E. I. (2020): Floods and rivers: a circular causality perspective. Scientific Reports, Vol. 10, 5175. https://doi.org/10.1038/s41598-020-61533-x

Susidko, M. M. (2000): Mathematical modeling of runoff formation processes as a basis of forecasting systems. Hydrology, Hydrochemistry and Hydroecology, Vol. 1, 32–40. (in Ukrainian)

Susidko, M. M., Luk'yanets, O. I. (2004): Zoning of the territory of Ukraine according to the degree of hydrological danger. Proceedings of Ukrainian Hydrometeorological Institute, Vol. 253, 196–204. (in Ukrainian)

Susidko, M.M., Maslova, T.B., Lipkan, O.A. (2011): Technology of interaction of mathematical models of runoff formation. Proceedings of Ukrainian Hydrometeorological Institute, Vol. 260, 158–174. (in Ukrainian)

Kaganer, M. S. (eds) (1969): Surface water resources of the USSR. Leningrad: Hydrometeoizdat, Vol. 6, no. 1. (in Russian)

Wang, W., Bruyère, C., Duda, M., Dudhia, J., Gill, D., Kavulich, M., Keene, K., Lin, H.-C., Michalakes, J., Rizvi, S., Zhang, X., Berner, J., Smith, K. (2015): Advanced Research WRF (ARW). Version 3 Modeling System User's Guide. NCAR. Available at: https://www2.mmm.ucar.edu/wrf/users/docs/user_guide_V3/contents.html

World Meteorological Organization (WMO) (2009): Guide to Hydrological Practices, Vol. II, Management of Water Resources and Application of Hydrological Practices, sixth edition, WMO-No. 168, World Meteorological Organization, Geneva, Switzerland.

Yang, Yu., Xu, Z., Zheng, W., Wang, S., Kang, Y. (2021): Rain Belt and Flood Peak: A Study of the Extreme Precipitation Event in the Yangtze River Basin in 1849. Water, Vol. 13, 2677. https://doi.org/10.3390/w13192677

Prof. Liudmyla Gorbachova, Dr.Sc. (*corresponding author e-mail: gorbachova@uhmi.org.ua)
Ing. Borys Khrystiuk, PhD
Mgr. Vitalii Shpyg, PhD
Ukrainian Hydrometeorological Institute
37, Prospekt Nauky
03028, Kyiv
Ukraine

DOI: 10.31577/ahs-2022-0023.02.0027

ACTA HYDROLOGICA SLOVACA

Volume 23, No. 2, 2022, 241–248

Empirical models to calculate the snow water equivalent in the high mountain catchments of the Western Carpathians

Ladislav HOLKO*, Michal DANKO, Martin JANČO, Patrik SLEZIAK

Empirical models based on the relationship between snow depth (*SH*) and density (ρ) are used to estimate the snow water equivalent (*SWE*) from SH. However, ρ is poorly correlated with *SH* while the correlation between *SH* and *SWE* which can be directly obtained from snow measurements, is much better. We derived models based on the *SH-SWE* correlations for two datasets obtained in the high mountain catchments in Slovakia (The Low and Western Tatra Mountains). The models consider time (months from January to April) and elevation zones. Evaluation of the models against independent data showed that they are transferrable to other climatic conditions. About a half of estimated point *SWE* values was well comparable to measured values, i.e. the differences were approximately within ±15%. Substantial overestimation of measured *SWE* by more than 35% was obtained for about 10% of the values in January when the same equation was used for all elevation zones. Our final validation employed independent data from the High Tatra Mountains. It showed that about 60% of *SWE* values calculated for the entire snow courses as an average of 20 values calculated by the derived models from *SH* compared well (±15%) to values obtained by the traditional approach, i. e. as a product of the snow course mean *SH* (20 measurements) and ρ (3 measurements). Although the results of our models can be comparable to those provided by models based on snow density, due to recurrent use of SH and almost no correlation between SH and ρ, the models based on the SH-SWE relationship represent in our opinion a more correct approach.

KEY WORDS: regression models, snow cover, hydrology, headwater catchments

Introduction

Snow water equivalent (*SWE),* i.e. the depth of water that would originate if the snowpack melts, is the most important hydrological characteristic of the snow cover. Point *SWE* values can be obtained from the weight of sampled snow core and area of the snow sampler while *SWE* characterizing greater distances (transects, snow courses) employs also snow density ρ. *SWE* is then calculated as a product of the snow course mean snow depth *SH* and mean density ρ (calculated from the point *SWE*s and associated *SH*s).

Accurate estimation of *SWE* in catchments is important for correct forecasting of spring runoff, quantification of the groundwater resources replenishment or manipulation of dams located in areas with significant snow accumulation. While the snow cover characteristics at lower elevations of Slovakia in the last decades exhibited decreasing trends (Siman and Slávková, 2019), snow accumulation in the highest mountain catchments, the headwater areas of the most important Slovak rivers, did not yet show such a trend (Holko et al., 2020). However, spatial variability of *SWE* in such catchments is high. Manual *SWE* measurement at snow courses distributed around a catchment remains difficult and time consuming and the automatic measurements (Kinar and Pomeroy, 2015) are expensive and cannot be done at any locations. The remote sensing does not provide a reliable information about the *SWE* variability in smaller mountain catchments (10^0–10^1 km^2). Therefore, emprirical models based on the relationships between snow depth and density taking into account also site altitude, temporal evolution of ρ during the winter or snow type, appeared recently to allow the *SWE* estimation from the more easily available SH data (e.g. Jonas et al., 2009; Sturm et al., 2010; McCreight and Small, 2014). Jonas et al. (2009) developed such a model with the aim to facilitate *SWE* monitoring on a catchment scale. It is based on the combination of the look-up tables, regression equations correlating *SH* and ρ and residuals between modelled and observed ρ. The authors concluded that the model and combination with a few SH measurements characterized a site similarly well as a single SWE measurement. Model validation suggested its robustness to transferability to independent data and even climatic conditions. Sturm et al. (2010) developed a model similar to that of Jonas et al. (2009) and calculated ρ taking into account *SH*, day of year and the climate class of snow. They concluded that 90% of the computed *SWE* values fell within ±8 cm of

the measured values. McCreight and Small (2014) modified the model of Jonas et al. (2009) for the use daily *SH* data. The complication with daily data is that ρ is small short after the snowfall and gradually increases with snow age due to snow densification. Bohrman et al. (2013) noted that linear snow density-time relationships do not allow for interannual variability in densification rates. They found out that total winter precipitation was the most important driver of snow densification rates while winter mean air temperature and melt-refreeze events were significant locally. Pistocchi (2016) developed an even simpler model that calculated ρ using an initial value at the beginning of the snow cover season and day of year.

Motivation for the development of empirical models estimating *SWE* from *SH* and modelled snow density is to obtain much more *SWE* data for various analyses utilizing the abundant and more easily measurable *SH* data. However, ρ is poorly correlated with *SH* (e.g. Jonas et al., 2009; López-Moreno et al., 2013). Another issue is that in the application of such a model, ρ is first calculated from the (poor) relationship with *SH* and then the same *SH* is used to calculate *SWE* as the product of calculated ρ and *SH*. The method is thus based on the recurrent use of only one independent variable, *SH*, to calculate two unknown variables ρ and *SWE*. Although the final results will not be much different, this could be avoided by calculating *SWE* using regression equations describing the relationships between *SH* and *SWE* which have high correlation coefficients. The equations should employ *SWE* data obtained without considering snow density. Point *SWE* is measured by weighting the snow core sampled by a snow tube. Assuming specific density of water 1000 kg m^{-3}, the snow water equivalent [in mm of water depth] can then be calculated as:

$$SWE = m*(10000/Sa) \quad (1)$$

where
m – is the mass of the collected snow core [kg],
Sa – is the area of the cutting part of the snow tube [cm^2].

SWE based on equation (1) does not need to consider snow density and can be easily derived from the general equation expressing density as a ratio of mass and volume. Various snow tubes and scales have been historically used in different countries (e.g. López-Moreno et al., 2020), but they all work on the same principle, i. e. weighting the snow core collected by the tube. Thus, any measurement employing the snow tube can directly provide *SWE* values. Although *SWE* can be determined directly by equation (1), ρ is used in the snow course measurements as well to obtain the *SWE* for the entire snow course. This is done by multiplication of the mean snow density calculated from a few (3–5) *SWE* measurements by the mean snow depth measured at many more points (10–20) points. Nevertheless, point *SWE* measurements do not need to consider snow density.

The objective of this study is to derive the parameters of equations correlating point values of *SH* and *SWE* and examine the transferability of such empirical models to other areas. The study is based on three datasets obtained in the highest mountains of Slovakia.

Material and methods

To the best of our knowledge, only two datasets containing the long-term *SH* and *SWE* data measured at the snow courses in small mountain catchments exist in Slovakia. The first one (hereafter called the Bystrianka dataset) was measured in the Bystrianka Creek catchment (southern part of the Low Tatra Mountains, catchment area 34.5 km^2, elevations 600–2043 m a.s.l., mean elevation 1200 m a.s.l.) in years 1969–1992. The measurements used in this study were conducted once per month in January, February, March and April. The snow courses were located in different parts of the catchment at elevations 600–2000 m n. m. (Holko, 2000). *SH* was measured by the graduated stick, the snow core was weighted five times at each snow course by the snow tube of Institute of Hydrology SAS which was derived from the US-federal sampler and had the diameter of 3.6 cm (Kozlík, 1967). We used only measurements in which the snow core height was at least 85% of measured *SH* and calculated *SWE* as the product of snow weight in kilograms and number 982.439 (as it follows from equation 1). The dataset contained 2785 values of *SH* and *SWE*. Characteristics of the dataset shown in Fig. 1 confirm poor correlation between *SH* and ρ (calculated from *SWE* and *SH*) and a much better correlation between *SH* and *SWE*.

The second dataset, hereafter called the Jalovčianka dataset, was measured in the Jalovecký Creek catchment (the Western Tatra Mountains, catchment area 22.2 km^2, elevations 820–2178 m a.s.l., mean elevation 1500 m a.s.l.) in years 2012–2022. The measurements were carried out at the end of January, February, March and in April. Methodology of the measurement was similar to that in the Bystrianka Creek catchment. *SH* was measured by the avalanche probe at 20 points and three *SWE* measurements per snow course were obtained with the snow tube Dolfi having the diameter of 8 cm (Hancvencl and Holko, 2019; López-Moreno et al., 2020). *SWE* was calculated by multiplying the snow core weight by 200. The dataset contained 865 values and its characteristics are shown in Fig. 2. Similarly, to the Bystrianka dataset, ρ was poorly correlated with *SH*.

The two datasets were obtained in mountain ranges that are not far from each other. They are divided only by one big mountain valley and the distance between the catchments is approximately 25 km. Yet, meteorological conditions in the catchments during individual winters can sometimes differ. Both catchments are located on the southern side of the mountains, i.e. on their leeward side. However, the Jalovecký Creek catchment is in the first mountain range on the route of moisture bringing air masses from the north and north-western directions (the main direction bringing precipitation to northern Slovakia). Snow cover at some snow courses in the catchment can also be influenced by the windward effects. The Bystrianka catchment is more isolated from the north and north-west. On the other hand, compared to

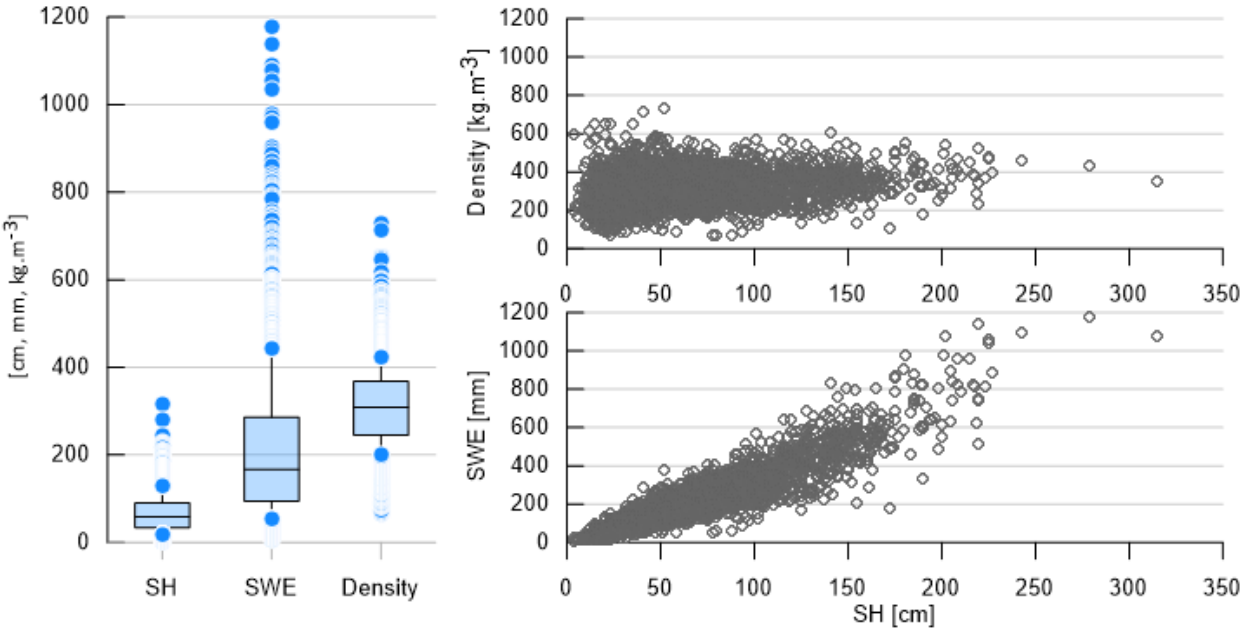

Fig. 1. The Bystrianka dataset (1969–1992); left- boxplots of SH [cm], SWE [mm] and ρ [km m^{-3}]; each boxplot represents 2785 values and shows percentiles 10 and 90 (whiskers), outliers (circles), interquartile ranges and medians (boxes); right – relationships between SH and SWE (calculated by equation 1) and SH and ρ (calculated from point SWE and SH).

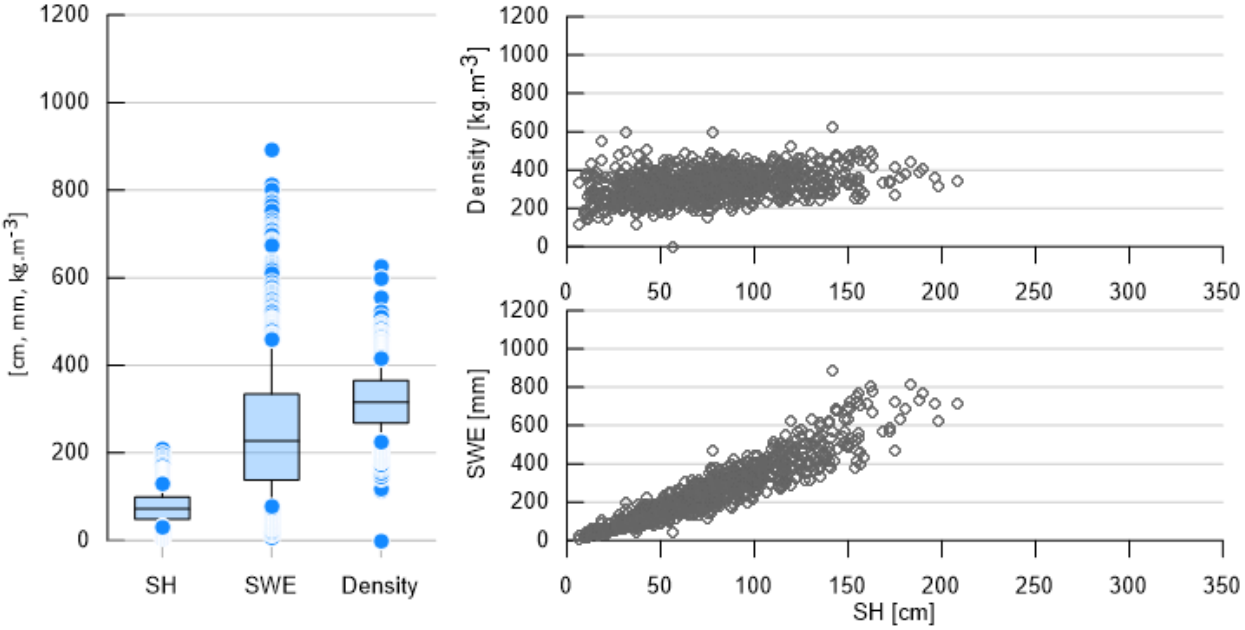

Fig. 2. The Jalovčianka dataset (2012–2022); left- boxplots of SH [cm], SWE [mm] and ρ [km m^{-3}]; each boxplot represents 865 values and shows percentiles 10 and 90 (whiskers), outliers (circles), interquartile range and median (boxes); right – relationships between SH and SWE (calculated by equation 1) and SH and ρ (calculated from point SWE and SH).

the Jalovecký Creek catchment, it can be more often affected by southern weather situations that are important for snow accumulation in some winters.

Slope and intercept of linear regression equations correlating *SH* and *SWE* for January, February, March and April were calculated for each dataset. Division of data into months did not take into account exact dates of measurements, i.e. all the values measured in January, were assigned to that month. In addition to regression equations based on all data from a particular month,

equations for three elevation zones were derived for each month too. The lowest zone (600–850 m a.s.l.) was chosen to represent the snow conditions in the foreland parts of the Slovak high mountain catchments. Zone 850–1400 m a.s.l. should represent the forest zone of mountain catchments and elevation zone 1400–2000 m a.s.l. was considered representative of their highest parts above the tree line.

Equations (empirical models) derived for each dataset were used to calculate SWE for the other dataset that represented independent data collected in different climatic conditions (period 1969–1992 was colder than period 2012–2022). Calculated and measured SWE were compared using the relative bias:

$$Relative\ bias = (SWE_{calculated} - SWE_{measured})*100\ /SWE_{measured}\ [\%] \quad (2)$$

Basic statistics of the bias were expressed in the boxplots for each month (January to April). Regression plots were used to examine the scatter of measured versus calculated values.

Finally, the performance of the empirical models obtained from the Bystrianka and the Jalovčianka datasets was examined for a smaller set of independent data measured in the neighbouring High Tatra Mountains in springs 2005 to 2007 (February, March, April). The snow courses were located at elevations 1030 to 2080 m a.s.l., their total number was 66 and they were located on the slopes of several mountains and mountain valleys (Patria peak, Gerlachovský štít peak, Slavkovský štít peak and the Velická dolina valley). Three *SWE* values were obtained for each snow course from the snow core sampled by the Dolfi sampler and *SH* measured by an avalanche probe. Relative bias and scatterplots between the measured and calculated *SWE* were used to compare the performance of the models. We also compared the *SWE* obtained for the entire snow course by the traditional approach (multiplication of mean ρ from three *SWE* measurements by the average *SH* from 20 measurements) with the *SWE* calculated as an average of twenty values obtained from *SH* and the empirical models derived from the Bystrianka and the Jalovčianka datasets. The comparison was designed to examine the idea of using the empirical models to provide more *SWE* data for the snow-related analyses.

Results and discussion

Regression analysis confirmed very good correlations between *SH* and *SWE*. Parameters of the obtained linear regression equations for different months and elevation zones are given in Table 1. The relative bias (Figs. 3 and 4) indicates that the performance of equations derived from the Bystrianka dataset (more data, results from a colder climate transferred to the warmer climate) was slightly better that of the models derived from the Jalovčianka dataset (less data, results from a warmer climate transferred to the colder climate). The mean bias (both mean and median) is close to 0%, i. e. measured and calculated values are on average similar, which is the property of correlation equations. However, the interquartile ranges of bias obtained from the Bystrianka dataset are smaller for all months except for April and the upper quartiles are also often smaller than for the Jalovčianka dataset (Table 2).

Table 1. Parameters of linear regression equations correlating point measurements of *SH* and *SWE* (*SWE=Slope x SH+Intercept*) calculated for the Bystrianka and the Jalovčianka datasets; R^2 is coefficient of determination; there was no data for the lowest elevation zone in April in the Jalovčianka dataset; the bold values were calculated for all data in a particular month without considering site elevation

		The Bystrianka dataset				The Jalovčianka dataset			
Month	Elevation	Slope	Intercept	*n*	R^2	Slope	Intercept	*n*	R^2
January	**600–2000**	**3.357**	**-31.225**	**853**	**0.876**	**3.429**	**-39.578**	**216**	**0.891**
	600–899	3.356	-25.413	273	0.860	2.618	-4.606	21	0.949
	900–1399	2.964	-22.133	345	0.829	2.834	-16.813	81	0.948
	1400–2000	3.683	-56.777	235	0.856	3.791	-62.762	114	0.869
February	600–2000	**2.987**	**-11.208**	**870**	**0.862**	**3.366**	**-21.444**	**257**	**0.928**
	600–899	2.667	1.886	412	0.822	2.963	-6.349	30	0.849
	900–1399	2.605	6.092	277	0.629	3.036	-11.755	95	0.956
	1400–2000	3.246	-29.881	181	0.790	3.521	-26.457	132	0.892
March	**600–2000**	**3.659**	**-26.937**	**477**	**0.825**	**4.088**	**-39.771**	**216**	**0.869**
	600–899	3.227	-7.022	69	0.933	3.543	3.430	6	0.963
	900–1399	3.019	1.856	239	0.820	3.542	-19.525	85	0.910
	1400–2000	4.146	-50.518	196	0.788	4.232	-43.328	125	0.832
April	**600–2000**	**3.882**	**-6.148**	**585**	**0.902**	**4.263**	**-40.078**	**176**	**0.856**
	600–899	3.348	-4.866	19	0.767	–	–	–	–
	900–1399	3.548	5.506	275	0.916	3.318	-4.335	60	0.748
	1400–2000	3.930	-0.097	291	0.880	4.323	-27.637	116	0.894

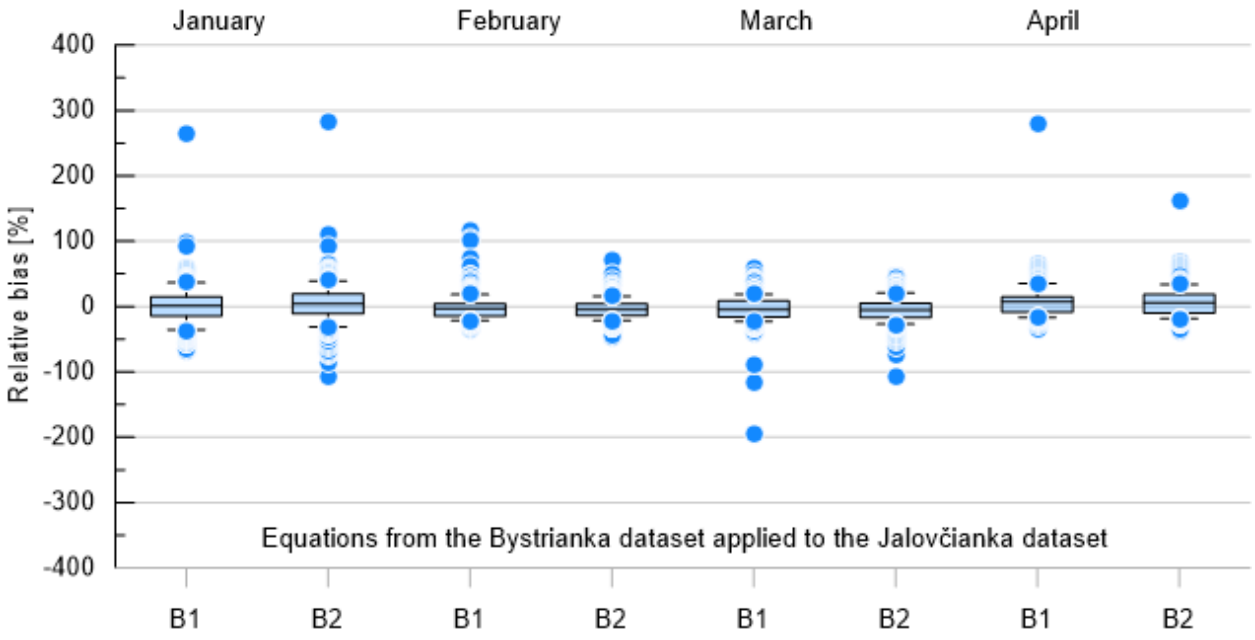

Fig. 3. Relative bias of SWE calculated for the Jalovčianka dataset using empirical models obtained from the Bystrianka dataset; B1 is the bias between measured SWE and SWE calculated by equations considering different elevation zones, B2 is the bias between measured SWE and SWE calculated by the same equation for all elevation zones (the bold numbers in the left part of Table 1); the boxplots show percentiles 10 and 90, outliers, interquartile ranges and arithmetic means.

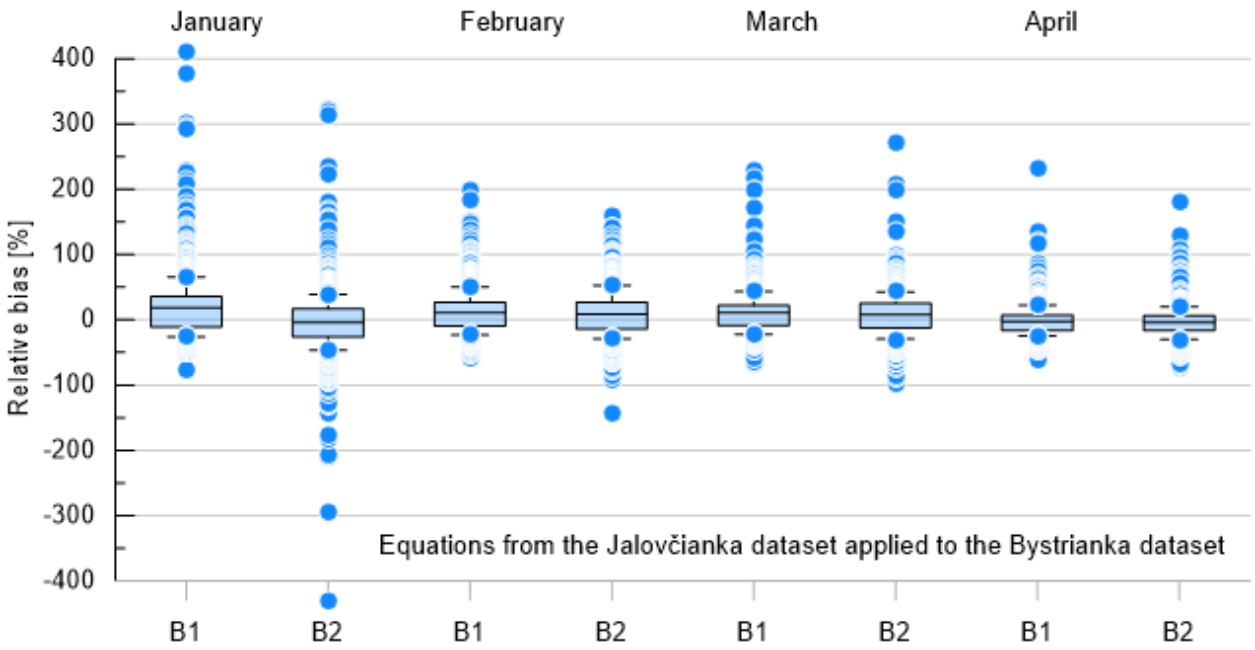

Fig. 4. Relative bias of SWE calculated for the Bystrianka dataset using empirical models obtained from the Jalovčianka dataset; B1 is the bias between measured SWE and SWE calculated by equations considering different elevation zones, B2 is the bias between measured SWE and SWE calculated by the same equation for all elevation zones (the bold numbers in the right part of Table 1); the boxplots show percentiles 10 and 90, outliers, interquartile ranges and arithmetic means.

Table 2 shows that generally the worst results were obtained for the models based on the Jalovčianka dataset for January (the largest upper quartile for B1, the lowest lower quartile for B2 and the largest interquartile ranges for both).

Figs. 3 and 4 and Table 2 provide the information about the accuracy of the SWE estimates. About a half of the estimates can differ from the measured values not more than by 15% which could be acceptable considering the effort needed to measure the SWE in mountains. However, it should be kept in mind that still a substantial number of the estimates can differ much more (see the whiskers and outliers in Figs. 3 and 4). The scatter of estimated SWEs (Fig. 5) is much smaller for the models based on the Bystrianka dataset. However, Fig. 5 also shows that for SWE of approximately 450 mm and more, the calculated values underestimate measured SWE. This phenomenon is less pronounced for the models derived from the Jalovčianka dataset where it becomes visible for the SWE values higher than approximately 600 mm. Fig. 5 shows the results based on the empirical models considering the elevation zones, but similar results were obtained also for the models that did not divide the catchments into elevation zones.

Greater negative intercepts in Table 1 mean that negative values of SWE can be calculated for very small SH.

Evaluation of the models obtained from both datasets against the data measured in the High Tatra Mountains showed that the differences between the models were very small (Fig. 6), although the models derived from the Jalovčianka dataset on average overestimated measured values slightly more. On the other hand, the snow course SWE values calculated with the models derived from the Jalovčianka dataset compare to values obtained by the traditional approach slightly better than those calculated with the models derived from the Bystrianka dataset (Fig. 7). The differences of 80% of calculated snow-course SWE valus (by models from the Jalovčianka dataset) were in the interval from -15% to +33%. Analogical differences for the models calculated from the Bystrianka dataset were within the interval from -25% to +24%. López-Moreno et al. (2020) concluded that the uncertainty in snow density measurements conducted by different snow tubes is approximately within 10–15%. Approximately 60% of the snow course SWE values estimated by the empirical

Table 2. Values of the lower and upper quartiles (P25, P75) and the interquartile ranges of SWE relative bias [%] when the equations from the Bystrianka dataset are applied to the Jalovčianka dataset (The Bystrianka dataset) and vice versa (The Jalovčianka dataset)

		The Bystrianka dataset			The Jalovčianka dataset		
		P25 [%]	P75 [%]	Interquartile range [%]	P25 [%]	P75 [%]	Interquartile range [%]
January	B1	-15	15	30	-11	35	46
	B2	-11	18	29	-26	17	43
February	B1	-15	4	19	-10	27	37
	B2	-14	4	18	-14	27	41
March	B1	-16	8	24	-9	22	31
	B2	-17	5	22	-12	25	37
April	B1	-9	15	24	-16	7	23
	B2	-10	18	28	-17	7	24

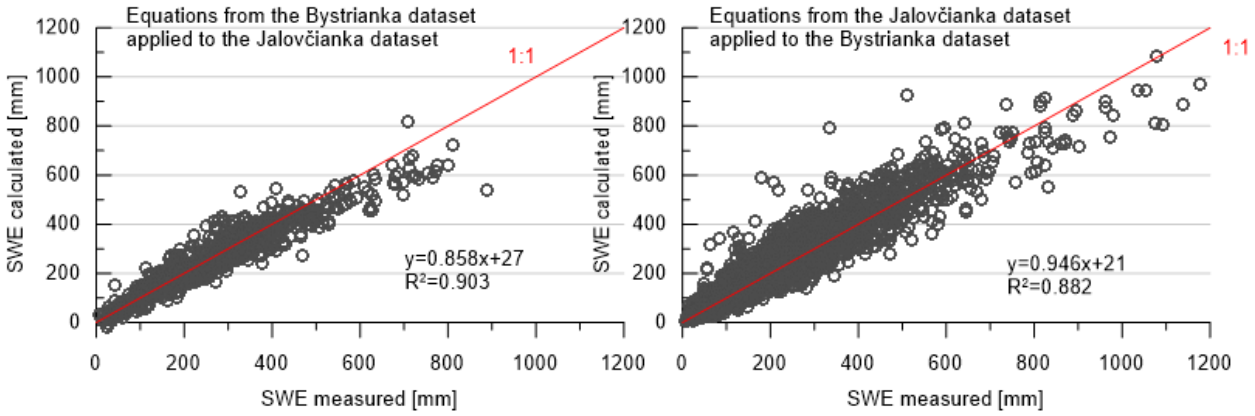

Fig. 5. Calculated versus measured SWE and parameters of linear regression equations describing the relationships between measured and calculated values; the calculated SWE values are based on the models considering elevation zones.

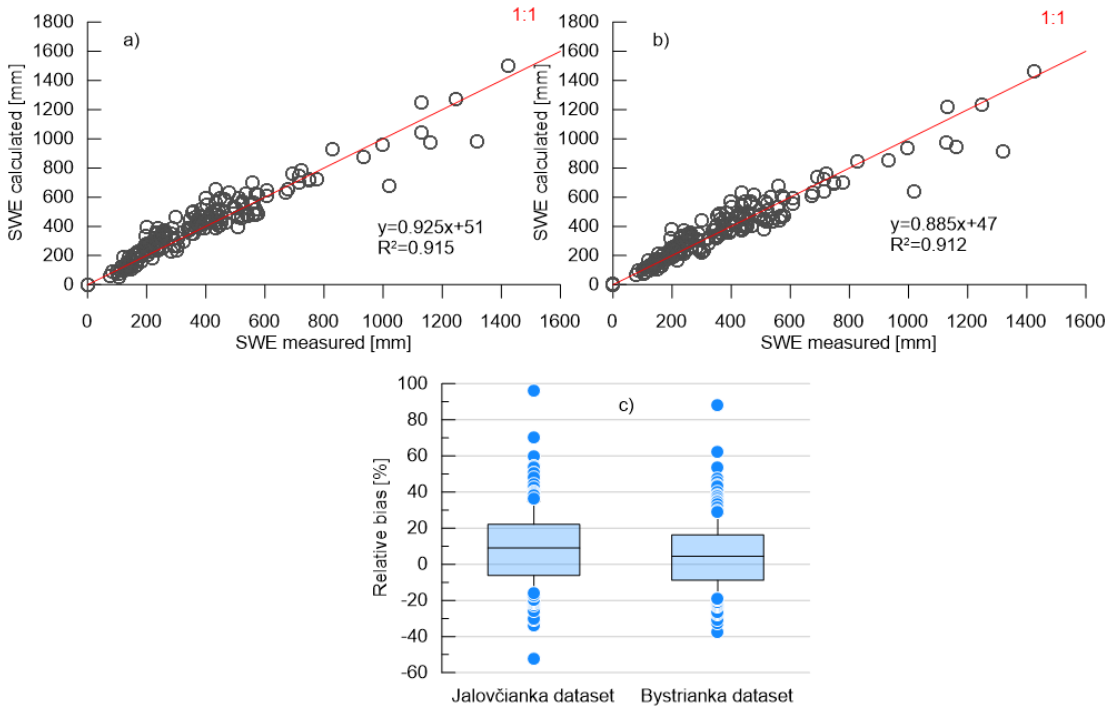

Fig. 6. Comparison of measured point SWE in the High Tatra Mountains and SWE calculated by the models derived from the Jalovčianka dataset (a) and from the Bystrianka dataset (b); the models took into account elevation of the sites; c) relative SWE bias, the boxplots show percentiles 10 and 90, outliers, interquartile ranges and arithmetic means.

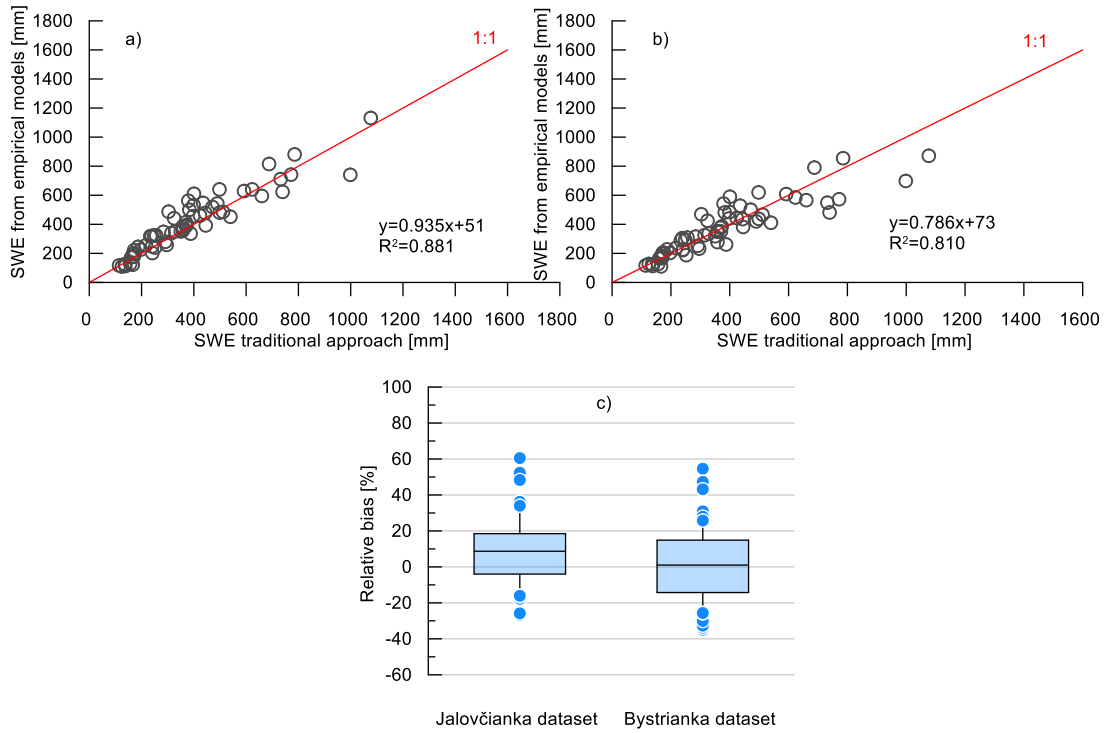

Fig. 7. Comparison of the SWE for the entire snow courses in the High Tatra Mountains calculated by the traditional approach (as a product of snow course mean SH and ρ based on measurements) and as the average of 20 SWE values calculated by empirical models derived from (a) the Jalovčianka dataset and (b) from the Bystrianka dataset that took elevation zones into account; c) relative SWE bias, the boxplots show percentiles 10 and 90, outliers, interquartile ranges and arithmetic means.

models differed from the measured values obtained by the traditional approach not more than by 15%. While this could be quite a good result for the simple empirical models, it also means that the accuracy of quite many SWE estimates (40%) can be substantially worse than the systematic errors in measured data. Users of such models should therefore carefully consider their application.

Conclusion

We proposed alternative empirical models to estimate the *SWE* from *SH* measurements based on the correlations of *SH* and *SWE*. The validation indicates that the models which we believe are more correct than earlier models based on the correlations between *SH* and ρ, could be useful to obtain more *SWE* data for some snow-related analyses.

Acknowledgement

This work was supported by the grants of the Slovak Academy of Sciences (project VEGA No. 2/0065/19) and Slovak Research and Development Agency (project APVV No. 19-0340).

References

Bormann, K. J., Westra, S., Evans, J. P., McCabe, M. F. (2013): Spatial and temporal variability in seasonal snow density. Journal of Hydrology, 484, 63–73.

Hancvencl, R., Holko, L. (2019): Laminátový snehomer DOLFI – vývoj a porovnanie s meraniami inými snehomermi. 23. Stretnutie snehárov 27. – 29. 3. 2019, Tále, Nízke Tatry (Eds. K. Hrušková, D. Kyselová, T. Trstenský) Slovenský hydrometeorologický ústav, Regionálne pracovisko Banská Bystrica, ISBN 978-80-99929-01-3, http://www.uh.sav.sk/en-gb/Research/Conferences/Snow-Meetings

Holko, L. (2000): Vyhodnotenie dlhodobých meraní parametrov snehovej pokrývky v horskom povodí. Acta Hydrologica Slovaca, 2000, 1, 1–8.

Holko, L., Sleziak, P., Danko, M., Bičárová, S., Pociask-Karteczka, J. (2020): Analysis of changes in hydrological cycle of a pristine mountain catchment. 1. Water balance components and snow cover. J. Hydrol. Hydromech., 68, 2, 180–191, DOI: 10.2478/johh-2020-0010

Jonas, T, Marty, C., Magnusson, J. (2009): Estimating the snow water equivalent from snow depth measurements in the Swiss Alps. Journal of Hydrology, 378, 161–167.

Kozlík, V. (1967): Výskum reprezentatívnosti snehomerných metód pre hydrologické výpočty a prognózy. Záv. správa ČÚ III-0-3/103, Ústav hydrológie a hydrauliky SAV, Bratislava.

Kinar, N. J., Pomeroy, J. W. (2015): Measurement of the physical properties of the snowpack. Rev. Geophys., 53, 481–544, doi:10.1002/2015RG000481.

López-Moreno, J. I., Fassnacht, S. R., Heath, J. T., Musselman, K. N., Revuelto, J., Latron, J., Morán-Tejeda, E., Jonas, T. (2013): Small scale spatial variability of snow density and depth over complex alpine terrain: Implications for estimating snow water equivalent. Advances in Water Resources, 55, 40–52.

López-Moreno, J. I., Leppänen, L., Luks, B., Holko, L., Picard, G., Sanmiguel-Vallelado, A., Alonso-González, E., Finger, D. C., Arslan, A. N., Gillemot, K., Sensoy, A., Sorman, A., Ertas¸, M. C., Fassnacht, S. R., Fierz, C., Marty, C. (2020): Intercomparison of measurements of bulk snow density and water equivalent of snow cover with snow core samplers: Instrumental bias and variability induced by observers. Hydrological Processes, 34, 1–14. https://doi.org/10.1002/hyp.13785

McCreight, J. L., Small, E. E. (2014): Modeling bulk density and snow water equivalent using daily snow depth observations. The Cryosphere, 8, 521–536, doi:10.5194/tc-8-521-2014

Pistocchi, A. (2016): Simple estimation of snow density in an Alpine region. Journal of Hydrology: Regional Studies, 6, 82–89.

Siman, C., Slávková, J. (2019): Trends of selected characteristics of snow cover in Slovakia in the period 1981/82–2017/2018. Meteorologický časopis, 22, 2, 95– 104.

Sturm, M., Taras, B., Liston, G. E., Derksen, Ch., Jonas, T., Lea, J. (2010): Estimating Snow Water Equivalent Using Snow Depth Data and Climate Classes. Journal of Hydrometeorology, 11, 1380–1394.

RNDr. Ladislav Holko, PhD. (*corresponding author, e-mail: holko@uh.savba.sk)
Ing. Michal Danko, PhD.
Ing. Martin Jančo, PhD.
Ing. et Ing. Patrik Sleziak, PhD.
Institute of Hydrology SAS
Dúbravská cesta 9
84104 Bratislava
Slovak Republic

DOI: 10.31577/ahs-2022-0023.02.0028

ACTA HYDROLOGICA SLOVACA

Volume 23, No. 2, 2022, 249–256

The generation of surface runoff in laboratory conditions using two portable rainfall simulators – an experimental study

Michaela DANÁČOVÁ*, Michal DANKO, Roman VÝLETA, Kamila HLAVČOVÁ

The use of laboratory methods in soil water erosion studies and rainfall simulation experiments has recently been considered more important because of the many advantages in controlling rainfall-runoff processes and sediment transport. In a laboratory study, rainfall simulation experiments (one alone and two identical rainfall simulators connected in a series) were focused on an analysis of the impact of the size of the irrigated area on the temporal distribution and volume of the surface runoff and the amount of eroded soil material. The experiments were conducted on a disturbed soil sample exposed to quasi-continuous 60-minute simulated rainfall events with an intensity of 2.7 mm min^{-1}. The two experiments were carried out on slopes of different lengths of 0.25 m (irrigated area: 0.0625 m^2) and 0.5 m (irrigated area: 0.125 m^2). The results showed the effects of the size of the irrigated area on surface runoff generation and changes in the soil structure, sediment concentration, and amount of soil loss. Knowledge of the rate of changes in the volume of the surface runoff and soil loss with respect to the size of the irrigated area in the laboratory conditions and subsequent generalization of the results provides essential information, which is irreplaceable for the preparation of field measurements and obtaining essential calibration and validation data for erosion and rainfall-runoff modelling.

KEY WORDS: laboratory experiment, rainfall simulator, surface runoff, eroded sediments

Introduction

In recent decades, rainfall simulators have become a popular tool for conducting research on topics such as infiltration, the generation of surface runoff, and soil erosion. Most of these studies mainly focus on sediment, nutrient, and pollutant transport as well as on evaluating the impacts of tillage management on compaction in agricultural soil (Aksoy et al., 2012). A portable rainfall simulator is easy to use, transport, and assemble in the field, making it possible to perform numerous repetitions of an experiment to draw reliable conclusions. The advantage of using a rainfall simulator is the elimination of the erratic and unpredictable variability of real rainfall and the enabling of the specific and reproducible assessment of several parameters that can be rapidly collected, while maintaining relatively uniform rainfall conditions (Iserloh et al., 2013). Simulators can provide substantial datasets that are necessary and essential for the calibration and validation of various processes in mathematical models (e.g., erosion, sediment transport, rainfall-runoff) of all types of complexity, including the empirical, conceptual, and physically-based (Aksoy and Kavvas, 2005). Small portable rainfall simulators are primarily used with a connection to agricultural land, where the quantification of erosion processes is of high importance (see Abudi et al., 2012; Iserloh et al., 2013; Hänsel et al., 2016). Nevertheless, numerous studies have shown that rainfall simulators can also be successfully used on different sites such as sloping olive groves (Palese et al., 2015), forest roads (Zemke, 2016), forested areas (Danáčová et al., 2017; Chouksey et al., 2017), headwater catchments (Holko et al., 2018), and alpine grasslands (see Schmidt et al., 2019).

In the previous field experiment campaign of Hlavčová et al. (2019), eight independent rainfall simulation experiments were carried out on south-facing slopes in the Myjava Hills (Myjava – Turá Lúka region of western Slovakia). All the experiments were carried out using different parameters such as the initial soil moisture (low, medium, high), the slope of the experimental plot (9% – 22%), and the vegetation cover (bare soil, winter crops, maize, rapeseed) to investigate the volume of the surface runoff and the weight of the eroded sediments. The rainfall simulations were conducted in the study using an Eijkelkamp-type rainfall simulator for erosion tests with a possible range of rainfall intensities of 180–420 mm $hour^{-1}$. This rainfall intensity is comparable with the real rainfall energy of a flash flood for the Myjava region (Myjava – Turá Lúka rain gauge, ID 15040). The results of the study showed that the field measurements were burdened by relatively uncertainties due to the small size of the experimental plots.

The objective was to test, in a simple laboratory experiment, the effect of the size of the irrigated area on bare soil with a low intensity of artificial precipitation and with a longer duration (more than 3 minutes), where the time to runoff, surface runoff volume, and sediment transport were monitored. This would allow for expanding knowledge about the possibility of using small portable rainfall simulators in parameterizing erosion-transport or rainfall-runoff models and shedding a light on the uncertainties of using parameters from either laboratory or field measurements in real-life studies (see Szabó et al., 2020; Dunkerley, 2021).

The main objective of the study was to carry out a series of laboratory experiments with rainfall simulators (one alone and two identical ones connected in a series) to analyse the impact of the irrigated area on the generation of surface runoff (amount and time distribution) and the amount of eroded soil material. The results of the study should answer the following questions: What effect will the size of the irrigated area (including the slope length) have on the generation of surface runoff? What will be the volume of water and eroded soil loss relative to the irrigated area? Can the results of laboratory experiments be used to calibrate parameters of erosion-transport or rainfall-runoff models?

Methodology and data

Rainfall simulators are key tools for investigating the dynamic processes of surface runoff, infiltration, and soil erosion characteristics (Iserloh et al., 2013). They are often used in laboratory or field experiments. The advantage of laboratory experiments is the elimination of uncertain natural conditions such as wind, solar radiation, soil moisture, and the antecedent soil conditions (Grismer, 2012).

In this experiment, the disturbed soil sample designated for the rainfall simulations in the laboratory conditions was taken from an agricultural field in the Myjava region, part of Turá Lúka. The soil sample used in the experiment was a type of loamy soil (according to Novak's soil classification system, see Novák and Hlaváčiková, 2016). The depth of the soil sample was 20 cm, and the sample was kept in a solid plastic container. The soil moisture was measured continuously using a soil moisture sensor. The sensor was placed at a depth of 5 cm in the lower part of the irrigated area. In order to simulate the vertical movement of water, the bottom side of the container was perforated and put into a container of the same type (see Fig. 1) that was used to store the infiltrated water. The Eijkelkamp Small Rainfall Simulator (Fig. 1) was used to generate artificial rainfall of a constant intensity. In the first experiment (A), a single rainfall simulator was used to irrigate the area of 0.0625 m^2 (length of slope: 0.25 m). The second experiment (B) used two identical rainfall simulators, which were put one after the other to extend the rainfall irrigated area to 0.125 m^2 (length of slope: 0.50 m).

In both experiments, the rainfall simulation was interrupted every 12 minutes at an intensity of 2.7 mm min^{-1} (quasi-continuous 60-minute rainfall simulation). The reason for these interruptions was the limitations of the rainfall simulator, whose reservoir enables the storage of only 2.3 litres of water. During the interruption, the surface runoff volume, the weight of the sediment, and the soil moisture were measured. Both experiments were preceded by the same initial conditions such as the initial soil moisture, the soil condition (disturbed sample) and management (cultivated bare soil), and the slope of the irrigated area. Table 1 shows an overview of the basic parameters and the initial conditions for both experiments.

Single rainfall simulator – EXPERIMENT **A**
(irrigated area: 0.0625 m^2)

Two rainfall simulators – EXPERIMENT **B**
(irrigated area: 0.125 m^2)

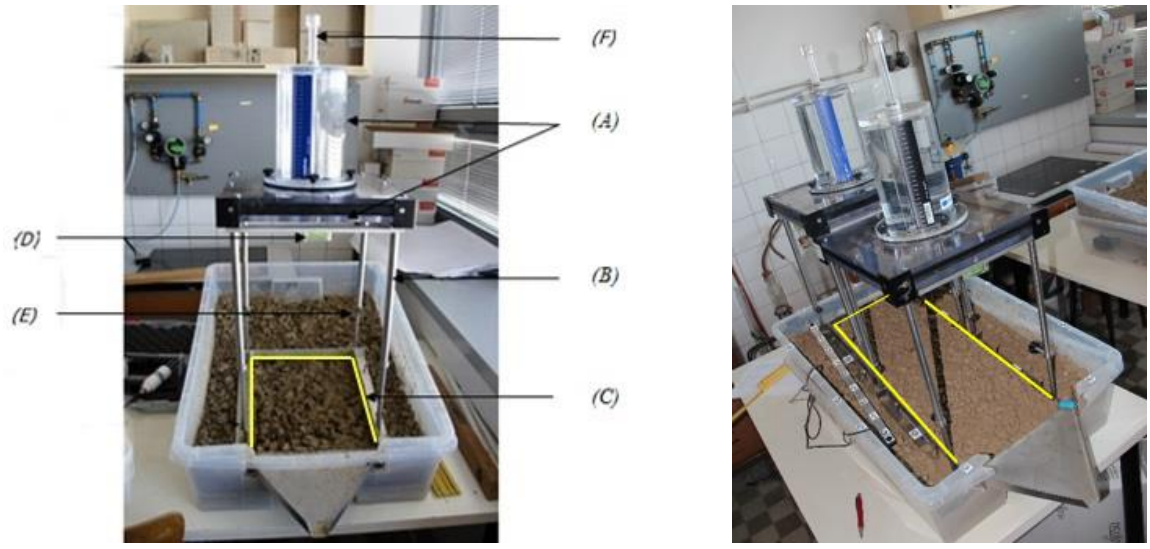

Fig. 1. The Eijkelkamp rainfall simulator: A – sprinkler plate and water reservoir, B – adjustable support, C – ground frame, D – small capillaries, E – adjustable support, F – aeration pipe.

During both experiments, the soil moisture and surface runoff were continuously measured using a soil moisture sensor and a camera that was recording the measuring cylinder collecting the surface runoff and eroded sediment (see Fig. 2A). These parameters were evaluated at 15-second intervals. Apart from the above steps, the weight of the eroded sediments was evaluated after each interruption by weighting the dried soil sample. The surface runoff along with the transported soil was captured in a measuring cylinder. The methodological procedure for processing the measured data during the quasi-continuous 60-minute rainfall simulation is shown in Fig. 2.

Table 1. Overview of the basic parameters and initial conditions for both experiments

Exp.	Length of slope	Irrigated area	Slope	Initial soil moisture	Rainfall intensity	Number of simulations	Total duration	Volume of simulated rainfall
	[m]	[m^2]	[%]	[%]	[mm min^{-1}]	[-]	[min]	[l]
A	0.25	0.0625	20	4.8	2.7	5	60	10.25
B	0.50	0.1250	20	4.2	2.7	5	60	20.5

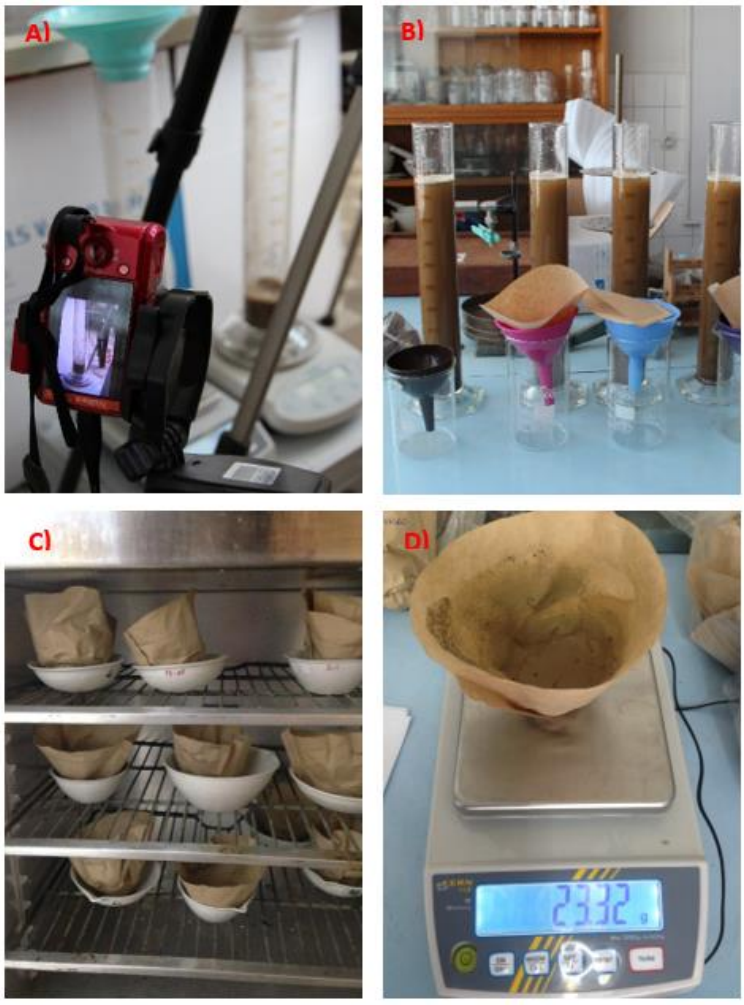

Fig. 2. The procedure of processing the measured surface runoff and eroded soil particles during the quasi-continuous 60-minute rainfall simulation: A) video recording of runoff generation and transport of soil particles; B) filtration of soil particles (sediments) from the measuring cylinders; C) drying of sediments; and D) weighting of sediments.

Results and discussion

For both the A and B experiments, the "time to runoff" (the time before the occurrence of any surface runoff) and its course over the whole experiment (15-second intervals) is shown in Fig. 3. The results showed that in the case of the experiment A with only one rainfall simulator used, the surface runoff appeared 251 s after the beginning of the experiment, while in case of experiment B, with two rainfall simulators arranged in a series, the time to runoff was reduced to 160 s. After the forced interruption of the rainfall simulation (after each 12-min simulation) due to the limitation of the amount of water in the simulator reservoir and its replenishment in both experiments, the surface runoff generation was resumed within 30 s (runs 2–5 of the 12–min simulation). The slope length of the irrigated area had an effect on the course and volume of the surface runoff. For experiment A (slope length 0.25 m), it can be seen that after each interruption at a time when the soil was already saturated, the surface runoff volume oscillated at an interval of 30–40 ml per every 15 s. For a slope length of 0.5 m (experiment B), it occurred in an interval of 60–80 ml per every 15 s, except for the first simulation. Thus, in general, it can be argued that once the soil becomes saturated and small erosion furrows are formed, the surface runoff volume becomes stable (the surface runoff becomes uniform) and varies within a certain range (the interval is also dependent on the amount of eroded soil, as this increases the volume of water in the measuring cylinder). The volume of the surface runoff mainly depends on the size of the irrigated area and on the intensity of the rainfall event (here constant in the all experiments).

A set of experimental parameters was collected within each 12-minute simulation to evaluate the dynamics of the surface runoff generation process, infiltration, and soil loss. Moreover, continuous monitoring of the soil moisture was also conducted. Table 2 gives an overview of the data obtained, which describes the erosion-transport processes within both experiments. The total surface runoff volume during the quasi-continuous rainfall simulation (intermittent 12-minute simulations) stabilized after the formation of small erosion furrows in the irrigated area and after the soil became saturated (during the second run of the simulation); it was stable during the remaining simulations. In both experiments, an increased volume of surface runoff was recorded in the second simulation run compared to the first simulation run. The probable reason is that the surface runoff volume was measured together with the transported sediment. The surface runoff stabilized for experiment A (simulation run 2–5) at 1.5–1.7 l per 12 min and at 2.8–3.3 l per 12 min for experiment B. The ratio of infiltration versus surface runoff was as expected. In the start for experiment A the infiltration was 51% from artificial the precipitation and decreased to 17% in the fifth simulation run (the start time to the surface runoff was 251 s). In the case of the double simulators in the series, the infiltration was 65% in the first simulation run and was decreased in the last simulation run to 19% (the start time to the surface runoff was 160 s). The highest soil loss values were measured for both experiments during the second simulation run (59 g for experiment A and 123 g for experiment B), which only confirms that from this simulation run onwards, the surface runoff increased significantly; moreover, small erosion furrows started to form, increasing the transport capacity of the irrigated area. Table 2 also shows that the concentration of the soil sediment as a component of the surface runoff decreased over time.

The time course of the soil moisture over the two experiments, which was measured by a soil moisture

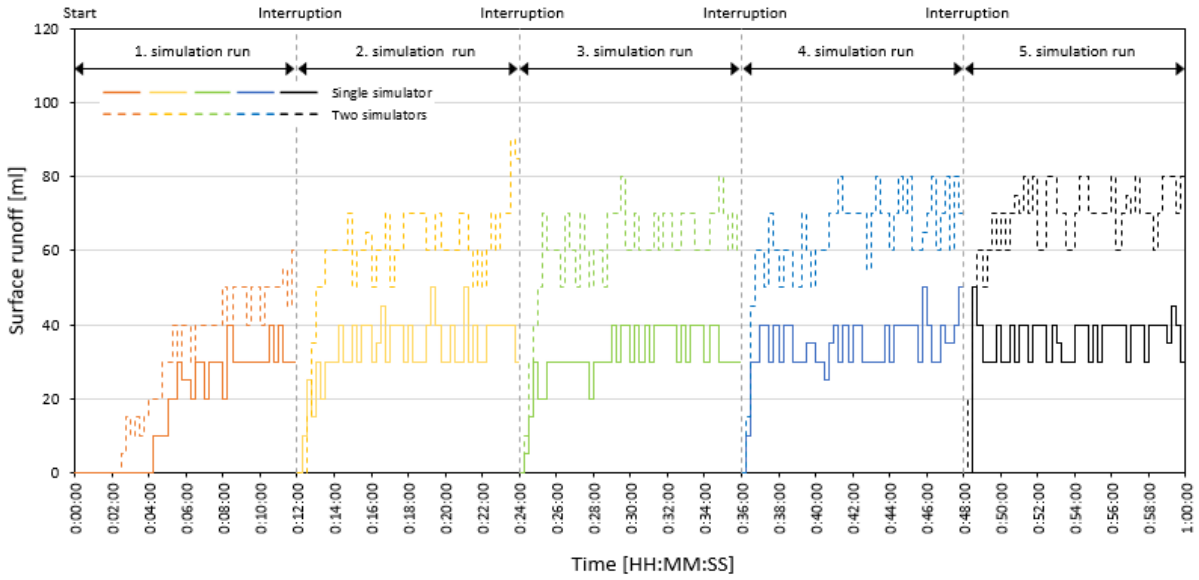

Fig. 3. Time course of the surface runoff under similar initial conditions: Experiment A (Single rainfall simulator), Experiment B (Two rainfall simulators).

sensor placed 5 cm under the surface in the lower part of the irrigated area, is shown in Fig. 4. In both experiments, the soil moisture began to increase at the end of the second simulation run (including a significant increase during the third simulation run), settling at around 45% of the soil moisture (experiment A) and 40% for experiment B by the fifth simulation run.

A comparison of the two experiments in terms of the size of the area on the surface runoff and soil particle transport for the quasi-continuous 60-minute rainfall event with an intensity of 2.7 mm min^{-1} is presented in Figs. 5–6.

Although the area and the length of the slope of the irrigated area in experiment B were two times greater than those in experiment A, the difference in the cumulative volumes of the surface runoff is different for the two experiments. It has been observed that with the increased time of the simulation, the surface of the irrigated area becomes more and more eroded, resulting in the creation of small erosion furrows and thereby causing an increased generation of surface runoff. Over time, the cumulative volume of the surface runoff in experiment B was almost twice as large as that in experiment A, which we believe was caused by the larger dynamic (kinetic energy) of the surface runoff in experiment B. Fig. 6 shows that the slope length significantly affects the transport of soil particles (sediment), as the mass of the dried sediment sample in each simulation run in experiment B significantly exceeds the values obtained in experiment A. The amount of sediment in the experiment with two simulators, and thus a longer slope length, increased by approximately 50–70 g during each 12-minute simulation run compared to the single simulator experiment. A possible explanation is that after reaching

Table 2. Measured characteristics of the 12-minute simulations for both experiments: Experiment A (Single rainfall simulator), Experiment B (Two rainfall simulators)

Exp.	Simulation run No.	Volume of simulated rainfall	Volume of surface runoff	Infiltration vs. Surface runoff	Soil moisture	Sediment soil mass	Concentration soil sediment
	[-]	[l]	[l]	[%]	[%]	[g]	[g l^{-1}]
A	1.	2.05	1.0	51% (49%)	4.8–4.9	36	36
	2.	2.05	1.6	22% (78%)	4.9–5.0	59	37
	3.	2.05	1.5	27% (73%)	5.0–22.7	31	21
	4.	2.05	1.6	22% (78%)	22.7–41.4	35	21
	5.	2.05	1.7	17% (83%)	41.4–45.1	32	19
B	1.	4.1	1.4	66% (34%)	4.2–4.3	103	74
	2.	4.1	2.8	31% (69%)	4.3–9.4	123	44
	3.	4.1	2.9	29% (71%)	9.4–34.1	95	33
	4.	4.1	3.0	25% (75%)	34.1–39.3	101	33
	5.	4.1	3.3	19% (81%)	39.3–40.0	82	25

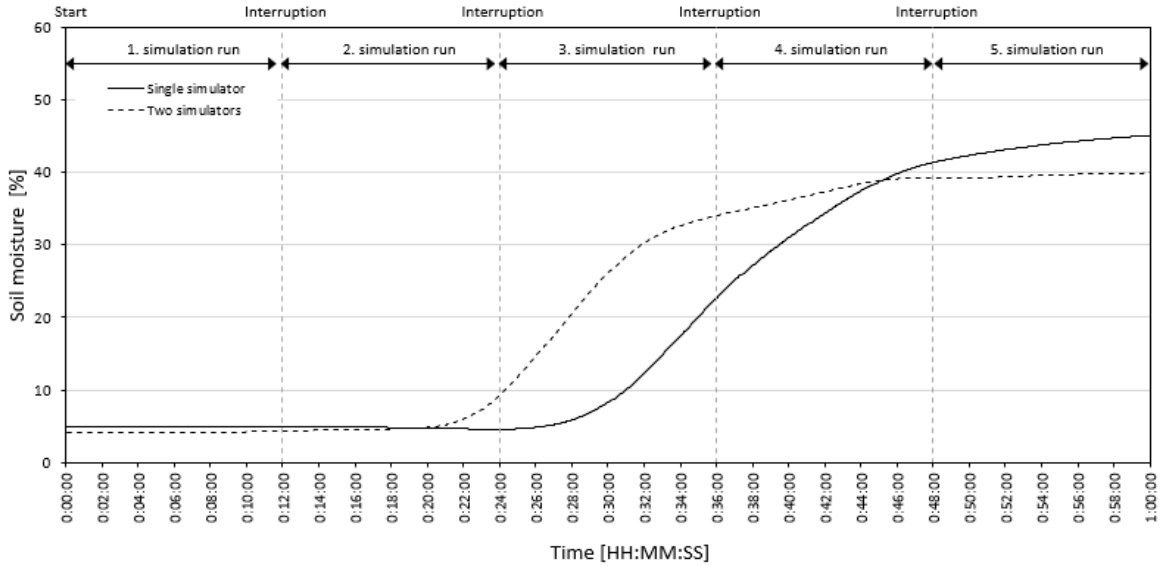

Fig. 4. Continuous course of soil moisture at a depth of 5 cm (soil moisture sensor situated in the lower part of the irrigated area): Experiment A (Single rainfall simulator), Experiment B (Two rainfall simulators).

the point of saturation of the rainfall area, there was approximately the same ratio of eroded sediments between the simulation runs.

A summary of the data obtained and a basic statistical comparison of the measured rainfall-runoff and transport parameters of the two experiments is presented in Table 3. The results presented in the table show the increase in the volume of the surface runoff during the quasi-continuous 60-minute rainfall simulation (intermittent after 12 min) in the two-simulator experiment was 81% (+6 l) higher compared to the one-simulator experiment; the sediment mass after drying was 161% (+311 g) higher; the sediment concentration in the surface runoff was 44% (+11 g l^{-1}) higher; and the infiltration values were 21% higher.

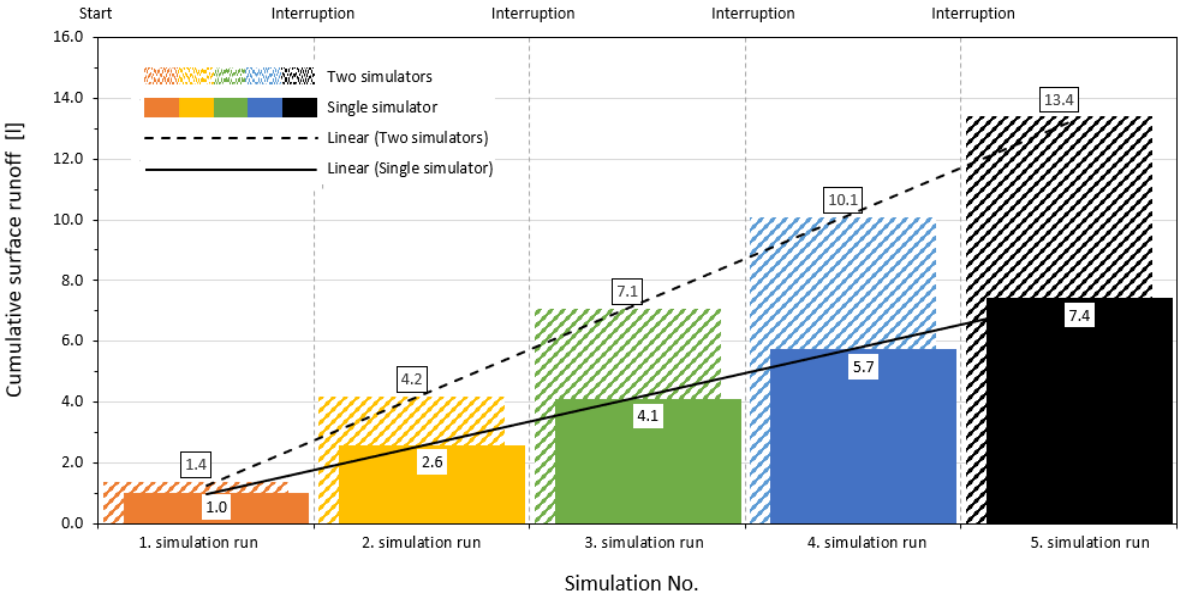

Fig. 5. Comparison of the cumulative surface runoff from a quasi-continuous 60-minute rainfall event (intermittent rainfall every 12 min) with an intensity of 2.7 mm min^{-1}: Experiment A (Single rainfall simulator), Experiment B (Two rainfall simulators).

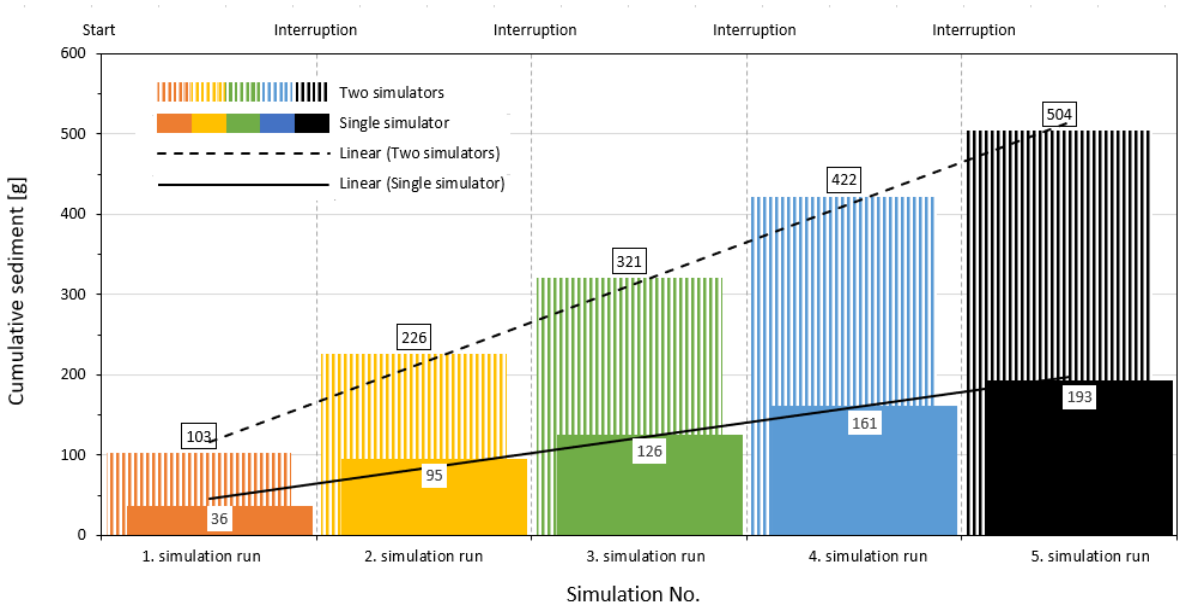

Fig. 6. Comparison of the cumulative soil loss (weight of the sediment sample after drying) from a quasi-continuous 60-minute rainfall event (intermittent rainfall every 12 min) with an intensity of 2.7 mm min^{-1}: Experiment A (Single rainfall simulator), Experiment B (Two rainfall simulators).

Table 3. Summary of the cumulative rainfall-runoff parameters: Experiment A (Single rainfall simulator), Experiment B (Two rainfall simulators)

Experiment	Cumulative surface runoff [l]	Cumulative sediments [g]	Concentration soil sediment [g l^{-1}]	Infiltration [%]
A	7.4	193	26.1	28
B	13.4	504	37.6	34
% increase	**+ 81%**	**+ 161%**	**+ 44%**	**+ 21%**

Conclusion

This study presents the results from two laboratory experiments investigating the effect of the slope length and irrigated area on the temporal distribution and volume of generated surface runoff and eroded soil material using compact and transportable rainfall simulators. The experimental measurements of the surface runoff generation were made using a rainfall simulator (irrigated area 0.0625 m^2) and two rainfall simulators connected in a series (irrigated area 0.125 m^2) on a disturbed soil sample subjected to a quasi-continuous 60-minute simulated rainfall event with an intensity of 2.7 mm min^{-1}. In addition to the volume and dynamics of the surface runoff generation, the sediment mass and the fraction of the infiltrated water from the surface runoff were measured under the same initial conditions for both experiments.

The results of the study showed that there is a direct relationship between the irrigated area and the volume of the surface runoff, as well as the slope length and the weight of the soil particles (sediments) transported. The surface runoff started to form about one-third of the time earlier in the experiment with the greater irrigated area compared to the experiment with half of the slope length. After the soil became saturated with water and the first small erosion furrows formed in the irrigated area (after a 12-minute rainfall simulation during both experiments), the volume of the surface runoff stabilized and became roughly uniform. The highest values of the transported soil particles were observed in both experiments between 12–24 min of the rainfall simulation, when the increase in the volume of the surface runoff was most significant.

Moreover, as the duration of the experiment progressed, the extent of the soil erosion increased together with the increased volume of generated surface runoff, especially in the case of the experiment with two rainfall simulators involved. The reason for this was the twofold slope length and irrigated area in experiment B compared to experiment A. Thus, the slope length significantly affects the transport of soil particles (sediment), as the mass of the sediment sample after drying in each simulation run in the two-simulator experiment significantly exceeded the values obtained in the one-simulator experiment. The concentration of the soil sediment as a component of surface runoff decreased with the increasing duration of the simulation in both experiments. In addition, the soil moisture began to increase after 20 minutes into the simulations in both experiments, followed by a significant step increase, with a plateau of around 45 min.

The study confirmed that the area of the experimental plot played an important role in the process of generating the surface runoff and soil erosion and transport (similarly as in studies e.g., Mayerhofer et al., 2017). Based on the results, not only could improvements be made for future experiments, but also unique information could be obtained that could be used in the process of the calibration and validation of mathematical models simulating soil transport and surface runoff. The results from this type of experiment could be used in the process of calibrating models when estimating their parameters and defining the initial conditions (initial soil moisture, time to runoff, surface roughness, runoff coefficient), as well as for validating models such as measuring the volume of the surface runoff and weight of sediments. This study is a good reference point for initiating or continuing future experiments related to rainfall-runoff and erosion-transport processes.

Acknowledgment

This work was supported by the Slovak Research and Development Agency under Contracts Nos. APVV-19-0340 and APVV-20-0374; and VEGA 1/0782/21.

References

Abudi, I., Carmi, G., Berliner, P. (2012): Rainfall simulator for field runoff studies, Journal of Hydrology, Vols. 454–455, 2012, 76–81.

Aksoy, H., Kavvas, M. L. (2005): A review of hillslope and watershed scale erosion and sediment transport models. Catena, 65, 247–271.

Aksoy, H., Unal, N. E., Cokgor, S., Gedikli, A., Yoon, J., Koca, K., Eris, E. (2012): A rainfall simulator for laboratory-scale assessment of rainfall-runoff-sediment transport processes over a two-dimensional flume, Catena, 98, 63–72.

Chouksey, A., Lambey, V., Nikam, B. R., Aggarwal, S. P., Dutta, S. (2017): Hydrological modelling using a rainfall simulator over an experimental hillslope plot. Hydrology, 4(1), p. 17.

Danáčová, M., Valent, P., Výleta, R., Hlavčová, K. (2017): The effects of rainfall on surface runoff and soil erosion from forest areas, 17th International Multidisciplinary Scientific GeoConference SGEM 2017, 641–648.

Dunkerley, D. (2021): The case for increased validation of rainfall simulation as a tool for researching runoff, soil

erosion, and related processes. Catena, 202, 105283.
Grismer, M. (2012): Standards vary in studies using rainfall simulators to evaluate erosion. Calif. Agric, 66, 102–107.
Hänsel, P., Schindewolf, M., Eltner, A., Kaiser, A., Schmidt, J. (2016): Feasibility of high-resolution soil erosion measurements by means of rainfall simulations and SfM photogrammetry. Hydrology, 3(4), p. 38.
Hlavčová, K., Danáčová, M., Kohnová, S., Szolgay, J., Valent, P., Výleta, R. (2019): Estimating the effectiveness of crop management on reducing flood risk and sediment transport on hilly agricultural land – A Myjava case study, Slovakia, Catena, 172, 678–690.
Holko, L., Danko, M., Hlavčo, J., Kostka, Z. (2018): Overland flow measurement in a mountain headwater catchment using a portable rainfall simulator, Acta Hydrologica Slovaca, 19 (1), 101–108.
Iserloh, T., Ries, J. B., Arnáez, J., Boix-Fayos, C., Butzen, V., Cerdà, A., Wirtz, S. (2013): European small portable rainfall simulators: A comparison of rainfall characteristics, Catena, 110, 100–112.
Mayerhofer, Ch., Meißl, G., Klebinder, K., Kohl, B., Gerhard Markart, G. (2017): Comparison of the results of a small-plot and a large-plot rainfall simulator – Effects of land use and land cover on surface runoff in Alpine catchments, Catena, 156, 2017, 184–196.
Novák, V., Hlaváčiková, H. (2016): Soil hydrology. Institute of Hydrology SAS. ISBN 978-80-224-1529-3
Palese, A. M., Ringersma, J., Baartman, J. E. M., Peters, P., Xiloyannis, C. (2015): Runoff and sediment yield of tilled and spontaneous grass-covered olive orchards grown on sloping land. Soil Research, 53, 542–552.
Schmidt, S., Tresch, S., Meusburger, K. (2019): Modification of the RUSLE slope length and steepness factor (LS-factor) based on rainfall experiments at steep alpine grasslands. MethodsX, 6, 219–229.
Szabó, J. A., Centeri, C., Keller, B., Hatvani, I. G., Szalai, Z., Dobos, E., Jakab, G. (2020): The use of various rainfall simulators in the determination of the driving forces of changes in sediment concentration and clay enrichment. Water, 12(10), 2856.
Zemke, J. J. (2016): Runoff and Soil Erosion Assessment on Forest Roads Using a Small Scale Rainfall Simulator. Hydrology 3, No. 3, 25.

Assoc. Prof. Ing. Michaela Danáčová, PhD. (*corresponding author, e-mail: michaela.danacova@stuba.sk)
Assoc. Prof. Ing. Roman Výleta, PhD.
Prof. Ing. Kamila Hlavčová, PhD.
Department of Land and Water Resources Management
Faculty of Civil Engineering
Slovak University of Technology in Bratislava
Radlinského 11
810 05 Bratislava
Slovak Republic

Ing. Michal Danko, PhD.
Institute of Hydrology SAS
Dúbravská cesta 9
841 04 Bratislava
Slovak Republic

DOI: 10.31577/ahs-2022-0023.02.0029

ACTA HYDROLOGICA SLOVACA

Volume 23, No. 2, 2022, 257–266

Improvement of runoff simulation efficiency using satellite soil moisture data for typical monthly runoff regimes in Austria

Martin KUBÁŇ*, Juraj PARAJKA, Ján SZOLGAY, Silvia KOHNOVÁ, Kamila HLAVČOVÁ, Patrik SLEZIAK, Adam BRZIAK

The availability of remote sensing data opened possibilities for assimilating these into rainfall-runoff models. We examined the quality of the simulated monthly runoff regime in catchments in which the inclusion of a new satellite soil moisture dataset (ASCAT SW1) into the calibration of the TUW rainfall-runoff model outperformed in the model verification the conventional runoff-only calibration in 198 Austrian basins. Using k-means clustering, catchments with similar mean monthly runoff regimes were grouped. Three variants of the multi-objective approach were analysed for each month of the year in Carinthia, Styria and Upper and Lower Austria regions. Improvement in the simulated monthly runoff using the ASCAT data was mainly noticeable in the winter and spring months. The runoff simulation efficiency decreased in the driest summer and autumn months. It has also been confirmed that improvements in the simulations can be expected in the flat river basins compared to the hilly types and in river basins with lower average slopes. The findings refine previous recommendations regarding when hydrological models could benefit from considering information beyond the runoff signatures in their calibration.

KEY WORDS: ASCAT, TUW dual-layer model, soil moisture assimilation, multi-objective calibration, runoff regime

Introduction

Recently the hydrological community significantly increased efforts to improve soil moisture estimation by incorporating remotely-sensed soil moisture data into hydrological studies. The potential of using remotely soil moisture through remote sensing in hydrology was described, e.g. in Brocca et al. (2017). The areas of applications of satellite-based soil moisture data in rainfall-runoff modelling cover three areas in general: Estimating antecedent soil moisture for rainfall-runoff models (e.g., Sunwoo and Choi, 2017; Jadidoleslam et al., 2019); assimilation of satellite data for runoff forecasting (e.g., Meng et al., 2017; Ciupak et al., 2019; Jun et al., 2021, Rončák et al., 2021); multi-objective calibration of continuous hydrological models (e.g., Li et al., 2018; Tong et al., 2021; Kuban et al., 2021, 2022).

Multi-objective calibration of rainfall-runoff models helps to reduce model and parameter uncertainty and improves predictions in general (Efstratiadis and Koutsoyiannis, 2010). The advantages of the multi-objective calibrations using satellite data were demonstrated in several case studies (see, e.g., Nijzink et al., 2018; Demirel et al., 2019; Széles et al., 2020). In addition, microwave satellite sensors increased the applicability of remote sensing of soil moisture. Consequently, the availability of satellite soil moisture datasets is growing, including a new ASCAT Soil Water Index (SWI) data product used in this paper (Paulik et al., 2014). The ASCAT application used here benefits from a new vegetation parameterisation of the ASCAT surface soil moisture retrieval algorithm and improved spatial representation based on a new directional resampling method (Tong et al., 2021; Kuban et al., 2021).

When calibrating rainfall-runoff models to soil moisture and discharge data concurrently, improvements in the representation of internal soil moisture state variables and fluxes were typically achieved. However, joint enhancement in soil moisture and runoff simulation efficiency has not always been observed (Kuban et al. 2021, 2022). Furthermore, other studies also noted deteriorated performance in runoff simulations (Brocca et al., 2017). Therefore, situations leading to benefits from including satellite soil moisture data in rainfall-runoff modelling (both for data assimilation and model calibration) need further clarification.

This paper is based on three various multi-objective calibrations of the dual-layer conceptual TUW rainfall-runoff model in 209 catchments in Austria (Kuban et al., 2021, 2022). It analyses the quality of the simulated monthly runoff regime in those catchments in which the inclusion of a new satellite soil moisture dataset (ASCAT SW1) into the calibration outperformed the conventional runoff-only calibration results in the model verification

for 198 catchments. We used identical model calibrations as in Kuban et al. (2021), which are based on the combinations composed of three multi-objective functions: on the runoff and soil moisture in the root zone; on the runoff and soil moisture in the topsoil layer; and on the runoff and soil moisture both in the root and topsoil layers, respectively. These included the exact finer spatial resolution of the ASCAT product for the topsoil and root zone, reported by Tong et al. (2021). Catchments with improvements in the multi-objective runoff simulations for each calibration scheme as compared to the single objective runoff-only calibration are selected and clustered based on the similarity of their interannual mean monthly runoff distribution. Comparisons of measured and simulated monthly runoff regimes are analysed. The results are expected to permit inferences about the physiographic properties of catchments with typical water balance, where the value of the scatterometer data for hydrological modelling proves helpful.

Material and methods

The TUW-dual rainfall-runoff model and its calibration and validation

In this paper, the TUW-dual conceptual rainfall-runoff model's output time series were used as calibrated by Kuban et al. (2021) in 209 Austrian catchments. The TUW hydrological model follows the structure of the well-known HBV model (Bergstrom, 1992). Parajka et al. (2009) developed it at the Vienna University of Technology as a lumped or semi-distributed conceptual rainfall-runoff model. Precipitation, air temperature, and potential evapotranspiration inputs are required to model catchment runoff on a daily or shorter-step basis. Model inputs can be spatially differentiated with the catchment elevation.

Consequently, the meteorological inputs, soil moisture and snow water equivalent were independently defined for each elevation zone. These were considered to have a 200 m altitudinal range in this research. The limitation of the approach used here was that the model parameters were identical in each elevation zone. Even with this limitation, the TUW-dual can still be regarded as a semi-distributed conceptual model.

Compared with the original TUW model, in the dual version, the soil layer was split into two zones, i.e., the shallow surface soil layer (topsoil) and the deep root zone soil layer. Separate storage represents each layer. The ASCAT data are directly indexed into the surface soil layer. The Soil Water Index (SWI) for the root zone layer is based on an infiltration model, which relates the surface and root zone soil moisture as a function of time. Conceptually it represents the soil moisture content in the first meter of the soil in relative units, ranging between the wilting level (0 %) and field capacity (100 %). Paulik et al. (2014) compared the ASCAT SWI dataset with at-site soil moisture measurements. They found that the SWI better agrees with the in-situ soil moisture from the deeper layers than the original ASCAT set of soil surface moisture data.

The surface zone soil storage is fed by rain and snowmelt and produces direct runoff. Bidirectional moisture flux connects both storages. The field water capacity parameter limits the root zone storage capacity, and it also produces (slow) runoff. In both soil storages, the water is reduced by the actual evapotranspiration, which is the function of the actual water level in these. Kuban et al. (2021, 2022) contain the detailed algorithm and the parametrisation of the layers.

The original TUW single soil layer model has 15 parameters, which need to be calibrated. In the TUW-dual model, 18 parameters had to be considered because of the dual soil layer structure. In addition, three new parameters for the surface soil storage layer were added. The single-objective and multi-objective calibration of the TUW-dual model methodology is described in Kuban et al. (2021, 2022). The analysis in this paper was based on the results achieved therein. For the sake of completeness, the main concepts are therefore repeated here.

The multi-objective calibrations were initially performed with data from the period 2007–2014 calibration period on 209 catchments and were published in Kuban et al. (2021). In this study, as in Kuban et al. (2022), we analysed the model performance to simulate runoff on a subset of 198 basins, where data were available for the validation period of 1991–2000. The model parameters from the calibration period were used (Kuban et al., (2021) in the verification. The validation catchments were divided into two groups, as in Kuban et al. (2022): catchments where the multi-objective calibration approach using the ASCAT SWI data improved or did not improve the values of runoff model efficiency criterion.

The multi-objective calibrations by Kuban et al. (2021) were performed with four functions (OF). The function labelled OF_Q was based on runoff only; OF_{Q+SR} was built from the runoff and soil moisture in the root zone; OF_{Q+SS} was assembled from data on the runoff and soil moisture in the topsoil layer, and $OF_{Q+SR+SS}$ was based on the runoff and soil moisture both in the root and topsoil layers.

The objective functions in multi-objective calibration were a weighted linear combination of the individual single-objective functions OF_Q, OF_{SR}, and OF_{SS}:

$$OF_{Q+SR} = OF_Q \times w_Q + OF_{SR} \times w_{SR} \quad (1)$$

$$OF_{Q+SS} = OF_Q \times w_Q + OF_{SS} \times w_{SS} \quad (2)$$

$$OF_{Q+SS+SR} = OF_Q \times w_Q + OF_{SS} \times w_{SS} \times OF_{SR} \times w_{SR} \quad (3)$$

where

w_Q, w_{SR}, w_{ST} – are the weights based on the results of Tong et al. (2021) and Kuban et al. (2021), and which were set as 1/2 and 1/3, respectively.

The Spearman correlation coefficient between the measured and simulated soil moisture values was used as an objective function for both soil moisture

layers. For the runoff, we chose the average of the Nash-Sutcliffe coefficient (NSE) and the logarithmic NSE as the objective functions (Nash and Sutcliffe, 1970):

$$NSE = 1 - \frac{\Sigma_{i=1}^{n}(Qobs(i)-Qsim(i))^2}{\Sigma_{i=1}^{n}(Qobs(i)-\bar{Q}obs)^2} \quad (4)$$

$$logNSE = 1 - \frac{\Sigma_{i=1}^{n}(logQobs(i)-logQsim(i))^2}{\Sigma_{i=1}^{n}(logQobs(i)-log\bar{Q}obs)^2} \quad (5)$$

where

Qsim(i), Qobs(i) – are the simulated and observed runoff at time *i*;

$\bar{Q}obs$ – is the average of the observed runoff.

The efficiency of the validation model runs was evaluated with respect to the simulated runoff. Therefore the same combinations of NSE and the logarithmic NSE were considered as the Runoff Model Efficiency RME:

$$RME = OF = \frac{(NSE+logNSE)}{2} \quad (6)$$

The evolution strategy by Storn and Price (1997), also known as the differential evolution (DE), was used to optimize the multi-objective parameter. DE is considered successful in finding the global optimum of a real-valued function of real-valued parameters and does not need continuous or differentiable objective functions. The DEoptim version was used here as described in Mullen et al. (2011).

The improvement in the multi-objective against the single-objective calibration was calculated as the difference between Relative Volume Errors (RVE):

$$RVE = \sum(\frac{Qobs(i)-Qsim(i)}{Qobs(i)}) * 100\% \quad [\%] \quad (7)$$

Improvement in the multi-objective calibration (IMO) = $|RVE_{single-objective}|$ - $|RVE_{multi-objective}|$ [%] (8)

In this study we decided to cluster the catchments into groups with a similar interannual distribution of normalised mean monthly runoff. We sought to determine how the inclusion of satellite data in such groups can improve the model efficiency in a typical runoff regime. Runoff simulations using the multi-objective approaches were considered separately.

We have applied the cluster analysis to group catchments according to the respective normalised runoff regimes represented by the interannual distribution of the long-term means of the monthly discharges divided by the long-term mean annual runoff. Cluster analysis is a multivariate method that aims to classify a sample of subjects (or objects) based on a set of measured variables into several different groups so that similar subjects are placed in the same group. The cluster analysis method has several variants; in this study, the *k*-means clustering was used (e.g., Hartigan, 1975).

This standard algorithm, which defines the total within-cluster variation as the sum of squared Euclidean distances between items and the corresponding centroid, has the following formula:

$$W(C_k) = \sum_{xi \in Ck}(x_i - \mu_k)^2 \quad (9)$$

where

x_i – is a data point belonging to the cluster C_k,

μ_k – is the mean value of the points assigned to the cluster C_k.

The choice of distance measures is a critical step in clustering. It defines how the similarity of two elements (*x, y*) is calculated and it will influence the shape of the clusters. The classical method for distance measure is the Euclidean distance calculated as:

$$d_{\text{euc}}(x,y) = \sqrt{\sum_{i=1}^{n}(x_i - y_i)^2} \quad (10)$$

where,

x and *y* – are two vectors of length *n*.

The K-means algorithm iteratively assigns each observation to the nearest centre and re-iterates this process until a new iteration no longer re-assigns any observations to a new cluster. The algorithm is considered to have converged at this point, and the final cluster assignments constitute the clustering solution. More details about this method are presented, e.g., in Hartigan and Wong (1979).

Data

In this paper, 198 catchments from the whole country of Austria were selected (Fig. 1). These catchments were also used in the previous studies (Kuban et al., 2022, 2021; Tong et al., 2021; Sleziak et al., 2020), and represent river basins with no significant anthropogenic influences. The catchments have various geomorphological characteristics. The catchments' area varies between 13.7 (Micheldorf, Krems River) to 6214 km^2 (Bruck an der Mur under Muerz, the Mur River), and the average slope varies from 1.74% to 43.91%. The mean annual precipitation is less than 400 mm year^{-1} in the east and more than 2500 mm year^{-1} in the west of Austrian. The mean daily air temperature was −2.83°C in the Alpine catchments and up to 10.30°C in the lowland catchments.

The Austrian hydrological and meteorological data that we used in this study were provided by the Central Hydrographical Bureau (HZB; https://ehyd.gv.at/, last access: 17 March 2021) and the Zentralanstalt für Meteorologie und Geodynamik (ZAMG). The data from all 198 gauged stations from the period 1991–2000 were used to validate the model in a daily time step. The discharge time series were not influenced by dams or hydropower structures. The climatic model inputs (mean daily precipitation and mean daily air temperature) have been derived from the gridded SPARTACUS data set (Hiebl and Frei, 2016, 2017). This data set provides daily 1 km gridded spatial resolution maps covering the whole territory of Austria. These data have been

available since 1961 and have been consistently interpolated using the same consistent station network throughout the entire period (Duethmann et al., 2020).
For the multi-objective calibration, the new experimental data of the Soil Water Index (ASCAT SWI) were used from the experimental version of the ASCAT DIREX Soil Water Index (ASCAT SWI) product, similarly as in Tong et al. (2021). The original ASCAT SWI surface soil moisture dataset at a 12.5 km spatial resolution is based on a new parametrisation for the correction of vegetation (Hahn et al., 2020), which has shown better soil moisture results for Austria (Pfeil et al., 2018). The process of disaggregation consists of a directional resampling method using a connection between regional (12.5 km) and local (0.5 km) scale Sentinel-1 backscatter observations, which temporarily retain stable soil moisture patterns that are also reflected in the radar backscatter measurements (EODC, 2021). The ASCAT SWI product provides estimates of the Soil Water Index describing the soil-water content profile on a 0.5 km spatial sampling grid, whereas the effective spatial resolution is believed to be within the range of 5–15 km, depending on the location. It is derived from directionally downscaled ASCAT surface soil moisture by computing the Soil Water Index. A key strength of this product is its consistency over long periods of time, as its temporal behaviour is only determined by the backscatter measurements acquired by the intercalibrated ASCAT sensors flown onboard the Metop-A/B/C, which belongs to the EUMETSAT-operated Metop ASCAT (Advanced Scatterometer) satellite mission.

Results and discussion

We apply the K-means clustering methods to cluster the catchments analysed with similar mean monthly runoffs for all three multi-objective variants of the runoff simulation. Only catchments with an improvement in the runoff simulation for the individual approaches of the model multi-objective calibration were considered.
Four clusters were formed for all three multi-objective approaches tested. Fig. 2 presents the spatial division of

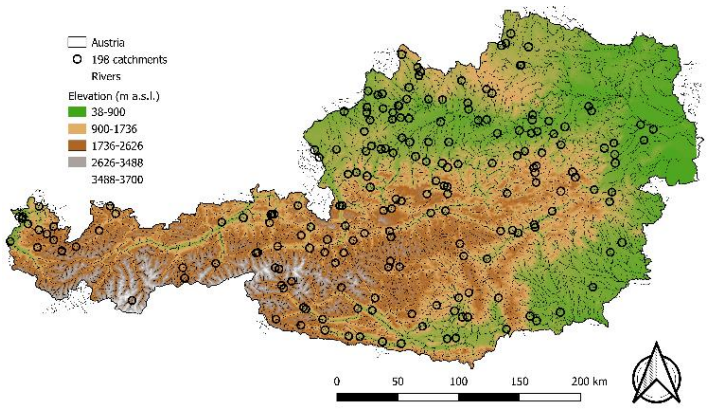

Fig. 1. Location of the 198 catchments selected on the territory of Austria.

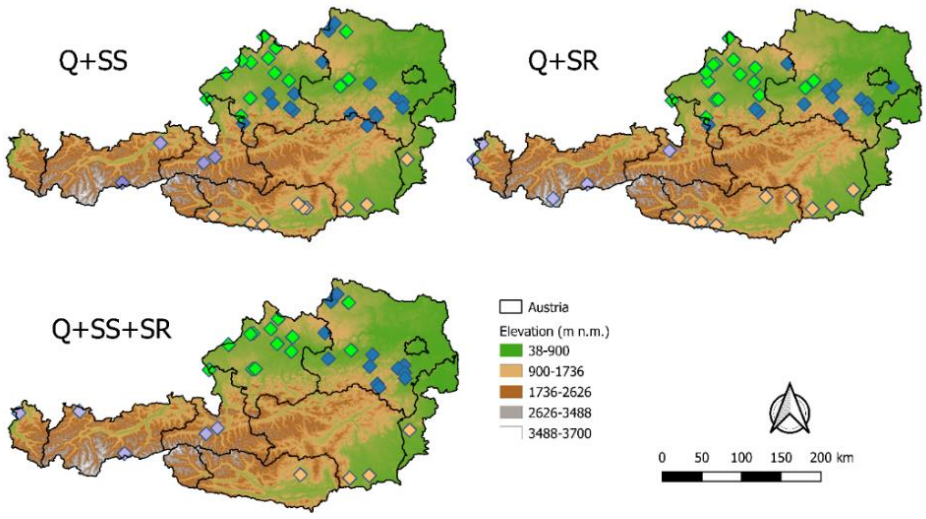

Fig. 2. Groups of the catchments with similar runoff regimes, with an improvement in the runoff simulation for the three multi-objective approaches (Q+SS, Q+SR, and Q+SS+SR) in the 1991–2000 validation period.

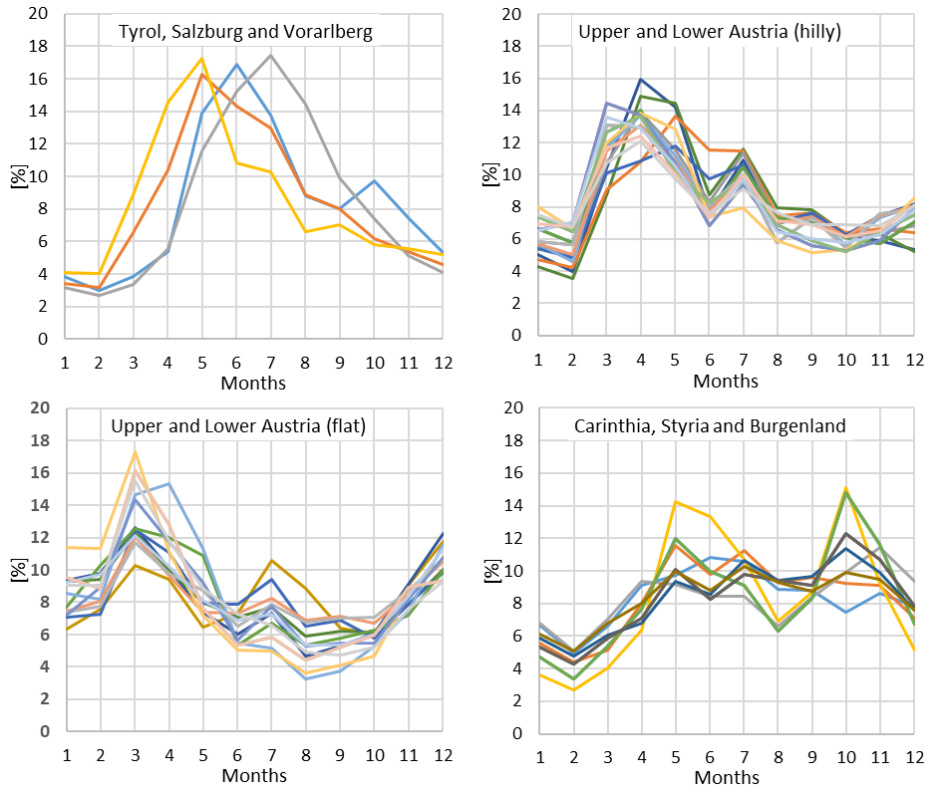

Fig. 3. Normalized mean monthly runoff for the catchments where we have detected an improvement in the runoff simulation with the multi-objective approach (Q+SS) for 1991–2000.

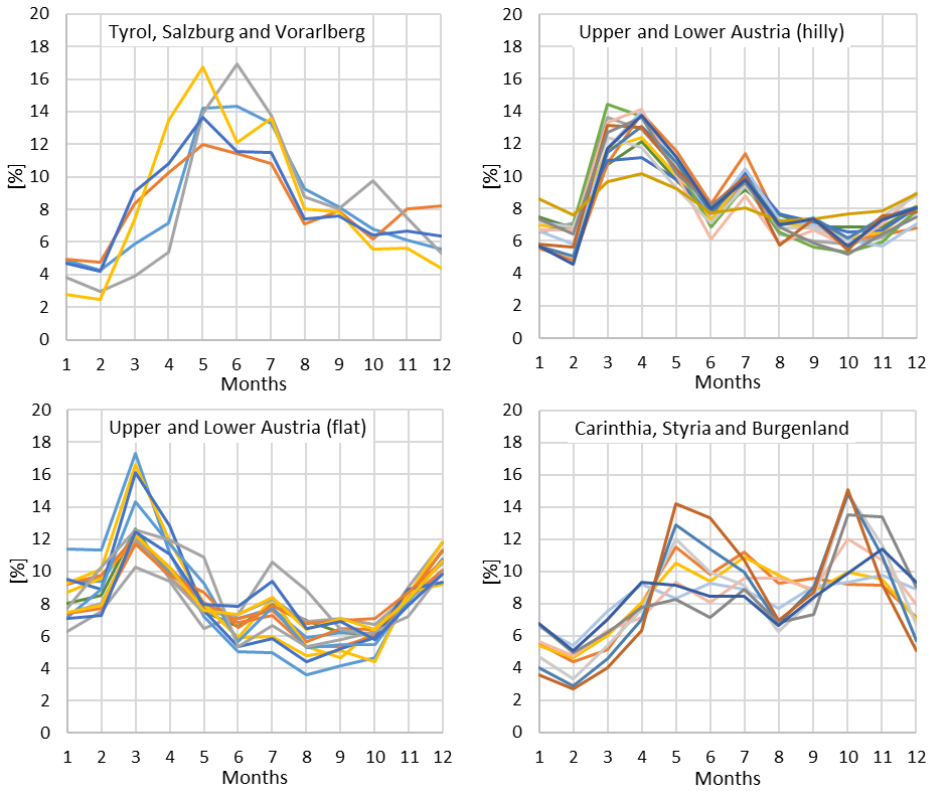

Fig. 4. Normalized mean monthly runoff for the catchments where we have detected an improvement in the runoff simulation with the multi-objective approach (Q+SR) for 1991–2000.

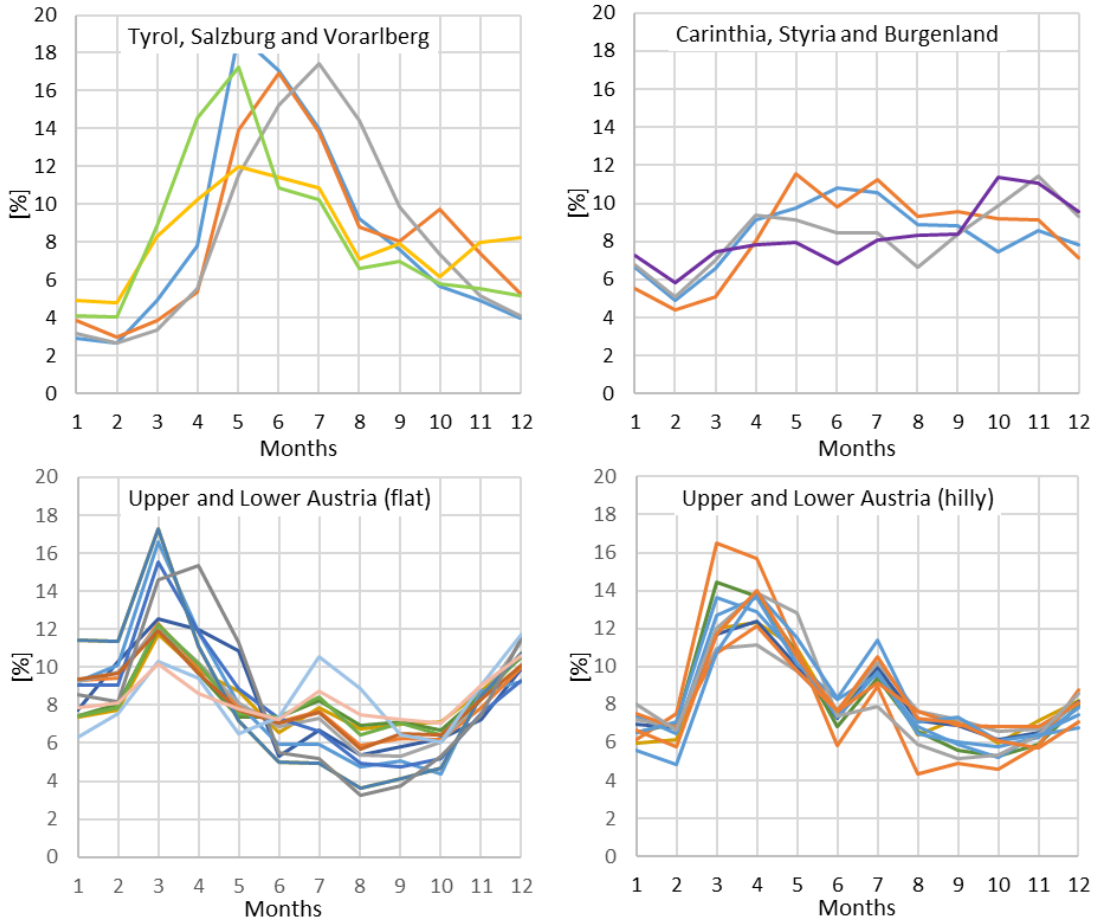

Fig. 5. Normalized mean monthly runoff for the catchments where we have detected an improvement in the runoff simulation with the multi-objective approach (Q+SS+SR) for 1991–2000.

the catchments into four clusters. We can see that the catchments form very comparable clusters, which are located in the following federal republics (regions) of Austria: Tirol and Salzburg (marked by purple colour points), Upper and Lower Austria (green and blue colour points), and Styria, Carinthia, and Burgenland (orange colour points).

Figs. 3–5 presents the typical mean monthly runoff regimes for the catchments analysed. We can see that the catchments located in the regions of Tyrol and Salzburg are characterised by the highest amount of runoff from May to July and by the driest periods in the winter months. This regime is typical of the high mountainous regions in the Alps. The catchments in the Upper and Lower Austria regions were divided by clustering into two groups, which represent hilly and flat catchments. The differences in these catchments can also be seen in the specific runoff and geomorphological characteristics. The runoff regime from snowmelt in the spring season is earlier in the flat catchments than the hilly ones. The catchments located in the regions of Carinthia and Styria are specific, with a higher monthly runoff regime in the spring and autumn that has an interconnection with the precipitation regime influenced by the cyclonic tracks from the Mediterranean Sea.

The comparison of the improvement in the runoff simulation using the multi-objective against the single-calibration approach was evaluated for the individual months using box plots, see Figs. 6–8. The box plots show the percentage of the improvement or deterioration in relative volume errors for the three multi-objective approaches (Q+SS, Q+SR, and Q+SS+SR) against the single-calibration approach for a specific month in the period 1991–2000 (Equations 7, 8).

The evaluation showed that the improvements occurred in different months for each group of catchments, where we detected an improvement in the runoff simulation with the multi-objective approach. For the Tyrol and Salzburg regions, there was a significant improvement in the runoff simulation between September and December and only a slight improvement from January to April. In the Upper and Lower Austria regions for the hilly river basins, there was only a slight improvement in the spring months of March-May for the multi-objective (Q+SS+SR) simulation and June. For the flat river basins in Upper and Lower Austria, there was a significant improvement in the runoff simulation from October to March, a slight decrease in May, and a subsequent improvement in June. In the states of Carinthia and Styria, there was an improvement in the runoff

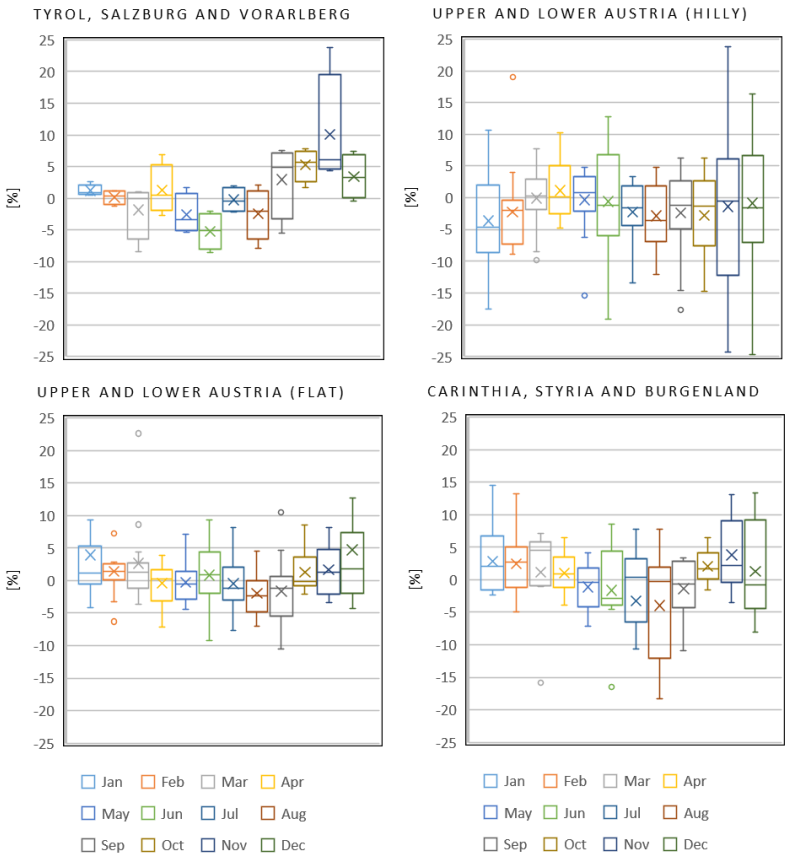

Fig. 6. Improvement in relative volume errors in [%] for multi-objective (Q+SS) calibration vs single-objective calibration in individual months for 1991–2000.

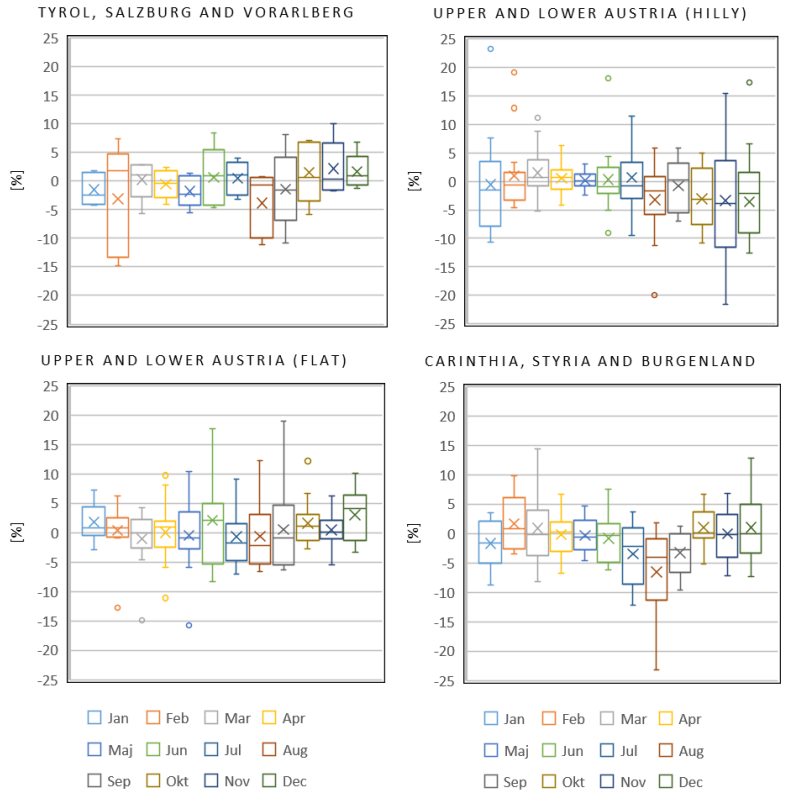

Fig. 7. Improvement in relative volume error in [%] for multi-objective (Q+SR) calibration vs single-objective calibration in individual months for 1991–2000.

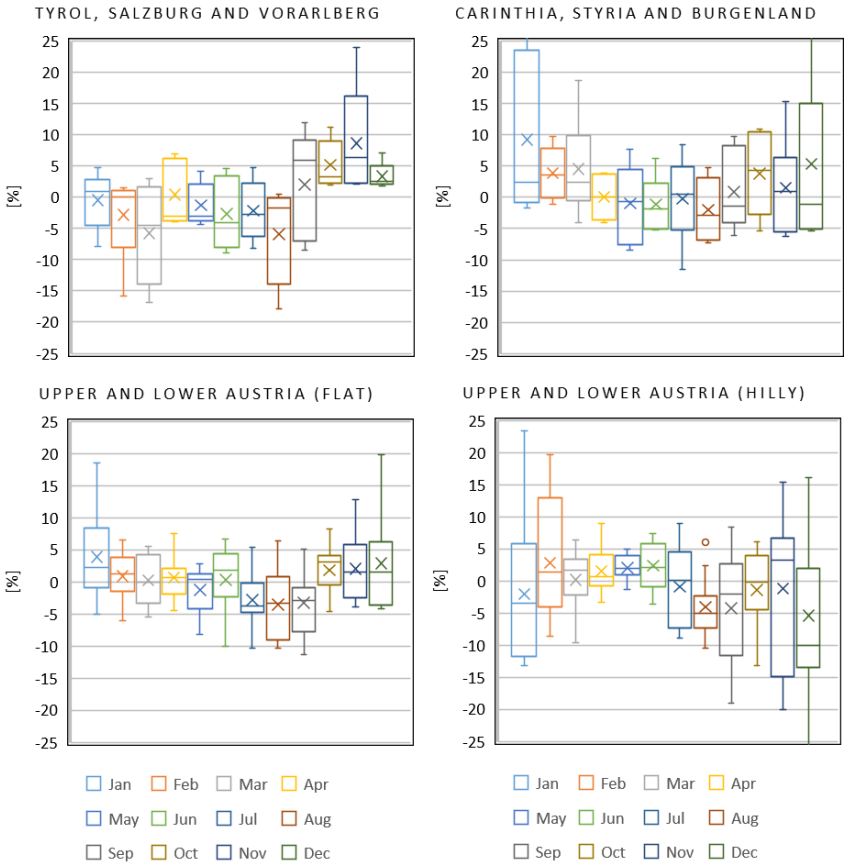

Fig. 8. Improvement in relative volume errors in [%]) for multi-objective (Q+SS+SR) calibration vs single-objective calibration in individual months for 1991–2000.

simulation using the multi-objective (Q+SS) approach from January to April and then in October to November, and for the multi-objective (Q+SR) approach from February to April. For the multi-objective (Q+SS+SR) approach, this improvement occurred in February-June and November.

Conclusion

In this study, we have examined the improvement of the simulated monthly runoff regime in catchments in which the inclusion of a new satellite soil moisture dataset (ASCAT SW1) into the calibration of the TUW rainfall-runoff model outperformed in the model verification, the conventional runoff-only calibration in 198 Austrian basins. Using k-means clustering, catchments with similar mean monthly runoff regimes were grouped for regions: Carinthia, Styria, and Upper and Lower Austria. Three variants of the multi-objective approach were tested for each month of the year. From the results, we can conclude that any improvement in the simulated runoff using ASCAT SWI data is mainly noticeable in the winter and spring months and vice versa; decreases in the simulation efficiency occurred in the driest summer and autumn months. This may be related to the ASCAT SWI product providing moderately distorted data for very dry soil (EODC, 2021). It has also been confirmed, e.g., in the Upper and Lower Austria regions, that better improvement in the simulations can be expected in the flat river basins compared to the hilly types, as well as in river basins with a lower average slope.

Acknowledgement

This work was supported by the Slovak Research and Development Agency under Contract No. No. APVV-19-0340 and the VEGA Grant Agency No. 1/0632/19. At the same time, we would like to acknowledge the support from the Stefan Schwarz grant of the Slovak Academy of Sciences.

References

Bergstrom, S. (1992): The HBV model - its structure and applications. Report No. 4, Swedish Meteorological and Hydrological Institute.

Brocca, L., Ciabatta, L., Massari, C., Camici, S., Tarpanelli, A. (2017): Soil Moisture for Hydrological Applications: Open Questions and New Opportunities. In Water 9 (2), p. 140. DOI: 10.3390/w9020140.

Ciupak, M., Ozga-Zielinski, B., Adamowski, J., Deo, R. C., Kochanek, K. (2019): Correcting Satellite Precipitation Data and Assimilating Satellite-Derived Soil Moisture

Data to Generate Ensemble Hydrological Forecasts within the HBV Rainfall-Runoff Model. In Water 11 (10), p. 2138. DOI: 10.3390/w11102138.

Demirel, M. C., Özen, A., Orta, S., Toker, E., Demir, H. K., Ekmekcioğlu, Ö., Tayşi, H., Eruçar, S., Sağ, A.B., Sarı, Ö., Tuncer, E., Hancı, H., Özcan, T. İ., Erdem, H., Koşucu, M. M., Başakın, E. E., Ahmed, K., Anwar, A., Avcuoğlu, M. B., Vanlı, Ö., Stisen, S., Booij, M. J., (2019): Additional Value of Using Satellite-Based Soil Moisture and Two Sources of Groundwater Data for Hydrological Model Calibration. Water 2019, 11, DOI: 10.3390/w 11102083.

Duethmann, D., Blöschl, G., Parajka, J. (2020): Why does a conceptual hydrological model fail to correctly predict discharge changes in response to climate change? Hydrol. Earth Syst. Sci., 24, 3493–3511, https://doi.org/10.5194 /hess-24-3493-2020, 2020.

Efstratiadis, A., Koutsoyiannis, D. (2010): One decade of multi-objective calibration approaches in hydrological modelling: a review. In Hydrological Sciences Journal 55 (1), 58–78. DOI: 10.1080/02626660903526292.

EODC (2021): Product User Manual ASCAT DIREX SWI 0.5 km, v1.0,.

Hahn, S., Wagner, W., Steele-Dunne, S., Vreugdenhil, M., Melzer, T. (2020): Improving ASCAT Soil Moisture Retrievals With an Enhanced Spatially Variable Vegetation Parameterization. IEEE Transactions on Geoscience and Remote Sensing. 1–16. 10.1109/TGRS.2020.3041340.

Hartigan, J. A. (1975): Clustering Algorithms. John Wiley & Sons, New York, ISBN 0-471-35645-X. 369 pp.

Hartigan, J. A., Wong, M. A. (1979): Algorithm AS 136: A K-means clustering algorithm. Applied Statistics, 28, 100–108. doi:10.2307/2346830.

Hiebl, J., Frei, C. (2016): Daily temperature grids for Austria since 1961—Concept, creation and applicability. Theor. Appl. Clim. 124, 161–178.

Hiebl, J., Frei, C. (2017): Daily precipitation grids for Austria since 1961—Development and evaluation of a spatial dataset for hydroclimatic monitoring and modelling. Theor. Appl. Clim., 132, 327–345.

Jadidoleslam, N., Mantilla, R., Krajewski, W. F., Goska, R. (2019): Investigating the role of antecedent SMAP satellite soil moisture, radar rainfall and MODIS vegetation on runoff production in an agricultural region. In Journal of Hydrology 579, p. 124210. DOI: 10.1016/j.jhydrol.2019.124210.

Jun, S., Park, J. H., Choi, H. J., Lee, Y. H., Lim, Y. J., Boo, K. O., Kang, H. S. (2021): Impact of Soil Moisture Data Assimilation on Analysis and Medium-Range Forecasts in an Operational Global Data Assimilation and Prediction System. Atmosphere, 12, 1089. https://doi.org/10.3390/ atmos12091089

Kuban, M., Parajka, J., Tong, R., Greimeister-Pfeil, I., Vreugdenhil, M., Szolgay, J., Kohnova, S., Hlavcova, K., Sleziak, P., Brziak , A. (2022): The effects of satellite soil moisture data on the parametrization of topsoil and root zone soil moisture in a conceptual hydrological model. Journal of Hydrology and Hydromechanics;70(3): 295–307. https://doi.org/10.2478/johh-2022-0021

Kuban, M., Parajka, J., Tong, R., Pfeil, I., Vreugdenhil, M., Sleziak, P., Adam, B., Szolgay, J., Kohnová, S., Hlavcova, K. (2021): Incorporating Advanced Scatterometer Surface and Root Zone Soil Moisture Products into the Calibration of a Conceptual Semi-Distributed Hydrological Model. Water, 13, 3366. https://doi.org/10.3390/w13233366

Li, Y., Grimaldi, S., Pauwels, V., Walker, R. N., Jeffrey, P. (2018): Hydrologic model calibration using remotely sensed soil moisture and discharge measurements: The impact on predictions at gauged and ungauged locations. In Journal of Hydrology 557, 897–909. DOI: 10.1016/j.jhydrol.2018.01.013.

Meng, S., Xie, X., Liang, S. (2017): Assimilation of soil moisture and streamflow observations to improve flood forecasting with considering runoff routing lags. In Journal of Hydrology 550, 568–579. DOI: 10.1016/j.jhydrol.2017.05.024.

Mullen, K. M., Ardia, D., Gil, D. L., Windover, D., Cline, J. (2011): DEoptim: An R Package for Global Optimization by Differential Evolution. Journal of Statistical Software, 40(6), 1–26. https://doi.org/10.18637/jss.v040.i06

Nash, J. E., Sutcliffe, J. V. (1970): River flow forecasting through conceptual models part I – A discussion of principles. Journal of Hydrology. 10 (3): 282–290. doi:10.1016/0022-1694(70)90255-6.

Nijzink, R. C., Almeida, S., Pechlivanidis, I. G., Capell, R., Gustafssons, D., Arheimer, B. Parajka, J., Freer, J., Han, D., Wagener, T., van Nooijen, R. R. P., Savenije, H. H. G., Hrachowitz, M. (2018): Constraining Conceptual Hydrological Models With Multiple Information Sources. In Water Resour. Res. 54 (10), 8332–8362. DOI: 10.1029/2017WR021895.

Parajka, J., Naeimi, V., Blöschl, G., Komma, J. (2009): Matching ERS scatterometer based soil moisture patterns with simulations of a conceptual dual layer hydrologic model over Austria. In Hydrol. Earth Syst. Sci. 13, DOI: 10.5194/hessd-5-3313-2008.

Paulik, C., Dorigo, W., Wagner, W., Kidd, R. (2014): Validation of the ASCAT Soil Water Index using in situ data from the International Soil Moisture Network. In International Journal of Applied Earth Observation and Geoinformation 30, 1–8. DOI: 10.1016/j.jag.2014.01.007.

Pfeil, I., Vreugdenhil, M., Hahn, S., Wagner, W., Strauss, P., Blöschl, G. (2018): Improving the Seasonal Representation of ASCAT Soil Moisture and Vegetation Dynamics in a Temperate Climate. Remote Sensing, 10, 1788. https://doi.org/10.3390/rs10111788

Rončák, P., Šurda, P., Vitková, J. (2021): Analysis of a Topsoil Moisture Regime Through an Effective Precipitation Index for the Locality of Nitra, Slovakia. Slovak Journal of Civil Engineering, 29 (1) 9–14. https://doi.org/10.2478/sjce-2021-0002.

Sleziak , P., Szolgay, J., Hlavčová, K., Danko, M., Parajka, J. (2020): The effect of the snow weighting on the temporal stability of hydrologic model efficiency and parameters, Journal of Hydrology, 583, 124639. ISSN 0022-1694, https://doi.org/10.1016/j.jhydrol.2020.124639.

Storn, R., Price, K. (1997): Differential Evolution – A Simple and Efficient Heuristic for Global Optimization over Continuous Spaces. Journal of Global Optimization 11, 341–359. https://doi.org/10.1023/A:1008202821328

Sunwoo, W., Choi, M. (2017): Robust Initial Wetness Condition Framework of an Event-Based Rainfall-Runoff Model Using Remotely Sensed Soil Moisture. In Water 9 (2), p. 77. DOI: 10.3390/w9020077.

Széles, B., Parajka, J., Hogan, P., Silasari, R., Pavlin, L., Strauss, P., Blöschl, G. (2020): The Added Value of Different Data Types for Calibrating and Testing a Hydrologic Model in a Small Catchment. In Water resources research 56 (10), e2019WR026153. DOI: 10.1029/2019WR026153.

Tong, R., Parajka, J., Salentinig, A., Pfeil, I., Komma, J., Széles, B. Kubáň, M., Valent, P., Vreugdenhil, M., Wagner, W., Blöschl, G. (2021): The value of ASCAT soil moisture and MODIS snow cover data for calibrating a conceptual hydrologic model. In Hydrol. Earth Syst. Sci. 25 (3), 1389–1410. DOI: 10.5194/Hess-25-1389-2021.

Ing. Martin Kubáň, Ph.D. (*corresponding author, e-mail: martin.kuban@stuba.sk)
Prof. Ing. Ján Szolgay, Ph.D.
Prof. Ing. Silvia Kohnová, Ph.D.
Prof. Ing. Kamila Hlavčová, Ph.D.
Ing. Adam Brziak
Slovak University of Technology
Faculty of Civil Engineering
Department of Land and Water Resources Management
Radlinského 11
810 05 Bratislava
Slovak Republic

Assoc. Prof. Ing. Juraj Parajka, Ph.D.
Centre for Water Resource Systems
TU Wien
Vienna, 1040
Austria

Ing. et Ing. Patrik Sleziak, Ph.D.
Institute of Hydrology SAS
Dúbravská cesta 9
84104 Bratislava
Slovak Republic

DOI: 10.31577/ahs-2022-0023.02.0030

ACTA HYDROLOGICA SLOVACA

Volume 23, No. 2, 2022, 267–272

Assessment of meteorological and hydrological drought using drought indices: SPI and SSI in eastern Slovakia

Tatiana SOĽÁKOVÁ, Martina ZELEŇÁKOVÁ*, Viktoria MIKITA, Helena HLAVATÁ, Dorota SIMONOVÁ, Hany ABD ELHAMID

The current article presents a one-dimensional frequency analysis of historical drought events in the years 1972 to 2014 in the eastern part of Slovakia. Two physical drought types: meteorological and hydrological are classified by SPI – standardized precipitation index and SSI – standardized streamflow index. These indexes have the same mathematical calculation, the difference is only in the input initial monitored data collected from seven rain gauge stations and seven river stations. The most appropriate theoretical probability distribution of selected data is performed using the Kolmogorov-Smirnov test, which is done in EasyFitt program. The basic parameters of meteorological and hydrological drought are determined by the application of the RUN method. One – dimensional frequency analysis of two physical droughts is created for a purpose of estimating the probability of their occurrence in time and identifying the spatial vulnerability of this area. The main benefit of this work is the identification of the average return time of drought events. On average we can expect a moderate meteorological drought in 18.14 to 36.8 months and a hydrological drought in 26 to 60 months.

KEY WORDS: frequency analysis, SPI, SSI

Introduction

Drought is a natural phenomenon with a temporary, negative and severe deviation from the average value of precipitation during a specific time period in an area that could lead to meteorological, agricultural, hydrological and socio-economic drought (COM (2007) 414 final). Scientists distinguish two kinds of drought: physical and non-physical drought. Meteorological and hydrological and agricultural droughts are classified as physical droughts because their origin depends on natural physical processes taking place in the atmosphere and on the earth's surface. Socio-economic drought is a non-physical drought and will still occur with at least one mentioned physical drought (Blain, 2012). Hydrological drought is later than meteorological drought, and the corresponding propagation time depends on persistent precipitation deficit, the occurrence of excessive temperature, evaporation and dry winds in the territory (Van Loon, 2013). The tendency of occurrence of intense droughts is increasing due to climate change all over the world, and the territory of the European Union is no exception. During the period 1976–2006, damages by drought were around 100 billion EUR (COM (2007) 414 final). In the years 2003, 2011–2012 and 2015 EU recorded the most severe manifestations of physical droughts (Fendeková et al., 2018). From the above-mentioned factors, the need to monitor and manage the risk of drought at the international, regional and local levels is increasing. Actual drought monitoring at the regional and local levels takes place with the help of a monitoring network throughout the territory of Slovakia. This monitoring network is available on the website of the Slovak Hydrometeorological Institute.

Various methods are used for monitoring and characterization of drought, but the most used methods are indexes (Tsakiris et al., 2007). There is at least one index form each type of drought. Standardized Precipitation Index SPI (McKee et al., 1993) or Standardized Precipitation and Evapotranspiration Index SPEI (Vicente-Serrano et al., 2010) are the indexes most commonly used to identify meteorological drought. To calculate the SPEI we need monthly data on precipitation totals and temperatures, while for SPI, only precipitation data for the given area is sufficient. The computation of SPI can be performed in various time intervals, which functionally distinguish different types of physical drought, as follows: i) 1 to 3-month intervals reflect soil moisture deficit, ii) 6 to 12-month intervals reflect changes in water accumulation in surface water sources, iii) 24 to 36 months reflect changes in groundwater reserves (McKee et al., 1993). The mathematical calculation of the index can be calculated in a parametric

and non-parametric way (Soľáková et al., 2013). In most cases, the non-parametric way is used because the data is usually not normally distributed. Identifying the most suitable probability distribution is possible according to the Kolmogorov-Shmirnov test (Kottegoda and Rosso, 1997), the L-moment distribution diagram (Peel et al., 2001) or the Akaike information criterion (Akaike, 1973). Some distributions such as Gamma, Generalized Gamma are zero-bounded, and if the data contains a high number of zero values, then a transformation of the cumulative probability function according to Wu et al. (2007) is necessary, so-called equiprobability transformation. In this way, we obtain a spatially and temporally stable index that can be compared with other indices from other regions (Blain, 2012).

Quantifying flow dynamics using an index: the SDI streamflow drought index was proposed by Nalbantis (2008). The SDI has a similar mathematical calculation to SPI, the monthly streamflow values are described by a lognormal distribution. The suitability of other three-dimensional statistical distributions such as lognormal, Pearson, log-logistic, Generalize Extreme Value, generalized Pareto and Weibull were studied by Vicente-Serrano et. al. (2012) in the Erbo basin in Spain and introduced the standardization of the SDI index by applying the statistical non-parametric Kolmogorov-Smirnov test or using the L-moment proportion diagram. Table 1 records the categorization of drought, which is the same for both indices: SPI and SSI and quantifies the risk of drought into classes according to severity. Such quantification of drought is issued when implementing measures in the basin or in the state (*Z* is a value of calculated index).

Identifying the occurrence of episodes of meteorological and hydrological drought makes the management of this event more efficient in the basin, thus ensuring the minimization of the negative impact on fauna and flora, as well as on human activities. The aim of this work was to identify episodes of moderate to extreme meteorological drought for the reference period 1972–2014 in a sub-basins: Dunajec and Poprad, Bodrog and Bodva, and also to identify the time of drought return with a 15.9% probability of occurrence.

Material and methods

The values of hydrometeorological data (values of average daily streamflows and total daily precipitation) for the selected time interval: 1971–2014 were provided for 7 river stations and 7 rain gauge stations (see Fig.1) by the Slovak Hydrometeorological Institute in Košice, only in the Ižkovce station is there a smaller time period: 1975–2014. SPI in a 12-month time frame (or SSI) is calculated using aggregated monthly precipitation totals (or monthly streamflows). Aggregation of precipitation totals (or streamflows) is performed with the help of a so-called moving window. The total precipitation value in December 2011 will have the sum of the total precipitation values from January 2010 to December 2011. And this is how we gradually obtain a statistical set of aggregated precipitation (or aggregated strreamflows), which we statistically analyze by identifying the most appropriate statistical distribution. Estimation of the most appropriate probability distribution f(x) for each month, by choosing from eight tri parameters distributions (General Extreme Value – GEV, Weibull, Lognormal,

Table 1. Categorization of drought

Index interval	Category	The probability of the event
$Z \geq 0$	No drought	50%
$-1 \leq Z < 0$	Mild drought	34.1%
$-1.5 \leq Z < -1$	Moderate drought	9.2%
$-2 \leq Z < -1.5$	Severe drought	4.4%
$Z < -2$	Extreme drought	2.3%

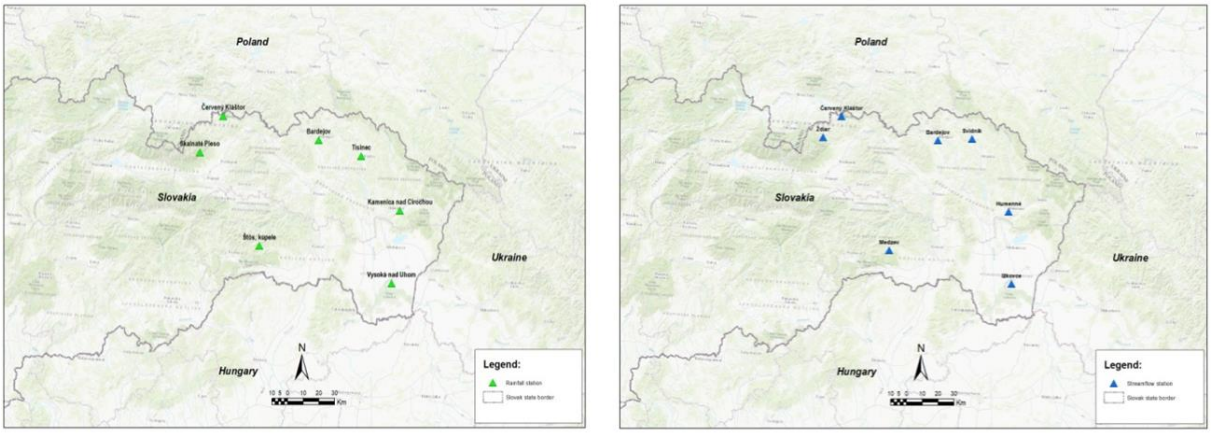

a) b)

Fig. 1. Map of the location of a) rain gauge stations and b) river stations.

Gamma, Generalized Gamma, Pearson 6, Burr, Normal) using the Kolmogorov – Smirnov test. The statistical test was done using the software: EasyFit 5.5 and Excel. The results of the statistical test at a significance level of 5% rank the probability distribution function in an Excel worksheet from the most appropriate theoretical function to the least appropriate.

Currently, the parameters of the best-fit probability distribution function are determined by the maximum likelihood method. Then we calculate the cumulative distribution function. By inverting its values in chronological time we obtain an index. Another important step is to verify whether the index values Z have a normal distribution according to the Wu et al. (2007) requirements. The identification of the beginning of a moderate drought is if Z<-1. Determining the total number of episodes and the duration. Duration is a continuous time interval during which Z is still less than -1) and the severity of individual episodes is a sum of all Z values during the continuous duration of the one drought episode. Inter-arrival time is the time that determines the period between two drought episodes or in other words, the time that elapses from the beginning of the first drought episode to the beginning of the next drought episode (Madadgar et. al, 2011).

Study area

The largest studied sub-basin, extending over the northeastern, eastern and southeastern parts of Slovakia, is the Bodrog sub-basin, where agricultural land use represents 51.2% of the total basin area of 7 272 km^2. The sub-basin of Bodrog is represented by four water meter/precipitation gauge stations, namely: Bardejov 312 m a.s.l. / Bardejov 312 m a.s.l., Svidník 216 m a.s.l. / Tisinec 192 m a.s.l., Humenné 155 m a.s.l. / Kamenica nad Cirochou 176 m a.s.l. and Ižkovce 100 m a.s.l. / Vysoka nad Uhom 230 m a.s.l. In the southern part of the studied territory there is a sub-basin of the Bodva, it is the smallest studied sub-basin with a total area of 858 km^2 and with 48.1% agricultural land use. It is characterized by a water meter station in the town of Medzev 318 m a.s.l. and approximately 12.3 km away, a precipitation gauge station in the town of Štós Kúpele 516 m a.s.l. in the northern part of the studied territory, there is a sub-basin of the Dunajec and Poprad with a total area of 1950 km^2 and with a total of 42% of the land used for agricultural purposes. This sub-basin is represented by two water meter stations and two precipitation gauge stations. There are stations in the cities: Červený Kláštor 469 m a.s.l. / Červený Kláštor 469 m a.s.l. and In Ždiar 896 m a.s.l. / Skalnaté Pleso 1778 m a.s.l.

Results and discussion

The results of the research are presented in the following. Over a 42-year time period, the total duration of long-term meteorological droughts ranged from 77 to 82 months, while in the Kamenica nad Cirochou was the most frequent occurrence of drought episodes. In January 1972 the maximum duration of the long-term meteorological drought was recorded in the north of the territory in Červený Kláštor, with a duration of up to twenty-four months. The greatest cumulative severity of the long-term meteorological drought was recorded in the south at Štós station, where rare occurrences of drought episodes are expected, but with greater duration and severity. The average inter-arrival time of a long-term meteorological drought ranges from 18.14 to 36.8 months (Table 2).

In the monitored area, the duration of long-term hydrological drought ranges from 78 to 86 months. The most frequent occurrence of the episode of a drop in the levels of surface water bodies and groundwater was recorded in the north of the territory at the Červený Kláštor station with a total of 22 drought episodes. In April, the longest twenty-five-month hydrological drought was recorded at the Medzev station, while this station is characterized as the most vulnerable station to this phenomenon during the observed period 1972–2014. The average inter-arrival time of long-term hydrological drought ranges from 23.6 to 60 months (Table 3).

Maps of the duration of meteorological drought (see Fig. 2) and hydrological drought (see Fig. 3) were created in the ArcGIS program using the spline function.

Table 2. Identification of the basic feature of long-term meteorological drought by index SPI-12 for the period 1972–2014

	Bardejov	Tisinec	Kamenica nad Cirochou	Vysoká nad Uhom	Štós	Červený Kláštor	Skalnaté Pleso
Duration	78	**82**	81	80	80	**82**	77
Max. duration	9	10	12	12	21	**24**	10
of drought	2003	1986	1986	1992	1992	**1972**	1979
episode	V.	XI.	XI.	VII.	VII.	**I.**	X.
Severity	-117.4	-116.9	-124.2	-122.2	**-127.2**	-121.4	-119.7
Drought episodes	28	26	**29**	20	14	22	20
Average inter-arrival time	19.42	20.36	**18.14**	26.78	36.8	24.23	26.78

We created six classes of drought duration, graded from the longest duration to the shortest duration based on interpolation from the maximum duration of the drought to the minimum duration of the drought in the observed period of 1972–2014 only in Ižkovce station for hydrological drought is a period: 1976–2014.
We consider the Červený Kláštor and Tisinec stations to be among the most vulnerable areas to long-term meteorological drought for the selected period. The north and northeast of Slovakia, the surroundings of Červený Kláštor and Humenne are among the areas most vulnerable to long-term hydrological drought. More results are published in the thesis of Soľáková (2017).
Similar results were published by Fendeková at el. (2018).

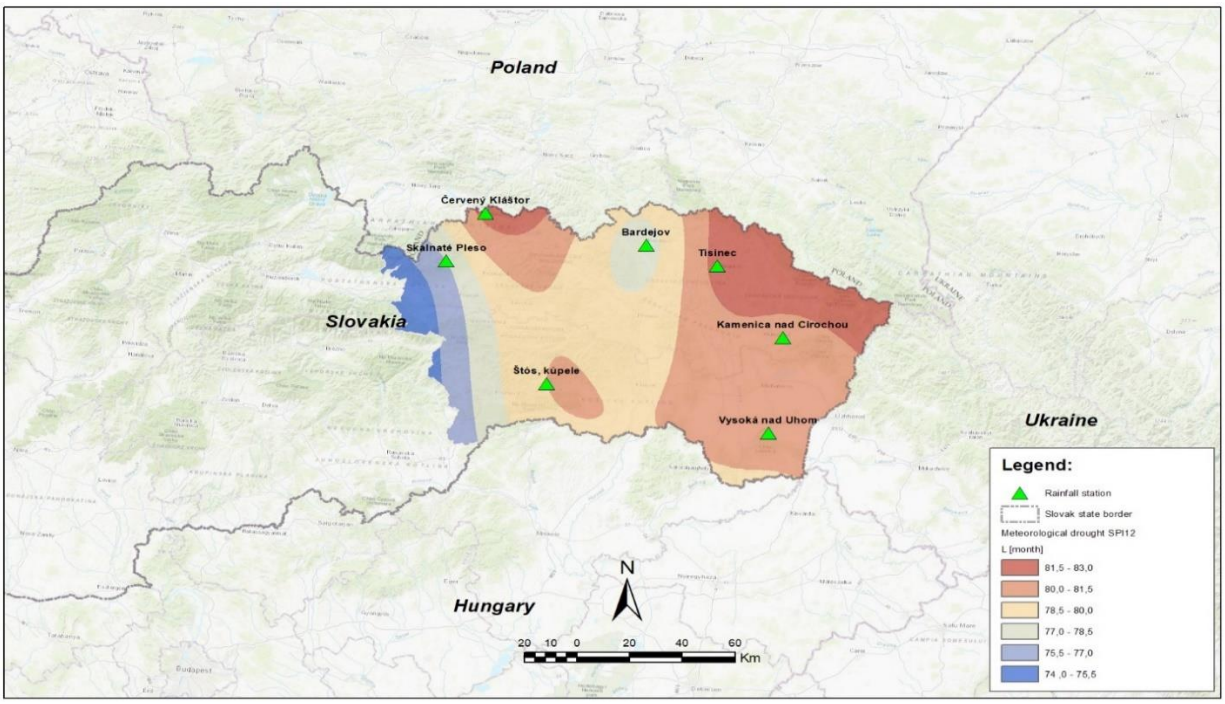

Fig. 2. Meteorological drought duration map over time period 1972–2014.

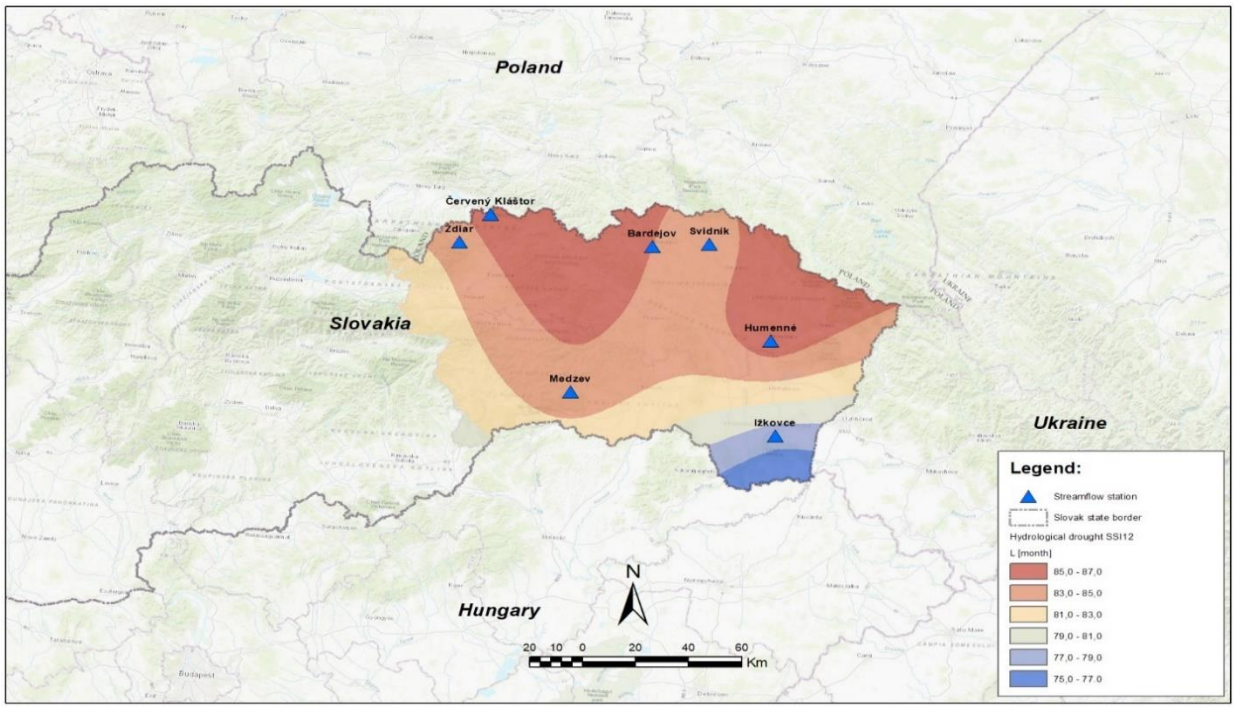

Fig. 3. Hydrological drought duration map over time period 1972–2014, for Ižkovce period: 1976–2014.

Table 3. Identification of the basic feature of long-term hydrological drought by index SSI-12 for the period 1972–2014 and for Ižkovce station from 1976 to 2014.

	Bardejov	Svidnik	Humenné	Ižkovce	Medzev	Červený Kláštor	Ždiar
Duration	85	84	**86**	78	84	**86**	84
Max. duration	15	13	12	13	**25**	13	17
of drought	1972	1984	1986	2003	**2002**	1993	1986
episode	I.	II.	XII.	II.	**IV.**	V.	VIII.
Severity	-127.6	-125.9	-127.3	-116.6	**-130.1**	-122.2	-119.9
Drought episodes	17	18	15	11	9	**22**	20
Average inter-arrival time	31.6	29.82	33.67	36.1	60	**23.6**	26

Conclusion

The primary cause of physical droughts is precipitation deficits in the basin, which, due to long-term effects, cause deficits in the levels of surface water bodies and the levels of underground bodies. The long-term persistence of these deficits in the basin leads to significant economic, social and environmental damage. The main task was the identification of long-term meteorological and hydrological drought for the time interval of 1971-2014 in three sub-basins located in eastern Slovakia. Events of long-term meteorological drought were recorded more often than events of hydrological drought, thus confirming the fact that occurrences of long-term deficit of surface water levels are largely compensated by underground water reserves in those sub-basins. The identification of the average inter-arrival time of drought tor each station contributes to the timely prediction and warning of these phenomena, as well as to their better management. In the future Slovakia could be vulnerable to a moderate meteorological drought approximately in 20 to 30 months and to a hydrological drought in 20 to 60 months. Future research in the drought risk assessment is inevitable especially due to climate change impacts.

Acknowledgement

This work was supported by the Slovak Research and Development Agency under the Contract no. APVV-20-0281. This work was supported by project HUSKROUA/1901/8.1/0088 Complex flood-control strategy on the Upper-Tisza catchment area.

References

Akaike, H. (1973): Information Theory and an Extension of the Maximum Likelihood Principle. Petrov, B.N. and Csaki, F., Eds., International Symposium on Information Theory, 267–281

Blain, G. C. (2012): Revisting the probabilistic definition of drought: strengths, limitations and an agrometeorological adaptation. Bragantia, Volume 71, No. 1, 132–141, DIO:10.1590/S0006- 87052012000100019

COM (2007): Commission of the European Communities: Addressing the challenge of water scarcity and droughts in the European Union. Communication from the Commission to the European Parliament and the Council. COM (2007) 414 final. Brussels, 18. 07. 2007.

Fendeková, M., Poórová, J., Slivová, V. Eds. (2018): Hydrologické sucho na Slovensku a prognóza jeho vývoja. 2018, Bratislava: Univerzita Komenského, Prírodovedecká fakulta

Kottegoda, N., Rosso, R. (1997): Statistics, Probability and Reliability for Civil and Environmental Engineers, New York: McGraw-Hill College, 1997; 768 p. ISBN: 0070359652.

McKee, T. B. N., Doesken, J., Kleist J. (1993): The relationship of drought frequency and duration to time scales. Proceeding of the Eighth Conference on Applied Climatology, Boston: American Meteorological Society, 1993; 179–184

Madadgar, S., Moradkhani, H. (2011): Drought Analysis under Climate Change using Copula. Journal of Hydrologic Engineering, DOI: 10.1061/(ASCE)HE.1943-5584.0000532

Nalbantis, I. (2008): Evaluation of a Hydrological Drought Index. European Water, Volume 23/24, 67–77.

Peel, M. C., Wang, Q. J., Vogel, R. M., McMahon, T. A. (2001): The utility of L-moment ratio diagrams for selecting a regional probability distribution. Hydrol. Sci. J., Volume 46, No. 1, 147–155

Soľáková, T, De Michele, C., Vezzoli, R. (2013): A comparsion between parametric and non-parametric approaches for the calculation of two drought indices: SPI and SSI. Journal of Hydrologic Engineering, Volume 19, No. 9, 1–11, DOI:10.1061/(ASCE)HE.1943-5584.0000942

Tsakiris, G., Loukas, A., Pangalou, D., Vangelis, H., Tigkas, D., Rossi, G., Cancelliere, A. (2007): Drought characterization [Part 1. Components of drought planning. 1.3. Methodological component]. Iglesias A. (ed.), Moneo M. (ed.), López-Francos A. (ed.). Drought management guidelines technical annex. Zaragoza: CIHEAM / EC MEDA Water, 2007, No. 58, 85–102

Van Loon, A. F. (2013): On the propagation of drought, How climate and catchment characteristics influence hydrological drought development and recovery. PhD thesis. Wageningen University. 2013. ISBN 978–94–6173–501–0.

Vicente-Serrano, S. M., Begueria, S., Lopez-Moreno, J. I.

(2010): A multi-scalar drought index sensitive to global warming: the Standardized Precipitation Evapotranspiration Index. Journal of Climate, Volume 23, 1696–1718. DOI: 10.1175/2009JCLI2909.1.

Vicente-Serrano, S. M., López-Moreno, J. I., Beguería, S., Lorenzo-Lacruz J., Azorin-Molina, C., Morán-Tejeda, E. (2012): Accurate Computation of a Streamflow Drought Index. Journal of Hydrologic Engineering, Volume 17, NO. 2, 229–358, DOI: 10.1061/(ASCE)HE.1943-5584.0000433.

Wu, H., Svoboda, M. D., Hayes, M. J., Wilhite, D. A., Wen, E. (2007): Appropriate application of the Standardized Precipitation Index in arid locations and dry seasons. International Journal of Climatology, Volume 27, 65–79

Ing. Tatiana Soľáková, PhD.
Prof. Ing. Martina Zeleňáková, PhD. (*corresponding author, e-mail: martina.zelenakova@tuke.sk)
Department of Environmental Engineering
Faculty of Civil Engineering
Technical University of Košice
Vysokoškolská 4
040 01 Košice
Slovak Republic

Viktoria Mikita, PhD.
Faculty of Earth Science
University of Miskolc
3515 Miskolc-Egyetemváros
Hungary

Ing. Helena Hlavatá, PhD.
Ing. Dorota Simonová
Slovak Hydrological Institute, branch office Košice
Ďumbierska 26
041 17 Košice
Slovak Republic

Professor Hany Abd Elhamid
Department of Water and Water Structures Engineering
Faculty of Engineering, Zagazig University
Zagazig, 44519
Egypt

Department of Environmental Engineering
Faculty of Civil Engineering
Technical University of Košice
040 01 Košice
Slovak Republic

DOI: 10.31577/ahs-2022-0023.02.0031

ACTA HYDROLOGICA SLOVACA

Volume 23, No. 2, 2022, 273–281

Spatial and temporal variability of Aridity Index in lowland areas of Slovakia

Viera RATTAYOVÁ*, Marcel GARAJ, Kamila HLAVČOVÁ

Changes in precipitation and temperature caused by global warming are reasons for the increasing occurrence of hydrological extremes such as floods or droughts. The aridity index is a significant indicator of local climate changes and is often used for quantifying the long-term climate conditions of a given location. In addition, the values of the aridity index are indicators of the water conditions of the area and their potential tendency to change in humidity. Therefore, understanding the spatio-temporal patterns of the aridity index is a crucial goal for agricultural and water management of watersheds.

This research investigates the spatial and temporal variations of the aridity indices at 27 climatological stations situated in the lowland areas of Slovakia. The stations were divided into three main lowland areas according to their spatial location. The United Nations Environmental Program (UNEP) method was used, and 40 years climatological measurements data from the Slovak Hydrometeorological Institute (SHMI) was considered for calculating the monthly and yearly mean values of the aridity index and assessing its spatial and temporal patterns.

Trends in the monthly and yearly spatial mean values of the aridity index showed significant variability between selected areas. The annual mean of the aridity index of stations situated in the Juhoslovenská kotlina lowland indicates increasing trends in the aridity index in winter months and in July. In the case of other lowlands, there were no trends in the monthly and yearly values. Other significant differences were observed in the seasonal variability of the mean monthly values of the aridity index in selected areas.

KEY WORDS: Aridity Index, Drought Assessment, Reference Evapotranspiration

Introduction

The aridity index is an often used index for characterising the long-term climatic conditions of a region. For example, studies of the aridity index have shown that under conditions of increasing concentrations of CO_2, the aridity values will increase (Greve et al., 2019).

Changes in the aridity index offer information about the impact of climate change and related climate variables on the availability of water. This index is also used as an indicator of climate change in many studies, where the trends of hydrological variables are investigated(Arora, 2002), and is used as an indicator of climate change (Huo et al., 2013; Kafle and Bruins, 2009). It has also been used for the determination of changes in crop yields (Bannayan et al., 2010; Ranjan et al., 2012).

Research of Tomlain and Škvarenina (2007) realized on 31 meteorological stations in Slovakia showed high variability of aridity index in selected stations. They divided the station into samples according to vertical vegetational zones. The aridity index calculated according to the Budyko method was moved in intervals 1.4–0.4, where *AI* value constantly decreases with the increasing altitude of stations. In the Region of central Europe, SPI and SPEI indexes are more frequently used to evaluate the drought. Vido et al. (2019) evaluated drought in the Horne Pozitavie region of Slovakia using the SPEI index. The results showed increasing humid conditions in winter and drier conditions in spring and summer, with a negative trend of SPEI in April, which can have consecutive impacts on agricultural yields. Study of Řehoř et al. (2021) shows gridded soil-drought values from the SoilClim model for the 1961–2019 period in four lowlands in central Europe at altitudes of below 400 m a.s.l.. In the winter half-year, linear trends in soil drought decrease progressively but are statistically insignificant for all four regions. Increasing annual temperature, increasing frequency of anticyclonic circulation types, and decreases in cyclonic types are probably the main drivers of the changing frequency and intensity of soil-drought episodes and their distribution over the year.

To calculation of aridity index, it is necessary to define the difference between incoming moisture totals and potential outgoing moisture. Several methods have been developed for describing and estimating moisture deficit, that use different input parameters to estimate the aridity

index. Thornthwaite (1948) calculated the values of the aridity index as the difference between reference evapotranspiration and precipitation divided by reference evapotranspiration. UNEP (1997) suggested using the ratio of total precipitation to the mean atmospheric evaporative demand (expressed as potential evapotranspiration). Calculating the aridity index according to the UNEP (1997) method requires determining the potential evapotranspiration from the measured climatological data that represents moisture losses. This method was originally developed for evaluations of the aridity index on a global scale and for its application. The Thornthwaite method was used for the calculation of potential evapotranspiration. The authors mention a more sophisticated method for estimating the evaporation rate, such as „calculating evapotranspiration rates for different crop types or calculating the soil moisture deficit in relation to precipitation and evapotranspiration". However, this method was not used in the study because it requires many inputs that are not available worldwide.

The aridity index calculated by this method does not consider the effect of seasonal variations in climatological inputs. The climate of an area can be categorized into five classes (Şarlak and Mahmood Agha, 2018):

- Humid $\rightarrow AI \geq 0.65$
- Drought sub-humid $\rightarrow 0.5 \leq AI < 0.65$
- Semi-arid $\rightarrow 0.2 \leq AI < 0.5$
- Arid areas $\rightarrow 0.05 \leq AI < 0.2$
- Hyper-arid $\rightarrow AI < 0.05$

For the calculation of the Aridity Index, a wide range of climatological variables measurements are necessary, especially for the estimation of reference evapotranspiration which is used instead of potential evapotranspiration. Reference evapotranspiration (ET_0) is a specific type of the potential value of evapotranspiration, which has been described as "the rate of evapotranspiration from a hypothetical reference crop with an assumed crop height of 0.12 m., a fixed surface resistance of 70 s m^{-1} and an albedo equal to 0.23, closely resembling an extensive surface of green grass" (Smith et al., 1990). FAO-56 Penman-Monteith equation for calculation of ET_0 (Eq.2) was utilized to calculate reference evapotranspiration. This method is commonly used as the benchmark method in research aimed at determining the water deficit of an area and evaluations of droughts (Ficklin et al., 2015).

Identification of the changes in the aridity index yields essential input for the management of watersheds and management of agricultural land. However, despite the many studies in various countries and regions on trends in the aridity index, only a few analyses are available for the Slovak Republic. This study aims to characterize temporal changes in the aridity index and determine the spatial distribution of *AI* values for identifying areas in the lowland regions of Slovakia the most endangered by aridity.

Materials and methods

Climatological data from 27 climatological stations of the maximum, minimum and mean air temperature, the wind speed at a 2 m height, actual water pressure, precipitation and duration of the sunsets in daily time step for the period from 1980 to 2019 was accessed from the Slovak Hydrometeorological Institute (SHMI). The 40-year period was considered to assess the spatial and temporal pattern of the aridity index. The list of 27 climatological stations (Fig. 1) was divided into three groups based on the lowland geomorphological units of Slovakia, i.e., a) Podunajská and Záhorská nížina lowland – the western part b) Juhoslovenská kotlina lowland – the central part and c) Východoslovenská nížina lowland – the eastern part. These three areas are the most important in terms of agricultural production in Slovakia; therefore, it is useful to get to know how they deal with water. Especially nowadays and recently when the impact of the soil drought, meteorological and hydrological drought is much stronger.

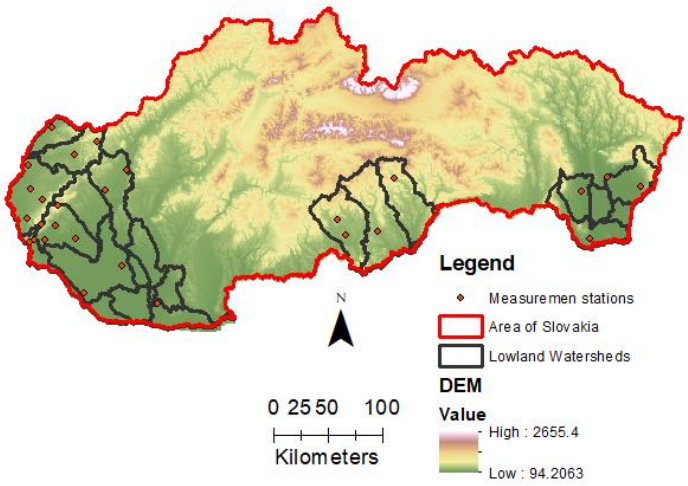

Fig. 1. Stations with measured meteorological data on selected lowland areas of Slovakia.

For calculating the aridity index (*AI*), the worldwide used UNEP (1997)method was selected. This method describes the aridity index as a deficiency of moisture under normal climatic conditions and is expressed as a ratio between total precipitation and potential evapotranspiration (Eq. 1, UNEP, 1997). According to Nastos et al. (2013), this method is suitable to use to appraise spatial patterns of aridity at a country or regional scale. The universal equation for calculating the Aridity Index is:

$$AI = \frac{P_i}{ET_{0_i}} \quad (1)$$

where
P_i – sum of precipitation for selected time step [mm i^{-1}]
ET_{0i} – sum of reference evapotranspiration for selected time step [mm i^{-1}]

The reference evapotranspiration in a daily step, which replaced potential evapotranspiration, was calculated using the FAO reference evapotranspiration equation for grass (Eq.2), according to the Penman–Monteith method (Allen et al., 1998). Replacement of the basic, low input required method for estimation of the potential evapotranspiration by a more sophistical method for calculating the reference evapotranspiration has been used in many studies (Koffi and Komla, 2015; Spinoni et al., 2015). This method provides better results for more specified regions, and, according to Sentelhas et al. (2010) and many other authors, is a universal standard for estimating *reference evapotranspiration*. The daily values of reference evapotranspiration were recalculated for monthly and yearly totals.

$$ET_0 = \frac{0.408*\Delta*(R_N-G)+\Upsilon\frac{900}{T+273}*u_2+(e_s-e_a)}{\Delta+\Upsilon*(1+0.34*U_2)} \quad (2)$$

where
ET_0 – reference evapotranspiration [mm day^{-1}];
R_n – net radiation at the crop surface [MJ m^{-2} day^{-1}];
G – soil heat flux density [MJ m^{-2} day^{-1}];
T – mean daily air temperature at 2 m height [°C];
u_2 – wind speed at 2 m height [m s^{-1}];
e_s – saturation vapor pressure [kPa];
e_a – actual vapor pressure [kPa];
e_s - e_a – saturation vapor pressure deficit [kPa];
D – slope vapor pressure curve [kPa °C^{-1}];
Υ – psychrometric constant [kPa °C^{-1}].

Fig. 2 shows the seasonal distribution of the monthly values of the reference evapotranspiration, calculated by the Penman–Monteith equation.

The Penman-Monteith method (Allen et al., 1998) requires input data of the air temperature, relative air humidity (or vapour pressure), wind speed, and solar net radiation. The dataset of the solar net radiation is not accessible in the SHMI database; and it is necessary to calculate it according to one of the available methods. The daily values of the solar net radiation were calculated according to the FAO-56 methodology(Allen et al., 1998), which is part of the methodology for estimation of reference evapotranspiration by the FAO method, where the most important input is the duration of the sunset (eq.3).

$$R_n=[(1-\alpha)*R_s]-\left[\sigma*\left[\frac{T_{max,K}+T_{min,K}}{2}\right]*(0.34-0.14\sqrt{e_a})*\left(1.35*\frac{R_s}{R_{s0}}-0.35\right)\right] \quad (3)$$

where
R_n – net radiation at the crop surface [MJ m^{-2} day^{-1}];
α – albedo or canopy reflection coefficient,
σ – Stefan-Boltzmann constant [4.903 10-9 MJ K^{-4} m^{-2} day^{-1}];
R_s – the incoming solar radiation [MJ m^{-2} day^{-1}];
R_{s0} – clear-sky solar radiation [MJ m^{-2} day^{-1}];
$T_{max,K}$ – maximum absolute temperature during a 24-hour period [K = °C + 273.16];
$T_{min,K}$ – minimum absolute temperature during a 24-hour period [K = °C + 273.16].

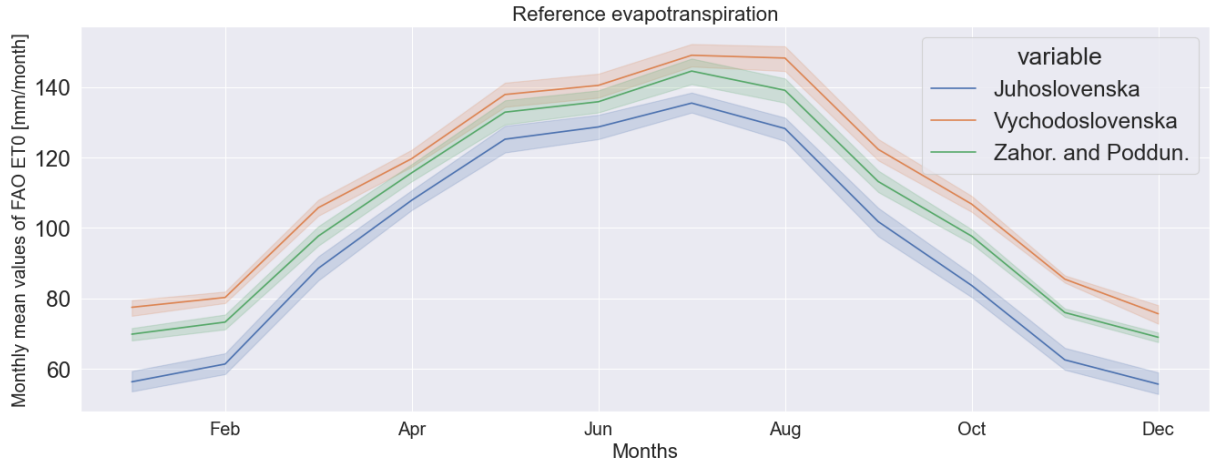

Fig. 2. Seasonal distribution of the monthly values of the reference evapotranspiration-areal mean value (the dark line is the median of the values, light border around the median is variance of the value).

Unfortunately, sunset duration data is unavailable in a length equal to length of the other climatologic data used. We cannot estimate this value from the value of any other accessible variable; therefore, the missing solar net radiation results were supplemented by reanalyzing the remote sensing data from the ERA5 dataset of the hourly data of net radiation on a single level, produced by Copernicus (2022). The values of the reanalyzed remote sensing data were calibrated by a simple linear model with net radiation derived from the measured data, with a Pearson correlation coefficient of 0.69, i.e., a moderate degree of correlation. The missing values of the calculated time series were replaced with data from these calibrated ERA5 net radiation datasets.

Mann-Kendall's non-parametric test was used for evaluating the monotonic tendencies of the aridity indices over time (Bevan and Kendall, 1971; Mann, 1945). This method for testing the trends was also recommended by the World Meteorological Organization (2009). The nature of the test is a correlation between the data ranks and sequences of a time series (Wang et al., 2020). For the calculation of the slope, the Theil–Sen (TS) method was applied (Sen, 1968; Theil, 1992).

Results

The results of the seasonal distribution show a different course of the mean monthly values of the aridity index in selected areas (Fig.3). The most significant difference in the seasonal distribution is in the case of stations in

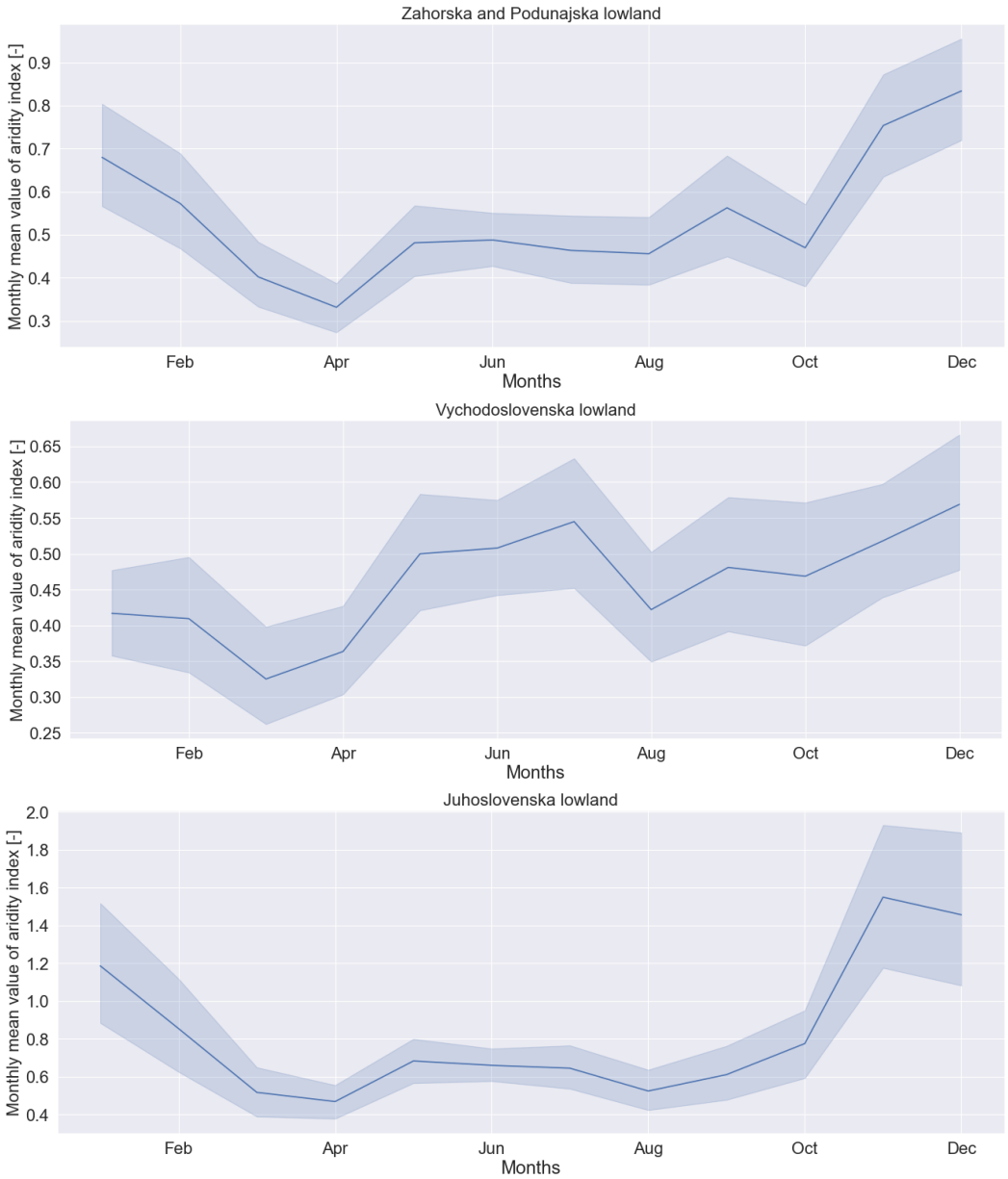

Fig. 3. Seasonal distribution of the mean monthly aridity index for selected areas (the dark line is median of the values, light border around the median is the variance of the values).

the Východoslovenská nížina lowland, where the mean monthly value of the aridity index is at its maximum in the summer months.

The seasonal distribution of the *AI* in the Záhorská and Podunajská nížina lowlands (Fig. 3) shows humid condition in the winter months and only becoming to semi-arid in April. The highest range of values appears in December. The seasonal distribution of *AI* in the stations in the Východoslovenská nížina lowland show a very similar course of AI; however, it is essential to point out that the values are higher than in other areas, and the Juhoslovenská kotlina lowland remains a dry humid area during all the months on average.

Moreover, the notable seasonal distribution of *AI* (Fig. 3) is for the Východoslovenská nížina lowland. At the end of the winter and in the early spring, the values of *AI* decrease below 0.5, which means that the area belongs to a semi-arid zone. This could be crucial for farmers in the spring season when vegetation and crops most demand water. It could increase costs for farmers to maintain healthy and vital plants. Another interesting fact is that the range of values is broad during all the months. This phenomenon is determined by the variability of the meteorological elements in the continental climate conditions representing the eastern part of Slovakia.

The linear regression with the trendline equation was derived from the yearly and monthly data (Fig. 4). To determine the significance of the trends, the Mann-Kendall trend test and the Thein-Sen slope were used. According to the results of the trends of the yearly values of AI, an increasing trend was identified by the Mann-Kendall test and the Thein-Sen slope on the monthly and yearly values in the case of the Juhoslovenská kotlina lowland. The trend analyses of the aridity index in the Juhoslovenská kotlina lowland with a significant level of α=0.05 showed a *p*-value of 0.0071 with a slope of 0.0059 for the yearly values and a *p*-value of 0.0000068 with a slope of 0.00066 for the monthly values.

The trend analyses of the monthly mean values for each month separately show the significant increasing trends of *AI* in the winter months- from December to February and in July (Table 1), in the station in the Juhoslovenská kotlina lowland. In the winter months of January and February, this phenomenon could be caused by a combination of an increasing precipitation trend and a decreasing trend of ET_0, the same situation occurs in July. In December, the increasing value of *AI* is probably caused by actual and previous months with decreasing

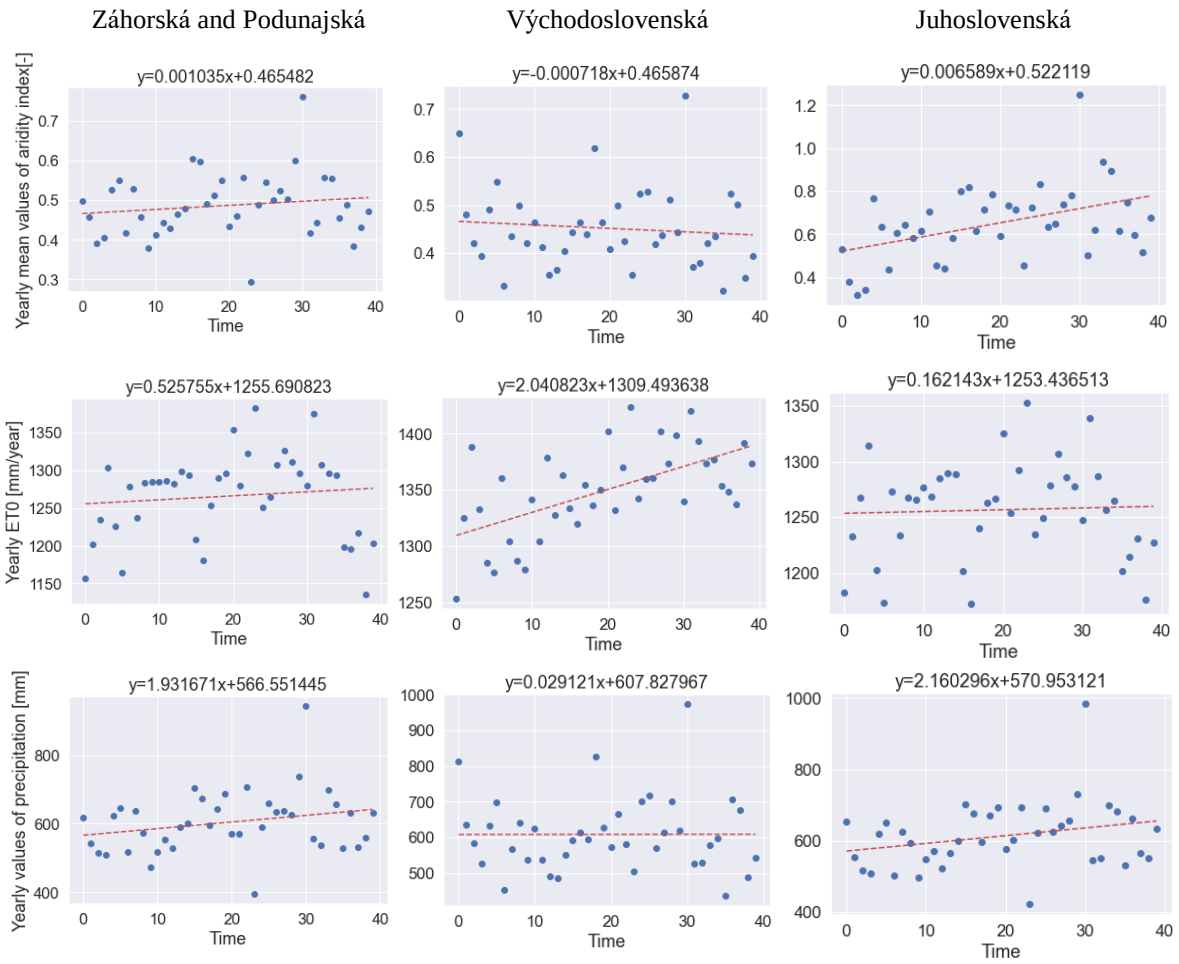

Fig. 4. Trends in the yearly mean aridity index and yearly sum of the reference evapotranspiration and precipitation for stations in selected areas – Linear regression.

value of ET_0, which continues to February. There is no trend in the monthly and yearly data in the spring and autumn months.

There were no recognized trends in the aridity index and precipitation in other areas. There is only a decreasing trend of ET_0, which is not significant enough to result in changes in the trends of the aridity index.

Another unexpected result is the difference between the seasonal distribution of the mean monthly precipitation and the seasonal distribution of the mean monthly aridity index values for the Juhoslovenská kotlina lowland. While the maximum monthly precipitation is concentrated in the summer months, i.e., from May to July (Fig. 5), the values of the aridity index are minimal in these months, with the maximum in the winter months, where the precipitation is in its minimal values. This impact is different in other selected areas, where the impact of the distribution of the monthly values of precipitation is discernible in the distribution of the monthly values of AI.

The pie charts (Fig. 6) below represent the fraction of each month allocated to a category of *AI* in the selected areas. Fig. 6 shows the highest frequency of months in the hyper-arid category (2.5%) and in the humid category of area in the stations of Juhoslovenská kotlina lowland with a fraction of 45.5% (Fig. 6). This area has the largethest ratio of months with edge categories of aridity index. Recognition of the spatial variability of the drought risk is significant for its management. On the other hand, the most considerable portion of the month adjunct to an area of semi-arid and dry sub-humid regions occurs in the stations in the Východoslovenská kotlina lowland, where is the highest fraction of months assigned like arid regions at the same time.

The range of the mean long-term values of the aridity index over the Slovak lowland stations is from 0.39 to 1.00 (Fig.7). The highest mean long-term values of the aridity index were estimated at the two stations of the Juhoslovenská kotlina lowland, i.e., Revúca and Malinec (0.99 and 1.0). The lowest value of the long-term aridity index was identified at the Gabčíkovo climatological station, where a value represents a semi-arida semi-arid climatic region.

In general, if we consider every area studied as a homogenous part, then we can assume that the climate of the central part of Slovakia in the Juhoslovenská kotlina lowland is categorized as a humid region according to the long-term mean value of the aridity index of 0.65. The Podunajská, Záhorská (*AI*=0.49) and Východoslovenská nížina lowland (*AI*=0.45) belong to semi-arid regions with a higher drought risk.

Table 1. Results from the Mann-Kendall trend analyses of the monthly values for each month separately (red-significant trend α=0.05, yellow-low significant trend α=0.1)

Zahorská and Podunajská lowland	Month											
	Jan	Feb	Mar	Apr	May	Jun	Jul	Aug	Sep	Oct	Nov	Dec
AI												
P												
ET_0				↑		↑						

Juhoslovenská lowland	Month											
	Jan	Feb	Mar	Apr	May	Jun	Jul	Aug	Sep	Oct	Nov	Dec
AI	↑	↑					↑					↑
P	↑	↑					↑	↑				
ET_0	↓	↓							↓	↓	↓	↓

Vychodoslovenská lowland	Month											
	Jan	Feb	Mar	Apr	May	Jun	Jul	Aug	Sep	Oct	Nov	Dec
AI												
P												
ET_0				↑		↑	↑	↑			↑	

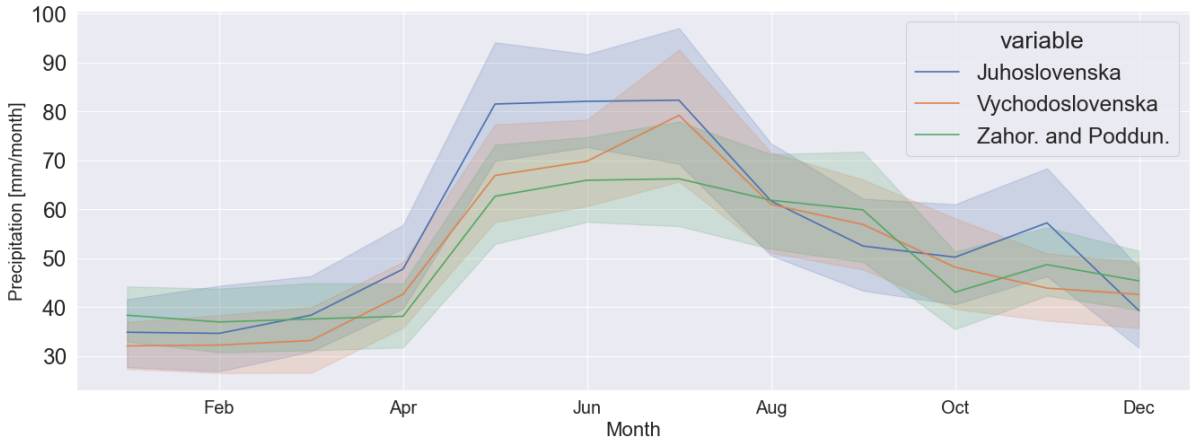

Fig. 5. Seasonal distribution of the long-term total monthly precipitation.

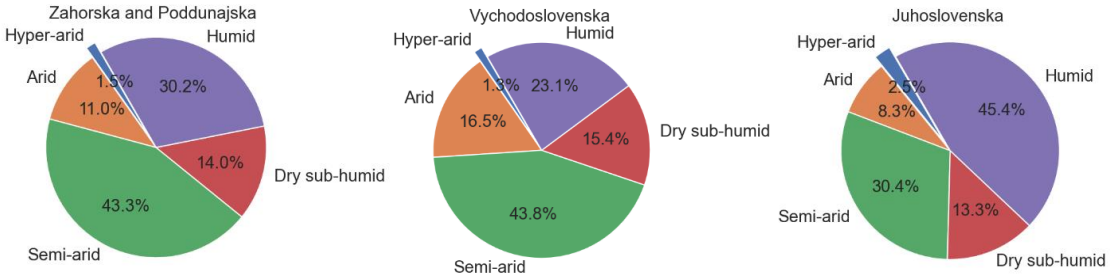

Fig. 6. Categorization of the months according the mean value of aridity index.

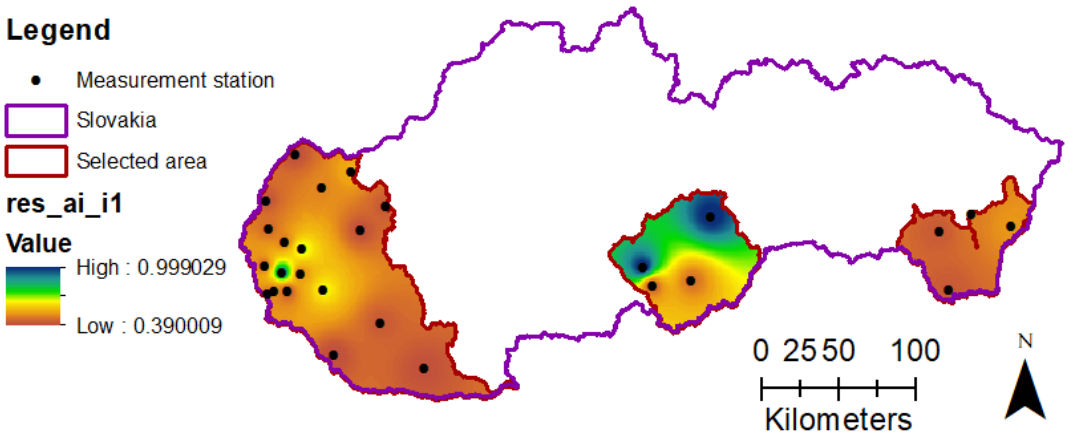

Fig. 7. Spatial distribution of the mean long-term aridity index.

Conclusion

The results show significant increasing trend in monthly values of *AI* (α=0.05) in the case of the Juhoslovenská kotlina Lowland, with the *p*-value $7*10^{-6}$ and Sen´s slope 0.0007 and *p*-value 0.007 and Sen´s slope 0.006 in yearly values. The seasonal distribution of the aridity index in the Juhoslovenská kotlina, Záhorská, and Podunajská nížina lowlands have two local minimums, the most significant in April (Juhosl. = 0.47, Zahor. and Pod. = 0.33) and the second local minimum in August (Juhosl. = 0.52, Záhor. and Pod. = 0.46). The maximum values of

the aridity index were identified in the winter months in both areas, in November on Juhoslovenska nížina lowland (*AI*=1.55) and in December for Záhorská and Podunajská nížina lowland (*AI*=0.83). The third local minimum can be recognized in October in the case of the Záhorská and Podunajská nížina lowland. In the Vychodoslovenská nížina lowland, the monthly distribution of aridity index values is different from other areas, and the maximum values are recognized in the late spring and summer – in May (*AI*=0.49) and July (*AI*=0.54). The minimum *AI* values was detected in March (*AI*=0.32), with a second local minimum in August (*AI*=0.42). These differences could be caused by differences in the climate of these regions because in the eastern part of Slovakia the climatic characteristics are more continental than in the western part of Slovakia. In the long-term trends of AI, we can find the significant increasing trends in the Juhoslovenská kotlina Lowland in the yearly and monthly mean values. Detailed trend analyses for each month separately show the significant increasing trends of *AI* in the winter months, i.e., from December to February and in July. The differing yearly distribution of the monthly mean values of the aridity index than in the monthly distribution of precipitation in the Juhoslovenská kotlina lowland may imply that in this area, the precipitation does not have the same impact on the distribution of the mean aridity values, as in the case of the other selected areas. To interpretation of the relationship between these characteristics, it is necessary to carefully and consider all possibilities, because in some cases, the ostensible relationship could occur by changes in other related characteristics caused by climate change. Describing the relationship between climatic characteristics and the aridity index will be the goal of our following research.

Acknowledgement

"This publication is the result of the project implementation: „Scientific support of climate change adaptation in agriculture and mitigation of soil degradation" (ITMS2014+ 313011W580) supported by the Integrated Infrastructure Operational Programme funded by the ERDF; and was supported by the Slovak Research and Development Agency under Contract No. APVV-18-0347; and grant number VEGA 1/0782/21."

References

Allen, R. G., Pereira, L. S., Raes, D., Smith, M. W. B. (1998): Crop evapotranspiration - Guidelines for computing crop water requirements - FAO Irrigation and drainage paper 56. *Irrigation and Drainage*. https://doi.org/10.1016/j.eja.2010.12.001

Arora, V. K. (2002): The use of the aridity index to assess climate change effect on annual runoff. *Journal of Hydrology*, *265*(1–4). https://doi.org/10.1016/S0022-1694(02)00101-4

Bannayan, M., Sanjani, S., Alizadeh, A., Lotfabadi, S. S., Mohamadian, A. (2010): Association between climate indices, aridity index, and rainfed crop yield in northeast of Iran. *Field Crops Research*, *118*(2). https://doi.org/10.1016/j.fcr.2010.04.011

Bevan, J. M., Kendall, M. G. (1971): Rank Correlation Methods. *The Statistician*, *20*(3). https://doi.org/10.2307/2986801

Ficklin, D. L., Letsinger, S. L., Gholizadeh, H., Maxwell, J. T. (2015): Incorporation of the Penman-Monteith potential evapotranspiration method into a Palmer Drought Severity Index Tool. *Computers and Geosciences*, *85*. https://doi.org/10.1016/j.cageo.2015.09.013

Greve, P., Roderick, M. L., Ukkola, A. M., Wada, Y. (2019): The aridity Index under global warming. *Environmental Research Letters*, *14*(12). https://doi.org/10.1088/1748-9326/ab5046

Huo, Z., Dai, X., Feng, S., Kang, S., Huang, G. (2013): Effect of climate change on reference evapotranspiration and aridity index in arid region of China. *Journal of Hydrology*, *492*. https://doi.org/10.1016/j.jhydrol.2013.04.011

Kafle, H. K., Bruins, H. J. (2009): Climatic trends in Israel 1970-2002: Warmer and increasing aridity inland. *Climatic Change*, *96*(1). https://doi.org/10.1007/s10584-009-9578-2

Koffi, D., Komla, G. (2015): Trend analysis in reference evapotranspiration and aridity index in the context of climate change in Togo. *Journal of Water and Climate Change*, *6*(4). https://doi.org/10.2166/wcc.2015.111

Mann, H. B. (1945): Non-Parametric Test Against Trend. *Econometrica*, *13*(3).

Nastos, P. T., Politi, N., Kapsomenakis, J. (2013): Spatial and temporal variability of the Aridity Index in Greece. *Atmospheric Research*, *119*. https://doi.org/10.1016/j.atmosres.2011.06.017

Ranjan, K., ·P., Goyari, P., Mishra, R. K. (2012): Measuring Weather Impact on Crop Yield Using Aridity Index: Evidence from Odisha. In *Agricultural Economics Research Review* (Vol. 1, Issue 26).

Řehoř, J., Brázdil, R., Trnka, M., Lhotka, O., Balek, J., Možný, M., Štěpánek, P., Zahradníček, P., Mikulová, K., Turňa, M. (2021): Soil drought and circulation types in a longitudinal transect over central Europe. *International Journal of Climatology*, *41*(S1). https://doi.org/10.1002/joc.6883

Şarlak, N., Mahmood Agha, O. M. A. (2018): Spatial and temporal variations of aridity indices in Iraq. *Theoretical and Applied Climatology*, *133*(1–2), 89–99. https://doi.org/10.1007/s00704-017-2163-0

Sen, P. K. (1968): Estimates of the Regression Coefficient Based on Kendall's Tau. *Journal of the American Statistical Association*, *63*(324). https://doi.org/10.1080/01621459.1968.10480934

Sentelhas, P. C., Gillespie, T. J., Santos, E. A. (2010): Evaluation of FAO Penman-Monteith and alternative methods for estimating reference evapotranspiration with missing data in Southern Ontario, Canada. *Agricultural Water Management*, *97*(5). https://doi.org/10.1016/j.agwat.2009.12.001

Smith, M., Segeren, A., Santos Pereira, L., Perrier, A., Allen, R. (1990): *Report on the Expert Consultation on Procedures for Revision of FAO Guidelines for Prediction of Crop Water Requirements. Rome, Italy, 28–31 May 1990*. https://doi.org/10.3/JQUERY-UI.JS

Spinoni, J., Vogt, J., Naumann, G., Carrao, H., Barbosa, P. (2015). Towards identifying areas at climatological risk of desertification using the Köppen-Geiger classification and FAO aridity index. *International Journal of Climatology*, *35*(9). https://doi.org/10.1002/joc.4124

Theil, H. (1992): *A Rank-Invariant Method of Linear and Polynomial Regression Analysis*. https://doi.org/10.1007/978-94-011-2546-8_20

Thornthwaite, C. W. (1948): An Approach toward a Rational Classification of Climate. *Geographical Review*, *38*(1). https://doi.org/10.2307/210739

Tomlain, J., Škvarenina, J. (2007): K charakteristike vlhkostných pomerov vegetačných stupňov Západných Karpát – index sucha a relatívna evapotranspirácia. *Vyskot, I. (Ed): „Klima Lesa"*.

UNEP. (1997): World atlas of desertification 2ED. *United Nations Environment Programme*.

Vido, J., Nalevankova, P., Valach, J., Sustek, Z., Tadesse, T. (2019): Drought Analyses of the Horne Pozitavie Region (Slovakia) in the Period 1966–2013. *Hindawi Advances in Meteorology*. https://doi.org/https://doi.org/10.1155/2019/3576285

Wang, F., Shao, W., Yu, H., Kan, G., He, X., Zhang, D., Ren, M., Wang, G. (2020): Re-evaluation of the Power of the Mann-Kendall Test for Detecting Monotonic Trends in Hydrometeorological Time Series. *Frontiers in Earth Science*, *8*. https://doi.org/10.3389/feart.2020.00014

World Meteorological Organisation (WMO) (2009): Guide to Hydrological Practices: Volume II: Management of Water Resources and Application of Hydrological Practices (sixth edition). In *WMO Report No. 168: Vol. II* (Issue 168). https://doi.org/10.1080/02626667.2011.546602

Ing. Viera Rattayová (*corresponding author, e-mail: viera.rattayova@stuba.sk)
Prof. Ing. Kamila Hlavčová, PhD.
Department of Land and Water Resource Management
Faculty of Civil Engineering
Slovak University of Technology
Vazovova 5
812 43 Bratislava 1
Slovak Republic

Mgr. Marcel Garaj, PhD.
Department of the Climatological Service
Slovak Hydrometeorological Institute
Jeséniova 17
833 15 Bratislava
Slovak Republic

DOI: 10.31577/ahs-2022-0023.02.0032

ACTA HYDROLOGICA SLOVACA

Volume 23, No. 2, 2022, 282–287

Design of detention spaces in the Ulička and Ublianka River catchment

Andrej ŠOLTÉSZ*, Martin ORFÁNUS, Jakub MYDLA

Based on morphological and hydrological data, a hydrodynamic model of surface water flow was created in the HEC-RAS program. The model simulated a 100-year flood wave propagation in the basins of the Ulička and Ublianka streams as a part of the upper Uzh River catchment. After calibration, protection measures were added to the model whose task was to transform the flood discharge. For the transformation of the flood wave, detention and multi-purpose reservoirs were proposed, which could improve the flow rates in the riverbeds in times of drought. The proposed measures were selected on base of the terrain recognition of the research team in September and October 2021 in several profiles of mentioned rivers as well as on their tributaries.

KEY WORDS: hydrodynamic modelling, flood transformation, HEC-RAS software, flood protection measures, detention reservoirs

Introduction

In frame of activities of the project of Cross-border cooperation Hungary – Slovakia – Romania – Ukraine HUSKROUA "Joint activities for the prevention of natural disasters in transboundary Uzh River basin" one of the goals was the analysis of the flood wave process in the river basin of the upper Uzh River, specifically the Ulička, Ublianka rivers and Zbojský stream. It should involve in the area of interest activities which ensure the mitigation of flood and drought consequences by increasing the retention capacity of the territory.

An integrated flood risk assessment approach based on coupled hydrological-hydraulic modelling was introduced by Smithers et al., 1997; Leskens et al., 2014; Garcia et al., 2020; Zhang et al., 2022; Uddin and Martin, 2021; Vyshnevskyi and Donich, 2021. The two-dimensional software HEC-RAS 2D was used to model the hydrodynamic runoff in the basin of the investigated streams. An implicit solution method was applied, which enables larger computational time steps and at the same time ensures a higher degree of stability and robustness of the calculation (compared to explicit solution options) and compared to traditional finite difference and finite element methods (Brunner, 2021).

Respecting certain simplifications and calculation assumptions, a hydrodynamic calculation model of the runoff was compiled, which was calibrated on the basis of the supplied hydrological and morphological data and subsequently used for calculations in the design of several variants of measures to retain water in the country with a subsequent evaluation of their effectiveness (Janík and Šoltész, 2021).

Material and methods

The modelled area is located in the north-eastern part of Slovakia in the district of Snina. In the northern part of the area of interest is the Ulička River basin, which leaves Slovakia near the village of Ulič and forms a right-hand tributary of the Uzh River. Ulička River flows parallel to the Zbojský stream which is its most important tributary, even the area of the watershed at the confluence is comparable (the area of the Ulička catchment at the confluence is approx. 98 km^2 and its left-hand tributary – the Zbojský stream catchment area is 96 km^2). Both streams have a feather-shaped watershed, are characterized by many torrents and flow in a south-eastern direction. The geological composition of the territory consists mainly of flysch. This area is characterized by significant forest cover with sparse population and a low area of agriculturally used land (Šoltész et al., 2022).

The Ublianka River catchment has a rather fan-shaped shape with a slight asymmetry and is close to the Ulička River in size (the total area of the Ulička catchment in the Slovak Republic is 206 km^2, Ublianka catchment is 194 km^2). Its most important tributary is Stežná, which forms the aforementioned asymmetry. Both rivers – Ublianka as well as Ulička flow towards Ukraine, where they create right-side tributaries of the Uzh River. The geological composition is somewhat more varied in this basin, apart from flysch, there is also a presence of

Quaternary rocks and, in the western part, neo-volcanic rests. The morphology is also different. Milder slopes form a suitable condition for agricultural land use, or for meadows or pastures. The diversity of the shape of the basin and the different morphology can be seen in Fig. 1, where the Ulička basin is shown on the left and the Ublianka basin on the right side. In the area of interest, the Poloniny National Park (NP) (primarily in the Ulička River basin) extends, and the part of the Vihorlat Protected Landscape Area (PLA) extends to the western edge of the Ublianka basin (Šoltész et al., 2022).

The HEC-RAS program in newer versions includes the option of modelling surface runoff based on precipitation (so-called rain on grid, HEC-RAS manual, 2021). This is 2D hydrodynamic model in which the precipitation episode can be entered as a boundary condition. They are then directly involved into the cells of the 2D network (Brunner, 2021).

The reason for using this tool was also the fact that it is possible to design measures such as water retention measures, detention or multi-purpose reservoirs in the same model. Such modelling is suitable to be used especially if the modelled area is large enough and precipitation is a significant component that creates a flood. On the contrary, modelling does not make much sense in the area of an existing large stream, where the flood will flow from an area far above the modelled area, which is not our case (Garcia et al., 2020).

The next step of the solution was the calibration of the assembled model. The aim of the model calibration was to quantify the accuracy of the mathematical model and the settings of individual parameters and to compare them with the design flood wave in the boundary profiles of the Ublianka and Ulička rivers according to the hydrological data provided by the Slovak Hydrometeorological Institute (SHMI), whether the modelling is accurate enough to be used as a relevant modelling tool.

Thus, the calibration mainly consisted in changing the precipitation as a boundary condition, but in order to obtain the most accurate results, the simulation settings (numerical scheme, grid resolution and parameters of existing structures) were also calibrated. In the calibration phase, the correct time step increment method and limits were also developed to ensure the stability of the calculation and the reliability of the results. The result of the calibration process is illustrated in Fig. 2, where the red line represents the design flood wave on the Ublianka River provided by SHMI and the blue line represents the simulation in the HEC-RAS program.

For the identification of suitable profiles in the valleys of both river basins the terrain recognition of the research team was carried out in September and October 2021. It made available to become familiar with the environment of the upper Uzh River basin. During the reconnaissance of the terrain, the existing measures, modifications on the streams were recorded and the locations of the water retention measures were preliminarily selected. Fig. 3a shows a fixed threshold on the Zbojský stream in the village of Ulič, and Fig. 3b shows an unmaintained detention structure on the Tapovec stream above the village of Klenová.

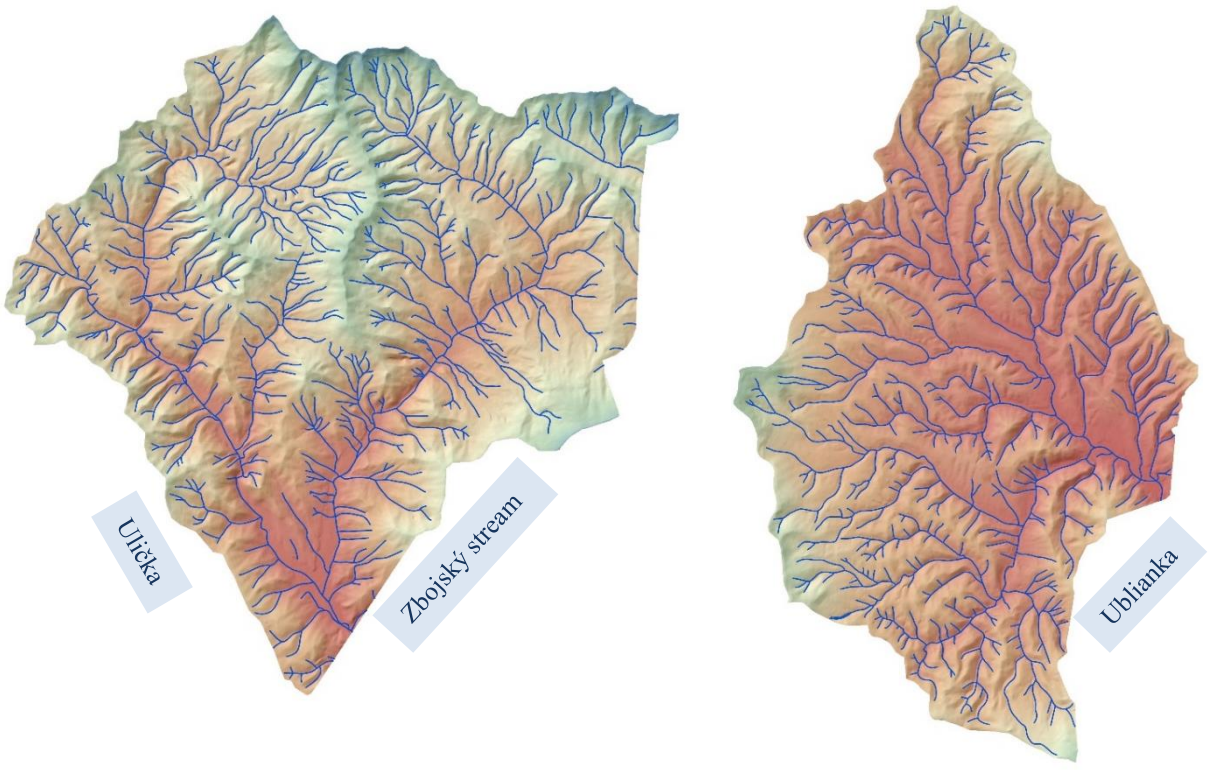

Fig. 1. The river basins of the Ulička and Ublianka rivers.

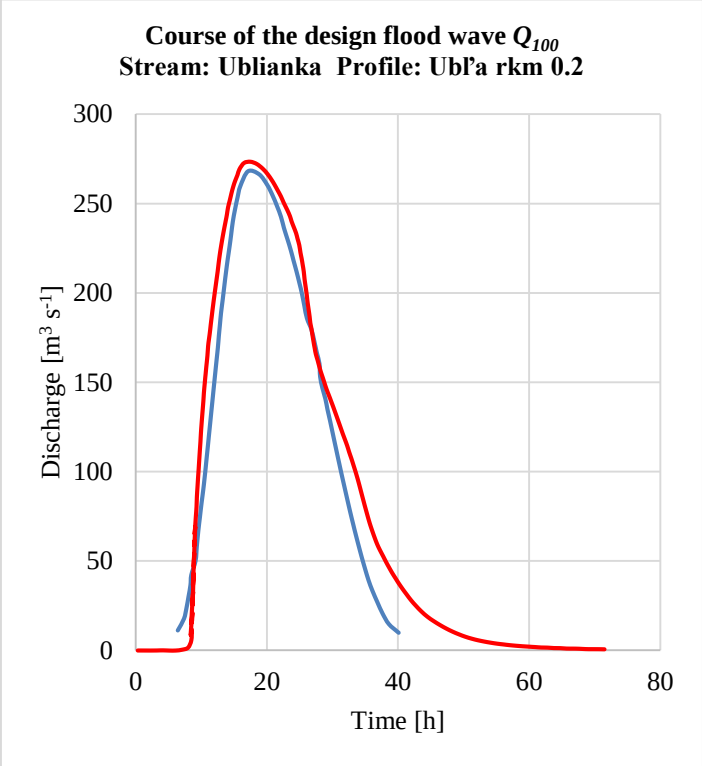

Fig. 2. Hydrogram of the proposed 100-year flood wave on the Ublianka stream.

Fig. 3. Existing measures on the Zbojský stream (a) and on the Tapovec stream (b).

To reduce the flood wave, measures such as the creation of polders, as well as multi-purpose small water reservoirs, were proposed. Several variants were proposed, which differed from each other in the number and location of polders and reservoirs.

Results and discussion

Fig. 4 shows one of the proposals for the location of multi-purpose reservoirs which was optimized in the next process. The location of detention reservoirs was limited by several factors such as residential areas, transport infrastructure, suitable morphological conditions, but also the territory of the Poloniny NP. Appropriate placement of water detention measures taking into account the mentioned factors was a rather difficult task, especially for the Uličká River basin, where the territory of the national park covers more than 55% of the basin.

All proposed measures were included into digital terrain model (DTM) of the investigated area which was the base for further analyses in HEC-RAS software environment. The exact determination of the retained volume was rather complicated according to accuracy of the DTM provided by Slovak Water Management Enterprise (SWME).

The detention and multipurpose reservoirs were placed in such a way that, even with smaller dam heights, they could provide a sufficiently large retained volume and at the same time capture a fairly large catchment. Fig. 5 shows a more detailed view of the location of the multi-purpose reservoir above the village of Nová Sedlica (green colour is representing the position of the Poloniny NP.

According to HEC-RAS series of hydrodynamic analyses the mentioned multi-purpose reservoir above Nová Sedlica (Fig. 5) can transform the local Q_{100} flood wave

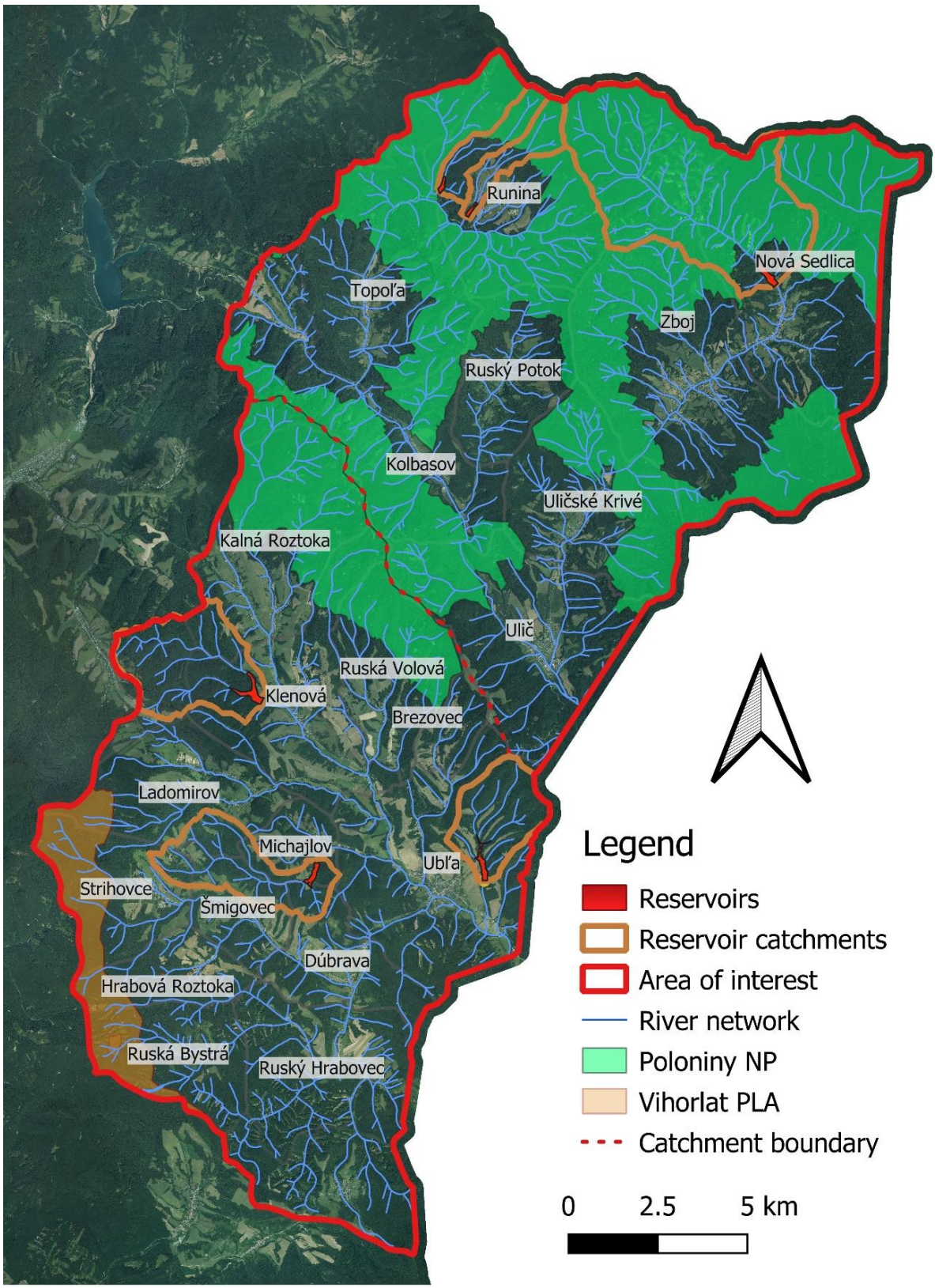

Fig. 4. One of the proposals of water retention measures (reservoirs only).

created in the basin belonging to the profile of the reservoir (rkm 12.4) with culmination of 49.4 $m^3 s^{-1}$ down to 34.8 $m^3 s^{-1}$, i.e. approximately by 30% (Fig. 6). The sudden decrease of the transformed flood wave is due to terrain morphology (DTM).

For illustration the hydrographs of flood wave for

the border profile of the Ublianka River (rkm 0.2) are presented in Fig. 7. The untransformed flood wave is culminated at discharge value of 270 $m^3 s^{-1}$. According to reservoir proposal in the upper part of the river basin, the culmination of the flood wave in the border profile is at 246 $m^3 s^{-1}$ what represents the flattening of flood wave by approx. 10%. Main parameters of proposed multi-purpose reservoirs are given in Tab. 1.

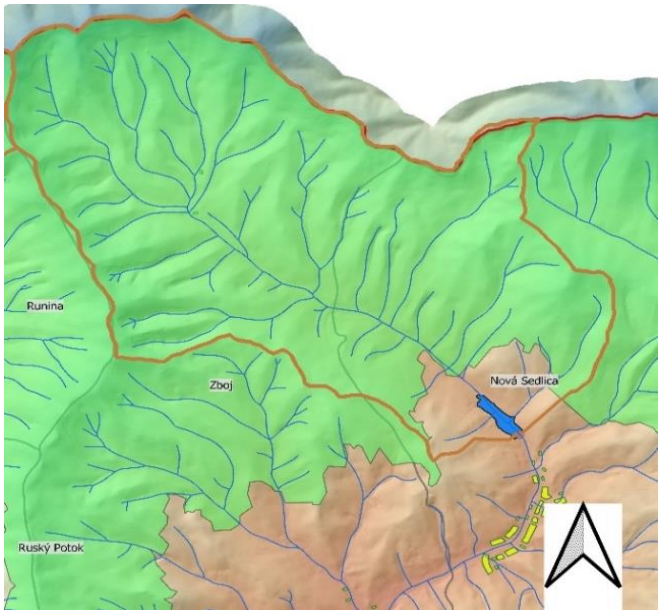

Fig. 5. Detail of the location of the reservoir above the village of Nová Sedlica.

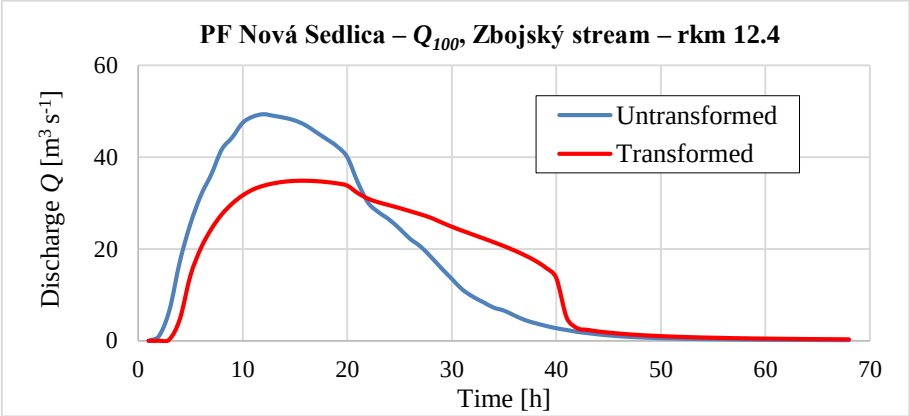

Fig. 6. Transformation of local Q_{100} flood wave on Zbojský stream in Nová Sedlica profile.

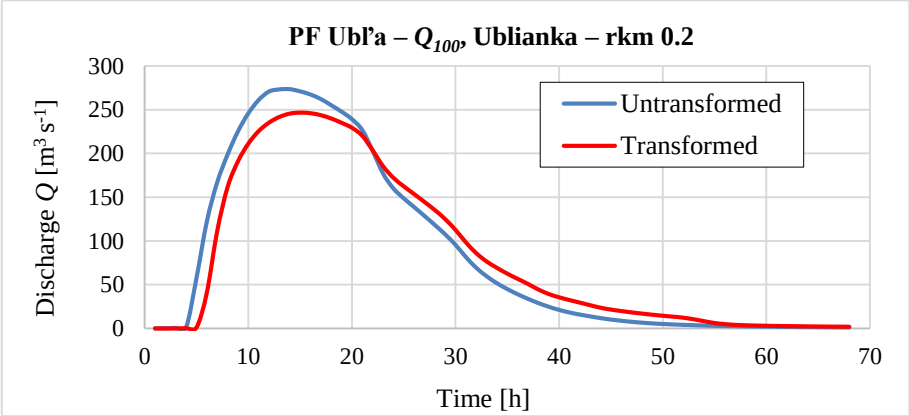

Fig. 7. Transformation of Q_{100} flood wave on Ublianka River in the Ubľa village border profile.

Table 1. Main parameters of proposed multi-purpose reservoirs

Basin	Name	Height [m]	Altitude [masl]	Max. volume [thous. m^3]	Max. flooded area [ha]	Basin area [ha]	Stream	River chainage [rkm]
Ulička	Nová Sedlica	21.0	432.0	864.0	12.9	2 430	Zbojský stream	14.2
Ublianka	Klenová	13.5	270.0	940.0	19.9	930	Tapovec stream	0.7
	Michajlov	11.0	255.0	500.0	10.0	730	Savkov stream	2.5

Conclusion

The goal of the submitted contribution was to illustrate the methodological procedure for possibilities of reducing flood situation using HEC-RAS 2D hydrodynamic modelling system using digital terrain model. Several variants of scenarios were analysed which differed from each other not only in the location and number of measures, but also in their type (detention reservoir, multi-purpose reservoir and other). The final proposal consisted of 12 detention reservoirs, which had a total volume of 3.3 mil. m^3 and from 3 multi-purpose reservoirs, which had a total volume of 2.3 mil. m^3. All flood protection measures were proposed taking several factors, such as residential areas, transport infrastructure, suitable morphological conditions, but also the territory of the Poloniny national park into account.

Achieving higher transformation is very difficult – even impossible – in the given conditions without significant interventions in the landscape, such as the relocation of existing roads or houses. However, the simulation showed a significant effect of flood protection measures in the upper parts of the river basins, where in some cases more than 50% reduction of peak flows was achieved.

Acknowledgement

Acknowledgment: This article was supported by the Research and Development Support Agency under contract no. APVV-19-383 "Natural and technical measures oriented to water retention in sub-mountain watersheds of Slovakia".

References

Brunner, G. W. (2021): HEC-RAS River Analysis System, 2D Modelling User´s Manual, Version 6.0. Davis: US Army Corps of Engineers, Institute for Water Resourcces, 562 p.

Garcia, M., J., Bedient, P. (2020): Integrating Reservoir Operations and Flood Modelling with HEC-RAS 2D. Water. 2020, Vol. 12, 2259; doi:10.3390/w12082259.

Janík, A., Šoltész, A. (2021): Analysis of flood protection in catchments of riversin Little Carpathians, Spektrum, STU, Bratislava, ISBN 978-80-227-5155-1, 124 p.

Leskens, J., Brugnach, M., Hoekstra, A. Y., Schuurmans, W. (2014): Why are decisions in flood disaster management so poorly supported by information from flood models? Environ. Model. Software 53, 53–61.

Smithers, J., Schulze, R., Kienzle, S. (1997): Design Flood Estimation Using a Modelling Approach: A Case Study Using the ACRU Model, vol. 240. IAHS Publication, 365–376.

Šoltész, A., Orfánus, M., Mydla, J. (2022): FLOOD UZH – Study of proposal of retention spaces in river basin of the upper Uzh River. Final scientific report, FCE STU Bratislava, 63 p.

Uddin, K., Martin, A. (2021): Potential flood hazard zonation and flood shelter suitability mapping for disaster risk mitigation in Bangladesh using geospatial technology. Prog. Disaster Sci. 100185.

Vyshnevskyj, V. I., Donich, O. A. (2021): Climate change in the Ukrainian Carpathians and its possible impact on river runoff, Acta Hydrologica Slovaca, Vol. 22, No.1, 3–14.

Zhang, K, Shalely, H., Ezaz, G. T., Chakraborty, A., Liu, L. (2022): An integrated flood risk assessment approach based on coupled hydrological-hydraulic modelling and bottom-up hazard vulnerability analysis. Environmental Modelling and Software, vol. 148, 11–22.

Prof. Ing. Andrej Šoltész, PhD. (*corresponding author, e-mail: andrej.soltesz@stuba.sk)
Assoc. Prof. Ing. Martin Orfánus, PhD.
Ing. Jakub Mydla
Slovak University of Technology in Bratislava
Faculty of Civil Engineering
Radlinského 11
810 05 Bratislava
Slovak Republic

DOI: 10.31577/ahs-2022-0023.02.0033

ACTA HYDROLOGICA SLOVACA

Volume 23, No. 2, 2022, 288–295

Dispersion process in conditions of real sewer systems – in situ experiments

Marek SOKÁČ*, Yvetta VELÍSKOVÁ

A general assumption of most current models used to simulate flow in sewer systems (pipes) is that the sewers are considered as prismatic channels. However, in real conditions there are many factors, which affect the real flow. One of them is the occurrence of the sediments and deposits in sewer pipes, which significantly changes the flow conditions, as well as the dispersion process in sewer systems by creation of "dead zones". Paper describes the effects of these zones on hydrodynamic dispersion process, which are particularly noticeable in hydraulic conditions of low flow rates in sewer system (sanitary, flow rates during dry period without rain …). In the study, there were applied two types of tracers and both used substances give identical results.

Experimental results show that even though sewer pipes are considered as prismatic hydraulic channels, in the real conditions some irregularities resulted with dead zones creation are presented. Their influence on the mass concentration time-course shape is depending on the sediment layer thickness. Gaussian approximation of the one-dimensional advection dispersion equation for instantaneous pollution entry is not suitable for the sewer pipes with sediments occurrence. In case of sediments presence, the GEV and Gumbel's approximation function looks to be more accurate.

KEY WORDS: sewer systems, sediments, hydrodynamic dispersion, dispersion coefficient, in situ-experiments

Introduction

Transport of substances in flowing water is influenced by the hydraulic conditions of streams. When dangerous substances are transported, the situation is much worse at low flow rates. In this case, there is a higher risk of exceeding the concentration limits of these substances (Čubanová et al., 2021). In real conditions on streams, the situation is even more complicated. Some rate of simplifications or schematizations is necessary for modelling, which of course also distorts the result. Therefore, when applying hydrodynamic models, one must be careful consider their appropriate application.

Sewer systems (pipes) are typically regarded as prismatic and regular hydraulic channels. This is also typical approach of most current models used for the simulation of the water quantity and quality in the sewer. However, in real conditions there are many factors, which affect and distort the flow and dispersion processes by forming so-called "dead zones". Generally, dead zones are formed in sewer systems by all obstacles and irregularities, which occur in the flow profile. These can be caused by various solid substances and objects that get into the sewer network, but also enlargements and narrowing of the flow profile (e.g. in shafts) as well as the irregularities in the sewer pipes slope and consequently caused backwater effects. This phenomenon becomes evident especially in conditions of low discharges (dry weather flows) and of course in case of lower sewer construction quality (irregular slopes, sewer settlement due to the ground consolidation) (Sokáč and Velísková, 2016).

We assume as the one of the most important factor of the of dispersion processes distortion the occurrence of the sediments and deposits in sewer pipes. These significantly changes the hydraulic conditions, as well as the dispersion process in sewer systems.

Modelling of the mass or pollution transport is currently practically an integral part of all hydrodynamic models, including models of runoff from urbanized areas to sewer systems. In this case, the transport models are typically reduced to 1D modelling, using the advection dispersion equation (1D ADE) in form (Martin et al., 2018; Rutherford, 1994).

$$\frac{\partial C}{\partial t} + v_x \frac{\partial C}{\partial x} = D_x \left(\frac{\partial^2 C}{\partial x^2}\right) + S_s \qquad (1)$$

where

v_x – is the velocity of water flow in a given direction of flow [m s^{-1}],

C – is the concentration of a substance [g m^{-3}],

D_x – is the dispersion coefficient in the longitudinal direction [m^2 s^{-1}],

S_s – is a function representing the sources of pollution [g m^{-3} s^{-1}],

x – is the spatial coordinate – distance [m],
t – is the time [s].

Such approach is fine from a formal point of view, but ADE does not take into account a very important fact (phenomenon), which occurs in real conditions: the occurrence of so-called dead zones. The dead zones are in fact water accumulation zones, where the water is temporarily stored and consequently released into the main flow (Czernuszenko and Rowiński, 1997; Gualtieri, 2010). Of course, this applies also to the substances suspended in the water.

As stated above, in the existing models sewer pipes are considered as a prismatic hydraulic channel with clearly defined hydraulic parameters. However, in the practice, after some time of the sewer pipe operation, the prismatic shape of the sewer pipes can be substantially changed due to the sediments and deposits at the bottom of the pipe. The deposits typically occur in sewer systems with small slopes (flat urban areas) and in sanitary sewer systems. In the combined sewer systems, the sediments are subject of spatial and temporary changes due to the stormwater flow in these systems. This phenomenon must be taken into account in the modelling the dispersion and flows in sewer systems (Manina et al., 2020).

However, also in combined sewer systems can fine sediment particles form so-called cohesive sediment, which is hardly removable by the self-cleaning ability of the sewer pipes (insufficient shear stress induced by the stormwater flows) (Stransky et al., 2016). Such sediments can be removed only by using mechanical cleaning procedures and technology, applied by the sewer system operator. Such cleaning shall be carried out regularly, but this is often omitted due to various reasons.

During our research, we encountered such conditions in sewer systems and we found out, that the sediments in sewer pipes significantly changes not only the hydraulic conditions compared to the original assumptions, but they also significantly change the dispersion process in sewer systems. The changes of the dispersion process are especially visible under low water flows conditions, e.g. sanitary flows (flow rates during dry period without rain in combined systems).

Material and methods

Dispersion coefficients characterise the intensity of dispersion or mixing, so it is one of the most important parameters for the pollution transport (dispersion) simulation. For application of the hydraulic model in real condition, it was necessary to verify the up-to date knowledge in this field as well as check if there are singularities, which distract the theoretical character of dispersion process (dead zones, deposits, sediments, obstacles etc.) (González-Pinzõn et al., 2013). For the most precise determination of dispersion coefficient value, we perform tracer experiments in real sewer pipes.

The experiments were performed in Petržalka, the right-bank part of the Bratislava city. The field experiments were performed in four campaigns, namely in May and June 2019, August 2021 and January 2022. All the experiments were performed within the research in the H2020 project SYSTEM. The research work in this project comprises laboratory as well as field experiments and development of a specific model, simulating the pollution spread in sewer systems (Fig. 1).

The first two campaigns were focused on experiments and data measurements for the dispersion coefficient determination in specific sewer sections (pipes) with various parameters and conditions, e.g. pipe diameter, pipe filling (flow depth). The third and fourth campaign was focused as complex experiments for the evaluation and calibration of the developed localisation model. In that case, large sections of the sewer systems were used, comprising several consecutive pipe sections with different diameters. This paper deals mainly with the first two campaigns, however it can be mentioned also some reference to the last campaign.

The lengths of the examined sewer sections were from 100 m up to 250 m. Experiments were performed in sewer pipes with diameter of 300 up to 3200 mm, in straight sections, without diameter changes. Because one of the main assumptions of the developed model was the presence of uniform and steady-flow, we performed all experiments during dry weather flows in sewer system, so only with the sanitary flow conditions in the sewer system.

As a tracer the kitchen salt and the colouring agent Rhodamine was used. The concentration of the salt (NaCl) was 1 kg of the salt in 10 litres of drinking water (approx. 110–115 mS cm^{-1}) and 1 ml of the 20% Rhodamine solution. Tracer dose (10 litres) was flushed in the upper manhole at a specific time. Measuring manhole was located in a specific distance downstream in the same sewers section. The measuring manhole was equipped with devices automatically registering time-courses of conductivity and fluorescence. The fluorescence was measured using portable fluorometric probe for Rhodamine (Turner designs) with data logger for data recording in specified intervals (the minimal interval can be set to 1 second). The conductivity was measured using portable conductivity meter (WTW Multi 3410) with data logger (the minimal record interval can also be set 1 second). The fluorescence / conductivity time-course data can be subsequently transferred into the concentration data.

Recorded time-courses were transferred into the MS Excel environment. Based on the registered concentration time-courses, it was possible to determine the dispersion coefficient value for the corresponding sewer section.

Values of dispersion coefficients obtained from the experiments were statistically evaluated.

Statistical evaluation was performed for each measured sewer branch using the specific approximation methods (Gauss, Gumbel and GEV). This procedure was focused on finding the best fit between the measured values and the approximation according to the considered method, i.e. to find the optimal set of the given method parameters providing the best goodness of fit based on the minimal root mean square error (RMSE) between the measured and approximated values, i.e.

Fig. 1. Documentation of the experiment steps: a) tracer preparation, b) tracer dosing, c) measuring probes in the confluence manhole, d) data loggers for recording the measured data.

$$RMSE = \sqrt{\frac{\sum_{t=t_1}^{t=t_2}(c_{m,t}-c_{a,t})^2}{n}} \quad (2)$$

where
RMSE – is the root mean square error [kg m^{-3}],
$c_{m,t}$ – is the measured value (concentration) at the time t [kg m^{-3}],
$c_{a,t}$ – is the approximated value in the time *t* [kg m^{-3}],
t_1 – is the measurement start time [sec],
t_2 – is the measurement end time [sec],

$$NRMSE = \frac{RMSE}{c_{max}-c_{min}} \quad (3)$$

where
NRMSE – is the normalised root mean square error [-],
c_{max} – is the maximal concentration in each particular experiment [kg m^{-3}],
c_{min} – is the minimal concentration in each particular experiment [kg m^{-3}].

The optimal sets of parameters were analysed and set up using the built–in Excel Solver function. The target value is the main indicator for the optimization process, looking for a minimum value for this indicator. In our case it was the RMSE value.

Results and discussion

Expected results of the first two campaigns of performed experiments were the determination of dispersion coefficient values for the selected pipes and the selection of the best applicable formula for the dispersion coefficient calculation. Another expected result was a verification, if the theoretical dispersion formulas fit with the experiment results. In case of differences, it was necessary to search for the reasons and try to modify

the theoretical model basis. A typical reason of the differences could be occurrence of dead zones.

One of the secondary goals was also assessment of the tracer experiments technology. As it was mentioned above, the kitchen salt as well as the florescent dye was used as a tracer in experiments. An example of the comparison of the results, achieved by both tracers can be seen on the Fig. 2.

When evaluating measurements and experiments, we came to result, that every tracer has its advantages and disadvantages. The advantage of the Rhodamine tracer is the fact, that its background concentration is zero (or values close to zero), so there is clear distinction of the experiment's concentration from all influences (released pollutants) that may occur in the sewer network during the experiment. This does not fully apply to the second tracer – the salt. The background concentration (measured as the conductivity) is not equal to zero and the measurement can be substantially affected by the fact that in the sewer network can be various sources of substances or pollutants affecting the wastewater conductivity (wastewater from washing, dishwashers, small industry). Such small disturbances can be also seen on the Fig. 2 in the time 12:14 and later (red line).

The disadvantage of the Rhodamine tracer was the high sensitivity of the measuring device – in many aspects, this fact is rather an advantage, but for this reason, it was necessary to clean the measuring probe regularly in the sewer environment. This can be also seen on the disturbances on the Fig. 2 – blue line before the time 12:07, where decreases of the measured values caused by the impurities on or close to the measuring probe appeared. The probe of the conductometric device was more practical in this respect and less prone to failures.

The common problem of both tracers was the determination of the dose to perform successful measurements in the entire device measuring range. With an insufficient tracer dose, the minimum detection sensitivity of the used device may be exceeded, and with an excessive dose, the measuring range of the device may be exceeded. The later one can be also seen on the Fig. 2 – the upper measurement limit for the fluorimeter was 500 000 RFUB (Raw Fluorescence Units Blanked) units. This limit was exceeded in the time around 12:07 (blue line), so the time course peak is "cut off".

From this point of view, it was very useful to use both tracers. This allows us during the evaluation of the measurements clearly determine whether it is a device error or a random fluctuation in the measured values.

Summary of field measurement parameters and result values of the dispersion coefficients are presented in Table 1.

Because the experimental area (Petržalka) is flat, the sewers are often in very small or minimal slopes. This naturally causes deposits to occur. This assumption was confirmed, and we really found large presence and thickness of sediments and deposits in some sewer branches (see Table 2). This concerns particular for the sewer branches with small diameters (less than 500 mm), where the flow rates were relatively small. In sewer branches with larger diameters, typically larger flow rate of wastewater was present, so the occurrence of sediments was more rarely. In large sewer collectors, no sediments were present.

As found by measurements evaluation, the presence of sediments affects (deforms) in large extent the shape of the concentration time-courses. This finding inspired us to continue this research also in laboratory conditions (Sokáč and Velísková, 2020).

Values of the dispersion coefficients D_x, calculated in this study, are in line with our results from previous studies (Sokáč and Velísková, 2016; Velísková et al., 2009). The range of the dispersion coefficient in these studies

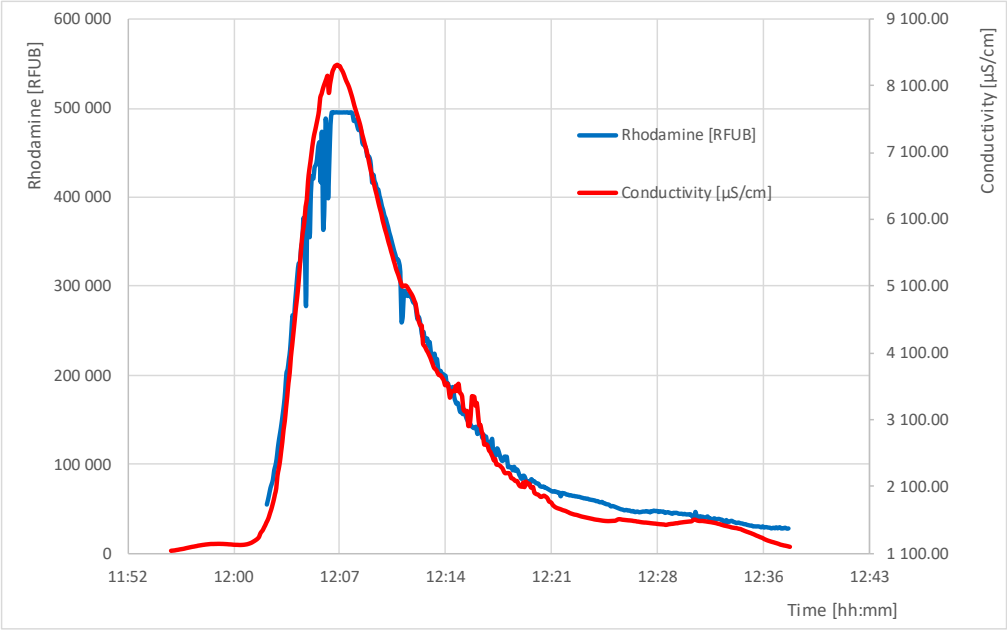

Fig. 2. Example of the experiment records (Rovniankova str., DN 400, 25th of June 2019).

Table 1. Results of field experiments

Exp. Nr	Sewer diameter (DN)	Sewer branch length	Flow velocity	Dispersion coefficient D_x-Gauss	Dispersion coefficient D_x-Gumbel	Dispersion coefficient D_x-GEV	Shape coefficient GEV
	[mm]	[m]	[m s^{-1}]	[m^2 s^{-1}]	[m^2 s^{-1}]	[-]	[-]
11	300	141	0.200	0.337	0.529	0.653	0.425
12	300	141	0.150	0.135	0.216	0.315	0.469
13	400	152	0.298	0.112	0.191	0.192	-0.049
14	400	152	0.280	0.111	0.192	0.192	-0.042
22	400	325	0.213	0.519	0.707	0.706	0.112
23	400	102	0.060	0.120	0.192	0.252	0.497
24	400	102	0.060	0.058	0.095	0.098	0.179
19	500	114	0.080	0.061	0.104	0.114	0.193
27	500	353	0.131	0.114	0.197	0.197	-0.025
17	600	130	0.195	0.035	0.059	0.060	0.111
18	600	130	0.192	0.025	0.042	0.043	-0.026
28	600	268	0.289	0.070	0.115	0.116	-0.095
15	3200	153	0.371	0.088	0.153	0.154	-0.116
16	3200	153	0.359	0.065	0.113	0.121	-0.246
25	3200	362	0.333	0.068	0.120	0.123	-0.197
26	3200	362	0.327	0.059	0.106	0.106	-0.192

Table 2. Results of field experiments – NRMSE

Exp. Nr	Estimated sediment thickness	NRMSE		
		Gauss	Gumbel	GEV
	[mm]	[%]	[%]	[%]
11	40	10.87	6.95	5.39
12	40	13.01	6.83	2.00
13	50	5.54	3.09	2.96
14	50	5.50	2.46	2.34
22	50	8.34	4.01	3.45
23	100	11.20	6.65	3.26
24	100	8.79	3.30	1.58
19	80	9.31	4.58	3.68
27	20	6.27	2.21	2.15
17	10	6.84	3.50	3.06
18	10	4.11	2.04	2.01
28	30	4.32	2.95	2.49
15	0	5.29	5.32	5.10
16	0	3.51	6.57	3.41
25	0	2.65	4.44	2.24
26	0	3.14	4.47	1.73
	Average	6.79	4.34	2.93
	Min	2.65	2.04	1.58
	Max	13.01	6.95	5.39

was determined in range 0.085–0.12 m^2 s^{-1}, but it is necessary to mention that this research was performed in clean and new sewer pipes. We can also state a good agreement with the study of (Rieckermann et al., 2005), where the average value of 0.16 m^2 s^{-1} was set up (10- percentile was 0.05 m^2 s^{-1} and 90-percentile was 0.36 m^2 s^{-1}).

The extent of dead zones and their influence on asymmetricity (distortion) of the dispersion process could be expressed by the value of the shape coefficient ξ, used in the GEV approximation (see eq. 7). This shape parameter (see Table 1) expresses the asymmetry of the concentration distribution in time. A 'neutral' value of the shape parameter, which corresponds to the shape of the Gaussian approximation function is -0.288 (in case of dead zones are not present). Higher values of this coefficient are caused by dead zones and corresponding asymmetricity of the concentration distribution in time

(represented by longer "tails" of the time concentration curves). Higher values of the shape parameter ξ in this way indirectly characterise the extent of dead zones.
As can be seen in Table 1, greater influence of the dead zones was found in case of smaller sewer pipe diameters and higher sediment layer thickness (see Table 2), whereas larger sewer pipe diameters showed less impact of the dead zones.
For the evaluation of all experiments we used the analytical solution of the equation presented in form (Rapp, 2016), (Cunge et al., 1980):

$$C(x,t) = \frac{M}{2A\sqrt{\pi D_x t}}\, exp\left(-\frac{(x-v_x\, t)^2}{4\, D_x\, t}\right) \quad (4)$$

where
D_x – is the longitudinal dispersion coefficient [m^2 s^{-1}],
$C(x,t)$ – is the concentration of solute in a particular distance and time [g m^{-3}],
G – is the mass of solute [g],
A – is the discharge area in a stream cross-section [m^2],
v_x – is the mean flow velocity [m s^{-1}],
t – is the time [s],
x – is the distance [m].

All measured results from tracer experiments were statistically evaluated, whereas the main result was the value of the dispersion coefficient D_x determination. Because experiments with the presence of sediments showed presence and influence of "dead zones", we found the evaluation of the dispersion coefficient using the eq. 4 as insufficient and therefore we used alternative equations based on asymmetrical probability (tracer concentration) distributions, e.g. on the Gumbel or GEV distribution (Sokáč et al., 2019).
As the 1-D analytic solution of the ADE (eq. 1) coming from the Gumbel statistical distribution (Loaiciga and Leipnik, 1999; Sokáč et al., 2019) this relation was applied:

$$c(x,t) = \frac{M}{A\sqrt{D_{x,G}\, t}} \exp\left[\frac{x-u\, t}{\sqrt{D_{x,G}\, t}} - \exp\left(\frac{x-u\, t}{\sqrt{D_{x,G}\, t}}\right)\right] \quad (5)$$

where
$D_{x,G}$ – is the longitudinal dispersion coefficient [m^2 s^{-1}] by the Gumbel's approximation model.

Both the Gaussian approximation model (eq. 4) and the Gumbel's approximation model (eq. 5) are two-parametric models, where the first parameter is the dispersion coefficient and the second parameter is the peak time (mean), expressed through the velocity of water flow u.
Even better results and conformity between models and data from real measurements can be obtained using the three parametric Generalised Extreme Value (GEV) distribution model (Sokáč et al., 2019):

$$c(x,t) = \frac{M}{A\sqrt{D_{x,GEV}\, t}}\, z(t)^{\xi+1}\, e^{-z(t)} \quad (6)$$

$$z = \left(1 + \xi\left(\frac{\bar{v}.t-x}{\sqrt{D_{x,GEV}\, t}}\right)\right)^{-\frac{1}{\xi}} \quad (7)$$

where
$D_{x,GEV}$ – is the longitudinal dispersion coefficient [m^2 s^{-1}] used in the GEV distribution model,
ξ – is the shape parameter. It express the asymmetry of the concentration distribution in time.

An example of one of measured parameter time courses (in this case a conductivity time course) is shown on Fig. 3. As it can be seen on this graph (Fig. 3), the approximation using eq. 4 (Gauss) is not appropriate, this approximation does not reflect the asymmetry of the tracer concentration time-course. Much better was the approximation based on the Gumbel's approximation and the best agreement was obtained by using GEV model approximation. This was also confirmed by the statistical tests – results of the statistical evaluation

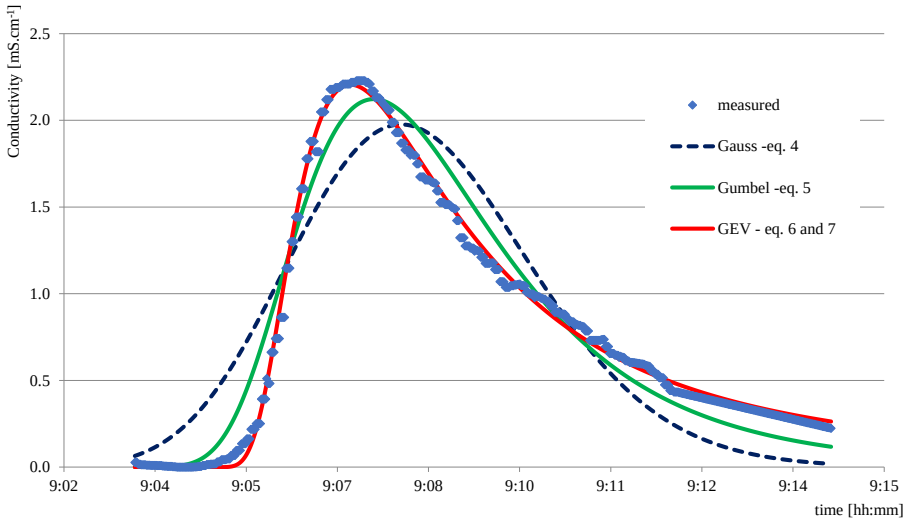

Fig. 3. Example of the experiment record and its approximations.

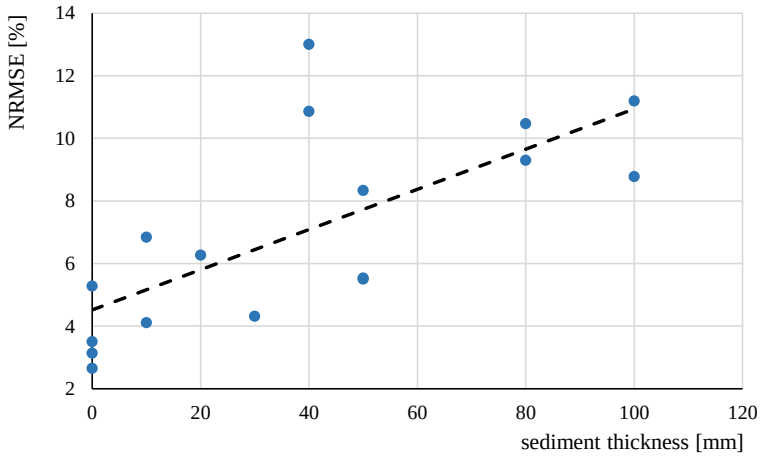

Fig. 4. Relation between the sediment thickness and the NRMSE of Gaussian approximation.

are presented in the Table 2.
As it can be seen in this table (Table 2), the best approximation results are achieved using different approximation methods than the Gaussian one. An interesting fact is that the NRMSE of the Gaussian approximation value increases with increasing sediment thickness, as documented on the Fig. 4. It points out that the Gaussian approximation (eq. 4) is suitable only for the clean sewer pipes without sediments. Larger sediment layers form in sewer pipes transient storage (dead) zones, which deforms the shape of the concentration time course in the downstream measuring profile of a tracer experiment. The correlation coefficient of the sediment thickness and the NRMSE is approximately R^2=0.5.

Conclusion

The performed tracer experiments give us a lot of experience and new knowledge. Regarding practical experience, the use of each tracer has its advantages and disadvantages. In terms of obtained results (dispersion coefficients, eventually other approximation parameters), both used substances give identical results. The use of both tracers simultaneously proved to be a great advantage, as this allowed us to distinguish random fluctuations and detect measurement errors.
Analyse of the obtained results shows following facts:

1. even though sewer pipes are considered as prismatic hydraulic channels without dead zones, in the real conditions the dead zones are present,
2. the presence of sediments and deposit in sewer pipes is one of the most important factor of the dispersion process distortion, especially in low flows conditions (dry weather flows),
3. the volume (size) of these dead zones and their influence on the time-course shape (deformation) is depending on the sediment layer thickness and
4. the Gaussian approximation of the one-dimensional advection dispersion equation for instantaneous pollution entry (eq. 4) is not suitable for the sewer pipes with sediments occurrence.

The comparison of the used approximation methods shows that the GEV approximation function (eqs. 6 and 7) was the most precise, thus the most suitable for application in real sewers. This approximation was in case of all experiments more precise than the Gaussian (eq. 4) and the Gumbel's approximation (eq. 5) functions. It is a result of the fact that the GEV approximation function is a three – parametric function, whereas the first two ones are only two – parametric functions. The Gumbel's approximation function proved to be more accurate for experiments with sediments presence, whereas for the clean sewer pipes the Gaussian approximation function was more accurate.
In the sewer pipes with large diameters, the effect of the dead zones was not so significant. This is because the self-clean ability of those sewer pipes is bigger than the small ones. In general, the flow rate in such big sewer pipes is larger, so the ratio of the sediment thickness and the water depth is small, thus the dead zones volume comparing to the flowing water volume is small, as well.

Acknowledgement

This work was supported by the Scientific Grant Agency VEGA–grant number VEGA 2/0085/20, by the project H2020–"SYSTEM", grant agreement No. 787128 and by the International R&D cooperation grant MVTS-SYSTEM.

References

Čubanová, L., Šoltesz, A., Mydla, J. (2021): Analysis of droughts due to the operation of water structures: Gidra river case study. *Pollack Periodica*, *17*(1), 111–116. https://doi.org/10.1556/606.2021.00463

Cunge, J. A., Holly, F. M., Verwey, A. (1980): *Practical aspects of computational river hydraulics.* Pitman Publishing Ltd.

Czernuszenko, W., Rowiński, P. M. (1997): Properties of the dead-zone model of longitudinal dispersion in rivers. *Journal of Hydraulic Research*, *35*(4), 491–504. https://doi.org/10.1080/00221689709498407

González-Pinzõn, R., Haggerty, R., Dentz, M. (2013): Scaling and predicting solute transport processes in streams. *Water Resources Research*, *49*(7), 4071–4088. https://doi.org/10.1002/wrcr.20280

Gualtieri, C. (2010): Numerical simulation of mass exchange processes in a dead zone of a river. In *Advances in Environmental Fluid Mechanics* (249–274). WORLD SCIENTIFIC. https://doi.org/10.1142/9789814293006_0012

Loaiciga, H. A., Leipnik, R. B. (1999): Analysis of extreme hydrologic events with Gumbel distributions: marginal and additive cases. *Stochastic Environmental Research and Risk Assessment 1999 13:4*, *13*(4), 251–259. https://doi.org/10.1007/S004770050042

Manina, M., Halaj, P., Jurík, L., Kaletová, T. (2020): Modelling seasonal changes of longitudinal dispersion in the Okna river. *Acta Scientiarum Polonorum Formatio Circumiectus*, *19*(1), 37–46. https://doi.org/10.15576/asp.fc/2020.19.1.37

Martin, J. L., McCutcheon, S. C., Schottman, R. W. (2018): Hydrodynamics and Transport for Water Quality Modeling. In *Hydrodynamics and Transport for Water Quality Modeling*. CRC Press. https://doi.org/10.1201/9780203751510

Rapp, B. E. (2016): Microfluidics: Modeling, mechanics and mathematics. In *Microfluidics: Modeling, Mechanics and Mathematics*. Elsevier Inc. https://doi.org/10.1016/c2012-0-02230-2

Rieckermann, J., Neumann, M., Ort, C., Huisman, J. L., Gujer, W. (2005): Dispersion coefficients of sewers from tracer experiments. In *Water Science and Technology* (Vol. 52, Issue 5). IWA Publishing. https://doi.org/10.2166/wst.2005.0124

Rutherford, J. C. (1994): *River Mixing*. Wiley, Chichester [England].

Sokáč, M., Velísková, Y. (2016): Dispersion process in urban sewer networks under dry weather conditions. *GAZ, WODA I TECHNIKA SANITARNA*, *90*(4), 152–155. https://doi.org/10.15199/17.2016.4.7

Sokáč, M., Velísková, Y. (2020): Impact of roughness changes on contaminant transport in sewers. *Acta Hydrologica Slovaca*, *21*(2), 145–151. https://doi.org/10.31577/ahs-2020-0021.02.0018

Sokáč, M., Velísková, Y., Gualtieri, C. (2019): Application of asymmetrical statistical distributions for 1D simulation of solute transport in streams. *Water (Switzerland)*, *11*(10). https://doi.org/10.3390/w11102145

Stransky, D., Kabelkova, I., Bares, V., Stastna, G., Suchorab, Z. (2016): Suitability of combined sewers for the installation of heat exchangers. *Ecological Chemistry and Engineering S*, *23*(1), 87–98. https://doi.org/10.1515/eces-2016-0006

Velísková, Y., Dulovičová, R., Sokáč, M. (2009): Určenie miery pozdĺžnej disperzie pri prúdení s voľnou hladinou v prizmatickom kanáli časť 1: priamy úsek trasy. (Determination of the longitudinal dispersion rate in the flow with free surface in prismatic channel. Part 1. Straight direct line. In Slovak. *Acta Hydrol. Slovaca*, *10*(1), 35–43.

Assoc. Prof. Ing. Marek Sokáč, PhD. (*corresponding author, e-mail: sokac@uh.savba.sk)
Ing. Yvetta Velísková, PhD.
Institute of Hydrology SAS
Dúbravská cesta 9
841 04 Bratislava
Slovak Republic

DOI: 10.31577/ahs-2022-0023.02.0034

ACTA HYDROLOGICA SLOVACA

Volume 23, No. 2, 2022, 296–304

Analysis of the water temperature in the Litava River

Zbyněk BAJTEK*, Pavla PEKÁROVÁ, Katarína JENEIOVÁ, Jakub RIDZOŇ

River water temperature is important in many environmental applications, hydrology, and ecology research. It mainly depends on several parameters of water bodies such as streamflow, groundwater interactions, and their surrounding atmosphere. It has been correlated with air temperature as a substitute due to the ease of applicability for rivers with some limitations over detailed meteorological data. An evaluation of integrated river water temperature and streamflow fluctuations is proposed to evidence biological activity, chemical specimen, oxygen solubility, self-purification capacity of a river system, and variation of flows due to hydro-climatic changes. The possibility of predicting the river water temperature at various locations over a river basin is vital for water quality management. Modelling of river water temperature is usually based on a suitable mathematical model and field measurements of various atmospheric factors. The aim of the study is the analysis and subsequent simulation of monthly and daily water temperatures in the Litava River at the Plášťovce station. First of all, the statistical analysis of a series of daily values of Litava water temperature and air temperature (Bzovík meteorological station) was done. In the second part of the study, the several multi-regression models of the daily water temperatures are analyzed.

KEY WORDS: Litava River, water temperature, simulation, multi-regression models

Introduction

The temperature of the river is an important factor that can be used to determine the health of water ecosystem. Forecast of the temperature of a river is an interesting topic since water temperature has an important ecological and economic impact (Lešková and Škoda, 2003; Grbić, et al., 2013). The flow temperature is influenced by many factors such as meteorological conditions, the condition of the river bed, river topography, and flow (Caissie, 2006). Meteorological conditions, especially air temperature, wind speed, solar radiation, and humidity are the factors that have the greatest impact as they determine the heat exchange and flows that take place at the surface of the river.

In river temperature regression analysis, air temperature is often used as the only independent variable because it can be used as a proxy for the net exchange of heat flows affecting water level and also because the estimated water temperature as the reference value temperature of the air temperature (Mohseni and Stefan, 1999; Caissie, 2006; Webb et. al., 2008). In addition, air temperature is widely measured and more readily available than other parameters. Therefore, it is very important to study and explain the relationship between air and water temperature. Many water temperature models have been successfully developed and applied in recent years. These can be divided into deterministic and statistical models (Benyahya et al., 2010). Deterministic water temperature models simulate spatial and temporal changes in river water temperature based on energy balances of heat fluxes and mass balances of currents in the river. These deterministic models require a large number of input variables, such as riverbed geometry, hydrological and meteorological conditions, and are therefore often impractical and time-consuming due to their complexity. On the other hand, statistical models are widely used in water temperature forecasts because these models are relatively simple and require fewer input data. Linear regression models (Morrill et al., 2005), non-linear regression models (Mohseni et al., 1998; van Vliet et al., 2013), and stochastics models (Ahmadi-Nedushan et al., 2007) have been successfully developed for data relating to different time scales in recent years.

Even though these statistical models relating water to air temperature offer relatively simple approaches to predicting water temperature, other statistical models such as Box-Jenkins and nonparametric models (Benyahya et al., 2010) and hybrid statistical-physical models such as air2water (Piccolroaz et al., 2016) can adequately model the water temperature. Artificial neural network (ANN) models have become widespread in recent years to predict the temperature of water. DeWeber and Wagner (2014) developed an ensemble ANN model to predict daily mean sea temperature using air temperature and terrain (Zhu et al., 2018). Even

though many models of river water temperature have been successfully developed and applied, several key issues in water temperature modelling need to be addressed as they can form the basis for developing effective mean river temperature model complexity. A relationship between air temperature and flow temperature is nonlinear for high or low air temperatures as proved by Mohseni et al. (1998).

When air temperatures are near or below 0°C, air and water temperatures are no longer synchronized, resulting in a poor relationship between air and river temperatures. The temperature of the river does not respond immediately to changes in air temperature due to thermal inertia versus hydrological mode fluxes (Isaak et al., 2017), so it may be necessary to account for time lags in the effects of air temperature on a practical temperature forecast (Benyahya et al., 2010). The solution may be splitted into two distinct components: a long-term periodic component, and a fluctuating short-term component. The long-term periodic component can be modelled by simple functions such as an invariant sinusoidal function, or more complex models like the Fourier series (Benyahya, et al., 2010). The selection of appropriate model inputs and appropriate time lags has not been explored in the literature, particularly in the case of estimating river water temperatures and other water quality parameters (Maier and Dandy, 2000). With recognizing that the river water temperature is increasing, it is a complex function of the interaction of climate change, hydrology, and human activities, there is a distinct lack of studies demonstrating their integrated influence on the spatiotemporal dynamics of water temperature as a result of lack of long term data. Such quantitative information is critical to the development of effective watershed management plans and water quality standards to protect aquatic species (Kaushal et al., 2010). In general, with the fact that water temperature is inversely proportional to river flow, reflecting reduced thermal buffering capacity due to decreasing flow rates, increased voyage time, and reduced thermal waste input dilution capacity of water (Moatar and Gailhard, 2006; Albek and Albek, 2009). Based on the global evaluation we can state, that reduction of the flow rate in rivers by 20% and 40%, respectively will increase water temperature by an average of 0.3°C and 0.8°C, another increase of 2 to 6°C can occur due to rising air temperature (van Vliet et al., 2012). Regarding to land use change, many studies indicate that shrinking forest cover (or decreasing vegetation shading) (Pekárová et al., 2011) and urban expansion (or increasing population density) in the area of the watershed, can significantly increase the temperature of the river water (Lepori et al., 2014; Orr et al., 2015). Although the relationship between air and water temperature is generally strong, the strength of such relationships varies regionally and temporally and may vary due to the complementary effects of local hydrology and human activities, such as changes in land use and population, can be of great importance for a site density (Orr et al., 2015; De Weber and Wagner, 2014; Cisty et. al., 2021).

So, for this reason the main task of this study was to better analyze fluctuations in water temperature during the year. The Litava River was chosen to find a model to simulate the relationship between the air temperature and the water temperature. For statistics and plotting the Cran R programing language (R Core Team, 2013) has been chosen because of the its complexity to provide analytical instruments and also great ability to visualize results.

Material and methods

River basin description and data

The Litava River (Slovakia) is a 45.4 km long left tributary of the Krupinica River (Fig. 1). The river has its source in the Krupinská planina in area below a saddle between the mountains Kopaný závoz (775 m a.s.l.) and Jaseňový vrch (724 m a.s.l) and flows initially in an approximately south-southwest direction through Senohrad, takes the Litavica on the left.

Further along, the Litava passes through the municipalities of Lackov, Litava, and Cerovo before continuing into a canyon-like valley and meeting the left-hand Malá Litava. Now the Litava turns to the west and makes its way through the Krupinská planina with five meanders. Then the valley opens to the south-west and the Litava passes the place Drienovo, joins with the right-hand tributary Vrbovok before it flows through Plášťovce and flows into the Krupinica on the left-hand side.

On Fig. 2, the average daily values of air temperature from the station Bzovík (latitude 48° 19’09’’, longitude 19°05’38’’; 355 m a.s.l.), and average daily discharges and water temperature from the gauging station Litava: Plášťovce (7600 – latitude 48°09’25’’, longitude 18°58’18’’) during the years 2006–2020 are presented (database of SHMI (Slovak Hydrometeorological Institute)).

Methods

In the past, linear regression models were often used, which succeeded in simulating stream temperatures with air temperatures when they were above 0°C. When air temperatures are below 0°C, the trend changes significantly, and therefore a new function was introduced to correctly simulate stream temperatures when air temperatures are low. This is mainly because at the highest and lowest air temperatures, the relationship between stream temperature and air temperature usually remains linear. The water – air temperature relationship can be well described by a continuous S-shaped function. Several mathematical functions were tested to represent this relationship, but the logistic function parameters are the most stable and its parameters have physical meaning Ratkowsky (1987)

$$To = \frac{\alpha}{1+e^{\gamma(\beta-Ta)}}, \quad (1)$$

where:

To – represents the average daily water temperature,

Ta – represents the average daily air temperature,

α – coefficient which estimates the highest value of water temperature,

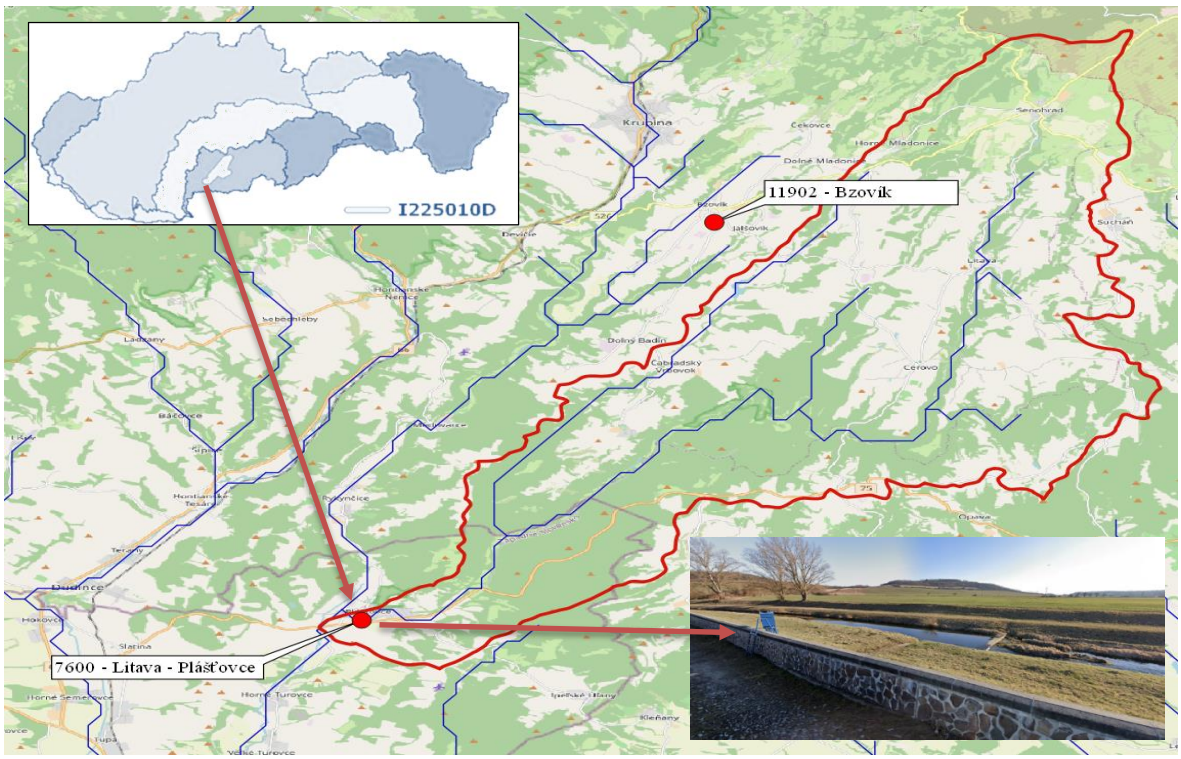

Fig. 1. Scheme of the Litava basin, Slovakia. Gauging station, SHMI Litava: Plášťovce, (Photo: Google Maps, 2022).

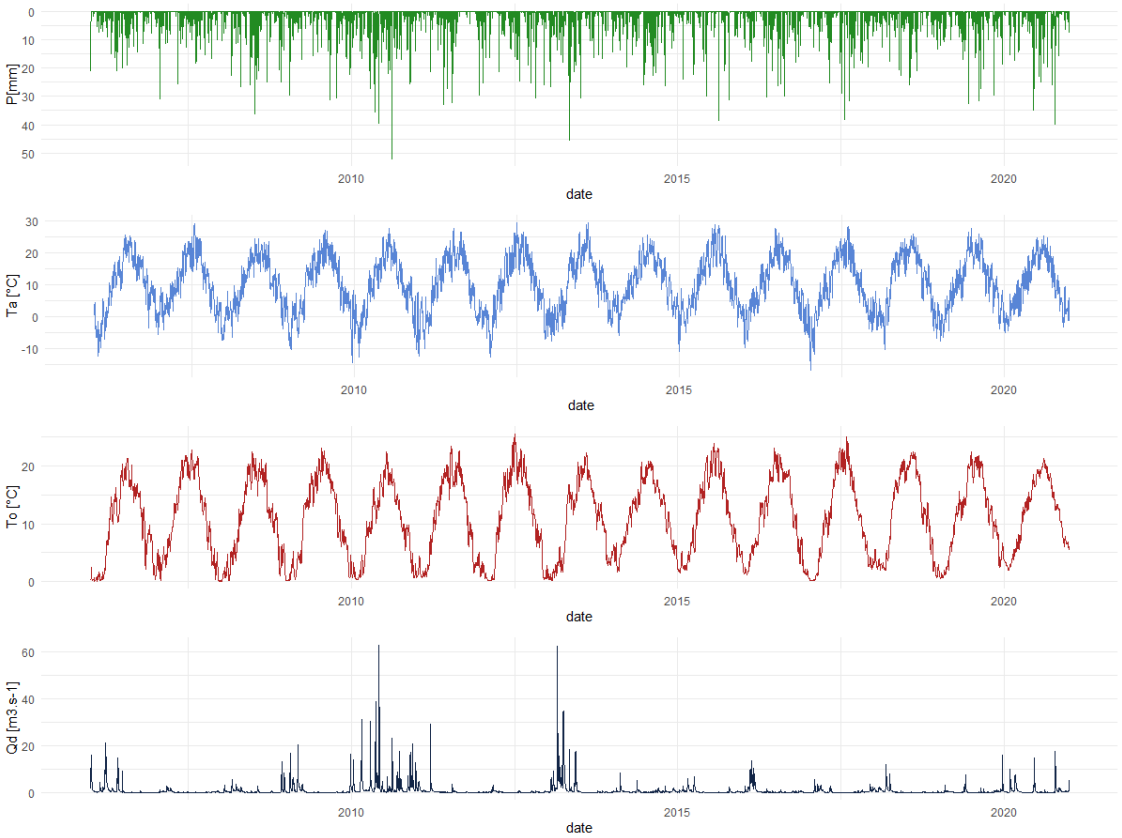

Fig. 2. Daily average water temperature To [°C], and daily average discharge Q [$m^3 s^{-1}$] of the Litava River at the Plášťovce station, the daily air temperature Ta [°C]and precipitation P [mm]at the Bzovik climatic station plotted for the period 2006–2020.

β – is the avarage daily air temperature at the inflection point,
γ – function of the steepest slope of the logistic function.

The basic logistic regression model proposed by Mohseni et al. (1998) for weekly data relates the stream water temperature with air temperature by using the following equation

$$To = c + \frac{d-c}{1+e^{(b.(Ta-e)}}, \quad (2)$$

where:
To – is the stream water temperature;
Ta – is the air temperature (the only input variable);
b, c, d, e – are four model parameters.

(Note that we use a different notation than Mohseni et al. (1998) to simplify the plot), which shows the lower (*a*) and upper (*b*) limits of water temperature, the slope at the inflection point of the logistic regression (*c*), and the air temperature at the inflection point (*d*). The parameter *c* can be estimated or it can be chosen directly.

Results

Statistical analysis of observed data

The water temperature of the Litava River depends mainly on air temperature and river bed temperature. Also groundwater inflows or spring-ups are thought to influence the surface water temperature of the Litava River. The water temperature is more stable than air temperature. The mean annual water temperatures exhibit a substantially lower range, in comparison with annual readings of air temperatures. Table 1 summarizes the descriptive statistical characteristics of water and air temperature time series for the 2006–2020 period. Long-term mean of water temperature at the Plášťovce gauging station for the 2006–2020 period was 10.95°C, and 9.94°C for air temperature in station Bzovík. It is in agreement with previous findings (Pekárová et al., 2011) that water temperature of a stream is determined by the air temperature of the environment through which it flows. This fact is of high relevance for indirect estimates of water temperature in streams using only air temperature observations.
The histogram of daily temperatures (Fig. 3) shows that the water temperature time series (similarly to the daily air temperatures) exhibit a bimodal distribution.

Daily fluctuation of water temperature

Both water and air temperature series show diurnal (daily) patterns. Daily fluctuations are, in general, higher in smaller streams, and also in deforested areas, where the bank vegetation does not prevent water against overheating during the day. The streams have their springs at higher altitudes from where they flow to lower locations, which causes a longitudinal increase in stream water temperature. Low temperature fluctuations are typical for large rivers, or for small streams close to their springs. This is because groundwater temperature – their main source of inflow, only slightly differs from the local mean yearly temperature. On the Figure 4 you can see the course of water temperature and air temperature in an hourly step during two periods in the month of September 2022. In the first series, it was a stable weather with a typical course of air and water temperatures, where the daily maximum air temperature is approximately between 1–2 pm and the maximum water temperature is between 6–8 pm. In the second case (September 17–20, 2022), there was a change in weather and also a change in the trend of daily temperature in the stream, where the typical diurnal variation practically does not occur, but the temperature drops linearly. Also considering this trend, we decided to use the diurnal step data for the analysis.

Model analysis and selection

In Tables 2–4 we can see the individual parameters of the regression models for the selected months. Table 2 shows the parameters for the whole data set and for

Table 1. Basic statistical characteristics of the daily water temperature in the Litava River *To* [°C], and daily air temperature in Bzovik Station *Ta* [°C] for the period 2006–2020

Characteristics	*To* Litava River	*Ta* Bzovik Station
Count	5479	5479
Mean	10.92	9.94
Minimum	0.00	-16.9
Maximum	25.6	29.4
Standard error	0.0917	0.1162
Median	11.4	10.3
Standard deviation	6.7922	8.602
Kurtosis	1.7004	2.1703
Skewness	-0.0284	-0.1340

selected monthly seasons (September – February and March – August).

The aim was to divide the year into a colder and a warmer period and thus to capture the hysteresis of the given data in the logistic regression curve, which we can also see in the graphs in Fig. 5 and 6. In Fig. 5 we can see a logistic regression curve from daily data for the whole period and in Fig. 6 for selected intervals of months.

After we have assessed these data, it was decided to divide the data into 4 series by seasons, specifically: December to February, March to May, June to August, and September to November. The parameters of the logistic regression function for these periods are listed in Table 3 and 4 and the logistic functions are shown in Fig. 7. As we can see, the shape of the curve is practically the same only for the months of December to February and March to May. If we consider the period from June to August, it does not reach the shape typical for logistic regression model, and during the months of September to November regression is almost linear. In general, we can conclude that the logistic regression model, divided into these 4 periods, has been refined.

Our goal was to find a model that can simulate the effect of air temperature growth to the water temperature in the Litava River. Since we are particularly interested in high air temperatures during summer heat and low flows, the above analyzes demonstrate that it is enough to use a linear model for data in the months of June-August. In the next step, we will add the effect of discharges on the water temperature in this model.

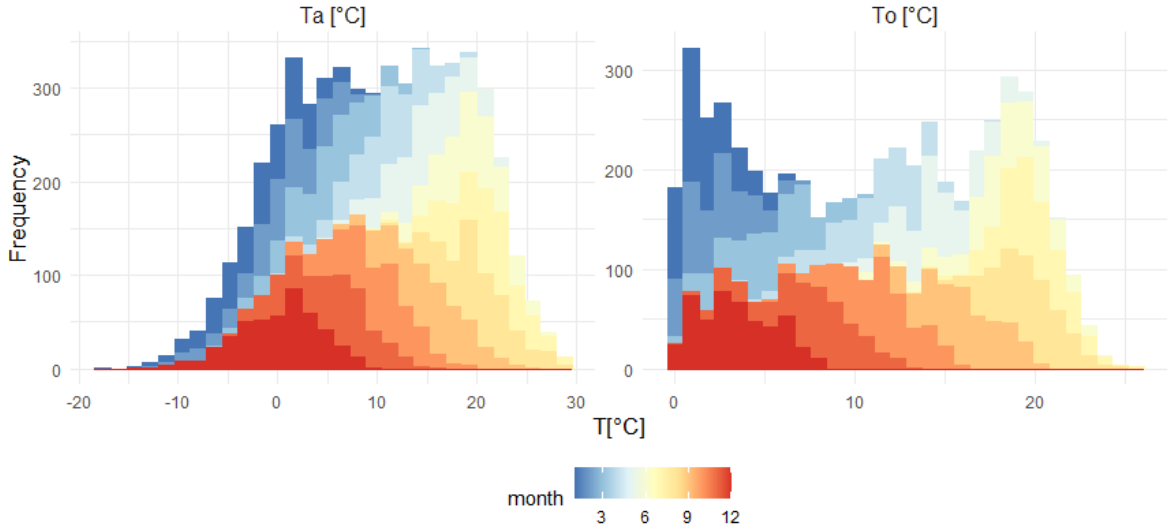

Fig. 3. Monthly histograms of average daily water (To) and air (Ta) temperature measured in the Litava River at station Plášťovce and Bzovik meteorological station, generated for the period 2006–2020.

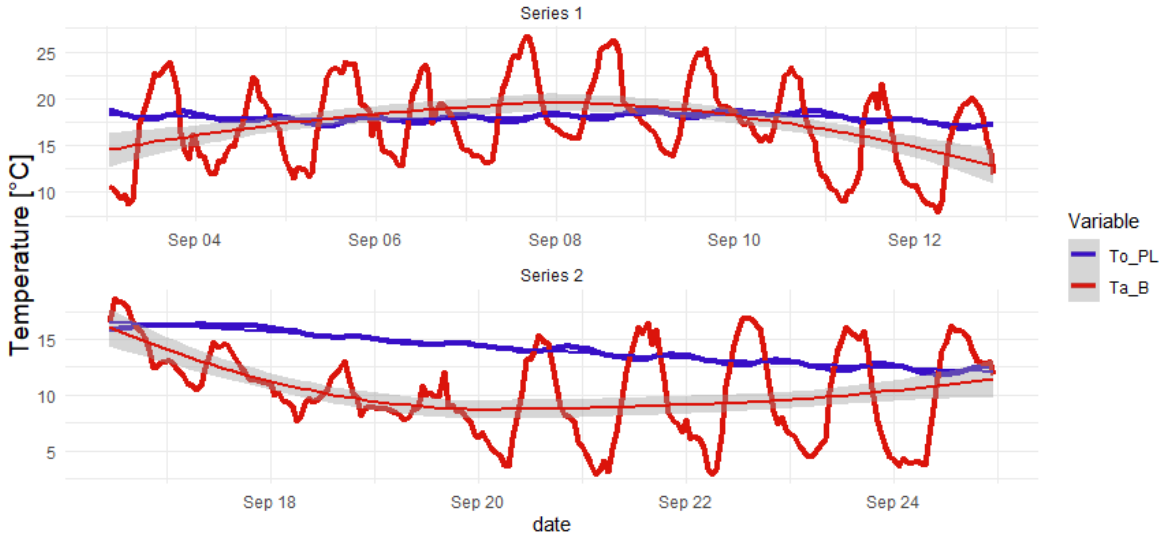

Fig. 4. Comparison of the water (To_PL, Litava: Plášťovce) and air (Ta_B, Bzovik) temperatures in the hourly time step (September 2022) polynomial trends.

Table 2. Regression model parameter for given period

	Complete dataset			September – February			March – August		
Parameter	**Estimate**	Std. Error	*t*-value	**Estimate**	Std. Error	*t*-value	**Estimate**	Std. Error	*t*-value
b	**-0.1630**	0.0040	-40.5624	**-0.2118**	0.0083	-25.6457	**-0.1690**	0.0078	-21.6569
c	**-0.7143**	0.1887	-3.7845	**0.1043**	0.1824	0.5718	**0.0269**	0.5095	0.0528
d	**23.0353**	0.2336	98.6023	**19.2269**	0.3517	54.6738	**23.1709**	0.3189	72.6576
e	**10.3963**	0.1273	81.6499	**8.5100**	0.1876	45.3635	**10.9980**	0.2318	47.4461
RSE		2.071349			2.06159			2.055851	

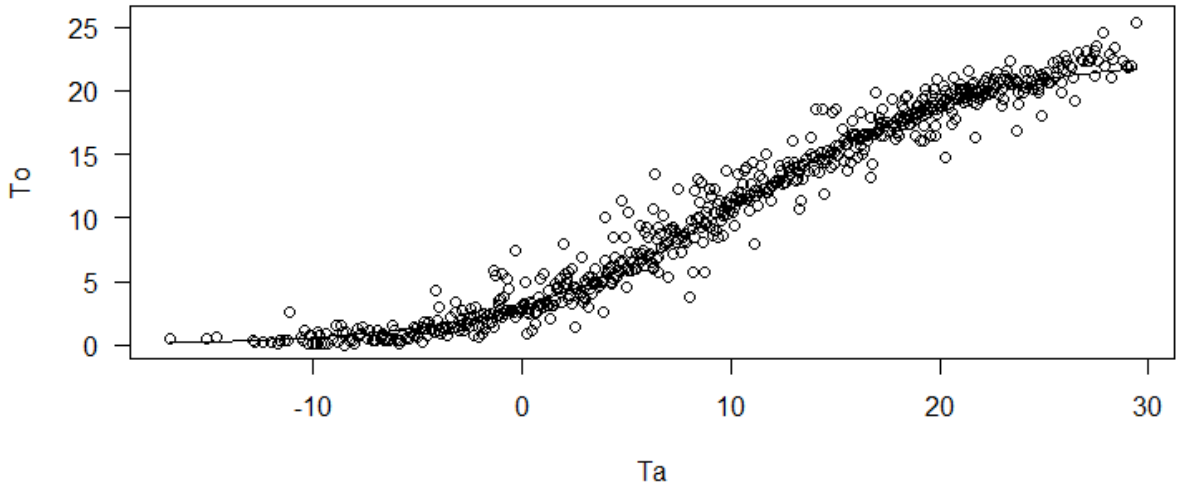

Fig. 5. Relationships between air Ta and water To temperature logistic (Mohseni) S-shaped regression. Daily values (2006–2020) To from Litava River (water gauging Plášťovce) and Ta Bzovik meteorological station.

Table 3. Regression model parameter for given periods (2006–2020)

	Months 12–2			Months 3–5		
Parameter	**Estimate**	Std. Error	*t*-value	**Estimate**	Std. Error	*t*-value
b	**-0.2267**	0.0493	-4.5946	**-0.1476**	0.0174	-8.4617
c	**0.0955**	0.3275	0.2918	**-1.3740**	1.1033	-1.2454
d	**6.4543**	0.9733	6.6317	**21.0219**	1.1403	18.4340
e	**2.3453**	1.1835	1.9817	**9.3481**	0.4956	18.8614
RSE		1.461298			2.126676	

Table 4. Regression model parameter for given periods (2006-2020)

	Months 6–8			Months 9–11		
Parameter	**Estimate**	Std. Error	*t*-value	**Estimate**	Std. Error	*t*-value
b	**- 0.0653**	0.0087	-7.5314	**- 0.0882**	0.0222	- 3.9613
c	**- 36.055**	23.0553	23.0553	**- 4.4801**	3.7653	- 1.1898
d	**26.5901**	1.3864	1.3865	**26.9152**	3.6071	7.4617
e	**- 11.019**	6.944	6.944	**9.4498**	1.1443	8.2575
RSE		1.607269			1.8802	

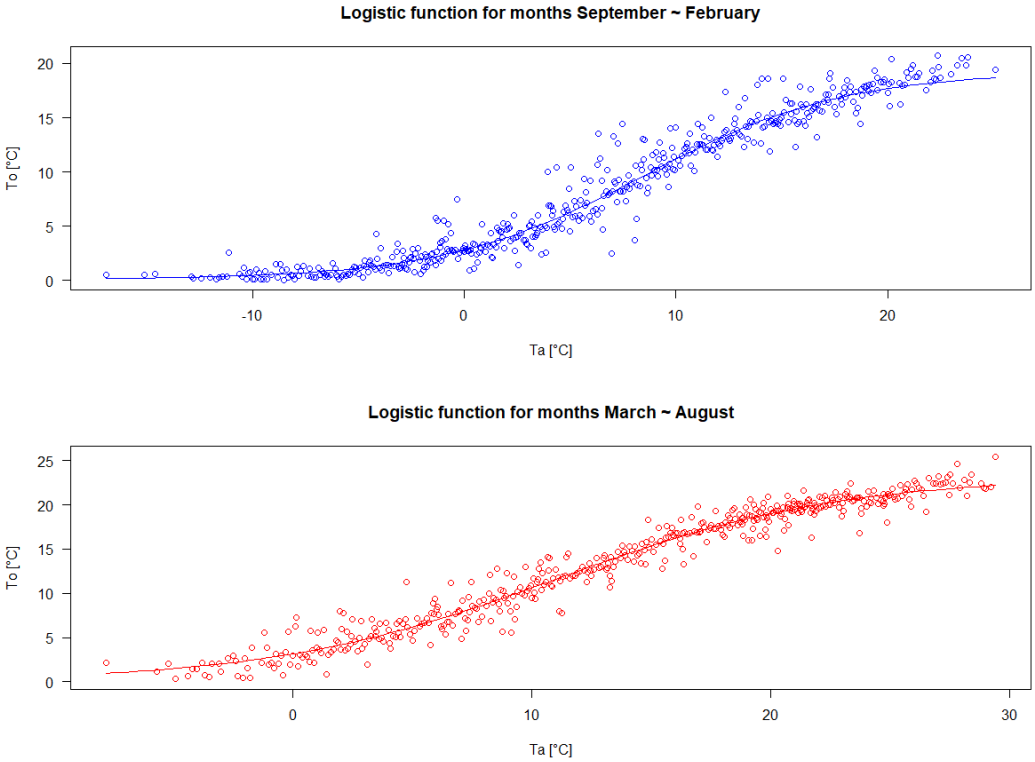

Fig. 6. Relationships between air and water temperature logistic (Mohseni) S-shaped regression. Daily values are splitted into two series according seasons, period 2006–2020.

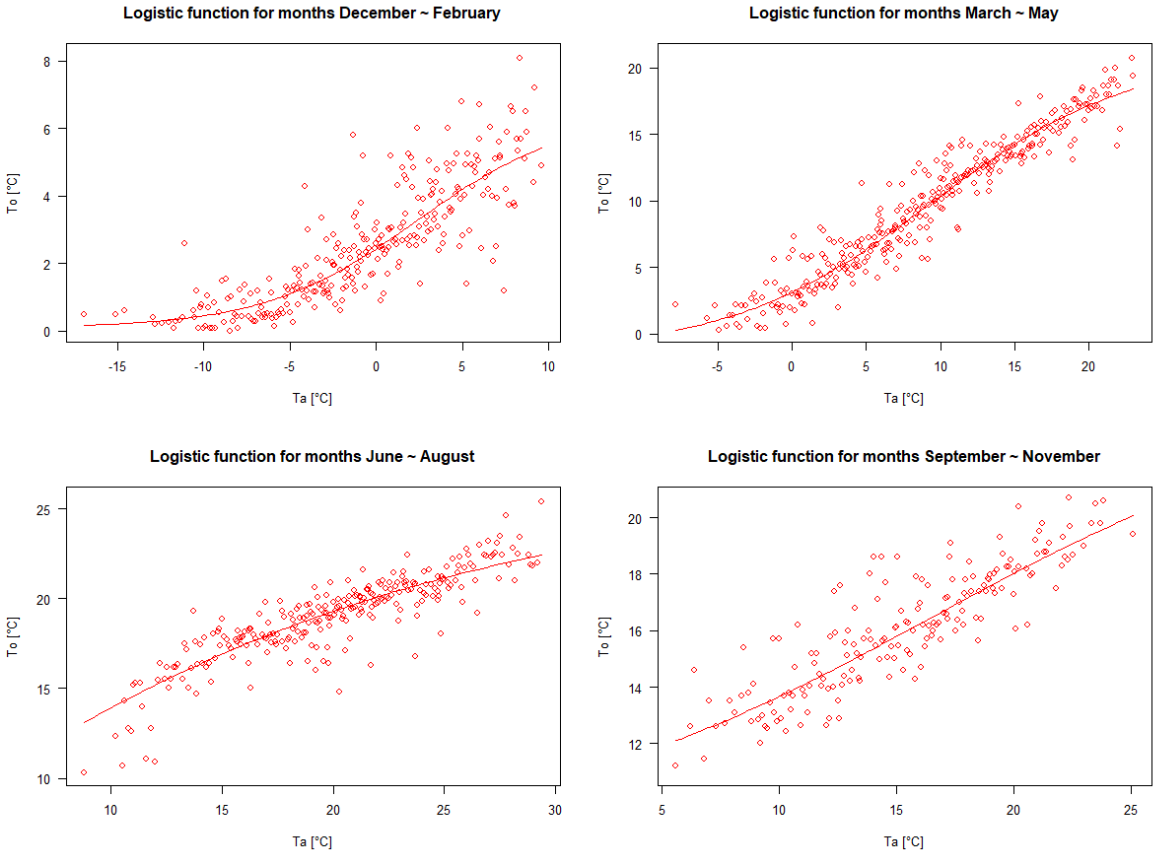

Fig. 7. Relationships between air and water temperature, logistic (Mohseni) S-shaped regression. Daily values (splitted into four series by seasons, period 2006–2020).

Conclusion

Both climatic changes and anthropogenic aspects affect the temperature of the stream. For this reason, it is very important for the future evaluation and prediction of the evolution of water temperature in rivers to know the dependence of water temperature on air temperature, which is also an ideal starting point for prediction models, given its availability and the amount of data from the station network. The logistic regression model used in the work was that of Mohseni et al. (1998). This model proved to be optimal for the purposes of this study. In this work, we examined daily temperature for the Litava River for the period 2006–2020, relying on data from the Plášťovce water gauging station and the Bzovík climate station.

We examined the effects of the data collection interval when we evaluated two short periods in the month of September 2022. For these two periods, we focused on the meteorological conditions. In the first series it was a period with a stable weather trend, where a typical diurnal step of the temperature in the frame of the bottom was captured by standard peaks of the daily maximum and minimum. In the second case, when the cooling occurred, a linear decrease in water temperature was recorded, which directly depended on the decrease in air temperature. Based on these facts, we decided to use the data in the given daily step in the next work.

In the next step, we focused on seasonality, the effects of which on the given logistic regression model have been little explored in the literature. In most cases, the models use data in the daily or weekly step, without taking into account the influence of the particular phase of the year. For this reason, we decided to explore two alternatives. In the first case, we divided the year into two seasons, September to February and March to August. In this case there was only a slight improvement, so in the next step we decided to divide the year into four seasons, largely copying the distribution of the annual periods. In this case, there was an improvement in the logistic regression model in three of the four periods. The only period in which there was virtually no improvement in the parameters was the period from March to May. For comparison, we created a logistic regression model for the entire observed period without dividing it into individual seasons. From the results presented, we can see the effects of seasonality on the estimation of water temperature in the river. It proved practical to divide the period into four periods when the model was refined to three of them. It follows that we need to examine more closely the effects of seasonality on our own control models, then on the transition from winter to spring months. In the future, we will add the effect of discharges on the water temperature in this model.

Acknowledgement

This research is supported by the project WATSIM "Water temperature simulation during summer low flow conditions in the Danube basin", and project APVV-20-0374 "Regional detection, attribution and projection of impacts of climate variability and climate change on runoff regimes in Slovakia".

References

Ahmadi-Nedushan, B., St-Hilaire, A., Ouarda, T. B. M. J., Bilodeau, L., Robichaud, É., Thiémonge, N., Bobée, B. (2007): Predicting river water temperatures using stochastic models: case study of the Moisie River (Québec, Canada) Hydrological Processes, 21, 1, 21–34 http://dx.doi.org/10.1002/hyp.6353

Albek, M., Albek, E. (2009): Stream temperature trends in Turkey. CLEAN –Soil, Air, Water 37, 142–149. https://doi.org/10.1002/clen.200700159

Benyahya, L., Caissie, D., El-Jabi, N., Satish, M. G. (2010): Comparison of microclimate vs. remote meteorological data and results applied to a water temperature model (Miramichi River, Canada). Journal of Hydrology, 380, 3–4, 247–259, https://doi.org/10.1016/j.jhydrol. 2009.10.039

Caissie, D. (2006): The thermal regime of rivers: a review. Freshwater Biology, 51, 1389–1406, https://doi.org/ 10.1111/j.1365-2427.2006.01597.x

Cisty, M., Soldanova, V., Cyprich, F., Holubova, K., Simor, V. (2021): Suspended sediment modelling with hydrological and climate input data. Journal of Hydroinformatics 23, 192–210, https://doi.org/10.2166/ hydro.2020.116

DeWeber, J. T., Wagner, T. (2014): A regional neural network ensemble for predicting mean daily river water temperature. J. Hydrol. 517, 187–200, https://doi.org/ 10.1016/j.jhydrol.2014.05.035

Grbić, R., Kurtagić, D., Slišković, D. (2013): Stream water temperature prediction based on Gaussian process regression, Expert Systems with Applications, 40,7407–7414, https://doi.org/10.1016/j.eswa.2013.06.077

Isaak, D., J., Wenger, S. J., Peterson, E. E., ver Hoef, J. M., Nagel, D. E., Luce, C. H., Hostetler, S. W., Dunham, J. B., Roper, B. B., Wollrab, S. P., Chandler, G. L., Horan, D. L., Parkes Payne, S. (2017): The NorWeST Summer Stream Temperature Model and Scenarios for the Western U.S.: A Crowd-Sourced Database and New Geospatial Tools Foster a User Community and Predict Broad Climate Warming of Rivers and Streams. Water Resources Research 53, 9181–9205, 10.1002/ 2017WR020969

Kaushal, S. S., Likens, G. E., Jaworski, A. N., Pace, L. M., Sides, M. A., Seekell, D., Belt, T. K., Secor, H. D., Wingate, R. (2010): Rising stream and river temperatures in the United States. Front Ecol Environ. 461–466, https://doi: 10.1890/090037

Lepori, F., Pozzoni, M., Pera, S. (2014): What drives warming trends in streams? A case study from the Alpine Foothills. River Res. Applic. https://doi.org/10.1002/rra.2763

Lešková, D., Škoda, P. (2003): Temperature series trends of Slovak rivers. Meteorologický časopis, 6, 2, 2003, 13–17.

Maier, H. R., Dandy, G. C. (2000): Neural Networks for the Prediction and Forecasting of Water Resources Variables: A Review of Modelling Issues and Applications. Environmental Modelling & Software, 15, 101–124. https://doi.org/10.1016/S1364-8152(99)00007-9

Moatar, F., Gailhard, J. (2006): Water temperature behaviour in the River Loire since 1976 and 1881. C. R. Geosci. 338, 319–328, https://doi.org/10.1016/j.crte.2006.02.011

Mohseni, O., Stefan, H. G. (1999): Stream temperature / air

temperature relationship: a physical interpretation. Journal of Hydrology 218: 128–141, https://doi.org/10.1016/S0022-1694(99)00034-7

Mohseni, O., Stefan, H. G., Erickson, T. R. (1998): A nonlinear regression model for weekly stream temperatures. Water Resource Research, 34, 10, 2685–2692, https://doi.org/10.1029/98WR01877

Morrill, J. C., Bales, R. C., Conklin, N. H. (2005): Estimating stream temperature from air temperature: Implications for future water quality. J. Environ. Eng. 131, 139–146, DOI:10.1061/(ASCE)0733-9372(2005)131:1(139)

R Core Team (2013): R: A language and environment for statistical computing. R Foundation for Statistical Computing, Vienna, Austria. URL http://www.R-project.org/

Orr, H. G., Simpson, G. L., Des Clers, S., Watts, G., Hughes, M., Hannaford, J., Dunbar, M. J., Laizé, C. L. R., Wilby, R. L., Battarbee, R. W., Evans, R. (2015). Detecting changing river temper-atures in England and Wales. Hydrological Processes, 29, 752–766, https://doi.org/10.1002/hyp.10181

Pekárová, P., Miklánek, P., Halmová, D., Onderka, M., Pekár, J., Kučárová, K., Liová, S., Škoda, P. (2011): Long-term trend and multi-annual variability of water temperature in the pristine Bela River basin (Slovakia). J. of Hydrol., 400, 333–340. ISSN 0022-1694. https://doi.org/10.1016/j.jhydrol.2011.01.048

Piccolroaz, S. (2016): Prediction of lake surface temperature using the air2water model: guidelines, challenges, and future perspectives. Adv. Oceanogr. Limnol., 7, 1, 36–50, DOI:10.4081/aiol.2016.5791

Plastovce – Litava [Street view].(2022), from https://www.google.com/maps/@48.1568829,18.972217,3a,75y,275.64h, 93t/dat a = !3m6!1e1!3m4!1sY51aFOguz2U8x7EtsGxZMQ!2e0!7i16384!8i8192).

Ratkowsky, D. A. (1987): Nonlinear Regression Modelling, Marcel Dekker, New York, 1983.

van Vliet, M. T. H., Franssen, W. H. P., Yearsley, J. R., Ludwig, F., Haddeland, I., Lettenmaier, D. P., Kabat, P. (2013): Global river discharge and water temperature under climate change. Global Environ. Change 23, 450–464, https://doi.org/10.1016/j.gloenvcha.2012.11.002

van Vliet, M. T. H., Yearsley, J. R., Franssen, W. H. P., Ludwig, F., Haddeland, I., Lettenmaier, D. P., Kabat, P. (2012): Coupled daily streamflow and water temperature modelling in large river basins. Hydrol. Earth Syst. Sci., 16, 4303–4321, https://doi.org/10.5194/hess-16-4303-2012

Webb, B. W., Hannah, D. M., Moore, R. D., Brown, L. E., Nobilis, F. (2008): Recent advances in stream and river temperature research. Hydrological Processes, 22, 902 – 918, https://doi.org/10.1002/hyp.6994

Zhu, S., Nyarko, E. K., Hadzima-Nyarko, M. (2018): Modelling daily water temperature from air temperature for the Missouri River. PeerJ. 6. 10.7717/peerj.4894, https://doi.org/10.7717/peerj.4894

Ing. Zbyněk Bajtek, PhD (*corresponding author, e-mail: bajtek@uh.savba.sk)
RNDr. Pavla Pekárová, DrSc.
Institute of Hydrology SAS
Dúbravská cesta 9
841 04 Bratislava
Slovak Republic

Ing. Katarína Jeneiová, PhD.
Mgr. Jakub Ridzoň
Slovak Hydrometeorological Institute
Jeséniova 17
833 15 Bratislava
Slovak Republic

DOI: 10.31577/ahs-2022-0023.02.0035

ACTA HYDROLOGICA SLOVACA

Volume 23, No. 2, 2022, 305–316

Three-dimensional numerical modeling of water temperature distribution in the Rozgrund Reservoir, Slovakia

Saeid OKHRAVI*, Marek SOKÁČ, Yvetta VELÍSKOVÁ

The Rozgrund water reservoir is one of the oldest reservoirs of the water supply system in the vicinity of Banská Štiavnica. In the past, it was one of the important reservoirs supplying the population with drinking water. Knowing the spatial and temporal variations of water temperature in the reservoir is the primary step to investigate and model water quality. Therefore, the present study was planned to simulate water temperature distribution in the Rozgrund Reservoir by incorporating atmospheric and bathymetric conditions using MIKE 3 FM model and took a step forward to model extreme hydrological and meteorological events impacts. The simulations were performed for July 2022 and the model provided 3D visualization of water temperature variations and corresponding temporal differences during the entire simulated period. The results revealed that the Rozgrund Reservoir experienced temperature stratification (i.e. non-isothermal layers) in the period of simulation when the initial temperature was given to the model, while the constant initial temperature condition needs a long time to reproduce water temperature stratification. In addition, this study assessed the impacts of high inflows on patterns of current flows and water temperature throughout the Rozgrund Reservoir. The present work has implications for improving the understanding of changes in water temperature distribution in the Rozgrund Reservoir and similar reservoirs and supports further works, as well.

KEY WORDS: 3D hydrodynamic model, Rozgrund Reservoir, spatial and temporal variability, water temperature distribution and stratification

Introduction

The reservoirs in Slovakia are part of a water impoundment system commonly used for domestic, drinking, irrigation and industrial purposes as well as for flood control (Negm and Zeleňáková, 2019). They have stored more than 1,890 M m^3 of water in Slovakia together with dams (GWP, 2011). Water temperature is a key variable in the hydrodynamic and water quality conditions of a reservoir. Additionally, water temperature plays an important role in the water flowing and mixing processes due to a developed cycle of temperature stratification, influencing the reservoir ecosystem functioning (Hlevca et al., 2015). The thermal structure of the reservoirs is relevant to internal influences such as lake morphometry (Han et al., 2000) and external influences such as wind forces, precipitation and heat exchange (Helfer et al., 2010).

There are a number of studies that have investigated reservoir water temperature distribution illustrating that all physical-chemical-biological processes are influencing temperature stratification and mixing processes (Lawson and Anderson, 2007; Kirillin and Shatwell, 2016; Zhang et al., 2020). The temperature stratification is subject to change by processes affecting heat transfer through the surface layer of a reservoir. These processes include heat exchange, heat flux caused by evaporation and precipitation and wave radiations from the sun, atmosphere and surface waters nearby (Boehrer and Schultze, 2008). The deep layers are less affected by mentioned processes and mainly influenced by turbulence, wind-induced currents and heat diffusion (Zhang et al., 2020). The temperature differences between the surface layer and deep layers result in water density stratification which introduces positive buoyancy gradients and directly affects reservoir hydrodynamic conditions (Kirillin, 2010).

Reservoirs consist of the main inflow with many tributaries and an outflow located near the dam wall such that three distinct zones in reservoirs are formed as riverine, transition and lacustrine. The longitudinal features in morphology, hydrodynamic and water quality properties are different in these three zones (Ji, 2017). The difference in water temperature between the inflow and reservoir water reverses the inflow current direction, known as thermocline erosion which significantly influences water temperature distribution over the transition and lacustrine zones (Zhang et al., 2020). Hence, three-dimensional (3D) numerical tools are useful to depict water temperature distribution in reservoirs and

decipher the temperature stratification. The vertical variations of water temperature in reservoirs are commonly measured by high-frequency in situ sensors (Webb et al., 2008) and more recently by the use of remote sensing methods (Sima et al., 2013). Nevertheless, both methods reflected flaws in visualizing the horizontal plane and vertical distribution of the water temperature. Sensor device suffers from the horizontal measurement of water temperature, and the remote sensing method is just only applicable for short-time monitoring of water temperature variations due to the coarse temporal resolution. To better understand spatial and temporal variations in water temperature over entire reservoirs and employ frequent changes in the heat exchange and flow pattern as well as changes in the morphological features of the reservoirs, hydrodynamic models have become powerful tools for representing present or future conditions of reservoirs.

Numerical hydrodynamic modeling has been widely applied for simulating the water movements within reservoirs (Zhang and Chan, 2003; Chao et al., 2010; Torriano et al., 2012; Zhang et al., 2020). León et al. (2007) and Li et al. (2018) have simulated spatial and temporal variations of water temperature using hydrodynamic models. Other water temperature modeling studies e.g. Mahanty et al. (2016) found that spatial variations of water temperature have been greatly influenced by wind forces and meteorological conditions. The study of Li et al. (2017) has numerically evaluated the dominant factors influencing water temperature stratification of Poyang Lake, China through the 2D hydrodynamic model MIKE 21. Zhang et al. (2020) have also investigated the thermal structure of a drinking water reservoir in Tarago, Australia, and shown the impacts of rainfall and wind on water temperature stratification using a 3D version of MIKE. In a recent study, Dadashzadeh et al. (2021) simulated flow patterns and water temperature distribution over a very large lake in Iran (Urmia Lake) with MIKE 3 to investigate the effects of a causeway structure located in the middle of the lake. The above-mentioned research studies have shown the strong applicability of using 3D numerical models for the investigation of water temperature stratification in natural water bodies like reservoirs. To date, the literature on water temperature distribution is less consistent in reservoirs and further studies should address horizontal and vertical variations of water temperature over morphological changes, and extreme meteorological and hydrological conditions with special attention to water quality properties.

The main objective of this study is to investigate and simulate the water quality of the Rozgrund Reservoir in Slovakia, mainly an indicator of water temperature. Rozgrund Reservoir was critical for domestic use in the previous time when it served as a reservoir for drinking supply, nowadays is in standby mode. The water temperature variations act as a basic element of water quality control such that the investigation of the spatial and temporal water temperature distribution and water temperature stratification in the Rozgrund Reservoir is of paramount importance. Also, Rozgrund is an example of a reservoir subjected to significant changes in water quality due to the seasonally dynamic river-reservoir system, hydrological events, and the size, shape and morphological conditions. Therefore, the goal of this study was to simulate the horizontal and vertical variations of water temperature during the summer time, for example specifically for July 2022 in the Rozgrund Reservoir as the preliminary stage for a greater simulation of water quality for strategic reservoirs in Slovakia with the purpose of the water resources management in extreme events. Accordingly, the present study used and validated the MIKE 3 hydrodynamic model to follow these specific goals:

1) visualizing hydrodynamic data and flow behavior using field measurements,
2) investigating spatial and temporal water temperature distribution over the reservoir using the simulation results,
3) exploring the effects of extreme hydro-meteorological events on water temperature distribution and stratification in the reservoir.

Study domain and material

Study area

The Rozgrund Reservoir is part of the Hron basin with a location of 6154800N and 2101200E (projection system: WGS84/World Mercator) and is approximately 6.5 km northwest of Banská Štiavnica in central Slovakia and has a maximum capacity of 960,000 m^3 of freshwater (Fig. 1), but current water storage is about 430,000–515,000 m^3. It was built in 1,744 to collect water for domestic people in the vicinity and the maximum depth of the reservoir is approximately 21 m near the earthen dam wall. The Rozgrund surface area in flooded conditions at the maximum allowed level is 53,820 m^2, almost 5.4 hectares (Fendek, 2019). The annual temperature range is -3 to 19°C and the average annual rainfall is about 950 mm. The reservoir is surrounded by mountains; the maximum water level in the reservoir is 705 m above mean sea level (amsl) and the elevation of the top of its dam is 706.20 m amsl. The Rozgrund Reservoir was the highest earthen dam in Europe until the second half of the 19th century and in former Czechoslovakia until the second half of the 20th century. The Rozgrund Reservoir used to provide a significant drinking water resource for the town of Banská Štiavnica since the beginning of the 20th century until the recent past. Currently, the Rozgrund Reservoir serves as a standby source of drinking water, for flood protection purposes and fish breeding with the aim of increasing the water quality in the reservoir through the biological system of the reservoir. The reservoir is characterized by lacustrine and riverine morphological processes that exhibit distinct seasonal variations (Chen et al., 2011). The reservoir receives inflow predominantly from two sources fed by creeks (small streams) (Fig. 1) as well as groundwater flow, rainfall, minor stream discharges and small ditches. The shape of the reservoir is narrow and long and its water depth gradually increases from the main inflow to outflow, reaching its maximum near the dam. Water surface elevation drop can be up to

approximately a level of 693 m amsl in the dry period.

Data availability

The bathymetry measurements of the Rozgrund Reservoir were carried out using an AUV (autonomous underwater vehicle) of type EcoMapper (manufactured by YSI) (https://www.ysi.com/ecomapper). The meteorological conditions of the reservoir, such as air temperature and precipitation were provided from the gauging station directly at the Rozgrund Reservoir locality. Additionally, this station provided daily records of water temperature and in-and-out flow discharge of the Rozgrund Reservoir. Other meteorological terms such as relative humidity, clearness, wind speed, and wind direction are available from the meteorological stations at Banská Štiavnica and Vyhne. We also performed measurements of water temperature in several vertical profiles during the field measurements on July 28 this year. The multi-parameter water quality probe (YSI Professional) was installed on the boat and the water temperature below the surface was measured by this vertical profiling system (Fig. 2). Fig. 3 shows the measured vertical variations of water temperature for the date 28/07/2022. Because the Rozgrund Reservoir is relatively large (Li et al., 2017), it could be assumed that the reservoir does not experience large daily changes in water temperature.

Methodology

3D hydrodynamic model description

The present study adopted the three-dimensional simulation model of DHI company, MIKE 3D FM (flexible mesh), to simulate the spatial and temporal variations of water temperature in the Rozgrund Reservoir by solving differential equations describing flow dynamics (integration of momentum and continuity), advection and dispersion, heat exchange and other processes driven by physical and climate conditions of the modeled reservoir. The mathematical foundation of the governing equations is based on the hydrodynamic module for solving 3D incompressible Reynolds Averaged Navier-Stokes (RANS) equations with the assumption of hydrostatic pressure together with a turbulent closure scheme and variable density, and the conservations of mass, momentum, temperature and salinity (DHI, 2017). Thus, the dynamically-coupled transport equations for water levels, velocity and temperature under external forces such as river inflows will result in the simulation of flow and temperature distribution in a 3D waterbody.

The heat exchange in the model must be included to represent the interaction of heat in the water with the atmosphere. The heat exchange calculation is based on four processes: latent heat flux (evaporation), sensible heat (convection), short wave radiation and long wave radiation. The heat exchange has a significant effect on water temperature simulation. In this study, the default values of latent heat, sensible heat, short and long wave radiations were used, while the constant values for the atmospheric conditions including relative humidity and clearness coefficient were set up to 71% and 60.4% according to mean values driven from data between 1991–2021 by the meteorological stations at Banská Štiavnica and Vyhne. In addition, the air temperature was included in the atmospheric conditions according to the daily averaged data series (Fig. 4).

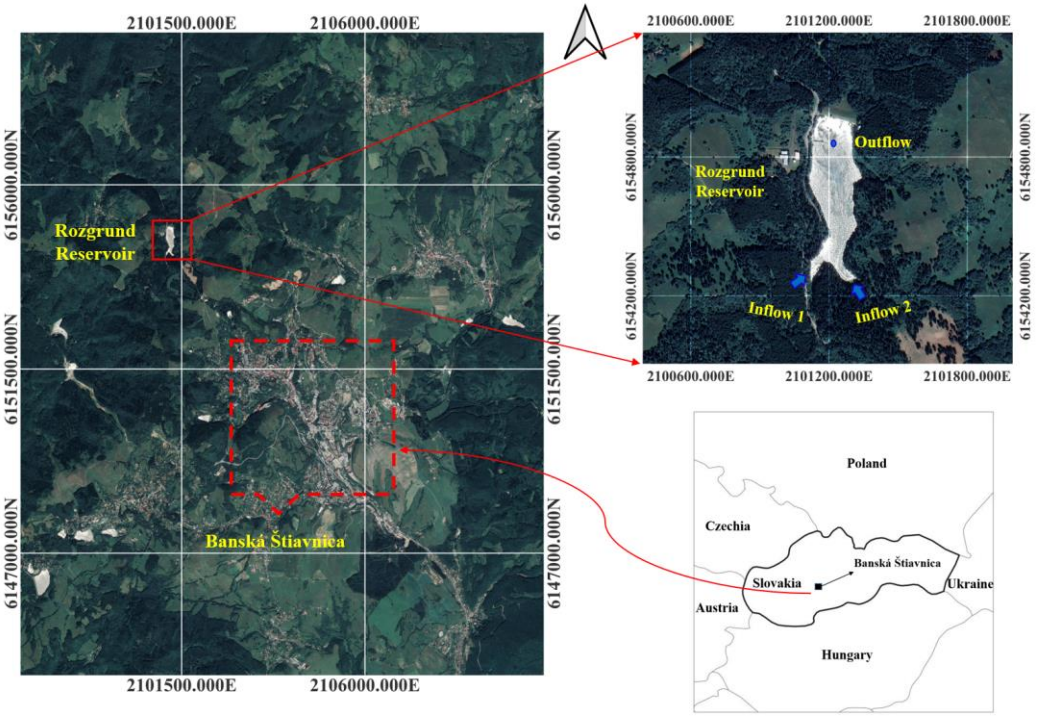

Fig. 1. Geographical map showing the location and shape of the Rozgrund Reservoir (map data: Google).

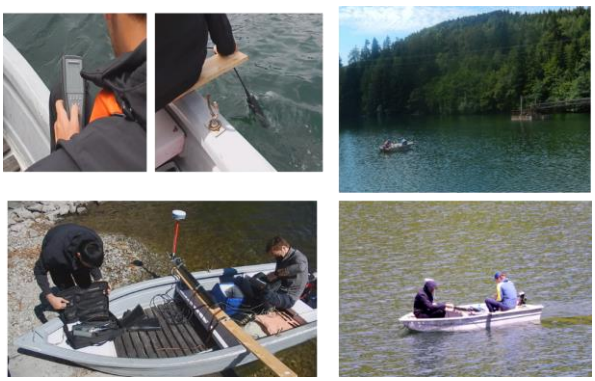

Fig. 2. Field boat measurements of vertical water temperature profiles in the Rozgrund Reservoir.

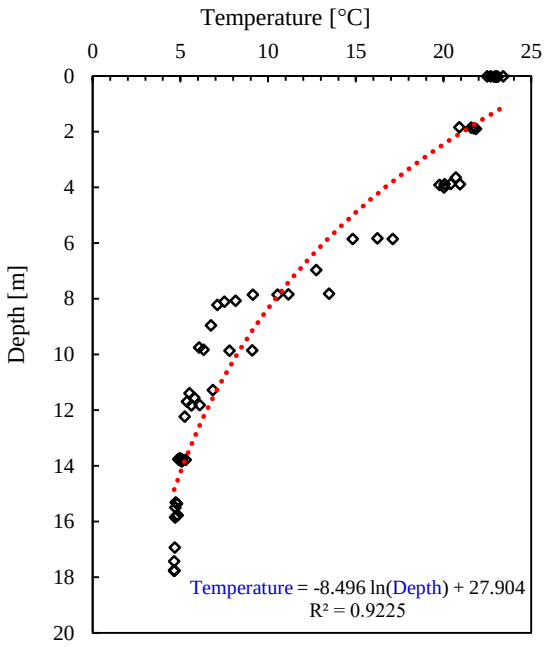

Fig. 3. Vertical changes in water temperature in July 2022 at the Rozgrund Reservoir.

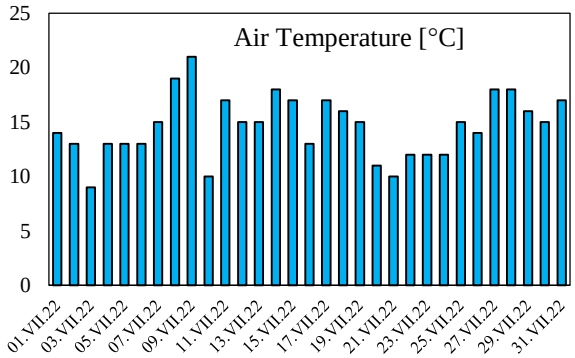

Fig. 4. Air temperature variations in July 2022.

Reservoir bathymetry and grid quality

The measured bathymetry (Fig. 5) data was used to make a flexible unstructured mesh of variable cell sizes. The grid map includes element sizes that vary between 5–15 m, resulting in a total number of 1159 nodes and 2057 triangular elements. The vertical distance was discretized uniformly with 1 m by a combined sigma and z-level method in which the sloping boundaries of the bathymetry are well-introduced. In detail, the vertical mesh was discretized into 19 layers with an equal distance of 1 m. In this hybrid *z*-sigma grid, 1 sigma layer for one meter below the water surface and 18 *z*-layers at the bottom of the sigma domain were defined. The cell sizes around the inflow and outflow boundaries are much denser due to the increased number of border points on the reservoir perimeter.

Boundary and initial conditions

The boundary conditions included the water discharge, water temperature and turbulence model characteristics at two inflows at the Rozgrund Reservoir. The bank of

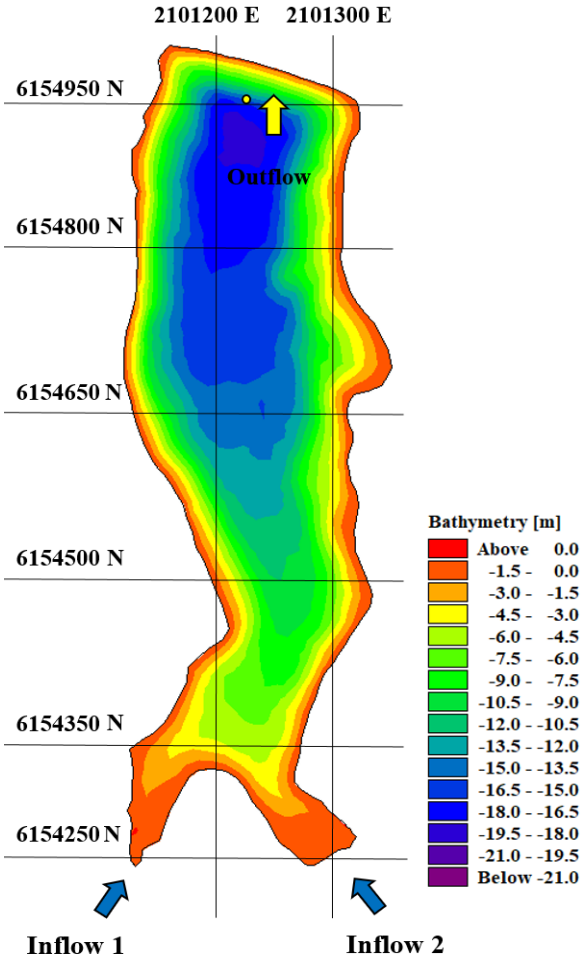

Fig. 5. Bathymetry of the Rozgrund Reservoir.

the Rozgrund Reservoir was defined as a zero normal velocity boundary. Furthermore, the water temperature at both inflows was 10°C and was assumed to be constant in the vertical direction. The water discharge and water temperature also have to be set to a point source outflow (Fig. 5). The initial conditions for the hydrodynamic module including surface elevation [m] and velocity in *x* and *y*-direction [m s^{-1}], temperature module including the vertical profile of water temperature (Fig. 3) and turbulence module including turbulent kinetic energy and its dissipation are also set for the start of simulations in the model setup.

Model setup

MIKE 3 FM model serves the hydrodynamic module as the basis to reproduce the water flow pattern and dynamics of water surface elevations in the reservoir. The shallow water equations were adopted for the solution technique to better reflect water temperature stratification with fewer errors from the steep slopes and wall boundaries. The time step is restricted to 300 *s* to keep the critical Courant–Friedrich–Lewy (CFL) number at 0.8 considering the numerical stability of the model. The water depth near the two inflow boundaries is very low, thus the wetting and drying in the hydrodynamic model were adopted with the rule following drying depth (0.001 m) < wetting depth (0.1 m) in the DHI MIKE flow manual to keep the inflows active in the model. The water temperature simulation package was activated in the model with the definition of density variations as a function of water temperature. To simulate and map the water temperature distribution in the *x-y* plane and a vertical direction, the meteorological conditions need to be adopted by heat exchange (refer to section 3.1). The simulation period of this study was for 1–31 July 2022 to ensure that the simulation could experience the mixing processes. In July 2022, the mean water flow was almost zero from inflow 1 and the reported mean water discharge in inflow 2 was 0.3 l s^{-1}, while the outflow discharge was reported as 5 l s^{-1}. This study adopted 'cold start' initial hydrodynamic condition in which the velocity values in the *x* and *y* directions were set to zero at the beginning of the simulated period (the simulation for warming up the model is not considered). The turbulence model is a mixed Smagorinsky / *k-ε* model for which the horizontal and vertical eddy viscosity are calculated by Smagorinsky and standard *k-ε* formulation respectively. These formulations contain several empirical constant and diffusion parameters interpreting dispersion throughout the reservoir, which were determined by the previous reports and literature description (DHI, 2017; Zamani and Koch, 2020). Notably, wind forcing is not included in the present numerical modeling. A brief description of the model setup of the Rozgrund Reservoir is incorporated in Table 1. The performance of the model is appraised by absolute mean error (*AME*) and the root-mean-square error (*RMSE*). Also, the index of agreement (*Ia*) is a good index to evaluate the similarity between observed and simulated data since of presenting proper weight to the errors and differences (Eslamian et al., 2019). It should be mentioned that the *AME* and *RMSE* values close to zero and *Ia* close to 1 specify the optimal

Table 1. Parameters used in the MIKE 3 FM simulations

Model component	Parameter description	Value and unit [] – note
Bed resistance	Bed roughness height	0.1 [m] – calibrated
Turbulence module coefficient	Horizontal eddy viscosity in Smagorinsky formulation	0.1 – default
	Vertical eddy viscosity in *k-ε* formulation	Minimum eddy viscosity: 1.8e-06 [m^2 s^{-1}] – default Maximum eddy viscosity: 180 [m^2 s^{-1}] – default
Dispersion coefficients	Horizontal and vertical dispersion in scaled eddy viscosity formulation	1 – default and 0.1 – default
Coriolis forcing	Coriolis type	Varying in domain
Heat exchange coefficients	Constant in Dalton's law	0.5 – default
	Wind coefficient in Dalton's law	0.9 – default
	Critical wind speed	2 [m s^{-1}] – default
	Transfer coefficient for heating and cooling	0.0011 – default
	Light extinction coefficient	1 [m^{-1}] – default
	Sun constant, *a* in Ångstrøm's law	0.295 – default
	Sun constant, *b* in Ångstrøm's law	0.371 – default
	Beta in Beer's law	0.3 – default
	Standard meridian for time zone	0 – default

values, thus indicating the best fit between the observed and simulated data (Okhravi et al., 2022).

$$AME = \frac{1}{N}\left(\sum_{i=1}^{N}|O_i - S_i|\right) \quad (1)$$

$$RMSE = \sqrt{\frac{\sum_{i=1}^{N}(O_i - S_i)^2}{N}} \quad (2)$$

$$Ia = 1 - \frac{\sum_{i=1}^{N}(O_i - S_i)^2}{\sum_{i=1}^{N}(|O_i - \bar{O}| + |S_i - \bar{O}|)^2} \quad (3)$$

where

$\bar{O}$ – is the mean value of observed data;

O_i and S_i – are the observed and simulated values, respectively;

N – is the number of data values.

Results and discussion

Previous studies have shown that the application of 3D hydrodynamic models is validated with the generally accepted or standard coefficients in the literature without the need for calibration (Chung et al., 2009; Zamani et al., 2018). The calibration is usually associated with 2D hydrodynamic models (e.g. MIKE 21) where the flow characteristics along the cross-section have been averaged. 2D models suffer from difficulties in the establishment of a reliable relationship between water surface elevation and volume since each mesh cell represents a different cross-sectional area (Zamani and Koch, 2020). In addition, a 3D water body such reservoir cannot be fully calibrated directly by the use of in-situ sample data since they have been not yet fully available for calibration in general. Therefore, the present study made an effort to illuminate the 3D flow behavior and water temperature distribution in space and time dimensions in the Rozgrund Reservoir and provide a preliminary understanding of 3D reservoir hydrodynamic modeling for further planned studies in water quality modeling in reservoirs for extreme events. Hence, three scenarios are devised to simulate water temperature variations in horizontal and vertical directions according to the above-mentioned descriptions. The MIKE 3 simulations are as follows:

1) Reservoir modeling based on July 2022 implementation using water temperature profile (Fig. 3) as the initial condition for temperature module (reference case).
2) The reference case simulation with the constant initial conditions for the temperature module.
3) The reference case simulation including high inflows.

Spatial and temporal variations of water temperature

The MIKE 3 model was run on a desktop PC with an AMD Ryzen 7 3700X 8-core processor (16 threads) and a Windows 10 operating system to simulate the one-month water temperature of the Rozgrund Reservoir (July 2022). The MPI (message passing interface) distributed memory approach allowed parallel computing within a multi-core processor. This approach assigns memory for several sub-domains saved in separate files, then they will be merged at the end of the simulation into the specified files. The one-month simulation with the grid mentioned before took 5 hours (CPU time).
According to the model setup, the simulation was initiated by the imported vertical variations of water temperature as was presented in Fig. 3. 2D map of water temperature distribution at surface in the horizontal plane

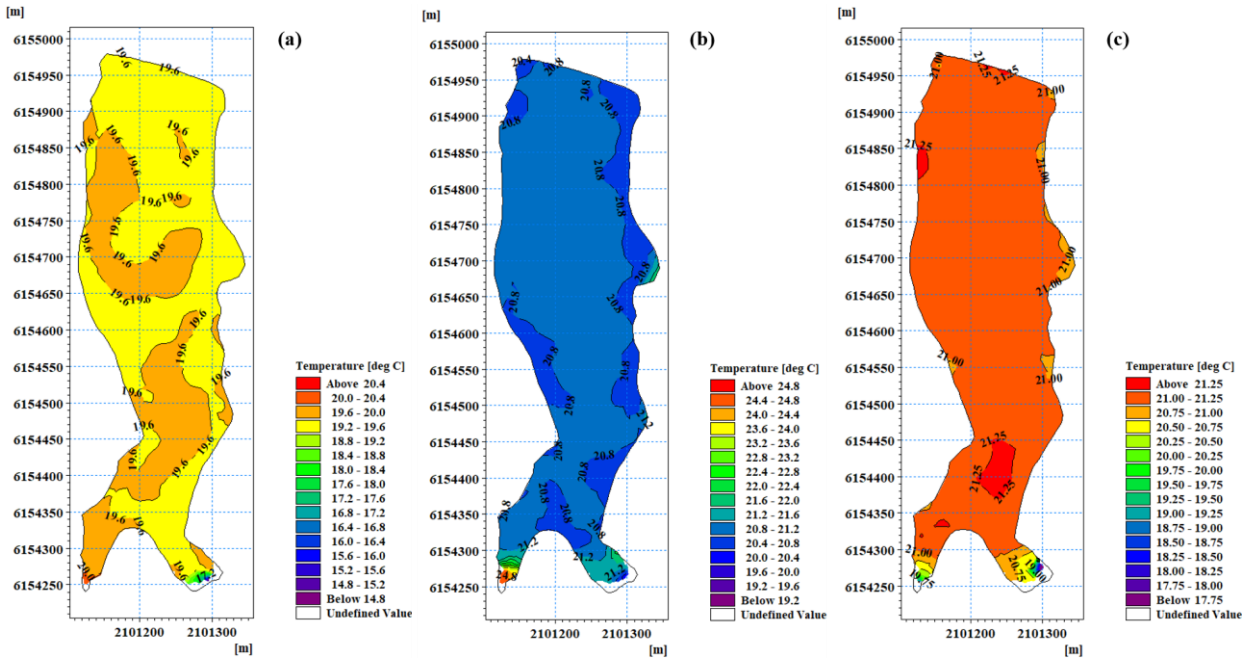

Fig. 6. Simulated water temperature distribution in July for Rozgrund Reservoir: a) 6 days, b) 15, c) 31 days.

for three moments is presented in Fig. 6. The minimum water temperature in July was recorded at 4.89°C in the deepest layer of the reservoir for a second time step in the simulation, while the initial water temperature in this location was 4.8°C. This interprets that the simulation follows the temperature stratification imported as an initial condition of the temperature module – the temperature difference is less than 1°C. The maximum value of water temperature was 22.33°C which is in the range of 10°C (inflow water temperature) <22.33°C<23.4°C (measured water temperature at surface, Fig. 3). The reservoir-averaged value of water temperature was 15.5°C.

A 2D display of current speed with current isolines at the surface of the reservoir (Fig. 7) in July showed very low velocities either in inflow 2 or near steep boundary slopes. It is worth noting that the current speed differences range from 0.001 to 0.05 m s^{-1} and are all less than 0.2 m s^{-1}, indicating that temperature stratification cannot be affected by inflows in the Rozgrund Reservoir (Li et al., 2016). Indeed, the very low inflows are not expected to significantly impact the initial temperature field within one month of simulation time.

The vertical cross-section plane of water temperature from inflow 2 (the only inflow current in July) toward the outlet shows water temperature changes (Fig. 8) from the beginning of the simulation till the end of the simulated period. The results show the water temperature at the surface layers was predicted

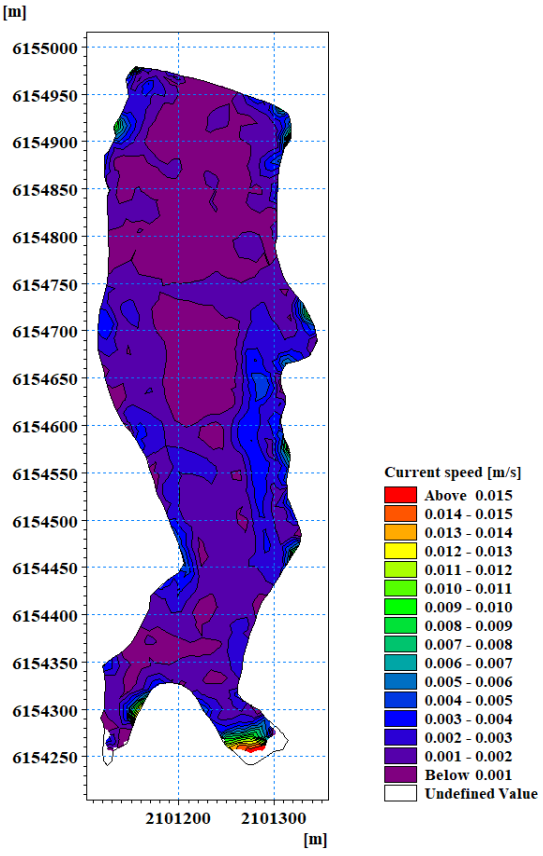

Fig. 7. Simulated current speed in July (reference case).

accurately in accordance with the initial measured water temperature. However, the water temperature at the deep layers experienced heating, and the water temperature rose to 16°C. The reasons for warming up deep layers could be attributed to a very small inflow and relatively large internal heat exchange in the reservoir when water mixing has not occurred. Notably, over a period of 1 month, the inflows will most likely not reach the sink at the north of the reservoir where the outflow is located (Fig. 5) and the water level was dropped to about 10 cm due to a significant unbalance of inflows and the outflow. Nevertheless, the results confirm that the model does retain water temperature stratification in the reservoir – the imported stratified water temperature for initial conditions has lasted up to the further time steps. The reservoir reveals non-isothermal and non-mixed layers for the entire waterbody since approximately all vertical temperature profiles show water temperature differences of more than 5°C (Fig. 8). According to Woolway et al. (2014), the reservoir is isothermal if the water temperature differences between the surface and deep layers decrease less than one unit (<1°C), which means that water temperature stratification can be neglected.

Temporal variations of water temperature (2 m below the water surface) are drawn in Fig. 9 for three different locations in riverine, transition and lacustrine zones. The value of the mean water temperature for each location was incorporated in Fig. 9. The temporal pattern of water temperature in the lacustrine and transition zones of the Rozgrund Reservoir is almost the same, while the temporal oscillations of water temperature in the riverine zone can be seen due to the influence of nearby inflow. As mentioned before, the water inside the reservoir cannot be mixed adequately over one month of simulation time such the water temperature at 2 m below the surface shows no distinct temporal changes in three zones. Additionally, the mean water temperature values between these zones are close and support the above-mentioned statements.

The next simulation was initiated with the constant water temperature as it was considered the same as the air temperature, 19.1°C (mean air temperature in July 2022 at the meteorological station in Banská Štiavnica). The water temperature distribution and current speed in the horizontal plane had similar patterns to the reference simulation while having different values. The results of this simulation also show that the Rozgrund Reservoir does not experience water temperature stratification during just a one-month simulation period when the initial water temperature was constant. Therefore, the vertically measured water temperature in July (Fig. 3) cannot be compared with simulation results and the model has to be extended for at least one year for the investigation of water temperature stratification in this reservoir (Li et al., 2017).

To assess the differences between results from these two simulations, the temporal changes in water temperature at a point location in the lacustrine zone at 2 m below the water surface were extracted and drawn in Fig. 10. The statistical analysis shows low values of *RMSE*

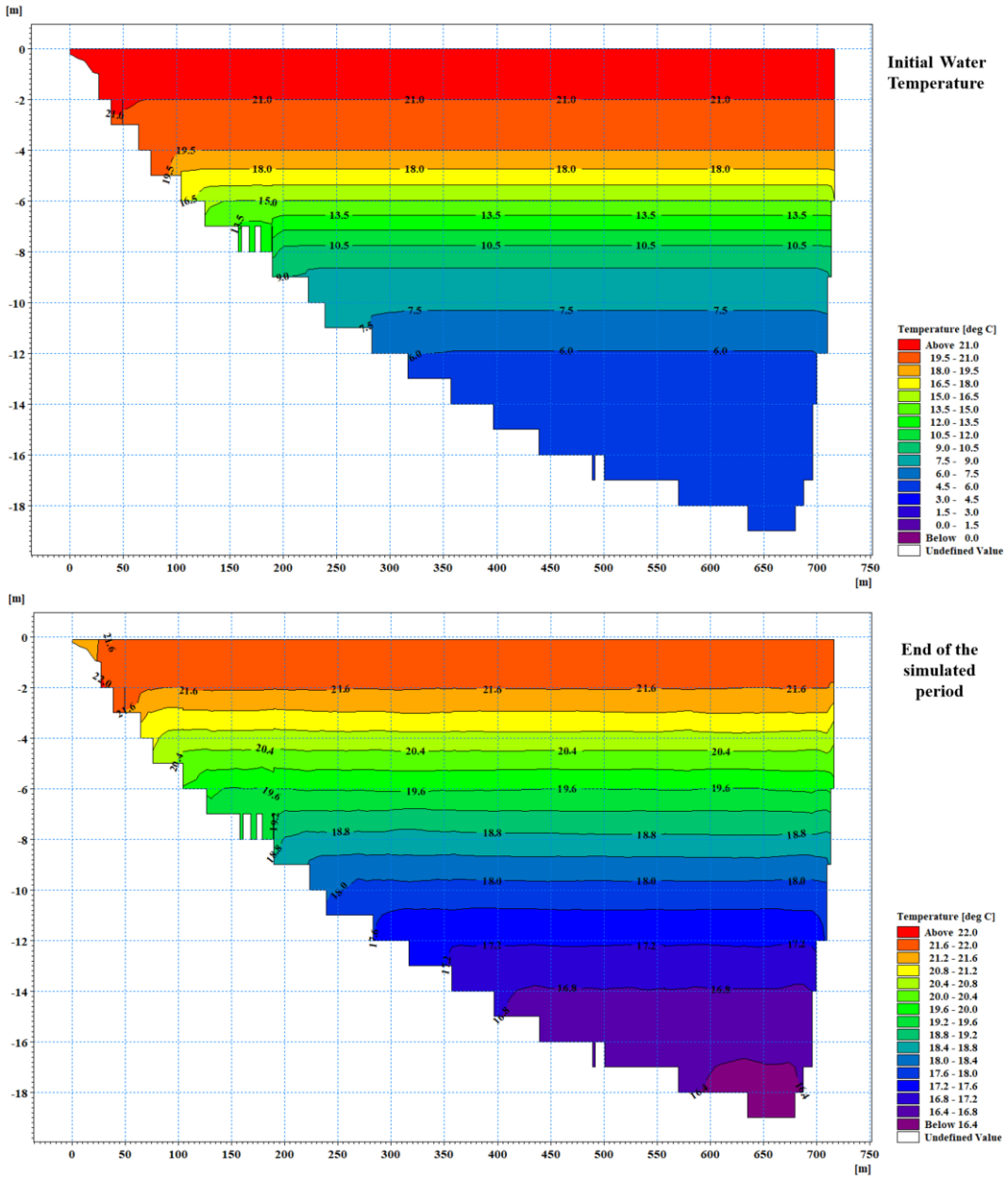

Fig. 8. Simulated vertical temperature distributions from the inflow 2 to the outflow.

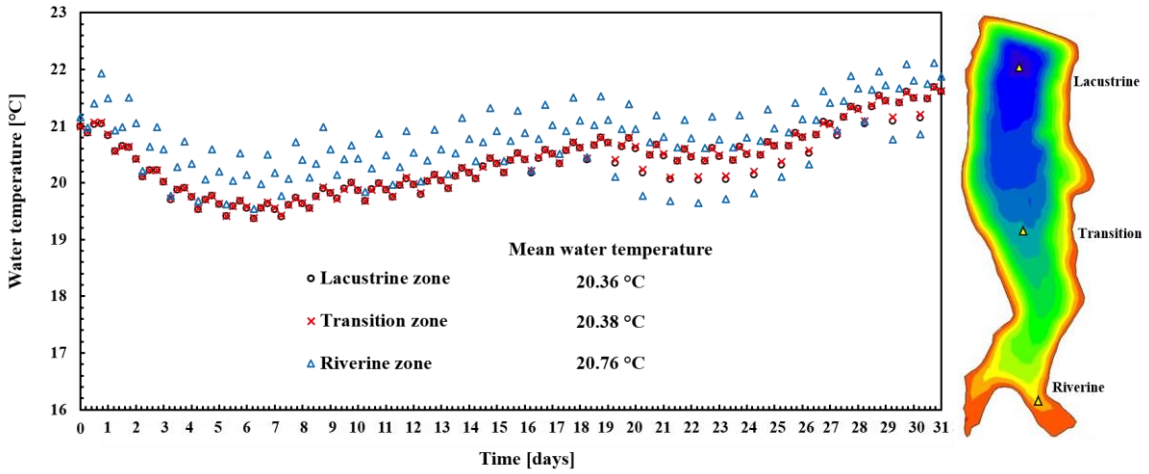

Fig. 9. Temporal variations of water temperature at 2 m below the surface in different parts of the reservoir.

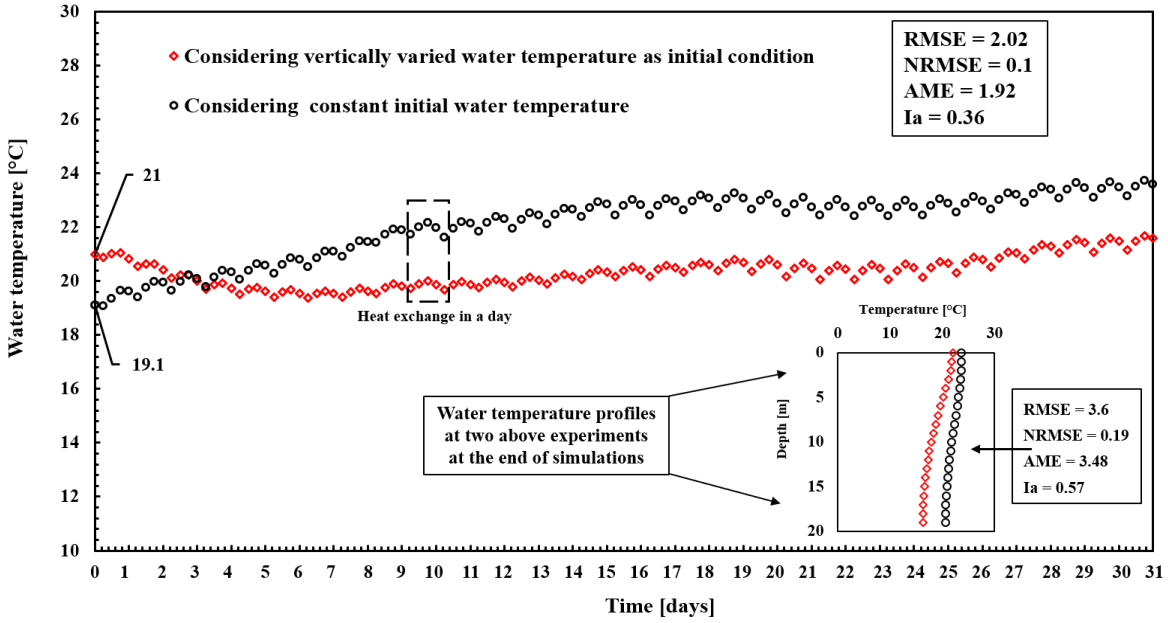

Fig. 10. Temporal variations of water temperatures at the point 2 m below the surface in different initial conditions together with the vertical variations of water temperature at the end of the two mentioned simulations.

(or $NRMES = RMSE/\overline{O}$) and *AME*, reflecting the good agreement between simulated water temperature in the case of the constant initial value for water temperature with vertically varied water temperature as an initial condition. Both the *AME* and *RMSE* are about 2°C, given that the range of numerical variations of water temperature was 19–24°C in July. Fig. 10 shows the significant effects of initial water temperature impact on temporal temperature variations such that the constant water temperature set for initial conditions always increase the water temperature during the simulation time unless the simulation continues for a long period. This fact could be confirmed with the vertical water temperature profile (Fig. 10), indicating the acceptable agreements ($Ia = 0.57$) in simulated water temperature in depth for the two mentioned initial conditions. The low *NRMSE* (= 0.1) reflects the potential fit that would have been achieved by further modifications of the simulations.

Effects of high inflows

In a reference simulation, the inflow to the computational model was only set to inflow 2 with 0.0003 $m^3 s^{-1}$ and an outflow discharge of 0.005 $m^3 s^{-1}$ (refer to model setup section). The planned third simulation was to investigate the effects of high flow on current speed and water temperature stratification of the reservoir. Thus, inflow 1 and inflow 2 were set with 0.003 and 0.007 $m^3 s^{-1}$, and the outflow was fixed with the previous value of 0.005 $m^3 s^{-1}$, which means that the inflow discharge was double of outflow discharge. The map of the current speed is shown in Fig. 11. Through comparing simulated results to the results from the reference simulation

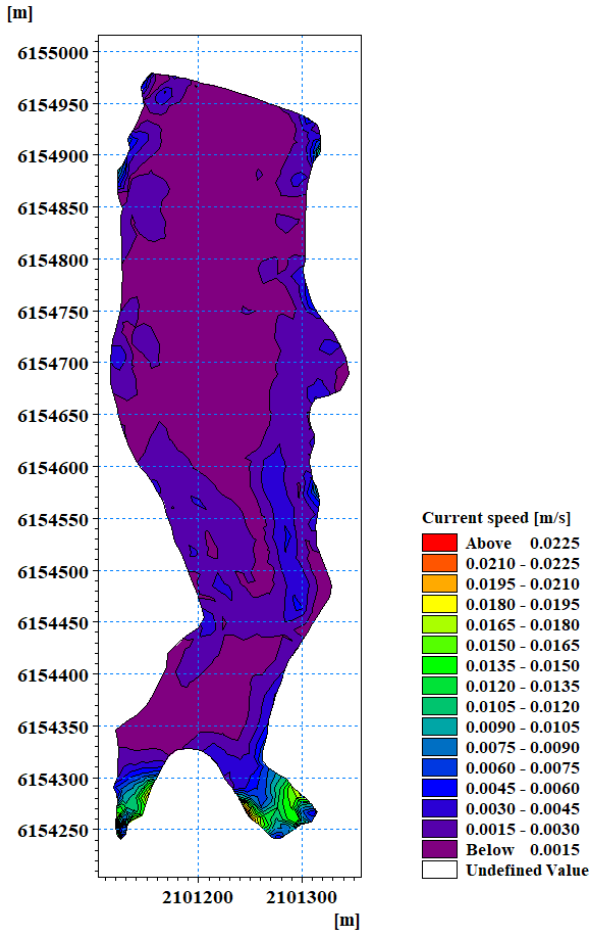

Fig. 11. Simulated current speed in July (high inflows scenario).

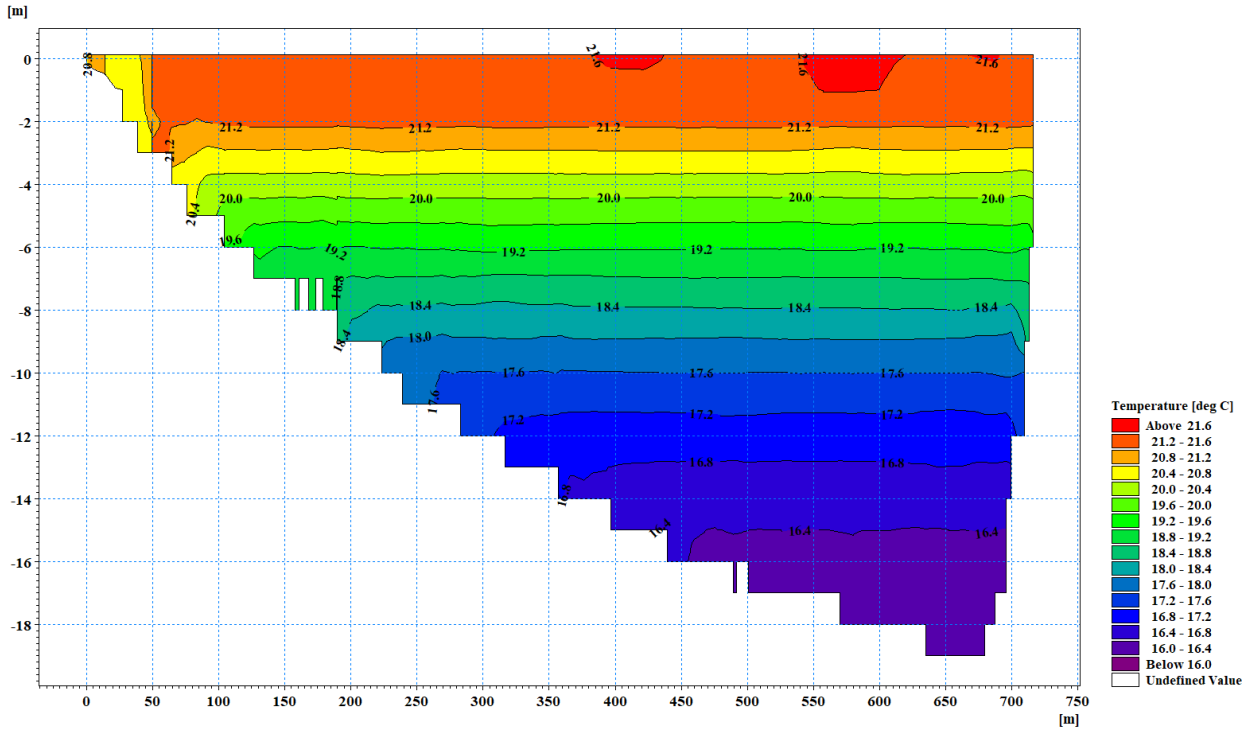

Fig. 12. Vertical varied water temperature from the inflow 2 to the outflow during a high inflows scenario.

(Fig. 7), the role of high inflows on the increase of current speed and probable mixing could be illuminated. The current speed was increased by more than 30% and the higher isolines appeared around two inflows.

The effects of high flow on water temperature stratification was also shown in Fig. 12. The water temperature profile did not reflect many changes compared to what was reported in the reference case in Fig. 8. The non-isothermal layers and temperature stratification were almost the same, but a 12 cm water level rise was predicted at the end of simulation time which is marked in Fig. 12.

Conclusion

The 3D hydrodynamic model of the Rozgrund Reservoir (located in Slovakia) was established using MIKE 3 FM model to elucidate spatial and temporal variations of water temperature in this reservoir for the simulated period (July 2022). The influence of high inflows (e.g. extreme hydrological conditions) on the current speed and water temperature was investigated using hydrodynamic modeling. The simulation results showed an acceptable performance in reproducing the water temperature and water level variations within the Rozgrund Reservoir.

The simulation results showed that the Rozgrund Reservoir experienced water temperature stratification in July and the very low inflows did not have effects on the thermal structure of the reservoir since the mixing did not occur over one month of simulation time. Additionally, velocity differences way less than 0.2 m s^{-1} confirmed non-mixed layers. Therefore, the spatial distribution of water temperature in three zones of the reservoir including riverine, transition and lacustrine was almost similar.

The water temperature results of two simulations with different initial conditions (vertically varied or constant initial water temperature) in the temperature module over one month, July, indicated the potential effects of constant initial water temperature to reproduce temperature stratification in the Rozgrund reservoir if long simulation time is grounded and further modifications on input files (e.g. heat exchange) are provided (the statistical analysis reported for Fig. 10).

The effects of high inflows on current speed showed rising water levels. Vertical stratification has not changed in the high inflows scenario over a one-month simulation. This research manifests time effects on the spatial and temporal variability of water temperature within the Rozgrund Reservoir, expressing that one month is a short time to simulate water temperature stratification changes. Thus, future research works would investigate long duration simulation e.g. one year of water temperature stratification changes. The focus of future research could be more on the degree and duration of water temperature stratification influenced by the intensity of external forces such as inflow, wind, precipitation and heat exchange conditions.

This present work aimed to depict water temperature distribution in scales of time and space in the Rozgrund Reservoir. The preliminary knowledge gained in this

research work will form the basis to study water temperature distribution and stratification in different reservoirs and finally benefit the investigation of water quality in a reservoir for better environmental management.

Acknowledgements

This work was supported by the project APVV-18-0205 with the title of ' Management of crisis situations in water supply with respect to climate change'.

References

Boehrer, B., Schultze, M. (2008): Stratification of lakes. Reviews of Geophysics, 46(2). https://doi.org/10.1029/2006RG000210

Dadashzadeh, M., Mojtahedi, A., Parsa, J. (2021): Evaluation the impacts of causeway remedial actions on Urmia Lake ecosystem using computational fluid dynamics and spatial analysis method. Journal of Civil and Environmental Engineering, 51(104), 41–53.

DHI (2017): User Guide of MIKE3: Estuarine and Coastal Hydraulics and Oceanography, Hydrodynamic Module.

Eslamian, S., Okhravi, S., Eslamian, F. (2019): Constructed Wetland: Hydraulic Design. Taylor and Francis Group, CRC Press, Boca Raton FL, USA.

Fendek, M. (2019): Assessment of water resources of Slovakia. In: Negm, A., Zeleňáková, M. (eds) Water Resources in Slovakia: Part I. The Handbook of Environmental Chemistry, vol 69. Springer, 21–62.

GWP (2011): Global Water Partnership Central and Eastern Europe, Slovak Hydrometeorological Institute. Bratislava, Slovakia. https://www.gwp.org/

Han, B. P., Armengol, J., Garcia, J. C., Comerma, M., Roura, M., Dolz, J., Straskraba, M. (2000): The thermal structure of Sau Reservoir (NE: Spain): a simulation approach. Ecological Modelling, 125(2–3), 109–122.

Helfer, F., Zhang, H., Lemckert, C. (2010). Evaporation reduction by windbreaks: Overview, modelling and efficiency. Urban Water Security Research Alliance. Technical Report No. 11.

Hlevca, B., Cooke, S. J., Midwood, J. D., Doka, S. E., Portiss, R., Wells, M. G. (2015): Characterisation of water temperature variability within a harbour connected to a large lake. Journal of Great Lakes Research, 41(4), 1010–1023.

Chao, X., Jia, Y., Shields Jr, F. D., Wang, S. S., Cooper, C. M. (2010): Three-dimensional numerical simulation of water quality and sediment-associated processes with application to a Mississippi Delta lake. Journal of environmental management, 91(7), 1456–1466.

Chen, M., Wei, X., Huang, H., Lü, T. (2011): Poyang Lake basin: A successful, large-scale integrated basin management model for developing countries. Water Science and Technology, 63(9), 1899–1905.

Chung, S. W., Hipsey, M. R., Imberger, J. (2009): Modelling the propagation of turbid density inflows into a stratified lake: Daecheong Reservoir, Korea. Environmental Modelling & Software, 24(12), 1467–1482.

Ji, Z. G. (2017). Hydrodynamics and water quality: modeling rivers, lakes, and estuaries. John Wiley & Sons.

Kirillin, G. (2010): Modeling the impact of global warming on water temperature and seasonal mixing regimes in small temperate lakes. Boreal Environment Research. 15 (2), 279–293.

Kirillin, G., Shatwell, T. (2016): Generalized scaling of seasonal thermal stratification in lakes. Earth-Science Reviews, 161, 179–190.

Lawson, R., Anderson, M. A. (2007): Stratification and mixing in Lake Elsinore, California: An assessment of axial flow pumps for improving water quality in a shallow eutrophic lake. Water research, 41(19), 4457–4467.

León, L. F., Lam, D. C. L., Schertzer, W. M., Swayne, D. A., Imberger, J. (2007): Towards coupling a 3D hydrodynamic lake model with the Canadian regional climate model: simulation on Great Slave Lake. Environmental Modelling & Software, 22(6), 787–796.

Li, Y., Yao, J., Zhang, L. (2016): Investigation into mixing in the shallow floodplain Poyang Lake (China) using hydrological, thermal and isotopic evidence. *Water Science and Technology*, 74(11), 2582–2598.

Li, Y., Zhang, Q., Ye, R., Yao, J., Tan, Z. (2018): 3D hydrodynamic investigation of thermal regime in a large river-lake-floodplain system (Poyang Lake, China). Journal of Hydrology, 567, 86–101.

Li, Y., Zhang, Q., Zhang, L., Tan, Z., Yao, J. (2017): Investigation of water temperature variations and sensitivities in a large floodplain lake system (Poyang Lake, China) using a hydrodynamic model. Remote Sensing, 9(12), 1231.

Mahanty, M. M., Mohanty, P. K., Pattnaik, A. K., Panda, U. S., Pradhan, S., Samal, R. N. (2016): Hydrodynamics, temperature/salinity variability and residence time in the Chilika lagoon during dry and wet period: Measurement and modeling. Continental Shelf Research, 125, 28–43.

Negm, A., Zeleňáková, M. (2019): Water Resources in Slovakia: Part I. The Handbook of Environmental Chemistry, vol 69. Springer.

Okhravi, S., Schügerl, R., Velísková, Y. (2022): Flow resistance in lowland rivers impacted by distributed aquatic vegetation. Water Resources Management, 36, 2257–2273.

Sima, S., Ahmadalipour, A., Tajrishy, M. (2013): Mapping surface temperature in a hyper-saline lake and investigating the effect of temperature distribution on the lake evaporation. Remote Sensing of Environment, 136, 374–385.

Torriano, F., Picher, P., Chaaban, M. (2012): Numerical investigation of 3D flow and thermal effects in a disc-type transformer winding. Applied Thermal Engineering, 40, 121–131.

Webb, B. W., Hannah, D. M., Moore, R. D., Brown, L. E., Nobilis, F. (2008): Recent advances in stream and river temperature research. Hydrological Processes: An International Journal, 22(7), 902–918.

Woolway, R. I., Maberly, S. C., Jones, I. D., Feuchtmayr, H. (2014): A novel method for estimating the onset of thermal stratification in lakes from surface water measurements. Water Resources Research, 50(6), 5131–5140.

Zamani, B., Koch, M. (2020): Comparison between two hydrodynamic models in simulating physical processes of a reservoir with complex morphology: Maroon Reservoir. Water, 12(3), 814.

Zamani, B., Koch, M., Hodges, B. R., Fakheri-Fard, A. (2018): Pre-impoundment assessment of the limnological processes and eutrophication in a reservoir using three-dimensional modeling: Abolabbas reservoir, Iran. Journal of Applied Water Engineering and Research, 6(1), 48–61.

Zhang, F., Zhang, H., Bertone, E., Stewart, R., Lemckert, C., Cinque, K. (2020): Numerical study of the thermal

structure of a stratified temperate monomictic drinking water reservoir. Journal of Hydrology: Regional Studies, 30, 100699.

Zhang, H., Chan, E. S. (2003): Modeling of the turbulence in the water column under breaking wind waves. Journal of oceanography, 59(3), 331–341.

Saeid Okhravi, PhD. (*corresponding author, e-mail: saeid.okhravi@savba.sk)
Assoc. Prof. Ing. Marek Sokáč, PhD.
Ing. Yvetta Velísková, PhD.
Institute of Hydrology SAS
Dúbravská cesta 9
84104 Bratislava
Slovak Republic